AN INVERSE TRANSMISSION LINE MODEL OF THE LOWER LIMB ARTERIAL SYSTEM

Lester Ryan John

THESIS SUBMITTED IN PARTIAL FULFILMENT OF THE REQUIREMENTS FOR THE DEGREE OF DOCTOR OF PHILOSOPHY IN THE DEPARTMENT OF BIOMEDICAL ENGINEERING

UNIVERSITY OF CAPE TOWN
AUGUST 2000

SYNOPSIS

The *theoretical objective* of this thesis was to investigate whether an inverse solution to a transmission line model of the human arterial system exists. The result of this research process was the development of the first Inverse Electrical Transmission Line Model of the human arterial system. This Inverse Model introduces a paradigm shift in the field of arterial modelling. It allows for direct application of inverse electrical transmission lines models to the clinical diagnosis of normal as well as stenotically diseased arterial states.

As a basis for the Inverse model, an underlying Forward Transmission Line Model was first developed. A novel set of graphical arterial modelling tools for use with both Forward and Inverse models, is also introduced. These tools are the result of a combination of Matlab™ subroutines, and Simulink™ models which together form a unique high-level visual algorithmic language ideally suited to modelling the complex branching geometry of the human arterial tree. The development of this set of visual arterial modelling tools was a *technical objective* of this thesis.

The Forward Model was validated by comparing its simulations to published qualitative and quantitative arterial data, as well as to published data from a physical arterial model. The comparison between a Forward Transmission Line Model and a complex Physical Arterial Model is the first such comparison between these two models.

The prerequisites for mathematical inversion of a Forward transmission line model are also discussed. The theoretical "hurdle" of inverting a transmission line based model of the arterial system has been overcome by the Inverse Model described in this thesis. The performance of the Inverse Model was tested under computer simulated conditions, by using it to analyse haemodynamic waveforms generated by the Forward Model (ie. a "virtual patient" with known arterial geometries) .

The 'normal' human arterial system is subject to age; body dimension; and gender-related variability. Quantification of this normal variability is an important step in improving the diagnostic accuracy of the proposed clinically-applied Inverse Model.

Therefore, for the sake of completeness, a literature review relating to the quantification of 'normal' cardiovascular variation is presented.

Having affirmed the theoretical objective, the *strategic objective* of this thesis was to prepare the groundwork for the introduction of the inverse arterial model into the non-invasive clinical diagnostic arena. Preliminary clinical investigation necessitated the development of custom haemodynamic data acquisition equipment (this was the second *technical* objective of this thesis). Because of the prototype nature of this equipment, it was not feasible to clinically implement the full theoretical Inverse Model. Consequently, a mathematically *underdetermined* version of the Inverse Model was also developed, for the sole purpose of carrying out preliminary clinical investigation. The results of this preliminary investigation are presented, in order to set a starting point for a proposed Pilot Clinical Study that would use the full critically determined version of the Inverse Model.

Both the Forward and the Inverse arterial transmission line models have been deliberately exposed to a variety of testing environments (existing transmission line models; published qualitative and quantitative subject data; a physical arterial model; normal clinical subject data; and clinical data from patients with a variety of arterial diseases). The successful implementation of these models in varied environments is a good indicator of their suitability for clinical use. The reason for this is that the clinical testing environment is very different from an idealized computer-simulated testing environment and it is difficult to infer the suitability of a model for clinical use simply on the basis of computer simulated tests.

The technical and logistical hurdles that stand in the way of a full clinical implementation of the Inverse Model are also discussed. Proposals are made concerning the direction of future theoretical inverse model research; prerequisite haemodynamic data-acquisition equipment development; and supplementary clinical studies.

" Two roads diverged in a wood, ...
I took the one less traveled by. "

Robert Frost

TABLE OF CONTENTS

CHAPTER 1
INTRODUCTION

The human arterial system is formed by a complex tree of arterial vessels. The characteristics of this system varies between groups of normal and arterially diseased individuals. Diagnostic equipment and techniques have been extensively developed for the clinical study of atherosclerotic disease. Mathematical research has focussed on the forward modelling of both the normal and diseased arterial states but has not been fully clinically exploited. The combination of mathematical and clinical diagnostic techniques requires the "key" of an inverse solution to existing mathematical models.

Diagnosis of atherosclerosis may be divided into three categories : Clinical Signs and Symptoms, Non-invasive tests, and Invasive tests. Clinical Signs and Symptoms are a qualitative indication of disease. Further investigation may be carried out using non-invasive diagnostic tests to quantify the extent and distribution of disease . These tests include the measurement of arterial blood pressure in the limb [Nicolaides, 1992]. Invasive Angiography is considered to be the 'gold-standard' in the diagnosis of arterial disease [Strandness , 1992].

Ultrasound has been used extensively to investigate arterial disease. Ultrasound imaging is used to visualise arteries. Doppler Ultrasound is used to detect arterial blood flow velocities. Duplex Doppler Ultrasound combines both techniques [Dauzat et al, 1992]. The Doppler velocity signal may be analysed using qualitative or quantitative techniques. Some methods of quantifying the Doppler flow velocity waveform include Pulsatility and Resistance Index [PI, RI : Nichols & O'Rourke , 1990]; Spectral Broadening Index [SBI : Labs & FitzGerald , 1992] ; and Laplace Transform Damping Factor [LTD : Skidmore , 1979].

Because of the similarity between haemodynamic fluid equations, and electrical circuit equations, haemodynamic analysis may be carried out using electrical circuit analogies. This approach which makes use of well established electrical circuit analysis techniques, despite being the subject of extensive academic research, has found little clinical application. Only the inverse lumped circuit model [Skidmore , 1979] has been clinically applied. Current non-invasive clinical diagnosis focuses on advanced imaging techniques (Ultrasound, CT, PET, MRI) , established clinical diagnostic techniques, and simple empirical indices.

The combination of non-invasively acquired arterial images and haemodynamic waveforms, with detailed circuit modelling techniques, has the potential to lead to improved methods of non-invasive diagnosis.

Non-invasive diagnostic techniques have numerous advantages over invasive techniques. For example there is little or no infection risk; no risk of surgical trauma; lower cost; lower time duration; and no need for surgical staff to be present. Non-invasive techniques also have disadvantages e.g. limited accuracy; inter- and intra-operator variability.

1.1 ELECTRO-HAEMODYNAMIC ANALOGY

A short segment of human artery may be represented by a section of compliant tubing. The fluid dynamics of circulating blood may be represented by the three dimensional Navier-Stokes equations and the continuity equation. Because of the similarity between the linearised Navier-Stokes equations for haemodynamics (Equations 1.1–1.2), and the propagating electro-magnetic wave equations in an electrical transmission line (Equations 1.3- 1.4), a compliant tube (hence the entire arterial system) may, in turn ,be mathematically modelled by a segment of an electrical transmission line (Figure 1.1) [LaCourse , 1986; Milnor , 1989].

$$\frac{-\delta P}{\delta x} = QR + L\frac{\delta Q}{\delta t} \qquad \text{[Equation 1.1]}$$

$$\frac{-\delta Q}{\delta x} = PG + C\frac{\delta P}{\delta t} \qquad \text{[Equation 1.2]}$$

Where : P = pressure; Q = flow; R = series hydraulic resistance; L = inertia of blood;
C = arterial wall compliance; G = conductance representing radial (leakage) flow ,
X = distance , t = time

$$\frac{-\delta V}{\delta x} = IR + L\frac{\delta I}{\delta t} \qquad \text{[Equation 1.3]}$$

$$\frac{-\delta I}{\delta x} = VG + C\frac{\delta V}{\delta t} \qquad \text{[Equation 1.4]}$$

where: V = electrical voltage; I = electrical current ; R = electrical resistance;
L = electrical inductance; C = electrical capacitance; G = electrical conductance;
X = distance; t = time

The advantage of an electrical model is that it allows powerful and well established circuit analysis techniques to be used to analyse blood flow and pressure waveforms. By using these electro-mechanical analogies, the effects of atherosclerotic disease on the arterial blood Flow and Pressure waveforms may be simulated. These characteristic waveform changes, may then be used as a clinical diagnostic aid.

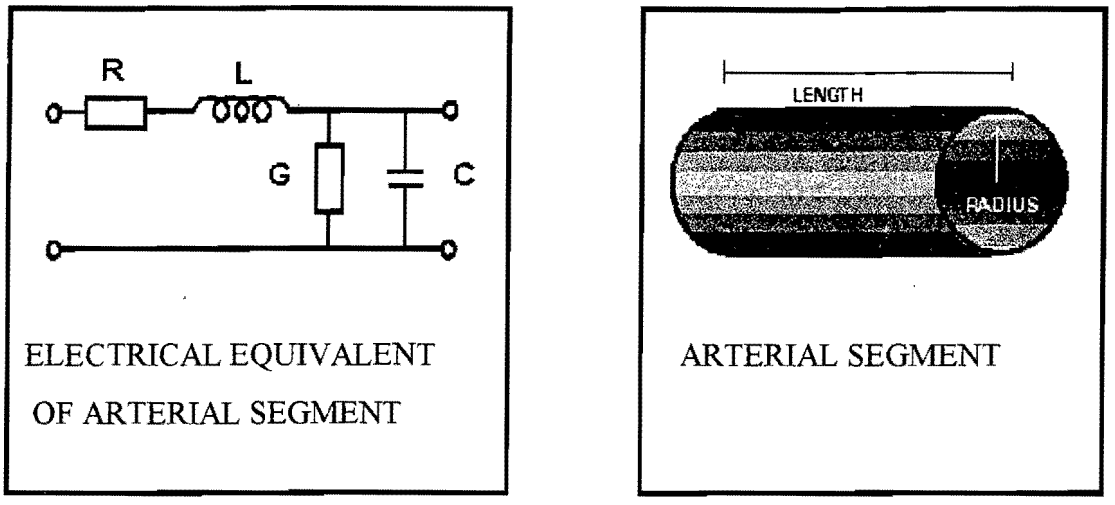

Electrical Parameters (per unit length)

Mechanical parameters

Figure 1.1 : Electrical Modelling of an Arterial Segment

Equations 1.5 - 1.7 , illustrate the mathematical analogy between a compliant arterial segment and a segment of an electrical transmission line (both of unit length), corresponding to [Figure 1.1].

$$\mathbf{R} = \frac{8.\mu}{\pi.r^4} \qquad \text{[Equation 1.5]}$$

$$\mathbf{L} = \frac{\rho}{\pi.r^2} \qquad \text{[Equation 1.6]}$$

$$\mathbf{C} = \frac{3.\pi.r^3}{2.E.h} \qquad \text{[Equation 1.7]}$$

With Mechanical Parameters : Length ; r = radius;
h = wall thickness; E = Young's modulus
ρ = blood density ; μ = blood viscosity

And Electrical Parameters : R = resistance; L = inductance;
C = capacitance; G = leakage conductance

Nonlinear frequency-dependent resistance and inductance is discussed further in Appendix VI.

1.2 FORWARD AND INVERSE ELECTRICAL MODELLING

A Forward arterial model is defined as a model where the inputs are the mechanical state of the arterial system, and the outputs are the corresponding haemodynamic waveforms . An Inverse arterial model is defined as a model in which the inputs are haemodynamic waveforms , and the outputs relate to the corresponding physiological / mechanical state of the arterial system (Figure 1.2).

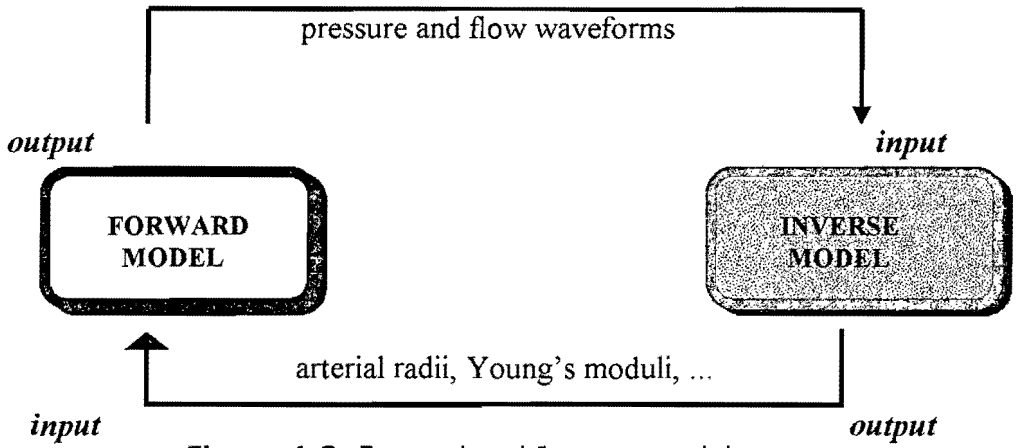

Figure 1.2: Forward and Inverse models

A forward model requires that the (physiological/mechanical) state of arterial disease be known, prior to the calculation of corresponding haemodynamic waveforms. This is the opposite of what is required for clinical diagnosis, where an inverse model (Figure 1.2) is needed. Forward modelling is therefore not directly applicable to clinical diagnosis. Indeed, a forward model may only be clinically applicable if it uncovers some features of haemodynamic waveforms which correlate with specific states of atherosclerotic disease, as a by-product rather than as a direct result. Forward models are further limited, in their clinical application, by the absence of research into inverse solutions for these models.

What is required, from a Clinical perspective, is an inverse electrical transmission line model, which would be able to transfer the huge body of academic research in forward/theoretical models, into the Clinical arena, and may therefore result in much improved diagnostic procedures. A good inverse model should include as many of the features of existing forward models as possible without compromising the 'invertability' of the model equations.

1.3 FORWARD MODELLING

The earliest electrical circuit models of the arterial system were **actual circuits** constructed using passive components (resistors, capacitors, inductors) These were, in effect, true analogue computers which could 'compute' the blood flow and pressure waveforms corresponding to the state of system being modelled [Jager et al, 1965; Westerhof et al, 1969] .

With the growing availability and increasing complexity of microcomputers, in subsequent years, these models were simulated on computer. **Computer simulated** models were more flexible (easier construction, modification) than actual circuits, and in addition were able to model non-linear behaviour that would be impossible to model using passive circuit components. [Snyder et al, 1968; Raines et al, 1974; Avolio, 1980; O'Rourke & Avolio, 1980; LaCourse et al, 1986; McIlroy et al, 1986, 1988.]

Further research modelled anatomically **tapered arteries**, corresponding closely to actual diameter tapers observed in human arterial segments [Einav et al 1988, 1992].

Forward modelling has progressed further, to include the **collateral circulation** (a common phenomenon in the human circulatory system) by modifying the representative transmission line equations to include the effects of circulatory loops (e.g. as in the circle of Willis in the cerebral circulation). This is a situation that is rarely encountered in an electrical circuit, and the development of this theory is therefore a direct consequence of the research in forward electrical modelling of the arterial system [Roller et al, 1969; Helal et al 1990,1994] .

Forward models are now also able to simulate arterial systems with physiological **feedback** (due to baroreceptor regulation of arterial blood pressure at the carotid bulb). Forward models are becoming increasing complex, and also more accurate in their representation of the human circulatory system [Calvalcanti et al, 1995; Ursino et al, 1995]. These research trends in Forward Modelling are illustrated in Figure 1.3.

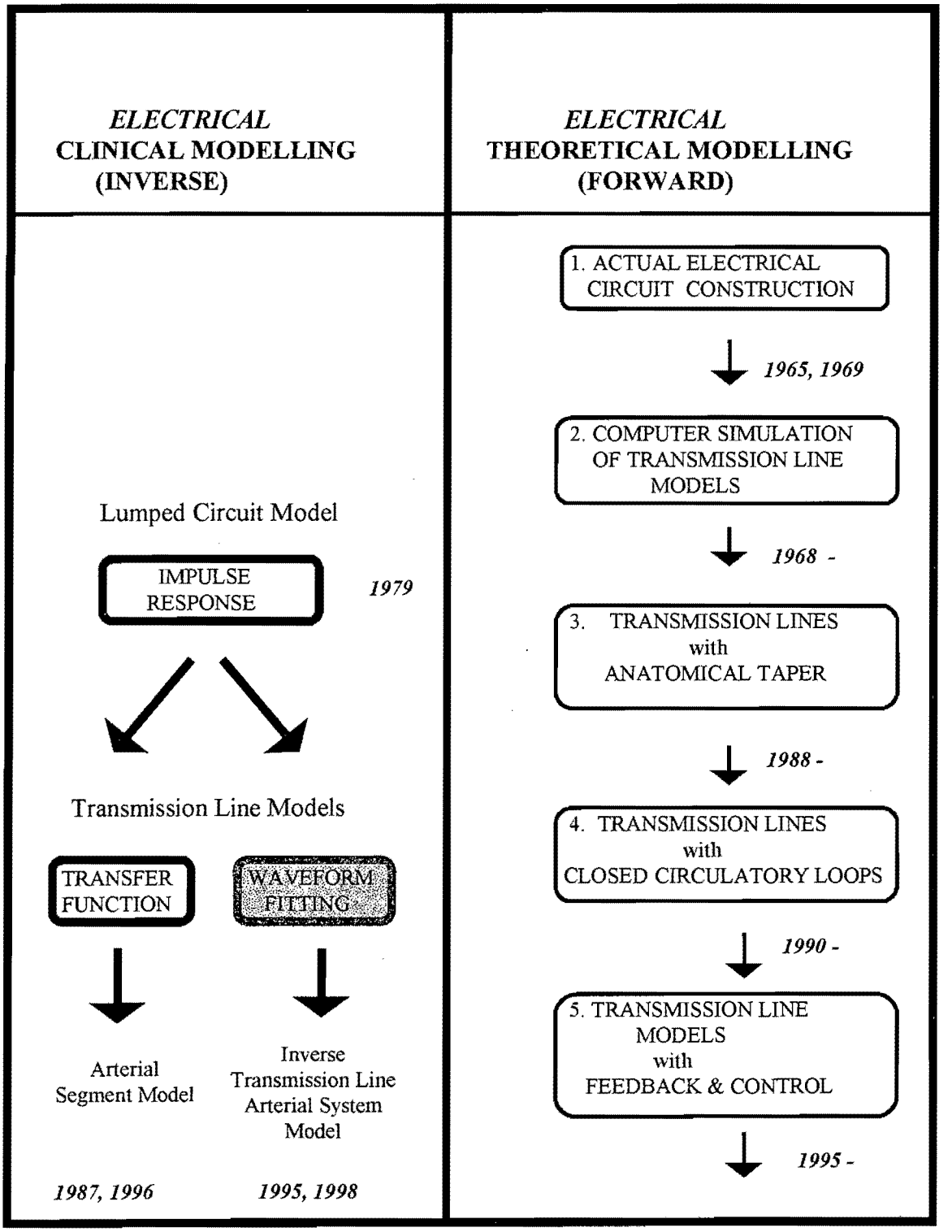

Figure 1.3 : Research trends in electrical modelling

1.4 INVERSE MODELLING

Electrical circuit models have been virtually ignored as an option for clinical diagnosis of atherosclerosis. This is in contrast to extensive academic research that has been conducted in this field . Among the reasons for this state of affairs is the mathematical complexity of the human circulatory system and the difficulty in obtaining anatomical and physiological information of the circulatory system in the living human, in sufficient detail, for accurate model implementation.

Another reason may be pinpointed by reviewing the trend of research in electrical modelling [Figure 1.3]. It is the hypothesis of this author, that this trend is directly responsible for the lack of a clinically applicable transmission line model. As a result of the increasing complexity of Forward models, it has become increasing difficult to compute the mathematical inverse of these models. Such research trends have resulted in the virtual abandonment of research into Inverse solutions. The inverse transmission line model (ITL) presented in this thesis, attempts to provide a starting point in shifting this trend.

A prerequisite for clinical application of any electrical circuit model (i.e. for diagnosis) is that a *unique* inverse solution should exist for the model. However, modern electrical circuit representations of the human arterial system have been structured to make a unique inverse of the representative equations mathematically impossible. Restructuring of these equations with a clear understanding of the pre-requisites for 'invertability', is necessary before any inverse transmission line model (ITL) may be implemented.

Very little research exists into inverse models applicable to the diagnosis of lower limb atherosclerosis.

Instead of inverse models, the earliest quantitative clinical diagnostics were in the form of very simple empirical indices RI (1974) and PI (1974) calculated from the Doppler Ultrasound blood flow velocity waveform. A more recent index, the spectral broadening index (SBI), quantifies the spectral broadening effects of turbulent flow in the arteries [see Figure 1.4: Mathematical Indices].

Principle Component Analysis [Evans, 1992] is another mathematical technique that uses a pattern recognition technique to characterise arterial waveforms into their diseased and healthy states [Figure 1.4 : Waveform Pattern Recognition]. These techniques differ greatly from Electrical Modelling techniques because they ignore the underlying physiological mechanisms .

The Impulse Response Model [Skidmore, 1979] was the first inverse electrical *lumped circuit* model. This simplified model adopted the approach of using 'lumped circuits' rather than more accurate transmission lines, as this allowed the model to be mathematically inverted. However it proved to be little improvement on earlier mathematical indices [Hoskins , 1990] [Figure 1.4 : Impulse Response]

A theoretical transfer function based model, which makes use of impedance plethysmography [Semnani & Smith , 1987], may be used to characterise an arterial segment (between two measurement sites). This technique represents the first published theoretical attempt at finding an inverse solution to the electrical transmission line equations. It attempts to bypass the problem of the large number of unknowns in a transmission line model, by dividing the arterial system into a number of segments , each of which is analysed separately. This method requires multiple readings at different points in an arterial tree by impedance plethysmography [Figure 1.4 : Transfer Function] . Another transfer function technique has also been implemented in the study of the normal upper limb (brachial to digits) arterial system [Mainardi et al, 1996] using Doppler Ultrasound and a Finger Pressure transducer.

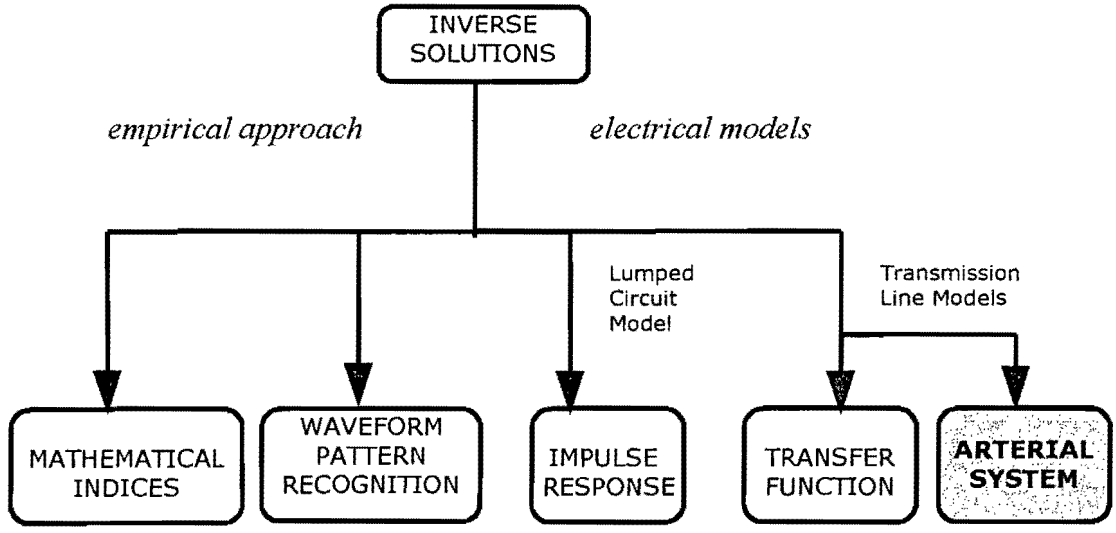

Figure 1.4 : Different types of Inverse Solutions

As illustrated in Figure 1.3, the Inverse Transmission Line (ITL) model bridges the gap between 'state of the art' forward transmission line models and simpler clinical models. It differs from the Transfer Function technique [Semnani & Smith , 1987] in that it includes the entire arterial system and requires measurement of arterial pressure and flow only at a single point . The emphasis of the ITL model is on waveform-fitting rather than on the use of a transfer function, and it's technical implementation makes use of arterial tonometry and Doppler ultrasound.

It's similarity with the Transfer Function model is that both of these techniques attempt to determine, via different methods, an inverse transmission line solution . Both of these techniques may be combined, in future research studies, for the purpose of arterial diagnosis.

CHAPTER 2
A MODEL OF THE NORMAL CARDIOVASCULAR SYSTEM

The human arterial system consists of a large number of interconnecting arteries of varying dimensions and wall properties. In order to develop an accurate model of the system, estimates of these dimensions and wall properties are necessary. In the Forward Model described in this thesis, the physical dimensions and static elastic moduli (Young's Moduli) of 128 discrete arterial segments were obtained from the literature [Avolio , 1980]. Avolio's data represented a modified version of data presented by [Westerhof et al ,1969] which improved the representation of the upper limb (arm) and carotid (head) regions. This data represents the arterial system of a "Physiologically Normal Male Subject" with a height of 1.75cm and a mass of 75kg [Westerhof et al , 1969].

In order to set up the vascular model each of the arteries was represented by a compliant walled elastic tube. The arterial system was divided into a series of uniform elastic tubes which were then connected together to represent the branching structure of the human systemic arterial system [Figure 2.2 - 2.3]. The dimensions of an individual tube correspond to the dimensions of the specific segment of artery that the tube represents.

2.1 ARTERIAL BLOOD

Human blood consists of plasma (colloidal suspension of proteins in an electrolyte solution) with a suspension of cells (98% erythrocytes, 2% platelets and leukocytes). The ratio of cells to the total blood volume, referred to as the haematocrit, normally ranges from 0.36 to 0.46 ie. approximately 36%-46% of the blood volume consists of cells. Blood is not a homogenous liquid, since the cellular component of blood tends to be lower near the walls of blood vessels. The cellular component of blood results in non-Newtonian fluid properties. The viscosity (μ) of blood varies with haemotocrit [Nichols & O'Rourke , 1990]. Under a range of conditions (eg. anemia, polycythemia) the blood viscosity in a subject may vary from 0.02 Poise to 0.07 Poise [LaCourse et al, 1986]. A normal value of 0.04 Poise was chosen for this simulation. Blood density (ρ) was assumed to be 1.05 g/cm^3.

2.2 LEFT VENTRICLE

The left ventricle of the heart provides the input to the systemic arterial system via the ascending aorta . A time domain volume flow rate (ml/s) waveform was used to represent the flow from the left ventricle [Figure 2.1]. This also corresponds to the flow waveform measured at the aortic root.

Figure 2.1 :
Aortic Volume Flow Rate waveform which was used as a basis for the input to the arterial model.

(diagram adapted from Milnor 1980 and Karamanoglu et al 1994)

The Matlab function "heart.m" in APPENDIX 3 was used to approximate this waveform.

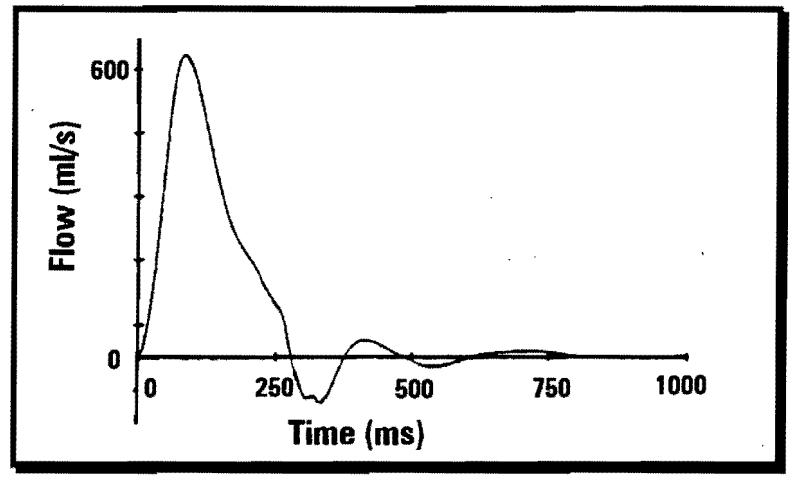

The time duration of this input waveform was adjusted according to a chosen heart rate (eg 75 beats per minute) by adjusting the length of the diastolic segment .The 'Fast Fourier Transform' (FFT) was used to calculate the frequency domain representation of this waveform, which was used as the input to the arterial model. Note that the Forward Model performs all analyses in the frequency domain.

2.3 VASCULAR GEOMETRY OF THE ARTERIAL SYSTEM

In modelling the vascular branching structure, only the geometry of the large and medium sized arteries have been included. The most detailed published arterial geometry, which includes sufficient data (experimental and estimated) to allow for computer simulation, was used for this purpose [Westerhof, 1969; Avolio, 1980]. This geometric structure corresponded closely to the accepted structure of the arterial tree as represented in most textbooks on human anatomy and physiology [Griffiths, 1981; Moore , 1985].

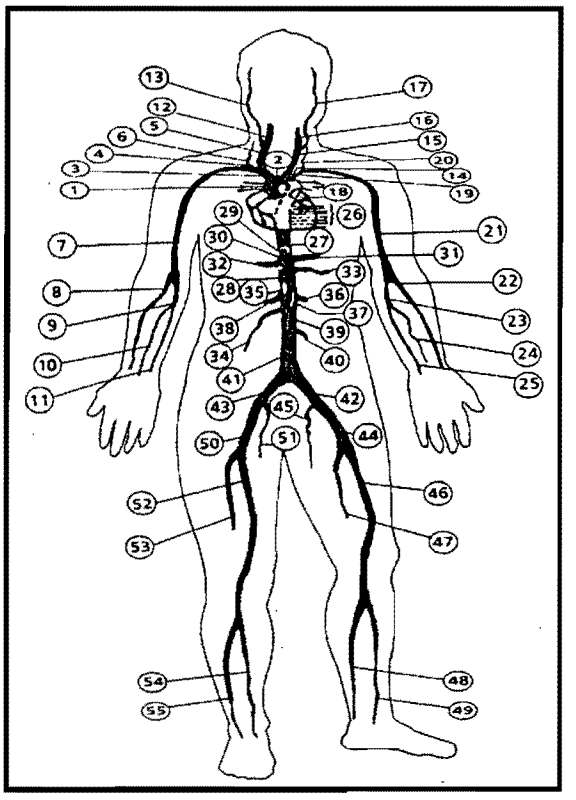

Figure 2.2 A model of the human arterial system (redrawn from Stergiopulos et al, 1992)

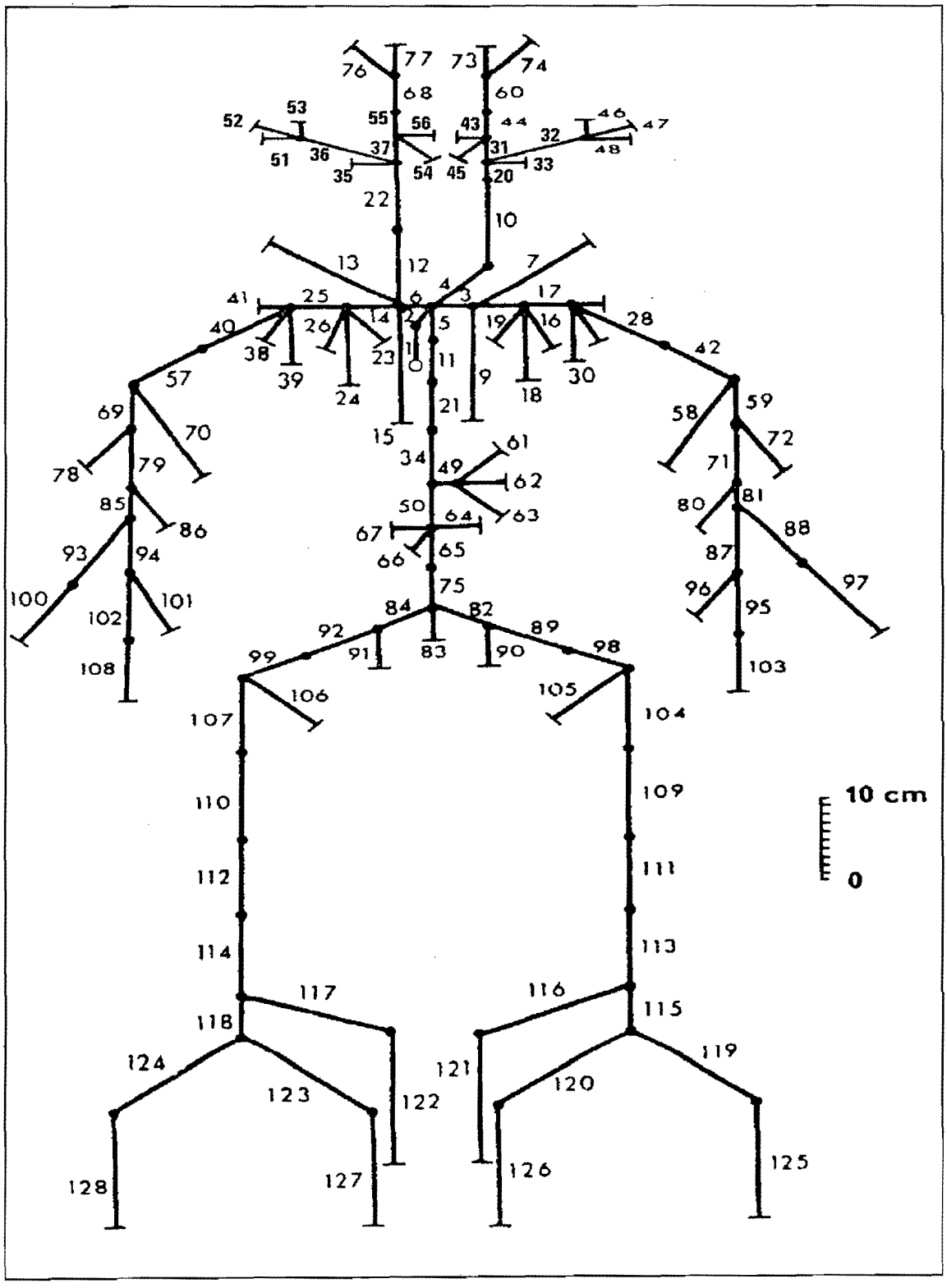

Figure 2.3 : Schematic model of the human arterial tree using 128 discrete tubes (redrawn, with minor numbering corrections, from Avolio , 1980)

2.4 VASCULAR DIMENSIONS AND ELASTIC MODULI

The arterial wall consists of a combination of rigid collagen fibres, compliant elastin fibres and smooth muscle cells (which are able to adjust vascular 'tone'). In the healthy state the aorta maintains diastolic blood pressure because of its large compliance . The radius of the aorta is not constant along its length, but tapers from its largest value in the ascending aorta, to its smallest diameter in the abdominal aorta at the iliac bifircation . This is referred to as *radial tapering*.

Radial tapering occurs to a smaller extent, in 'daughter' arteries that branch off from the 'parent' aorta. In the vascular tree the radii of these 'daughter' vessels are smaller than the radius of the parent vessel. Radial tapering was modelled by dividing an artery into a series of segments, with decreasing radii.

The medium-sized arteries that branch out from the aorta supply various regions of the body. Medium sized arteries also contain relatively more smooth muscle than the aorta, and are therefore less compliant. This is referred to as *'elastic taper'*. The presence of smooth muscle fibres also allows the radii and elasticities of these arteries to be varied under different physiological states.

In this physiological model, the Static Young's modulus of Elasticity was approximated as $4*10^6$ dyne/cm^2 . Further down the arterial tree this Elastic modulus was increased to $8*10^6$ dyne/cm^2 (eg superficial femoral artery, segments 104 and 107 in Figure 2.3 and Table 2.3, [Avolio 1980]) and to $16*10^6$ dyne/cm^2 (in the internal iliac artery , segments 90 and 91 in Figure 2.3 and Table 2.3) in the most distal branches. In reality, the true elastic behaviour of an arterial segment is frequency dependent, and is also influenced by blood pressure . The dynamic Young's Modulus remains virtually constant from 2Hz upwards [Nichols & O'Rourke , 1990].

For the purposes of this model the Static Young's Modulus was also used for harmonic analysis. This was done to reduce the number of model parameters. Once a working clinical version of the Inverse Model has been implemented, additional

mathematical features such as the dynamic Young's Modulus may be used, provided they do not compromise the mathematical conditions for a unique inverse solution. The viscous component of blood is represented by it's Poiseuille resistance [Figure1.1 and Equation 1.5]. This resistance is only theoretically valid for steady flow with a parabolic velocity profile. Arterial blood flow is however pulsatile. Under stenotic disease conditions , turbulence also increases. Therefore the use of the Poiseuille resistance only approximates the conditions that exist in an artery. It does however, serve as a useful, and simple approximation.

2.5 ARTERIAL PERIPHERAL RESISTANCE AND IMPEDANCE

Arterioles and capillaries are present at the junction between the arterial and the venous systems. The vascular beds are situated, in this physiological model, at the distal end of the terminal arteries . These vessels have small physical dimensions and (in the healthy state) provide the greatest hydraulic resistance to flow. The dimensions of the arterioles are not constant, but are physiologically regulated to provide for the dynamic needs of the different arterial beds (eg. increasing blood flow to the muscles in response to exercise).

A simple resistor is used to DC model these terminal vessels. Its resistance is equal to the ratio of mean arterial pressure to volume flow rate . No detailed published data on terminal resistance (mean pressure / mean flow) has been located, even in papers that have described the arterial system in detail [Avolio , 1980], [Westerhof et al, 1969] . Mean pressure is relatively constant in the larger arteries, because most of the arterial pressure is lost across the large resistance of the arterioles and capillaries of the vascular beds (terminal impedance). A mean arterial pressure of 100mm Hg was therefore assumed for all the large and medium sized arteries.

The mean peripheral resistance (mean pressure / mean flow) of the arterial model therefore depends wholly on the estimates of volume flow rates in the various arterial subsystems. Volume flow rates have been estimated using a variety of data from Physiological textbooks. Where no regional flow data was available, this data was approximated (eg. upper limbs in Table 2.1).

Head and Upper Extremities :	**25%**	[Corey and Wemple, 1975]
Brain	15%	[Millar, 1977]
rest of Head	2%	*estimated* : 0.2* (25%-15%)
Upper Limbs	8%	*estimated* : 0.8* (25%-15%)
Abdomen	**55%**	[Corey and Wemple, 1975]
Liver (arterial)	6%	[Guyton, 1981]
Kidneys	22%	[Guyton, 1981]
rest of Abdomen	27%	*estimated* : 55%-6%-22%
Pelvis and Lower Extremities	**20%**	[Corey and Wemple, 1975]
Lower Limbs	18%	[Raines et al, 1974]
Inferior Mesenteric	2%	*estimated* : 20%-18%

Table 2.1 Estimates of percentage of total arterial flow in different regions

It should be noted that the percentage flow was estimated for a 'normal' healthy person under resting conditions. Actual flow percentages in an individual subject may vary due to body size and proportions, age, state of health or disease, and gender. In addition flow percentages are also altered after physical activity (increased blood flow to skeletal muscles) and after a meal (increased blood flow to the gastrointestinal organs).

The percentage flows to the 61 terminal branches of the 128 element model (Table 2.2) have been calculated using the estimates of Table 2.1, and the arterial model represented in Table 2.3 and Figure 2.3. Where no prior flow information existed, regional flow percentages were divided equally amongst the terminal branches.

	SEGMENT NUMBER			FLOW PERCENTAGES	
	COMMON	LEFT	RIGHT	REGIONAL % FLOW	SINGLE BRANCH % FLOW
HEAD & UPPER LIMBS				***25%***	
Brain int. carotid				*15%*	
*Lingual artery		43	56		15% / 8 = 1.875%
*Facial artery		45	54		15% / 8
*Superficial Temporal		73	77		15% / 8
*Maxillary artery		74	76		15% / 8
Rest of Head ext carotid				*2%*	
*Middle cerebral artery		46	53		2% / 8 = 0.25%
Cerebral artery		47	52		2% / 8
*Opthalmic artery		48	51		2% / 8
*Superior Thyroid artery		33	35		2% / 8
Upper Limbs				*8%*	
*Internal mammary		7	15		8% / 28 = 0.2857%
Vertebral		9	13		8% / 28
*Costo-cervical artery		16	26		8% / 28
*Suprascapular		18	24		8% / 28
*Thyrocervical		19	23		8% / 28
*Thoraco-acromial		27	41		8% / 28
*Circumflex scapular		29	39		8% / 28
*Subscapular		30	38		8% / 28
*Profunda brachi		58	70		8% / 28
*Superior ulnar collateral		72	78		8% / 28
*Inferior ulnar collateral		80	86		8% / 28
Interossea artery		96	101		8% / 28
Radial artery		97	100		8% / 28
Ulnar artery		103	108		8% / 28
ABDOMEN				***55%***	
Liver (arterial)				*6%*	
Hepatic artery	63				6%
Kidneys				*22%*	
Renal artery	64				22%
Rest of Abdomen				*27%*	
Gastric artery	61				27%/4 = 6.75%
Splenic artery	62				27%/4
Superior mesenteric	66				27%/4
Gastric artery	67				27%/4
PELVIS & LOWER LIMBS				***20%***	
Lower Limbs				*18%*	
*Internal iliac		90	91		9% / 2 = 4.5%
Profundis artery		105	106		9% /4 = 2.25%
Anterior tibial artery		125	128		9% / (4*3) = 0.75%
Posterior tibial artery		121	122		9% / (4*3) = 0.75%
*Peroneal artery		126	127		9% / (4*3) = 0.75%
Inferior Mesenteric				*2%*	
Inferior mesenteric	83				2%

Table 2.2 Estimates of the percentage of total arterial flow in the different terminal branches of the arterial model illustrated in Figure 2.3

2.6 VENOUS SYSTEM

The systemic venous system returns blood back to the heart. Venous pressures are much lower than arterial pressures. For the purposes of this analysis, the venous pressure was assumed to be 0 mm Hg. In the electrical equivalent model, the venous system was represented by the 'ground' or 'negative' return path connecting the ends of all the terminating impedances back to the negative terminal of the signal source (ie the heart). Chen et al [1997] has modelled the effect of including a venous system (with veins and valves) on the input impedance of an arterio-venous system. The effects of including a modelled venous system were found to only be significant in the very low frequency range (below 0.2 Hz).

2.7 FEEDBACK AND CONTROL IN THE ARTERIAL SYSTEM

The model described in this thesis represents an open loop control system. In reality, the cardiovascular system is a complex closed loop system in which multiple local and global feedback loops are present, in order to dynamically adjust for optimum physiological performance . A closed loop control system has not been included in the arterial model presented here. It is conceivable that future revisions of this model may include closed loop systems, such as have been implemented in a number of recently published forward models [Calvalcanti et al, 1995; Ursino, 1995].

		Left	Right	Length	Radius	Wall Thickness	E x 10^6	fo
				L(cm)	(cm)	(h cm)	dyn/cm	(Hz)
Ascending aorta	1			4	1.45	0.163	4	34.7
Aortic arch	2			2	1.12	0.132	4	16.7
Aortic arch	5			3.9	1.07	0.127	4	36.6
Thoracic aorta	11			5.2	1	0.12	4	27.6
Thoracic aorta	21			5.2	0.95	0.116	4	27.8
Thoracic aorta	34			5.2	0.95	0.116	4	27.8
Abdominal aorta	50			5.3	0.87	0.108	4	27.5
Abdominal aorta	65			5.3	0.57	0.08	4	29.3
Abdominal aorta	75			5.3	0.57	0.08	4	29.3
Coeliac artery	49			1	0.39	0.064	4	167.8
Gastric artery	61			7.1	0.18	0.045	4	29.2
Splenic artery	62			6.3	0.28	0.054	4	28.9
Hepatic artery	63			6.6	0.22	0.049	4	29.6
Renal artery	64			3.2	0.26	0.053	4	58.4
Superior mesenteric	66			5.9	0.43	0.069	4	28.1
Gastric artery	67			3.2	0.26	0.053	4	58.4
Inferior mesenteric	83			5	0.16	0.043	4	42.9
Common carotid (L)	4			8.9	0.37	0.063	4	19.2
Common carotid (L)	10			8.9	0.37	0.063	4	19.2
Common carotid (L)	20			3.1	0.37	0.063	4	55.1
Common carotid (R)	12			9.9	0.37	0.063	4	19.2
Common carotid (R)	22			8.9	0.37	0.063	4	19.2
Left subclavian artery	3			3.4	0.42	0.067	4	48.6
Brachiocephalic artery	6			3.4	0.62	0.086	4	45.4
Common iliac		82	84	5.8	0.52	0.076	4	27.3
External iliac		89	92	8.3	0.29	0.055	4	21.3
*Internal iliac		90	91	5	0.2	0.04	16	74.1
External iliac		98	99	6.1	0.27	0.053	4	30.1
Femoral artery		104	107	12.7	0.24	0.05	8	21.1
Profundis artery		105	106	12.6	0.23	0.049	16	30.3
Femoral artery		109	110	12.7	0.24	0.05	8	21.1
Popliteal artery		111	112	9.4	0.2	0.047	8	30.2
Popliteal artery		113	114	9.4	0.2	0.05	4	22
Anterior tibial artery		115	118	2.5	0.13	0.039	16	181.5
Anterior tibial artery		119	124	15	0.1	0.02	16	24.7
Anterior tibial artery		152	128	15	0.1	0.02	16	24.7
Posterior tibial artery		116	117	16.1	0.18	0.045	16	25.7
Posterior tibial artery		121	122	16.1	0.18	0.045	16	25.7
*Peroneal artery		120	123	15.9	0.13	0.039	16	28.5
*Peroneal artery		126	127	15.9	0.13	0.019	16	28.5
Internal carotid		31	37	5.9	0.18	0.045	8	49.6
External carotid		32	36	11.8	0.15	0.042	8	26.3
*Superior thyroid artery		33	35	4	0.07	0.02	8	78.3
*Lingual artery		43	56	3	0.1	0.03	8	106.9
Internal carotid		44	55	5.9	0.13	0.039	8	54.4
*Facial artery		45	54	4	0.1	0.03	16	113.4
*Middle cerebral artery		46	53	3	0.06	0.02	16	159.4

Table 2.3 : Anatomical Data for the human arterial tree synthesised with *128* elastic tube segments [Avolio, 1980]. (Note that segments 98 & 99 are referred to in this thesis as the Common Femoral artery rather than External Iliac). E = Static Young's Modulus. fo = cut-off frequency for each discrete segment.

		Left	Right	Length	Radius	Wall Thickness	E x 10^6	fo
				L(cm)	(cm)	(h cm)	dyn/cm	(Hz)
Cerebral artery		47	52	5.9	0.08	0.026	16	80
*Opthalmic artery		48	51	3	0.07	0.02	16	147.6
Internal Carotid		60	68	5.9	0.08	0.026	16	80
*Superficial Temporal		73	77	4	0.06	0.02	16	119.6
*Maxillary artery		74	76	5	0.07	0.02	16	88.6
*Internal mammary		7	15	15	0.1	0.03	8	21.4
Subclavian		8	14	6.8	0.4	0.066	4	24.7
Vertebral		9	13	14.8	0.19	0.045	8	19.2
*Costo-cervical artery		16	26	5	0.1	0.03	8	64.2
Axillary artery		17	25	6.1	0.35	0.062	4	28.2
*Suprascapular		18	24	10	0.2	0.052	8	29.9
*Thyrocervical		19	23	5	0.1	0.03	8	64.2
*Thoraco-acromial		27	41	3	0.15	0.035	16	133.4
Axillary artery		28	40	5.6	0.31	0.057	4	31.7
*Circumflex scapular		29	39	5	0.1	0.03	16	90.7
*Subscapular		30	38	8	0.15	0.035	16	50
Brachial artery		42	57	6.3	0.28	0.055	4	29.1
*Profunda brachi		58	70	15	0.15	0.035	8	18.9
Brachial artery		59	69	6.3	0.26	0.053	4	29.7
Brachial artery		71	79	6.3	0.25	0.052	4	29.9
*Superior ulnar collateral		72	78	5	0.07	0.02	16	88.6
*Inferior ulnar collateral		80	86	5	0.06	0.02	16	95.6
Brachial artery		81	85	4.6	0.24	0.05	4	41.1
Ulnar artery		87	94	6.7	0.21	0.049	8	42.2
Radial artery		88	93	11.7	0.16	0.043	8	25.9
Ulnar artery		95	102	8.5	0.19	0.462	8	33.9
Interossea artery		96	101	7.9	0.09	0.028	16	58.5
Radial artery		97	100	11.7	0.16	0.043	8	25.9
Ulnar artery		103	108	8.5	0.19	0.046	8	33.9

Table 2.3 ***continued*:** Anatomical Data for the human arterial tree synthesised with *128* elastic tube segments [Avolio, 1980]

CHAPTER 3
ELECTRICAL TRANSMISSION LINE MODELLING

The physiological model described in Chapter 2, may be converted into an equivalent electrical transmission line model. Each of the 128 model segments of Figure 2.3 were represented as a section of an electrical transmission line. Electrical circuit theory was then used to predict the voltage and current waveforms at specified points in the simulated arterial system using the approach described below.

3.1 TRANSMISSION LINE SEGMENT - MECHANICAL TUBE ANALOGY

At rest the human heart rate is fairly steady (5% beat to beat variation), which allows the arterial system to be approximated as a steady state system. This allows for the use of steady state transmission equations, rather than the more mathematically complex, transient form of the transmission line equations.

Consider a segment of an artery of unit length which is approximated by a compliant tube, and in turn represented by a unit length segment of an electrical transmission line (Figure 1.1).

The mechanical variables may be converted to their electrical equivalents of resistance , inductance, conductance and capacitance all expressed per unit length (ie the RLCG parameters). These electrical variables together with the physical length of the artery/tube/transmission line uniquely define the transmission line .

Further variables such as the transmission line characteristic impedance (Z_0) and the propagation constant (γ_0) may also be calculated from the RLCG parameters according to the equations below :

$$Z_0 = \sqrt{(R + j.\omega.L)/(G + j.\omega.C)} \qquad \text{[Equation 3.1]}$$

$$\gamma_0 = \sqrt{(R + j.\omega.L).(G + j.\omega.C)} \qquad \text{[Equation 3.2]}$$

These equations are defined for each discrete angular frequency ($\omega = 2\pi f$) , in a steady state system. In mathematical terms Z_0 and γ_0 are functions of the angular frequency and the electrical variables RLCG, which are in turn functions of the mechanical parameters (radius, wall thickness, Young's modulus).

3.2 MODELLING A SINGLE TRANSMISSION LINE SEGMENT

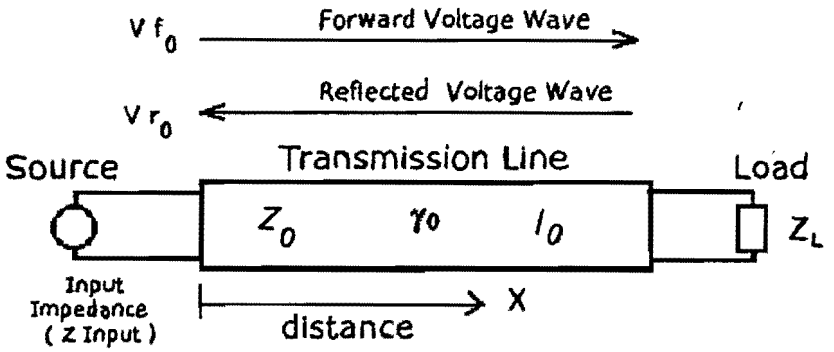

Figure 3.1 Single transmission segment, terminated by load Z ,

where :	Length	=	l_o,
	Characteristic Impedance	=	Z_o
	Propagation Constant	=	γ_o
	Forward Travelling Voltage at source end	=	Vfo
	Reverse Travelling Voltage at source end	=	Vro

If a transmission line segment is connected to a signal source and terminated by a load impedance Z_L (corresponding to the Hydraulic Impedance = Pressure / Flow) , the resulting forward and reverse travelling voltage and current waveforms (corresponding to the pressure and volume flow rate waveforms in the mechanical model) may be calculated.

The input impedance of this segment is the ratio of total voltage and total current at the source end [Equation 3.3].

$$Z_{input} = Z_0 \cdot \left[\frac{(Z_L - Z_0)e^{-\gamma_0 . l_0} + (Z_L + Z_0)e^{+\gamma_0 . l_0}}{(Z_0 - Z_L)e^{-\gamma_0 . l_0} + (Z_L + Z_0)e^{+\gamma_0 . l_0}} \right] \qquad \text{[Equation 3.3]}$$

The Fast Fourier Transform (FFT) of the aortic volume flow waveform (Figure 2.1), (analogous to the total current (*It*) at the source of the transmission line), is used as the input waveform. The corresponding total voltage (*Vt*) at the source is the product of total current and the input impedance.

$$Vt = It \cdot Z_{input} \qquad \text{[Equation 3.4]}$$

$$(Vro + Vfo) = (Ifo - Iro) \cdot Z_{input} \qquad \text{[Equation 3.5]}$$

The forward and reverse travelling voltage waves , at the input (assuming a source impedance matched to the characteristic impedance), are related by the voltage reflection coefficient at the input (ρ_{INPUT}).

$$Vro = Vfo. \left[\frac{Zinput - Z_0}{Zinput + Z_0} \right] = Vfo.\rho_{INPUT} \qquad \text{[Equation 3.6]}$$

The corresponding reflection coefficient at the load end (ρ_L) is defined by :

$$\rho_L = \frac{Z_L - Z_0}{Z_L + Z_0} \qquad \text{[Equation 3.7]}$$

Using Equation 3.6 and Equations 3.4- 3.5 gives :

$$Vfo = \frac{Vt}{(1 + \rho_{INPUT})} \qquad \text{[Equation 3.8]}$$

The input and load-end voltage reflection coefficients are related by :

$$\rho_{INPUT} = \rho_L . e^{-2.\gamma_0 . l_0} \qquad \text{[Equation 3.9]}$$

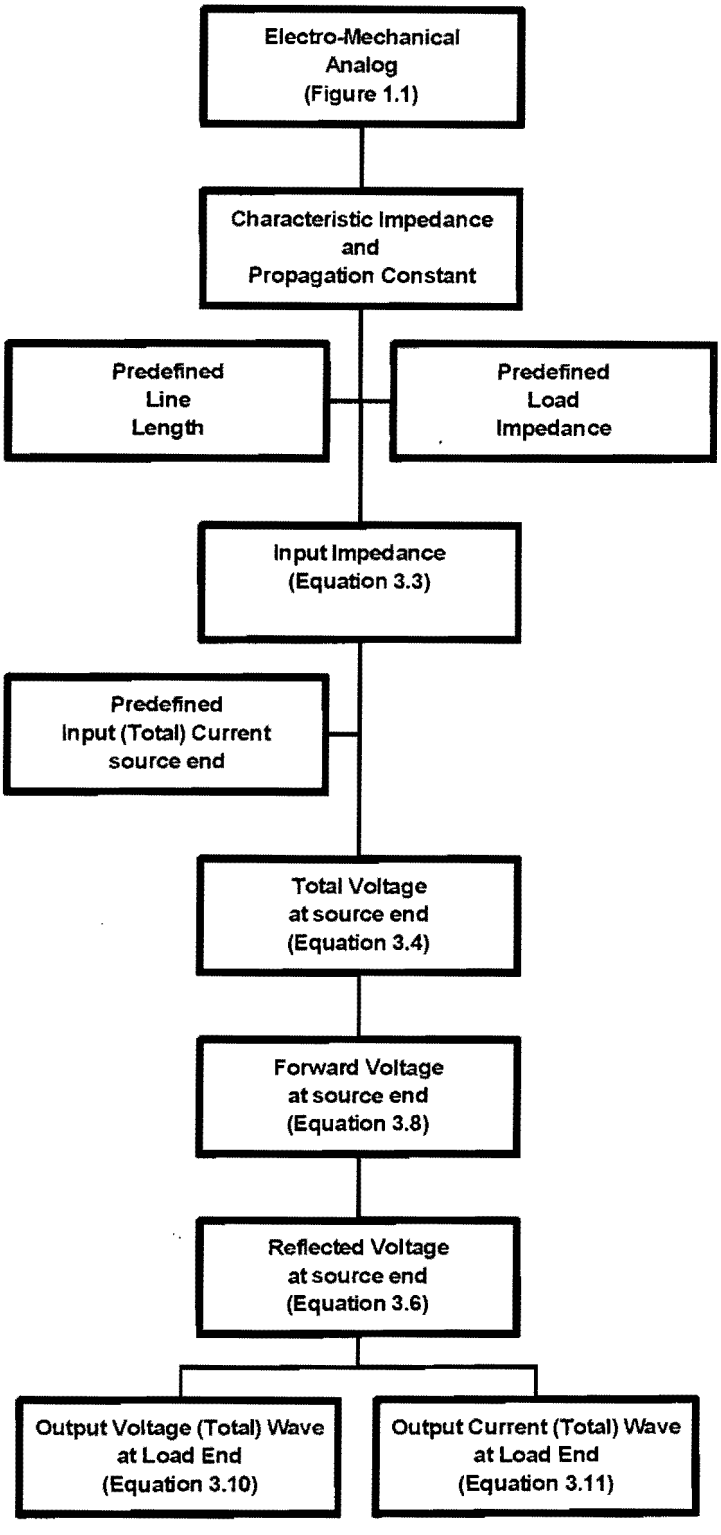

Figure 3.2 : Algorithm to solve for the load voltage and current of a single transmission line segment

3.3 MODELLING TWO TRANSMISSION LINE SEGMENTS IN SERIES :

Consider two transmission line segments in series, with a perfectly matched source generating a forward voltage (Vf1) . [Figure 3.3]

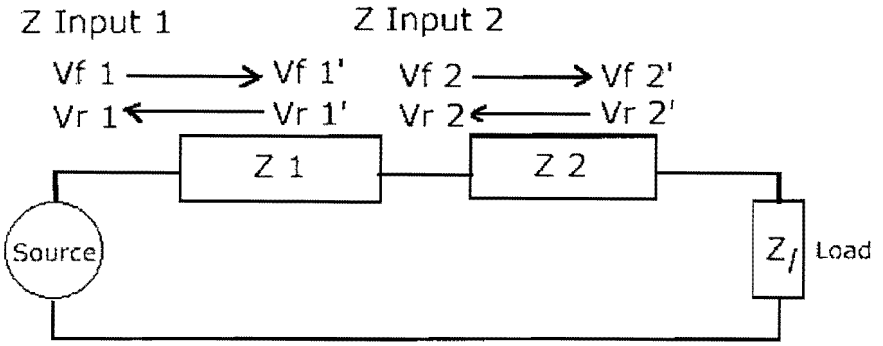

Figure 3.3 : Two series transmission line segments terminated by a Load Impedance Zl

The input impedance of line Z2 may be calculated using Equation 3.3 . This impedance (Zinput2) represents the steady state load at the load-end of line Z1. The input impedance of line Z1 may hence be calculated using the same procedure. By using the algorithm described in Figure 3.2, the voltage (and current) at the load end of line Z1 may be calculated. Hence, from a voltage analysis viewpoint, the problem of solving for the load voltage is reduced to the situation illustrated in Figure 3.4

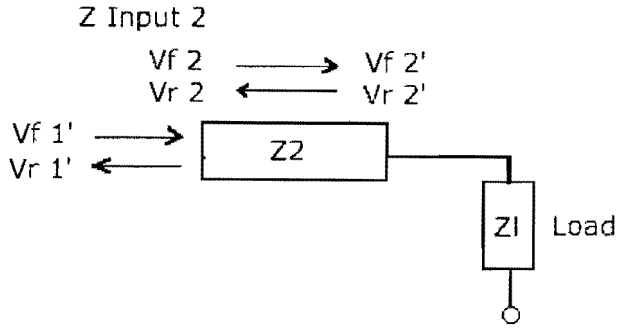

Figure 3.4 : Voltage analysis of second transmission segment (Z2) in a series

The method of equivalence of node voltages [LaCourse et al, 1986] allows Equations 3.12 and 3.13 to be defined at the junction of the two transmission line segments :

$$Vf_1` + Vr_1` - Vf_2 - Vr_2 = 0 \qquad \text{[Equation 3.12]}$$

$$Vf_1 . e^{-\gamma_1 l_1} + Vr_1 . e^{+\gamma_1 l_1} - Vf_2 - Vr_2 = 0 \qquad \text{[Equation 3.13]}$$

(In the equations above, the voltages with a superscript (e.g. $Vf_1`$) represents the load end voltages i.e. $Vf_1`$ represents the load end forward voltage of line 1, whilst Vf_1 represents the source end forward voltage of that same line.)

However, Vf_2 and Vr_2 are related by Equation 3.6, with the input impedance of line Z2 represented by Zinput2. Combining Equations 3.6. and 3.12 , allows Equation 3.12 to be rewritten as :

$$Vf_1` + Vr_1` - Vf_2 . \left[1 + \left[\frac{Zinput2 - Z_2}{Zinput2 + Z_2} \right] \right] = 0 \qquad \text{[Equation 3.14]}$$

The only unknown variable is Vf2. The problem (for line Z2) now reduces to the same situation outlined in Figure 3.1. Hence the load voltage may be calculated. The algorithm for solving for the load voltage and current of two series transmission lines is illustrated in Figure 3.5

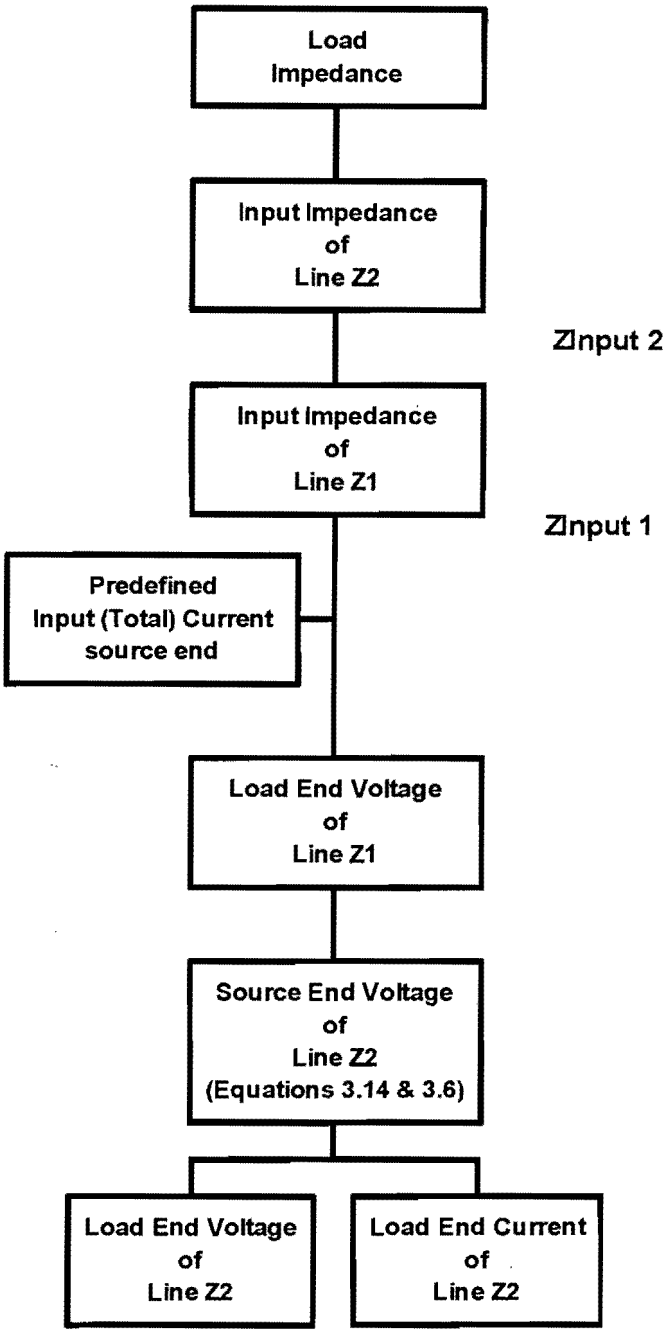

Figure 3.5 : Algorithm to solve for the load voltage and current of two transmission line segments in series

3.4 MODELLING A 'TREE' OF TRANSMISSION LINE SEGMENTS :

Now consider a number of transmission line blocks connected in a 'tree' [Figure 3.6]

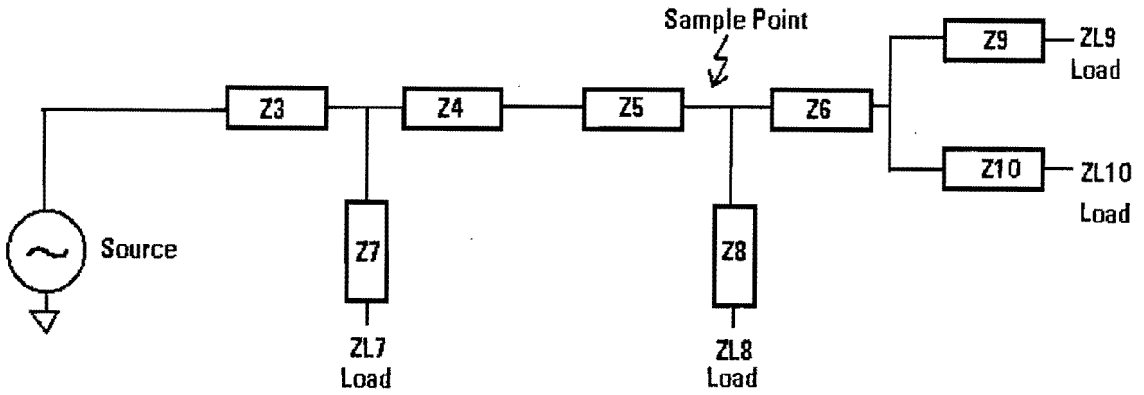

Figure 3.6 : Tree of transmission line segments terminated by Load Impedances ZL7, ZL8, ZL9, ZL10

The four terminal lines : Z7, Z8, Z9, Z10, are connected to their respective load impedances : ZL7, ZL8, ZL9, ZL10.

The first step in solving for the voltage at a specific point in the tree is to calculate the input impedance at the source-end of the tree by working from the load-ends towards the source-end. At bifurcations (e.g. the junctions Z4-Z7 and Z6-Z8 and Z9-Z10) the input impedance is the parallel combination of the input impedances of the individual branches.

Then the corresponding voltages are calculated by working from the source end towards the point at which the voltage is required (i.e. the 'sample' point). At bifurcations, the equivalence of node voltages [LaCourse et al, 1986] is still valid for the 'parent' segment (e.g. Z5) and each daughter segment (e.g. Z6 and Z8) individually. Electrical current waveforms may be calculated from the corresponding voltage waveforms at that point by using Equation 3.11

This general method allows for the calculation of voltages and currents at any point on the simulated transmission line system ('tree'), given an input function, and the load impedance at the end of each terminal segment.

A similar method described by LaCourse et al [1986] does not allow for the inclusion of unmatched load impedances at the ends of a transmission line tree. It therefore implies that the synthesis of voltages on a transmission line tree is independent of the terminal load supplied by that tree. However, the effect of load impedances has been included in the method of analysis (Figure 3.2 and 3.5) described thus far, by using Equations 3.3 and 3.6. to relate the load impedance to the forward and reverse travelling voltages.

3.5 MODELLING A LOAD IMPEDANCE

The load impedance (ZL) used at the terminal end of a transmission line is a lumped circuit. There are no suitable models that model both the DC and AC terminal load adequately. Terminal impedance modelling is still the subject of much research. Therefore the approach of using separate DC and AC models has been adopted with one circuit for DC (mean) and another for the AC (harmonics).

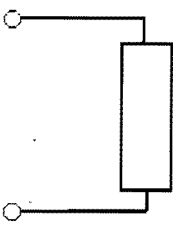

$$\text{mean Resistance} = \frac{\text{mean Pressure } (\text{dyn/cm}^2)}{\text{mean Flow } (\text{ml/s})}$$

Figure 3.7 Mean Load Resistance of terminal artery

For the analysis of the mean Flow and Pressure , a resistive termination is used (Figure 3.7). In this circuit the mean resistance is defined as the ratio of the mean Pressure to the mean Flow. Mean Pressure is assumed to be 1.334×10^5 dyn/cm^2 (=100mmHg) , and mean Flow in the various branch arteries of the arterial model (Figure 2.3) is determined from Table 2.2

For harmonic analysis, a different equivalent circuit is used. Using a simple resistive termination for harmonic analysis results in an 'un-physiological' mismatch between the load impedance and the characteristic impedance of an artery . Therefore, the indirect method adopted by Avolio [1980] is used.

A voltage reflection coefficient (ρ_L) is defined, for the first harmonic, at the load end of the transmission line. With the load end reflection coefficient, and line characteristic impedance known, the corresponding first harmonic load impedance may be calculated using Equation [3.15] below, and referring to Figure 3.8 and 3.1

$$Z_L = \left[\frac{1+\rho_L}{1-\rho_L}\right].Z_0 \qquad \text{[Equation 3.15]}$$

For the circuit described in Figure 3.8, Z_L is frequency dependent. Therefore, in order to determine the corresponding impedance at higher harmonics, the result of Equation 3.15 above must first be resolved into its shunt resistive (R_L) and capacitive (C_L) components. The load impedance equation is :

$$Z_L = \left[\frac{R_L}{1+j.\omega.R_L.C_L}\right] \qquad \text{[Equation 3.16]}$$

From Equation 3.16 R_L may be determined using the equation :

$$R_L = \frac{1}{\text{real component of}\left(\frac{1}{Z_L}\right)} \qquad \text{[Equation 3.17]}$$

Likewise, C_L may be determined using the equation :

$$C_L = \frac{imaginary \quad component \quad of\left(\frac{1}{Z_L}\right)}{\omega} \qquad \text{[Equation 3.18]}$$

Therefore once R_L and C_L have been determined, the load impedance Z_L may be calculated at any angular frequency using Equation 3.16.

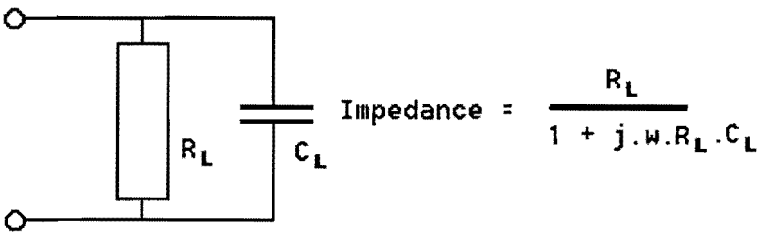

Figure 3.8 Harmonic Load Impedance model of terminal artery

The Simulink models and Matlab functions that are implemented and the associated theory described in this Chapter, are in Appendices 2-3.

CHAPTER 4

A NOVEL VISUAL IMPLEMENTATION OF THE FORWARD ARTERIAL TRANSMISSION LINE MODEL

The transmission line equations described in Chapter 3 have been incorporated into a custom-developed flexible, graphical forward model. Flexibility, in this context refers to the ease with which a model may be restructured. This is an important requirement for a model of a system as complex as the human arterial system. In addition, model flexibility is also important in a research tool as the end result of the modelling process is unknown.

For these reasons, a new graphical programming approach was developed. This method is a novel way of combining the ease of development using Matlab for Windows, with the flexibility of the graphical interface of Simulink. The result was a custom designed flow-chart-like 'Visual Matlab' language.

4.1 OVERVIEW OF COMPUTER SIMULATED MODEL

Simulink was used to develop a visual library for computer simulation of the forward arterial model. A section of compliant tube with a known diameter, wall thickness, Young's Modulus and length was implemented as a Simulink "Arterial Segment Block" [Figure 4.1] . The underlying transmission line equations for the tube sections are contained in visual form within each block [Figure 4.2]. These blocks were then connected together to form a 128 segment model of the human arterial system [Figure 4.3].

Simulink (which is a *graphical equation solver*) was not used to directly perform any equation solving. By setting the simulation parameters of Start Time = Stop Time , Simulink is 'tricked' into acting as a *graphical flow chart.* Matlab Function Blocks, Mux's , Constant, To Work Space, Input Port, and Output Port Blocks were used to synthesise the flow chart. Each Matlab Function block is a graphical implementation of a function with inputs and outputs. The relationship between input and output is determined by a custom written Matlab function. This approach results in the conversion of Matlab from a normal programming language, into a flow chart language. As such, it is very useful for the easy synthesis of a program from a flow chart or algorithm.

Simulink was used to define the branching structure of the arterial model; to define the physical dimensions and elastic properties of each of the 128 tube segments; and to define the algorithmic relationship between the underlying transmission line equations for each tube segment.

Matlab was used to define custom Matlab functions (or 'm files') that implemented all the relevant electro-mechanical analogies and transmission line equations. These Matlab functions were then 'linked' to the corresponding Simulink block.

The simulation of the model is controlled by a Matlab driver program. This driver program determines the input waveform (aortic flow waveform) to the Simulink model, and reads the output waveforms (peripheral blood flow and pressure waveforms). The relationship between the Matlab driver program and the Simulink component of the model is illustrated in Figure 4.4 .

4.2 ARTERIAL SEGMENT BLOCKS

The basic Simulink sub-unit is an ARTERIAL SEGMENT BLOCK. Each arterial segment block represents a section of uniform elastic tube with pre-defined mechanical parameters of radius, wall thickness / radius ratio, static Young's modulus, and length (see also Table 2.3). The arterial segment block has two inputs and two outputs (Figure 4.1).

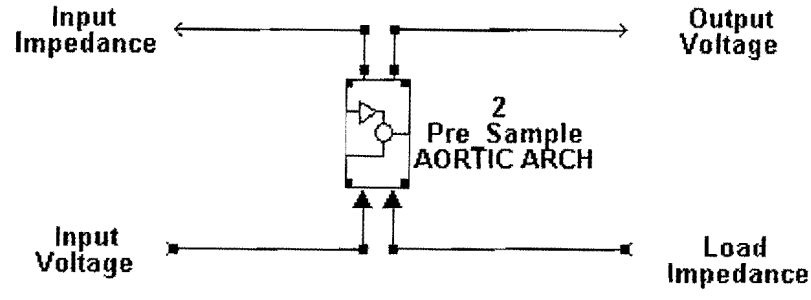

Figure 4.1 : SIMULINK ARTERIAL SEGMENT BLOCK representing an electrical transmission line segment model of a uniform elastic tube.

Each arterial segment block is a 'mask' for a set of flowchart-like algorithms, contained within it. This flowchart may be accessed by a 'double mouse click' over the arterial segment block.

The flowchart solves the steady state electrical transmission line equations, according to the method described by the algorithm in Figure 3.2. This approach has the advantage of illustrating the mathematical flowchart underlying the haemodynamics of a segment of artery. If required, the flowchart may be modified easily by adding or deleting function blocks, and by making or breaking links between different function blocks using a mouse. This allows a very complex mathematical process, to be adjusted very easily.

There are 5 different types of ***arterial segment blocks.*** The Graphics of these 5 blocks are in Appendix 2.1.1 - 2.1.2.

arterial input block	input segment i.e. ascending aorta.
arterial presample block	segments between *input block* and *arterial sample block* e.g. thoracic aorta
arterial sample block	segment where flow & pressure waveforms are sampled.
arterial distal block	simplified form of *presample block* which only transmits impedance information.
arterial terminal block	block representing a terminal artery e.g. peroneal

4.3 ARTERIAL BRANCHING BLOCKS

At branching sites (e.g. aorto-iliac bifurcation) in the arterial tree, an ***arterial branching block*** is used. Multiple branches are synthesised from an arterial bifurcation block. The type of arterial branching block depends on the number of daughter branches at branching site : (Appendix 2.2)

arterial bifurcation connector	2 daughter branches
arterial trifurcation connector	3 daughter branches
arterial quadfurcation connector	4 daughter branches

4.4 ARTERIAL SUBSYSTEM BLOCKS

Trees of interconnected arterial segment blocks may be grouped together and represented as a ***subsystem block*** . This allows for a compact graphical representation, but has no effect on the actual structure of the model. A number of subsystem blocks are defined in the original model. Simulink models of the various subsystem blocks are in Appendix 2.3.1 - 2.3.2.

left carotid	**subsystem**
right carotid	**subsystem**
left arm	**subsystem**
right arm	**subsystem**
left leg	**subsystem**
right leg	**subsystem**
coeliac artery	**subsystem**
renal, superior mesenteric, gastric	**subsystem**

Subsystem blocks may be included within subsystems e.g. the femero-distal subsystem block (representing the circulation distal to the right external iliac artery), within the right leg subsystem block (Appendix 2.3.2).

4.5 DETAIL WITHIN AN ARTERIAL SEGMENT BLOCK

The arterial segment blocks described in Chapter 4.2 contain a visual algorithm of the electrical analogue and transmission line equations. This visual algorithm [Figure 4.2] may be viewed or modified by a double mouse click on the arterial segment block [Figure 4.1].

Referring to Figure 4.2 , the Matlab function blocks call the respective Matlab function files that are defined within the function block. The 2 input and 2 output ports of Figure 4.2 correspond to the inputs and outputs of Figure 4.1

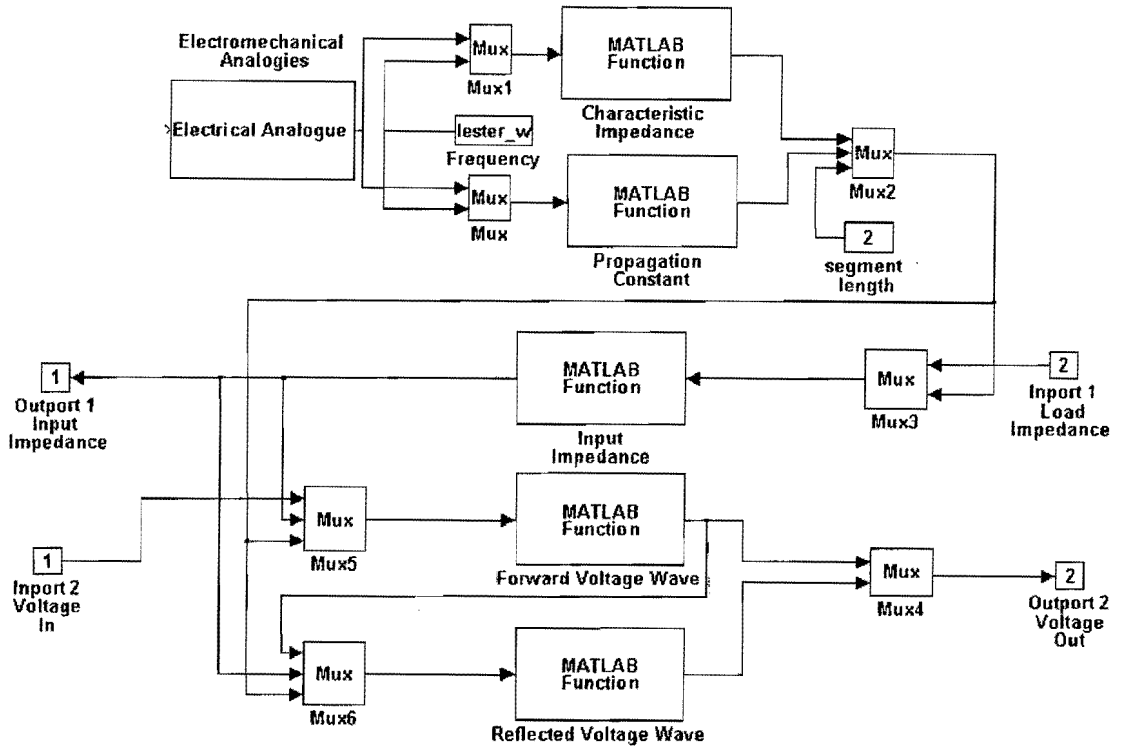

Figure 4.2 : Simulink System (flow chart) underlying the Arterial PreSample Segment block (figure 4.1). This flowchart is accessed by a double mouse click on the block illustrated in Figure 4.1

Multiplexors (MUX in Figure 4.2) are used to combine inputs into a single input vector , before feeding into a Matlab function block. This is necessary because a Simulink Matlab Function Block only allows a single vector input. The vector may have multiple elements representing different input variables.

Similarly, the output of a Simulink Matlab Function Block is a vector with multiple elements representing different output variables. Complex numbers are represented by two vector elements (i.e. real and imaginary parts), because Simulink 1.3c does not allow complex inputs to a Matlab function block. The input vector elements are converted into their complex form within the body of the Matlab function. A complex

output (e.g. characteristic impedance in Figure 4.2) is converted into a [real and imaginary] vector representation before being output as a single output vector (see programs in Appendix 3)

4.6 MATLAB FUNCTIONS CALLED BY ARTERIAL SEGMENT BLOCKS

The "MATLAB Function" blocks of Figure 4.2 are linked to custom written Matlab functions .These Matlab functions may be unmasked by a double mouse click on the corresponding MATLAB Function Block. The custom Matlab functions are listed below, with the corresponding programs in Appendix 3.1 – 3.11.

Electrical Analogue	*converts mechanical parameters into RLC electrical parameters*
Characteristic Impedance	*calculates the characteristic impedance of a segment*
Propagation Constant	*calculates the propagation constant of segment*
Input Impedance	*calculates the input impedance of a segment*
Forward Voltage Wave	*calculates the forward voltage at the load end of a segment*
Reflected Voltage Wave	*calculates the reverse voltage at the load end of a segment*
Arterial Bifurcation	*calculates equivalent impedance of two parallel impedances*
Forward and Reflected Current	*calculates forward and reflected current at the load end*
Peripheral Impedance	*calculates the load impedance of a terminal transmission line*

The implementation of arterial branching follows the procedure described in Chapter 3.4.

4.7 SUMMARY OF VISUAL FORWARD ARTERIAL MODEL

Using the Simulink blocks described thus far, a 128 segment model of the human arterial system corresponding to the arterial tree of Figure 2.3, and the arterial segment data presented in Table 2.3, has been synthesised (Figure 4.3). Analysis of the Simulink arterial model was carried out in the frequency domain. An Arterial Sample Block corresponding to the external iliac artery has been defined on the Right Leg of the model, by the inclusion of the ***Arterial Sample Block*** at segment 92. The outputs of this model are therefore the arterial flow rate (cm^3/s) and pressure waveforms from the external iliac artery, in man (Figure 4.3).

A Matlab Program (Appendix 3.12.2) converts the input function (Figure 2.1) into a frequency domain function by a Fast Fourier Transform (i.e. Matlab 'FFT' function) . The output time domain waveforms are synthesised by calculating the model outputs for it's mean value, and for each harmonic frequency (15 harmonics are analysed).

At each discrete frequency , the outputs are stored in a vector. At the completion of 16 simulations (i.e. DC and 15 harmonics) the time domain output waveforms are synthesised using the Inverse Fast Fourier Transform.(i.e. Matlab 'IFFT' function).

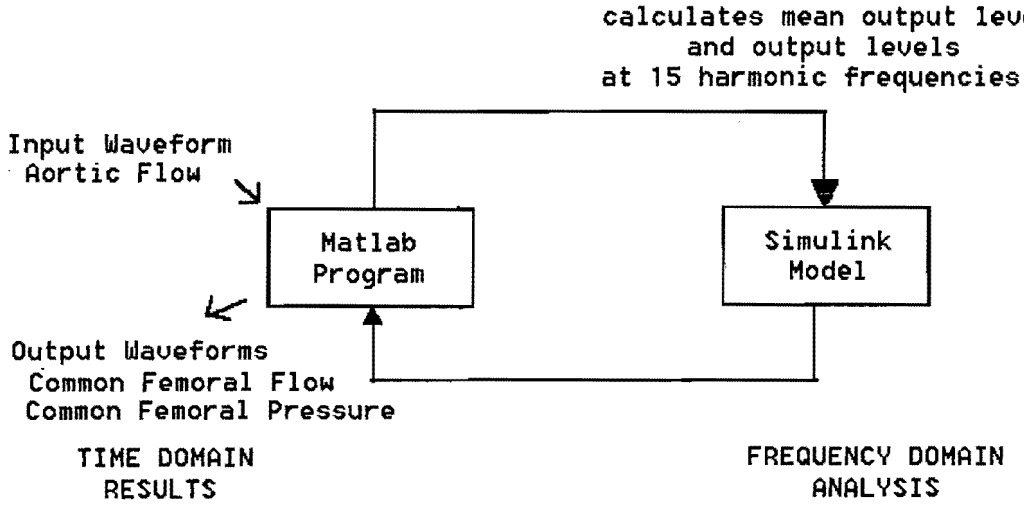

Figure 4.4 : Illustration of the interface between the Matlab driver program and the Simulink component of the arterial model. The Simulink component of the model is shown in greater detail in Figure 4.3 and the Matlab driver program for the Forward Model ('simavol.m') is shown in detail in Appendix 2.

The physiological data of Chapter 2, has been converted into a computer simulated (Chapter4) transmission line model (Chapter 3), by the use of a novel Matlab - Simulink

interfacing technique. The Simulink model (Figure 4.3) is ideally designed for arterial modelling studies. Arterial tree geometries may be easily modified. In addition, the underlying model equations may be modified according to any algorithm that the researcher may require.

CHAPTER 5

VALIDATION OF THE FORWARD MODEL UNDER NORMAL AND STENOTIC CONDITIONS

Validation of the Forward Arterial Model is a necessary intermediate process, before it may be implemented in its inverse form. This process was carried out in 3 steps :

5.1 Validation of transmission line equations
5.2 Validation of the equivalence of the forward model to other computer simulated models, and actual physiological data for the 'normal' subject
5.3 Validation of the ability of the forward model to simulate the effects of stenotic disease on haemodynamic waveforms.

5.1 VALIDATION OF TRANSMISSION LINE EQUATIONS

This is an important step that verifies that transmission line theory (Chapter 3) was correctly implemented in the computer simulation (Chapter 4). Two standard undergraduate textbooks on electrical transmission lines were used for this purpose [Plonus, 1978; Chipman ,1968] . By using the same data as was used in the worked examples within the texts, the results of computer simulations were compared to the results provided by the textbooks. These simple tests confirmed that the transmission line equations were correctly implemented in the computer simulated model.

5.2 VALIDATION OF THE 'NORMAL' FORWARD MODEL

Using a cardiac stroke volume of 60ml, a heart rate of 75 bpm, and the arterial data presented in Chapter 2, the 'normal' resting state of the human systemic arterial was simulated.

The results of the simulation were compared to data from the literature, in the following areas :

5.2.1 Input Impedance of the systemic arterial system
5.2.2 Blood Pressure and Blood Flow waveforms
5.2.3 Arterial Pulse Wave velocities

5.2.1 Arterial Input Impedance

The input impedance spectrum (at the aortic root) of the Simulink Forward Model was compared to input impedance graphs for 7 human subjects (averaged) , and the [Avolio, 1980] arterial model in Figure 5.1.

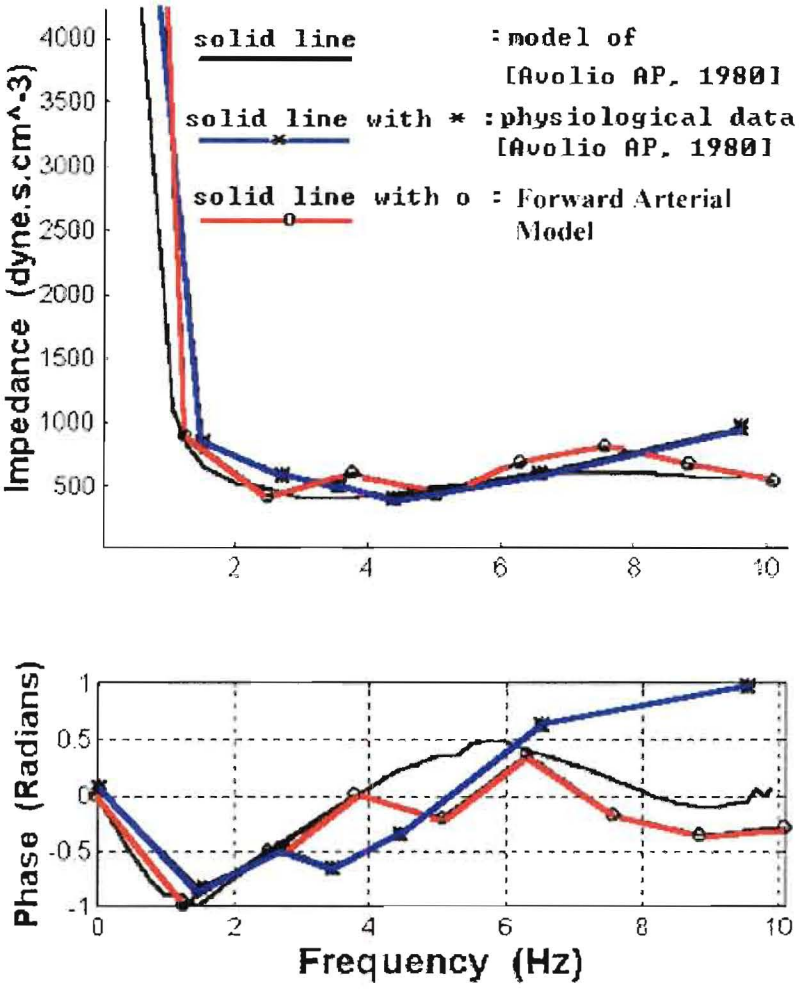

Figure 5.1 : The Input Impedance of the human systemic arterial system. The solid **red** line with circles "o" represents input impedance of the Forward Model presented in this thesis. The solid **blue** line with the star "*" represents clinical data. The solid line alone represents the computer simulated arterial model of Avolio [1980]. Note that the Forward Model DC Impedance was calculated using a mean pressure of 133 300 dynes/cm5, and a mean flow rate of 60ml/s = 9.1cm/s (in Segment 1 : Table 2.3). Equivalent DC values and mean flow velocities were unavailable for Avolio's data.

Before the data was superimposed, it was necessary to convert the impedance spectrum data from the Forward Model from units of dynes.s.cm^{-5} (with flow = volume flow rate) to the units of dynes.s.cm^{-3} (with flow = flow velocity). This was done by dividing the simulated aortic flow waveform by the area of the aortic root segment (π.r ^{2}) to convert it from volume flow rate (cm^3/s) to mean velocity (cm/s). The arterial impedance was then calculated as the ratio of pressure and flow velocity at each of the harmonics.

While the Forward Model uses the same arterial data and geometric structure (Figure 4.3, 2.3 and Table 2.3) as the [Avolio , 1980] model , it differs in four respects :

1. The Avolio model uses a nominal terminal (load) reflection coefficient of ρ_L = 0.8. For the Forward Model, a terminal voltage reflection coefficient of ρ_L = 0.2 (determined by trial and error) was used instead. This affected only the AC component of the terminal impedance spectrum (see Chapter 3.5) and resulted in 'better' haemodynamic waveforms, by damping out excessive oscillation.

2. The DC component of terminal impedance in the Forward Model was evaluated according to Tables 2.1 and 2.2. The [Avolio , 1980] model did not publish data for DC terminal impedance

3. [Avolio , 1980] modelled the effects of arterial wall viscoelasticity, and the non-linear frequency dependent variation of resistance and inductance (using Womersley's equations), compared to the simpler electromechanical approximations used by the Forward Model (Figure 1.1). When the Womersley equations were included in the Forward Model (see Appendix VI), it was found that the computation time increased significantly, whilst there was no significant change in the haemodynamic waveforms or the impedance spectrum. It was therefore concluded that the Womersley equations were not necessary for the initial development of the Inverse Model, although they may included in future more advanced versions.

4. The algorithm used within each arterial segment, also differs in the two models. The Forward model algorithm (Figure 4.2) allows for the resolution of voltage and current waveforms into their forward and reflected components, whilst the [Avolio , 1980] algorithm only evaluated total voltage and current waveforms.

As a result, the impedance waveforms, whilst similar (Figure 5.1), do have minor differences.

Other published studies of aortic input impedance are also similar to Figure 5.1 [O'Rourke & Avolio, 1980; Mills et al, 1970; Snyder et al, 1968; Chen et al, 1997].

5.2.2 BLOOD PRESSURE AND BLOOD FLOW WAVEFORMS

Blood Pressure waveforms at specified points in the human arterial tree, corresponding to the model presented in Figure 4.3, are illustrated in Figure 5.2

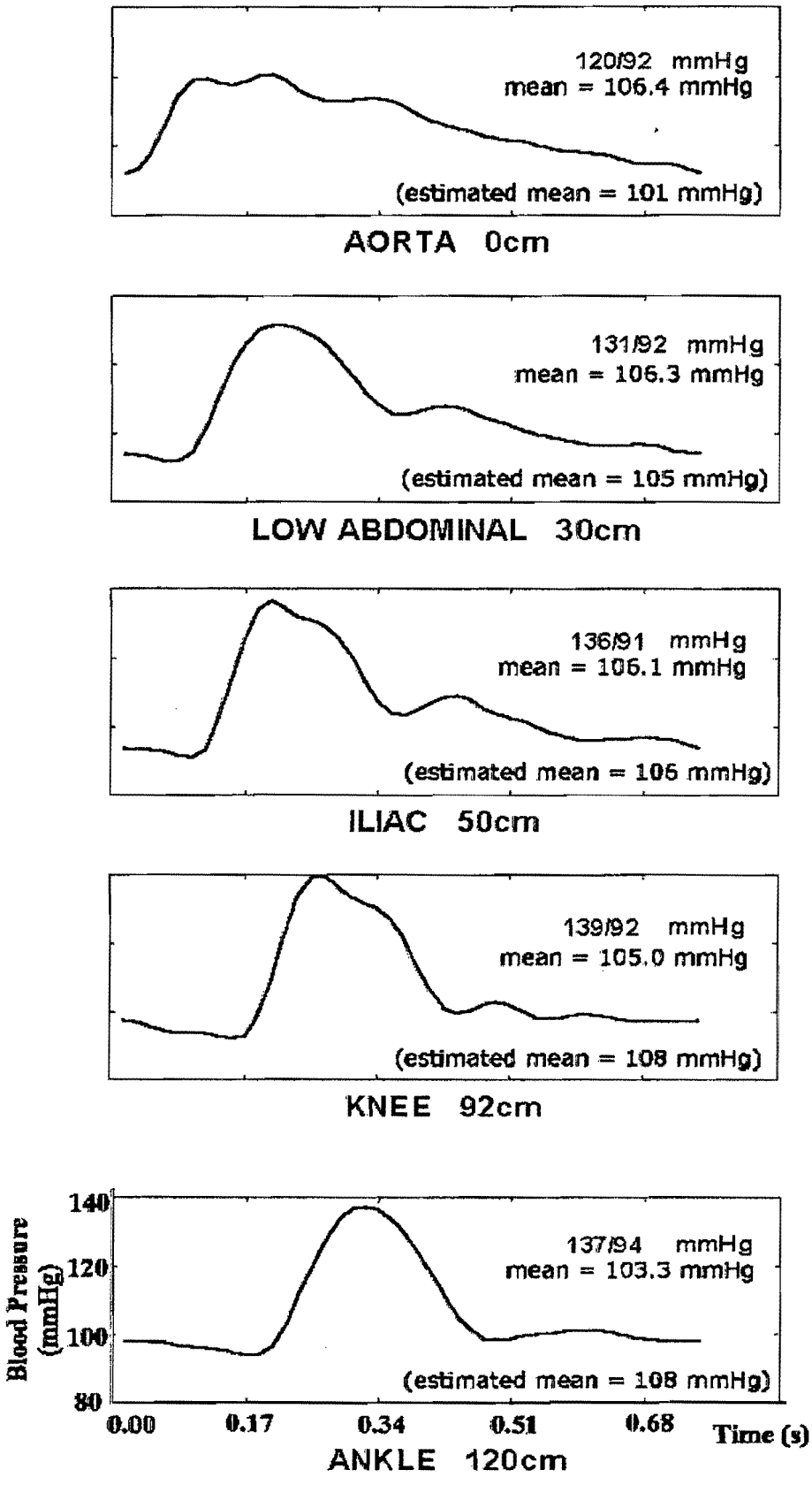

Figure 5.2 : Computer Simulated Blood Pressure waveforms, generated using the model from Figure 4.3. Note estimated mean refers to the mean Blood Pressure using the clinical formula (mean = (Systolic+2*Diastolic)/3). The distances in the graphs are downstream-relative to the aortic valve.

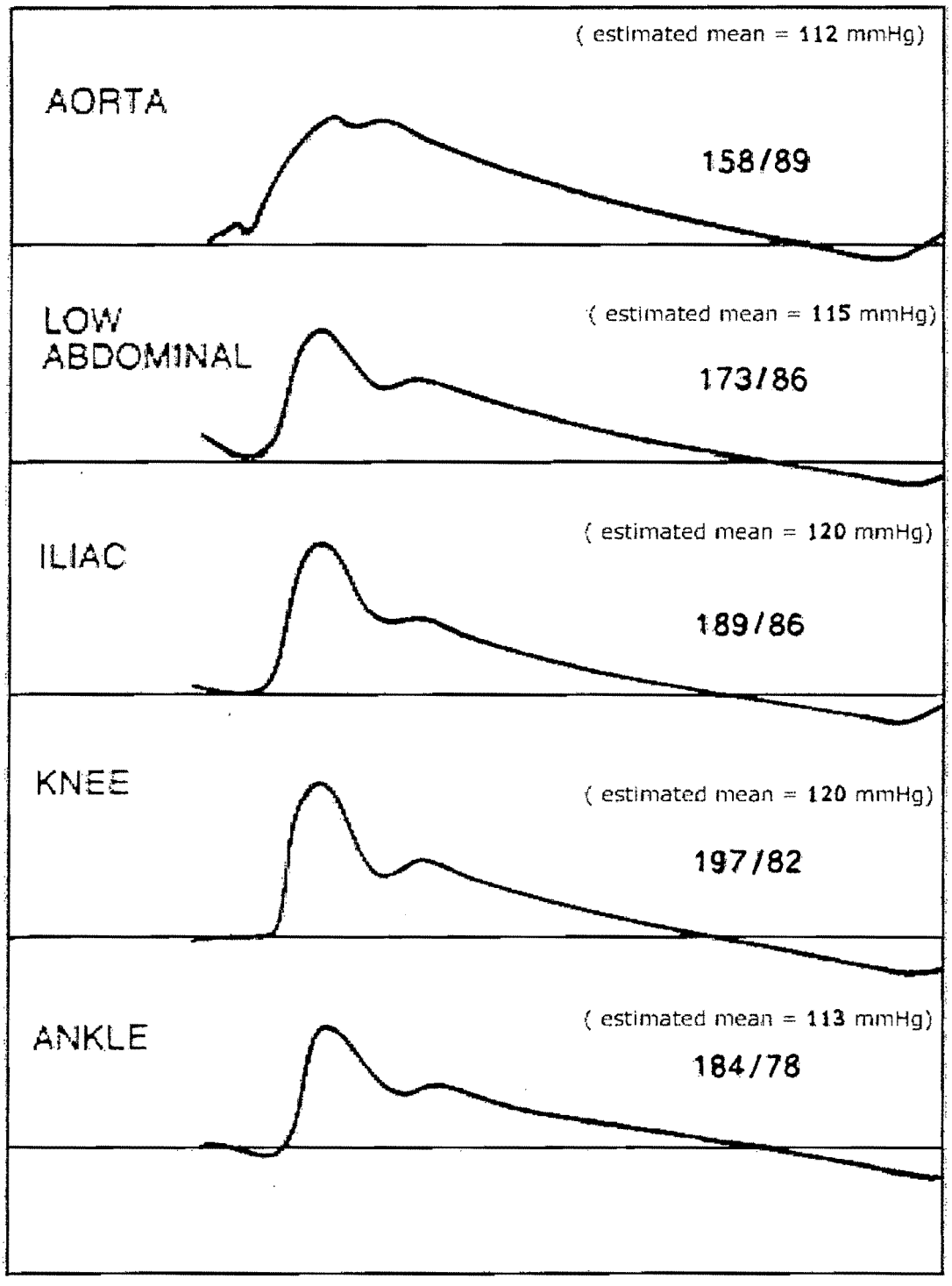

Figure 5.3: Canine Blood Pressure Waveforms from a 12.6kg dog [Remington & O'Brien , 1970]. The original paper provided only waveform shapes as well as systolic and diastolic pressures, but with no values on the axes. The mean pressures in this figure were estimated by this author using the same formula as used in Figure 5.2

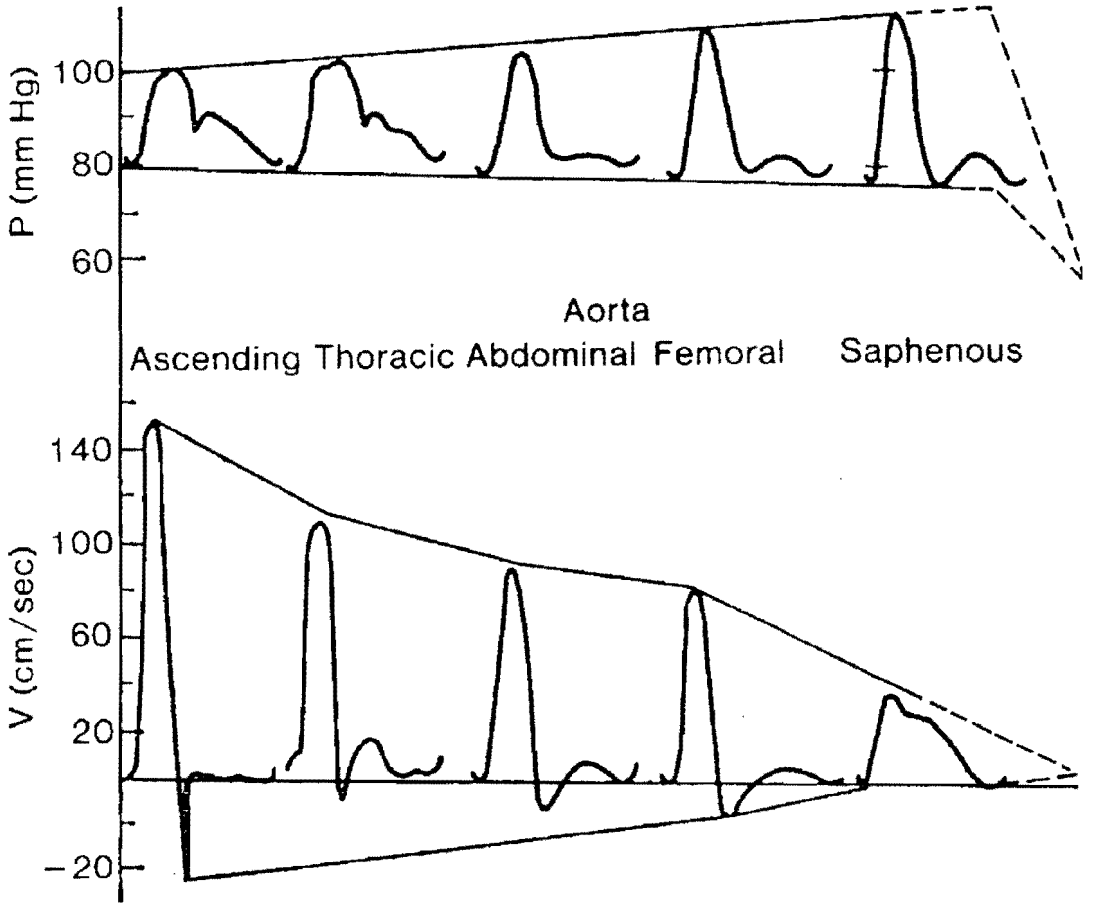

Figure 5.4: Canine Blood Pressure and Flow Waveforms [Nichols & O'Rourke , 1990]

Canine arterial waveforms are reproduced in a number of research papers because they are considered to be representative of human arterial waveform trends, whilst being easier to acquire clinically. The Simulated human waveforms of Figure 5.2 may be compared with equivalent canine data [Remington & O'Brien, 1970] in Figure 5.3 , and [Nichols & O'Rourke, 1990] in Figure 5.4. as well as with known characteristics of the human arterial system. Mean pressure decreases slightly whilst Diastolic Pressure changes very little along the simulated arterial tree, as is the case physiologically. Systolic Pressure increases towards the periphery (despite the slight decrease in mean Pressure), which also agrees with known physiology. Note that there is a difference between the actual mean pressure and the estimated mean pressure . The actual mean pressure [available in Figure 5.2 only] clearly illustrates the well established trend of a slight decrease in mean pressure towards the periphery. The estimated mean pressure [Figure 5.2 – 5.3] however does not illustrate this trend because it is only a crude mathematical approximation of the true mean pressure. Pulse propagation delays are apparent in the computer simulated (Figure 5.2), as well as the canine waveforms (Figure 5.3). The depth of

the dicrotic notch of the computer simulated pressure waveforms increases towards the periphery. This is also observed in the canine waveforms.

The main discrepancy between the waveforms, was the pressure level of the dicrotic notch. In [Nichols & O'Rourke , 1990] canine data (Figure 5.4), the notch reaches the diastolic pressure level from the level of the abdominal aorta . The computer simulated data, the dicrotic notch approaches the diastolic pressure level at the level of ankle. Canine data from [Remington & O'Brien , 1970] (Figure 5.3) clearly illustrates a much smaller dicrotic notch at the level of the ankle (note that Figure 5.3 does not unambiguously indicate the level of diastolic pressure. It was assumed that horizontal line represented the diastolic pressure.)

Specific modelling of the *femoral* haemodynamics has been described in a dog [Guha, 1970] and in a human [Raines et al, 1970]. Comparison between Forward Model external iliac waveforms in Figure 5.6 and the measured waveforms of a 12.6kg dog , in Figure 5.7, show a marked similarity.

Whilst Raines et al [1970] models the *human* leg (Figure 5.5), no actual patient data was supplied for comparison (i.e. only computer simulated data was provided). The results of his simulation, whilst showing a typical normal waveform for the flow pulse, illustrate an atypical pressure waveform, with the dicrotic notch being very close to diastolic pressure. The Raines et al [1970] model, whilst reasonably modelling the flow waveforms, does not model the normal pressure waveform adequately.

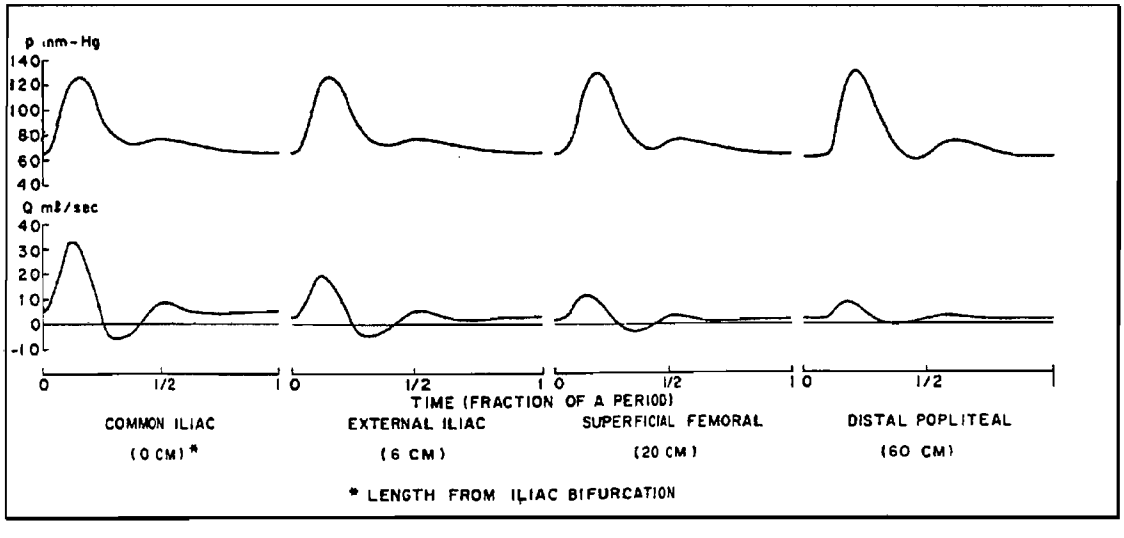

Figure 5.5: Femoral Pressure and Flow Waveforms from an Arterial Model [Raines et al, 1970]

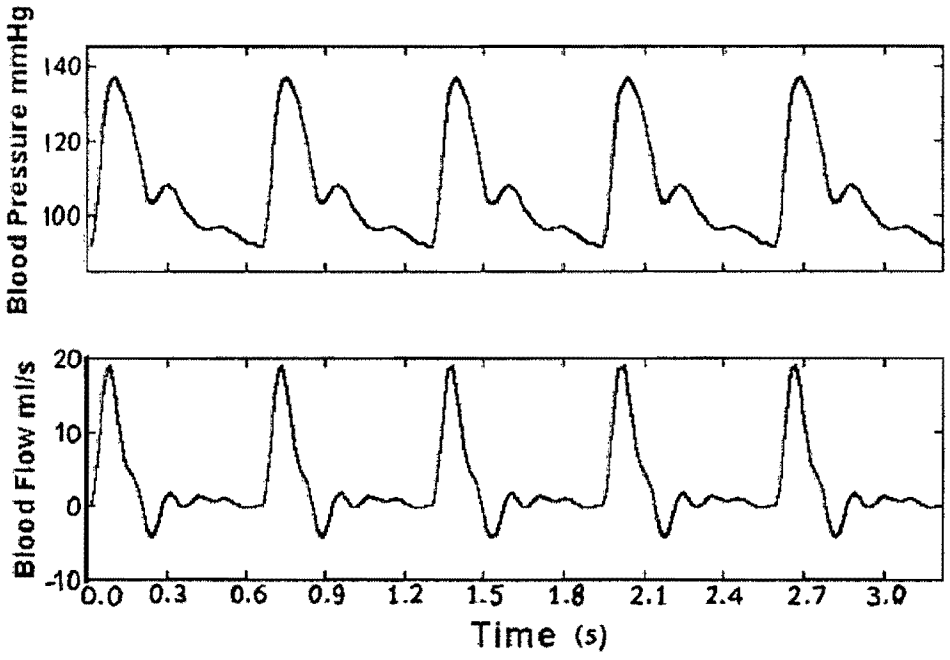

Figure 5.6: External Iliac Pressure and Flow Waveforms from the Forward Model (model illustrated in Figure 4.3)

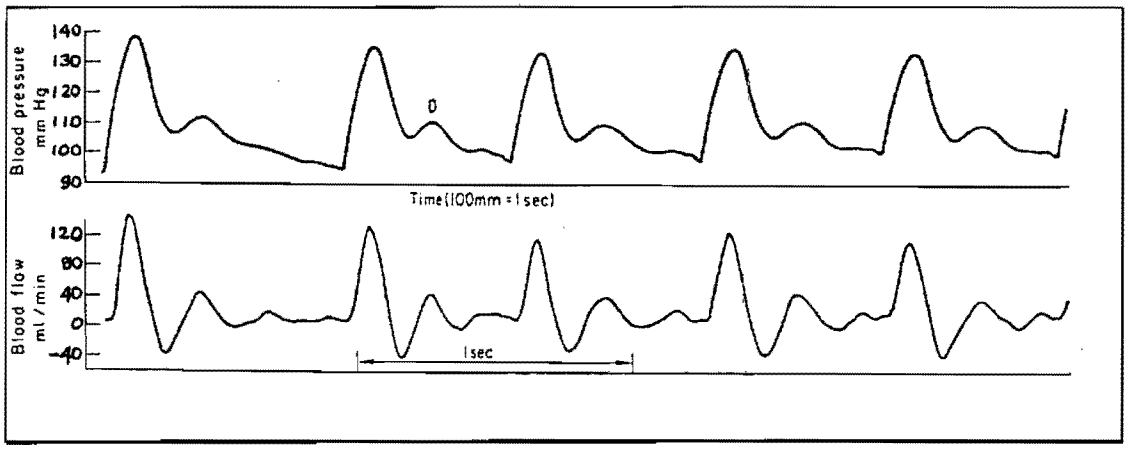

Figure 5.7: Experimental Femoral Pressure and Flow recordings from a 12.6kg dog [Guha , 1970]

5.2.3 ARTERIAL PULSE WAVE VELOCITIES

Pulse wave velocities in the Forward Model were calculated using transmission line Equation 5.1.

$$c = \frac{\omega}{\beta} \qquad \text{[Equation 5.1]}$$

β is the imaginary component of the propagation constant ($\gamma = \alpha + j\beta$) and represents the phase delay of a travelling wave. In the electrical analogue, this value has been shown to be equivalent to the wave velocity as calculated from the Moens- Korteweg [Equation 7.1]

The corresponding time delay is calculated by dividing the wave velocity, by the distance travelled (i.e. arterial segment length)

$$t_{delay} = \frac{c}{length} \qquad \text{[Equation 5.2]}$$

Computer simulated wave velocities (note that this is the true wave speed which has very small frequency dependence under the 'normal' physiological conditions modelled, in contrast to the apparent wave velocity which has a much larger frequency dependency), and time delays, from the Simulink Forward Model of Figure 4.3, are shown in Table 5.1

ARTERY		WAVE SPEED cm/s	TIME DELAY ms
ascending aorta	1*	494	8.1
aortic arch	2	504	4
aortic arch	5	505	7.7
thoracic aorta	11	508	10.2
thoracic aorta	21	511	10.2
thoracic aorta	34	511	10.2
abdominal aorta	50	515	10.3
abdominal aorta	65	542	9.8
abdominal aorta	75	542	9.8
common iliac	84	551	10.5
femoral/ext iliac	92	608	13.6
* number refers to Figure 2.3 and Table 2.3			

Table 5.1 : Computer Simulated Forward Model wave velocities and delay times

ARTERY	SUBJECT	METHOD	WAVE SPEED cm/s	REFERENCE
Ascending Aorta	man	H	520	(Luchsinger et al, 1964)
	man	W	440	(Latham et al, 1985)
Thoracic Aorta	man	H	400	(Luchsinger et al, 1964)
	man	W	550 - 650	(Wezler & Boger, 1939)
	man	V,E	580	(Learoyd & Talyor,1966)
	man	W	520	(Latham et al, 1985)
Iliac	man	V,E	700	(Learoyd & Talyor,1966)
	man	W	800	(Latham et al, 1985)
Femoral	man	W	800	(Kapal et al, 1951)
	man	V,E	1800	(Learoyd & Talyor,1968)
note : Method : H = averaged higher frequency harmonics, W = wavefront or foot-to-foot, V = in vitro, E = computed from				
note : data refers to average wave velocities				elastic modulus
note : Table redrawn from [Milnor WR, 1980]				

Table 5.2: Experimental pressure wave velocities, redrawn from [Milnor , 1980]

The data in Table 5.1 shows the mean velocity and time delays for specific arterial segment blocks, in the Forward Model of Figure 2.3, 4.3 and Table 2.3 . The mean velocity and mean time delays were calculated from the mean of velocities and time delays calculated at 15 harmonics. These *theoretical* velocities (and time delays) vary very little across the frequency spectrum and are known as the *true wave velocities.*

However practical measurement of these variables, often use the 'foot to foot' method [Milnor WR, 1970]. Wave reflections distort the waveforms resulting in *apparent wave velocities* (Table 5.2) which differ from the *real wave velocity* (Table 5.1). Figure 5.8 illustrates the approximated frequency-independent *true wave velocity* (solid line), compared to the frequency-dependent *apparent wave velocity* (solid line with circles).

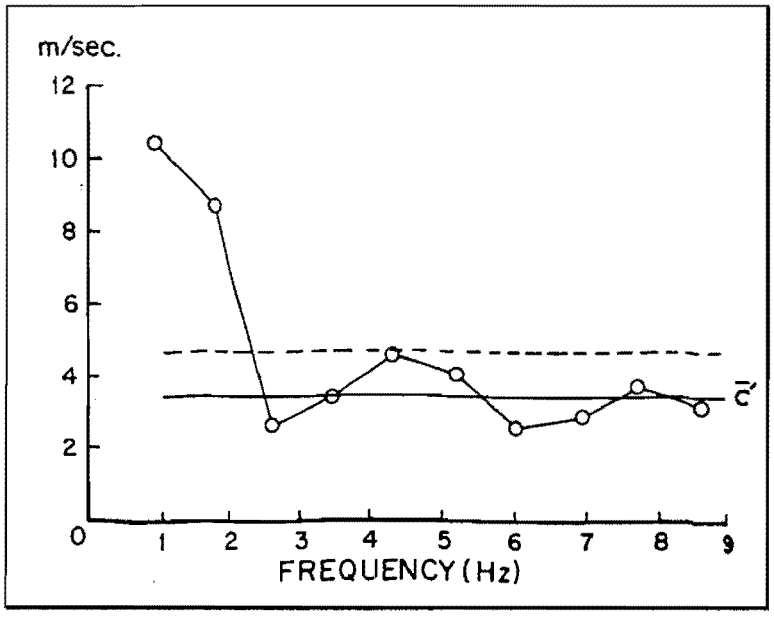

FIGURE 5.8 : *Wave Velocities* in the Ascending Aorta. The dashed line represents the average velocity of all harmonics of the apparent wave velocity, whilst the solid line represents only the average velocity of harmonics of the apparent wave velocity above 2 Hz (note that this line was shown extended to 1 Hz in the original paper). The solid line approximates the *true wave velocity* better than the dashed line. The solid line with circles "o" represents the *apparent wave velocity*, which is frequency dependent (*figure from* [Nichols & O'Rourke , 1990])

Comparison of simulated results (Table 5.1) with data from actual subjects (Table 5.2) shows a close correlation between the Forward Model simulation and experimental results in the aorta. A relatively larger error is present in the iliac and femoral arteries. This may be due to experimental results showing the *apparent wave velocities* which are influenced by wave reflections especially at peripheral sites. Wave reflections are more pronounced in the periphery. Inadequate modelling of the peripheral arterial tree would also result in some error.

Wave reflections in the human arterial system have different effects on the pressure and flow waveforms. Where reflections result in an increased apparent wave velocity when measured using pressure waveforms, they would decrease apparent wave velocity measured by the corresponding flow waves [Milnor, 1980]

5.3 VALIDATION OF THE 'STENOSED' FORWARD MODEL :

Stenotic arterial disease was simulated in the Forward Model (Figure 4.3) by reducing the radius of the arterial segment under investigation. Arterial stenosis in the external iliac artery was simulated by decreasing the radius of arterial segment 92 (sample region in Figure 8.2) in Figure 4.3. The computer simulated waveforms were compared quantitatively and qualitatively to known characteristics of clinical waveforms. Quantitative comparisons were carried out be comparing the Pulsatility Index (PI) of the computer simulated waveforms to the known clinical threshold of PI for a 'critical' isolated proximal stenosis. Qualitative comparisons were carried out by comparing computer simulated waveform trends (with progressive stenosis) to known clinical trends [Table 5.4].

5.3.1 QUANTITATIVE VALIDATION OF THE 'STENOSED' FORWARD MODEL

Existing clinical diagnostic tests for arterial stenosis predict the degree of stenosis by using the flow velocity waveform. The arterial pressure waveform is not used directly for this purpose, since the arterial flow velocity waveform may be easily obtained non-invasively using Doppler ultrasound.

The flow velocity waveform (or estimated flow rate if a duplex Doppler system is used) shows characteristic changes, depending on the severity of arterial stenosis. The Pulsatility Index is a simple index used to quantify the flow velocity waveform . Because PI is independent of the absolute velocities of a waveform it would give the same result for the flow rate (ml/s) and flow velocity (cm/s) waveforms at the same site , if the arterial diameter is constant or does not change significantly.

$$\mathbf{PI} = \frac{\textbf{peak to peak velocity}}{\textbf{mean velocity}} \qquad \text{[Equation 5.3]}$$

The Pulsatility Index of simulated flow waveforms was therefore computed in order to determine if this index gave results in the computer simulated model that corresponded to the clinically observed variation of PI with proximal stenosis.

% AREA STENOSIS	% RADIUS STENOSIS	PULSATILITY INDEX
0	0	8.2762
12.5	6.5	8.0532
24.5	13.1	7.7511
37.5	21	7.3422
50	29.3	6.7201
62.5	38.8	5.784
75	**50**	**4.1872**
87.5	64.7	1.9535
91	70	1.2084
93.8	75	0.6522
96	80	0.2901
97.8	85	0.0954
99	90	0.0187

Table 5.3 : Pulsatility Index of External Iliac blood flow waveforms at various levels of computer simulated stenosis

Critical stenosis is defined as a 70%-80% *area* stenosis. Before a stenosis reaches this critical value, it has little effect on the pressure and flow waveforms, and hence also on the blood supply to the distal bed [Strandness, 1986]. At critical stenosis the Pulsatility Index (PI) of the computer simulated model is approximately 4.2 (Table 5.3).

This $PI_{critical}$ of 4.2 corresponds closely with a clinically observed mean PI for critical stenosis of 4.3 [Clifford et al, 1981]. Some investigators have selected a critical level of 5.0 for Clinical PI [Nichols et al , 1990] which is still within the critical range demonstrated by Table 5.3. Clinical PI does however have a larger standard deviation, and is therefore not always able to differentiate between below critical , and above critical stenosis [Clifford et al, 1981].

The presence of 'critical stenosis' does have implications for an Inverse Model. An Inverse Model, based on haemodynamic waveforms, will not be able to detect arterial radii reductions that are not manifested by changes in the flow or pressure waveforms. Levels of stenosis below critical stenosis, would be defined as 'normal' in such an inverse model.

5.3.2 QUALITATIVE VALIDATION OF THE 'STENOSED' FORWARD MODEL

Computer simulations of normal External Iliac Flow and Pressure waveforms are illustrated in Figures 5.9 and 5.10 respectively. The effects of progressive stenosis of the External Iliac artery (i.e. segment 92 in the Figure 4.3) on the shapes of flow and pressure waveforms are illustrated in Figures 5.11 and 5.12 respectively. Below 60% area (40% diameter) stenosis, the shape of the external iliac waveform is the normal triphasic. Above 60% area stenosis, the systolic peak decreases rapidly, reverse flow disappears, and the waveforms becomes damped and monophasic. These computer simulated disease waveforms correspond closely to the behaviour of clinically observed stenotic waveforms as described in Table 5.4.

0% - 50% diameter stenosis	.....	normal triphasic waveform, with large *systolic forward flow* , followed by *late systolic reverse flow*, and *late diastolic secondary forward flow*
50% + diameter stenosis	.....	*forward systolic flow* peak blunted, loss of *reverse flow* component
		[Strandness DE, 1991]

Table 5.4 : Estimation of the degree of proximal radius by qualitative analysis of the Doppler flow velocity waveform.

Appendix 9 contains plots of the effect of computer simulated stenoses on upstream and downstream pressure waveforms. Forward models may be used to e.g. generate the downstream waveform given the arterial dimensions and upstream waveform, provide that the anatomical state of the arterial segment is known.

Quantitative (Aortic Input Impedance : Figure 5.1, Ext. Iliac PI : Table 5.3) and qualitative (Blood Pressure along the arterial tree; Normal External Iliac Artery Blood Pressure and Flow; External Iliac artery Stenosis) similarities between the Simulink Forward Arterial Model, and other computer simulated models and clinical studies has been demonstrated. The Forward Model, models the arterial system in health and disease, with sufficient accuracy, for inverse implementation, as a possible clinical diagnostic model. Having validated the accuracy of the Forward Model, it may now be restructured so that an inverse solution is possible (Chapters 8-10).

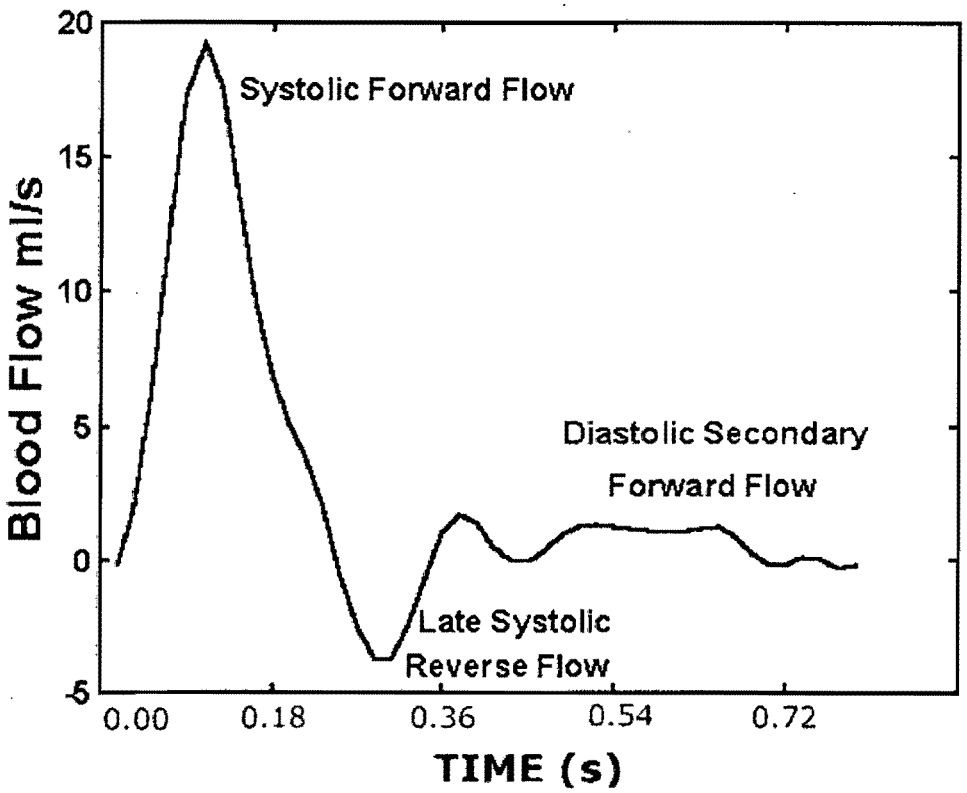

Figure 5.9 Computer simulation of a normal external iliac flow waveform

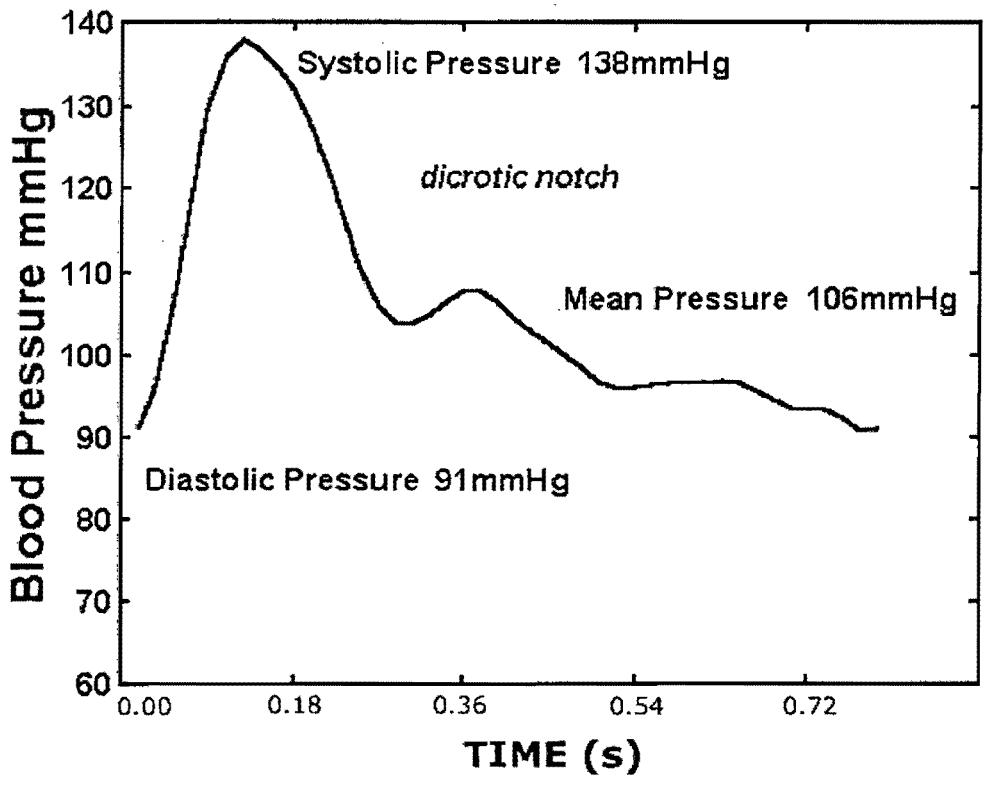

Figure 5.10: Computer simulation of the normal external iliac pressure waveform

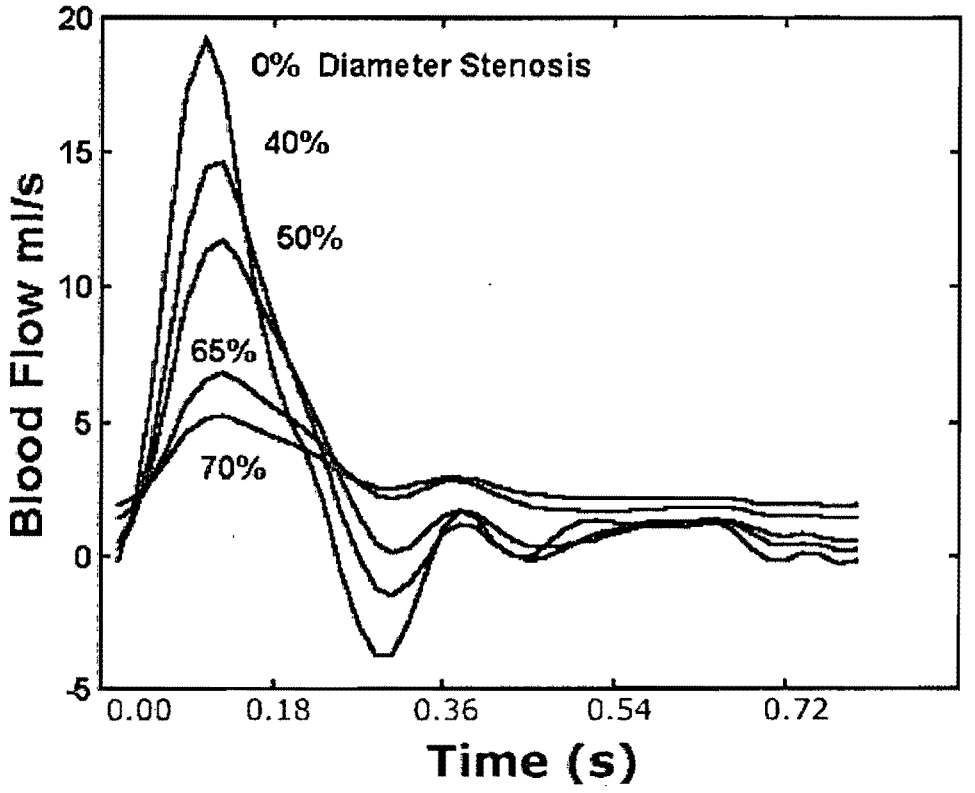

Figure 5.11: Computer simulation of the variation of ext. iliac flow with stenosis

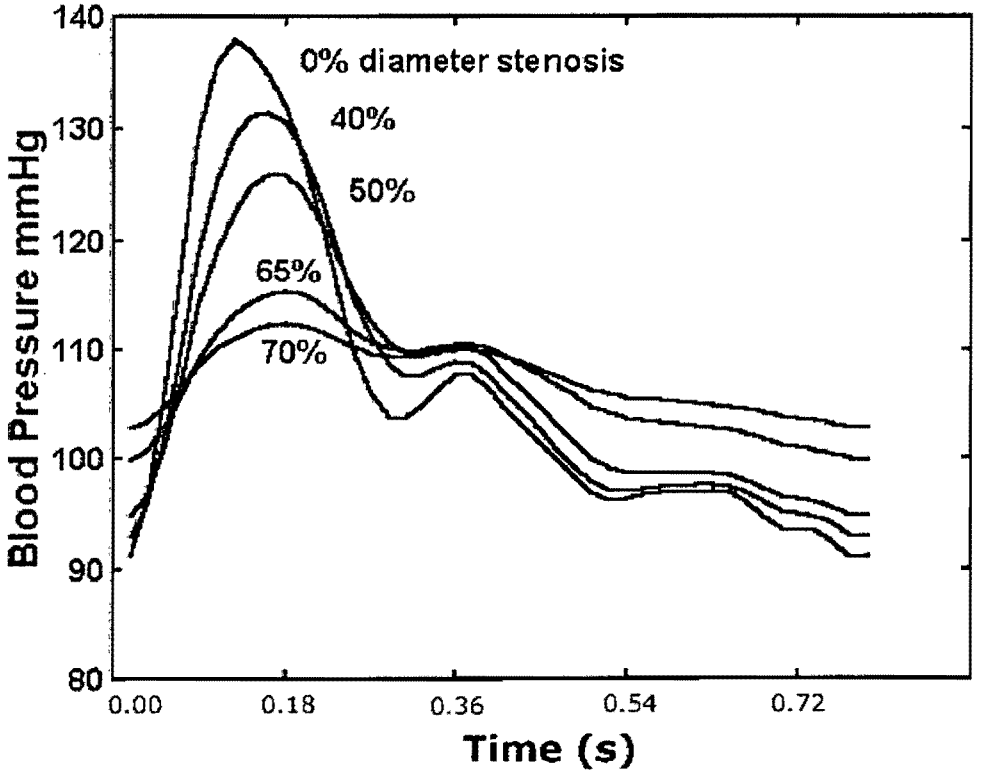

Figure 5.12 Computer simulation of the variation of external iliac pressure with stenosis. Note that this measurement site is upstream from the stenosis.

CHAPTER 6
NORMAL AND PATHOLOGICAL VARIATION OF THE CARDIOVASCULAR SYSTEM

The forward model described in the previous chapters is based on the dimensions of a young, physiological normal male. Atherosclerotic disease is however more prevalent amongst the elderly. The cardiovascular system also undergoes normal age related changes. In addition, physical size (height, weight, proportion), gender, and race also affect the structure of the vasculature. Coexisting diseases such as diabetes mellitus and hypertension also have an influence on haemodynamic waveforms. Therefore, for the sake of completion, and in order to put preliminary clinical studies (Chapter 13-15) in perspective, some aspects of normal and pathological variation of the data described in Figure 2.3 and Table 2.3 are introduced in this chapter.

Most research papers publish only graphical data (i.e. scatter graphs with a closest fit line). A custom program "degraph.m" was written by this author (see Appendix 3.13, and available via anonymous ftp from http://www.mathworks.com) to convert the graphical data into it's corresponding tabular form. The equation of the best fit line was calculated from the extracted table.

6.1 NORMAL CARDIOVASCULAR VARIATION

6.1.1 : CARDIAC STROKE VOLUME

The aortic flow waveform (Figure 2.1) was used, as the input waveform to the arterial model. This waveform may also be scaled, to take into account the variation of cardiac output (or stroke volume) with size and age.

Cardiac output is defined as the product of cardiac stroke volume and heart rate.

Cardiac Output = Stroke Volume * Heart Rate [Equation 6.1]

Therefore, if the stroke volume is known, the cardiac output of a subject with a known heart rate may be calculated.

The 'normal' resting heart rate is 72 bpm, and 'normal' resting cardiac output is 5L/min. Thus the 'normal' resting stroke volume is about 70ml.

A variety of allometric formulae are available for the estimation of stroke volume (SV) from body size :

$\mathbf{SV\ (ml) = 3.59 * Weight^{0.71}\ (kg)}$ ...	$r^2=0.28$, $p<0.0001$ [Equation 6.2]
$\mathbf{SV\ (ml) = 35.38 * Body\ Surface\ Area^{1.19}\ (m^2)}$ ...	$r^2=0.32$, $p<0.0001$ [Equation 6.3]
$\mathbf{SV\ (ml) = 23.99 * Height^{2.04}\ (m)}$ ...	$r^2=0.28$, $p<0.0001$ [Equation 6.4]

Table 6.1 Three different formulae for estimating adult cardiac stroke volume [de Simone et al, 1997]

The relationship between SV and Body Surface Area (BSA) is the most linear. BSA may be estimated from a subjects height and weight (i.e. mass) using the well known DuBois formula :

$$\mathbf{BSA(m^2) = 0.2025 * Height(m)^{0.725} * Weight(kg)^{0.425}} \quad \text{[Eq 6.5]}$$

Using Equations 6.3 and 6.5, a stroke volume of 76ml is estimated for a 1.75m, 75kg subject.

Stroke volume varies with the *age* of a subject as well. This age variation must be taken into account in elderly subjects. Adult male stroke volume decreases with increasing age, whilst adult female stroke volume increases with age [deSimone et al, 1997].

Using the Stroke Index (stroke volume normalised to BSA), the age related variation of stroke volume in the adult male, may be estimated using data from the literature :

Stroke Index = SV / BSA [Equation 6.6]

Stroke Index = -0.2 Age + 54 ml/m^2 ... $\sigma = 9.5$ [Equation 6.7]

[Branfonbrener et al, 1955]

Using Equations 6.7 and 6.5 for a 21 year old, 1.75m, 75kg male, predicts a stroke volume of 95ml. The stroke volume estimate of Equation 6.7 is 25% greater than the estimate of Equation 6.3 . The equations of Branfonbrener et al [1955], predict a 0.5% decrease in stroke volume per year, in adult males.

6.1.2 ARTERIAL LENGTH

Arterial length varies with the size of a subject. The general form of the allometric equation, which relates body weight to the size of corresponding vascular parameters (Y) is shown below :

$$Y = a.\ Weight^{\,b} \qquad \text{[Equation 6.8]}$$

where :	b = 0	Y is independent of body weight
	b = 0.33	Y is dependent on body height
	b = 0.67	Y is dependent on body surface area
	b = 1	Y is dependent on body weight

Examination of the exponent (b) gives an indication of what body size parameter most directly influences the vascular parameter Y [Li , 1996].

The theoretical allometric equation for estimation of aortic length (L_{aorta}) from body size is :

$$L_{aorta} = 17.5 * Weight^{0.31} \qquad \text{[Equation 6.8]}$$

[Li , 1996]

The exponent 0.31 indicates that a better approach would be to relate aortic length to body height. Using the anatomical data from Table 2.3 a linear equation relating aortic length to body height was extracted . With Height = 1.75m and aortic length = 42 cm, the linear relation was

$$L_{aorta} = 0.24 * Height \qquad \text{[Equation 6.9]}$$

Arterial length also varies with age [Milnor , 1989], [Nichols & O'Rourke , 1990] . Experimental results also indicate that the influence of height on abdominal aortic length decreases with age [Toda et al, 1980].

The change in length of the aortic arch with age has been studied [Mohaiddin et al , 1990]. Using the program 'degraph.m', to analyse the graphical data of [Mohaiddin et al , 1990] the increase in length of the aortic arch was estimated at 0.6 % per year (relative to length at an age of 21 years).

6.1.3 ARTERIAL RADIUS

Arterial radius varies with body size and the position within the body. In addition, the larger arteries (especially the aorta) exhibit 'radial taper'.

The allometric formula relating Aortic diameter and Weight is :

$$D_{aorta} = 0.48 * Weight^{0.35} \quad \text{[Li , 1996]} \quad \text{[Equation 6.9]}$$

By comparison with Table 2.3, this value corresponds to the aortic diameter 6cm downstream from the aortic root. The exponent of 0.35 implies that D_{aorta} may in fact be more dependent on body height than weight.

Arterial radius increases with age. The percentage increase in arterial radius with age as estimated by three published sources are shown below :

Ascending aorta	0.9 % per year	[Milnor WR, 1989]
Ascending aorta	1.4% per year	[Mohaiddin RH et al, 1990]
Ascending aorta	1.6% per year	[Bazett HC et al, 1935]
Aortic arch	1.1% per year	[Mohaiddin RH et al, 1990]
Descending aorta	1.4% per year	[Mohaiddin RH et al, 1990]
Abdominal aorta	1.8% per year	[Bazett HC et al, 1935]

Table 6.2 : Increase in arterial radius, per year(* estimates using degraph.m)

Another study generated linear equations relating aortic diameter to age, body surface area, and gender : (ages ranged from 17 to 87 years)

Thoracic	Aorta	=	0.14 Age + 10.05 BSA + 1.11 Male - 0.84	(mm)	[Eq 6.10]
Renal	Aorta	=	0.08 Age + 4.66 BSA + 2.44 Male + 4.07		[Eq 6.11]
Infrarenal	Aorta	=	0.07 Age + 3.63 BSA + 2.55 Male + 4.77		[Eq 6.12]
Celiac	Aorta	=	0.11 Age + 5.24 BSA + 2.02 Male + 4.35		[Eq 6.13]

Table 6.3 : Increase in arterial diameter with Age, BSA, and Gender. Male=1 for males, and Male=0 for females [Pearce et al, 1993]. R^2 Thoracic = 0.69 ($p < 0.001$); R^2 Renal = 0.54 ($p<0.0001$); R^2 InfraRenal=R^2 Celiac = 0.55 ($p<0.0001$)

6.1.4 ARTERIAL WALL THICKNESS

Arterial wall thickness is generally represented as the wall thickness (h) to diameter (D) ratio (wall thickness ratio, see Table 2.3). Wall thickness ratio is also affected by the internal blood pressure [Learoyd & Taylor , 1966] and age.

The descending thoracic aorta has been studied by Pearson et al [1994] , who gives the following equation:

$\mathbf{h/D_{\text{thoracic aorta}}} = -2.815*10^{-4}\ \text{Age} + 0.069$ ... $r^2 = 0.187,\ p<0.0007$ [Equation 6.14]

Although arterial diameter (D) increases with age, the corresponding increase in wall thickness (h) is greater. This results in an overall increase in the wall thickness to diameter ratio (h/D) with age [Milnor , 1989].

6.1.5 ARTERIAL ELASTICITY (and ARTERIOSCLEROSIS)

Arteriosclerosis refers to the age-related increase in arterial stiffness. This is not considered to be pathological (in contrast to Atherosclerosis). Between the ages of 20 and 60 years, the elastic modulus of the aorta is more than doubled [Milnor , 1989]. This variation in Elastic Modulus with age is not uniform in the arterial tree. The elastic modulus of the common carotid artery increases with age, whilst that of the femoral artery is not affected by age [Benetos et al, 1993]. The 'young' thoracic aorta is more elastic than peripheral arteries, whilst the 'old' thoracic aorta is stiffer than peripheral arteries (e.g. iliac and femoral arteries) [Learoyd & Taylor, 1966].

The variation of the Static Young's Modulus ($\mathbf{E_s}$) in the thoracic aorta is non-linear. It varies little up to the age of 45 years, and thereafter varies linearly with age :

$\mathbf{E_{s\ \text{thoracic aorta}} = 6.772 - 0.181\ Age + 0.004\ Age^2}$ **(*10⁶ dynes)** [Eq 6.15]

... $r^2 = 0.61,\ p = 0.0001$ [Pearson et al, 1994]

6.2 PATHOLOGICAL VARIATION

6.2.1 ATHEROSCLEROSIS

Atherosclerosis results in the narrowing of the arterial lumen, which reduces flow to the distal arterial bed. This disease has 3 effects on the dimensions of the arterial segment involved. The segment *radius* is decreased , the *effective wall thickness* is increased, and the *wall elasticity* is decreased. For the purposes of this thesis, only the reduction in radius was used to simulate atherosclerosis, as this was the dominant factor (see also Chapter 5.3). In addition to the local stenotic effects of atherosclerosis, it also results in vasodilation of the distal arterial bed, as the circulatory feedback system attempts to compensate for the reduced blood flow.

6.2.2 ANEURYSMS

Arterial aneurysms result initially in an increase in the arterial diameter. The wall thickness is reduced, and wall elasticity is increased. With the increase in diameter a point may be reached where the artery will burst. However, the presence of an arterial aneurysm may also result in the formation of a thrombus, which may be viewed hemodynamically as having similar effects to an atherosclerotic stenosis.

6.2.3. HYPERTENSION

Hypertension refers to elevated blood pressure. There is a general normal increase in blood pressure with increasing age. Hypertension is an increase in the blood pressure above the normal age related value. The higher blood pressure distends arteries resulting in an increase in radius and wall thickness [Pearson et al , 1994], and a reduction in elasticity [Pearson et al, 1994; Learoyd & Taylor, 1966] i.e. increase in Young's Modulus. The increase in wall thickness is probably a result of the cardiovascular feedback system response to hypertension, as one would expect the wall thickness to decrease with increasing distending pressure. The wall thickness to diameter ratio (h/D) decreases with increasing blood pressure [Learoyd & Taylor , 1966].

6.3 DISCUSSION

Allometric and empirical formulae which quantify the effects of age, gender, and body dimensions may be integrated with electrical transmission line models to form a more accurate representation of the normal human arterial system. Furthermore the parameters of these formulae (age, gender, and body dimensions) may be recorded with relative ease in a clinical setting, and therefore would not add further mathematical unknowns to the model. Note that reducing the number of unknowns is an important prerequisite for inversion of a transmission line model. This requirement is discussed in detail in Chapter 8. At this stage it is just important to note that the use of these allometric and empirical equations would not mathematically compromise the Inverse transmission line model.

An electrical transmission line model is an extremely complex representation of the human arterial system. However there is much more complexity that is not included in such a model. The test of any theoretical model is its ability to imitate physical reality. Because of the complexity of the arterial system, it is virtually impossible to include all physical effects into a mathematical model. It is also very easy to compromise the accuracy of a model by adding a myriad of equations in an unsystematic manner. In this authors opinion, the correct approach to this complex problem is a "bottom up" approach. Such an approach begins with a simple model that includes only some of the dominant variables. If the simple model proves either unsuccessful or has potential for improvement, then further effects may be added to the model until the model is considered to be sufficiently accurate for its intended purpose. The bottom-up approach has the added effect of identifying what the dominant variables are. The more dominant a variable, the greater its effect on the accuracy of a model.

Two questions remain :

1. What constitutes a "bottom level" model for the purposes of this thesis ?
2. Is it feasible to systematically apply the allometric and empirical equations presented in this chapter to the chosen "bottom level" model in the context of the preliminary clinical feasibility study (Chapters 12-15) ?

This thesis defines a basic transmission line model of the entire arterial system as its "bottom level" model. This chosen bottom-level model succeeds the previous

bottom-level (clinically applied) inverse electrical circuit model which was the lumped circuit model described by Skidmore [1979]. It is an incremental step up from the Skidmore model because it also models the effects of wave propagation delays and wave reflections .

The feasibility of applying the allometric and empirical equations presented in this chapter depends on the structure of the preliminary clinical study. This study (described in Chapters 12-15) could not implement the over-determined Inverse Model (described in Chapters 8-10) , but rather used an underdetermined version of the Inverse Model (Chapter 14). Because of the theoretical limitations of the underdetermined model, it was not considered feasible to implement the allometric and empirical equations for this Inverse Model component of preliminary study. Their integration into the inverse model may only be systematically carried out (in a clinical setting) if the over-determined version of the Inverse model is used. However the equations were used to a limited extent in an isolated analysis of the Arterial Pre-Sample Region (Chapters 12-13).

CHAPTER 7

COMPUTER SIMULATION OF A PHYSICAL ARTERIAL MODEL

A physical circulatory model may be synthesised using fluid-filled compliant tubes to simulate arteries; a fluid pump to simulate the heart; mechanical valves to simulate cardiac valves; and a data acquisition system to record fluid dynamic waveforms. This physical model of the human arterial system may be considered to be an *intermediate* step between a computer simulated transmission line model and the actual physiological system because it models fluid dynamic effects that cannot be included in an electrical circuit model. These include turbulence, a velocity profile that changes with time and complete three dimensional flow.

There are extensive published articles on physical circulatory models. The literature included articles on physiological pump design [Law et al, 1987]; a windkessel-based physical model [Westerhof et al, 1971]; single rigid-tube steady flow models [Bascom et al, 1993; Law et al, 1989]; single compliant-tube steady flow models [Allard et al, 1995; Elad et al,1992], single rigid-tube pulsatile flow models [Tutty, 1992], and more complex multi-tube pulsatile flow models [Helal et al, 1994; Reul et al, 1974; Segers, 1997]. A study of chaotic oscillations in a compliant tube has also been published [Jensen, 1992].

There are no detailed published mathematical simulations of complex multi-tube physical arterial systems with pulsatile flow that compare actual and predicted pressure and flow waveforms at a number of locations. Helal et al [1994] describes the computer simulation of a multi-tube model which uses a simple sinusoid (rather than a physiological waveform) as the input waveform.

The research situation relating to the divergence between the current clinical diagnostic research direction and the research direction of theoretical transmission line models of stenotic arterial disease discussed in Chapter 1, also appears to be present in the virtually non-existent relationship between physical arterial modelling (specifically complex multi-tube models) and transmission line modelling, albeit for very different reasons. It is the hypothesis of this author, based on a review of the literature as well as research experience in the construction and testing of a relatively simple physical arterial model [1,p66] , that

the reason for this research divergence is that the presence of artefact in waveforms acquired from multi-tube physical models makes it difficult to compare them with waveforms acquired from electrical transmission line models. However this missing research direction must be included in this thesis not only for the sake of completeness, but also because an accurate multi-tube physical arterial model would prove to be an invaluable "arterial phantom" for future researchers of Inverse Transmission Line Models of the human arterial system.

The multi-tube pulsatile flow model described by Seger's [1997], was mathematically simulated using the Forward Model. A total of 81 individual tube segments were included in the simulation. At first glance, it may appear to be easier to mathematically model a physical arterial system than a real physiological system. However, for a number of reasons (discussed in Section 7.1) this is not true. The graphical arterial modelling tools described in Chapter 4 allowed the Seger's physical model to be simulated on computer with relative ease. Seger's multi-tube model used a physiologically realistic input waveform in contrast to the sinusoid input waveform used by Helal et al [1994] . This chapter therefore presents a unique comparison between a physiologically realistic multi-tube physical model and a computer simulated transmission line model of the human arterial system.

---

[1] *A two tube (one with 8 resistive branches, and another with a single resistive branch) physical model was designed by this author and constructed by M. Price, for the initial purpose of testing the ability of the Forward Model to simulate the pressure and flow waveforms. This model used a "physiological pump" to simulate the pumping action of the human heart which was designed by D. Boonzaier , and also built by M.Price (Department of Biomedical Engineering, University of Cape Town). Because of the artefacts described in Section 7.1 this physical system did not consistently produce repeatable waveforms, and was therefore unsuitable for computer simulated analysis.*

The process of building and testing this model did however serve as a good basis for evaluating of the use and accuracy of physical models in representing the human arterial system. The Segers model was chosen (instead of the two-tube model) for analysis because it provided a detailed representation of the human arterial system , and because of the availability of multiple flow and pressure waveforms.

7.1 NON-PHYSIOLOGICAL EFFECTS IN A PHYSICAL ARTERIAL MODEL

Despite its ability to simulate complex haemodynamic effects, a physical model may also introduce artefacts which are not present in the normal human circulation. The most important artefact results from the presence of *air bubbles* which are difficult to eliminate in a physical system. These bubbles often collect at points in a physical system, resulting in a progressive reduction of the effective radius at that point. This may also cause local obstructions, especially in smaller diameter tubes. Unless the tubes are transparent, and the fluid opaque, it is very difficult to locate these 'air emboli' and remove them. The presence of air bubbles also increases the compliance of a system.

Another factor to consider in a physical model is the *'tethering'* of tubes. Arteries in the human body are constrained by longitudinal stress. If this were not the case then the arteries would be subject to longitudinal, in addition to radial, deformation as a pulse wave travels through them. Existing electro-mechanical analogies are only valid for tethered arteries. Because of this, un-tethered elastic tubes in a physical model would produce fluid dynamics waveforms that would differ from those produced by an electrical transmission model of the same system.

Excessive *vibration* of the physical model would also tend to induce turbulence at lower velocities than indicated by the critical Reynold's number for the different tubes (and flow velocities). External vibration would disturb a laminar streamline resulting in turbulence. The longitudinal elastic compliance of an un-tethered physical model would be one of the causes of system vibration. For thin walled tubes, the system should be submerged in a fluid e.g. water, so that the tubes maintain a circular cross-section. If the physical system is submerged in a fluid then a holding tank is necessary. The presence of surrounding fluid with inertia further influences the vibration of the system. The fluid holding tank may develop waves (as a result of tube longitudinal and radial vibration) which would in turn become an external stimulus to the system of tubes. The effect of turbulence is not modelled by existing transmission line models.

At *arterial branching points* in a physical model there would be areas of low compliance. This is due to the presence of e.g. plastic connectors; extra silicone rubber glue or excess rubber depending on the method of construction of the

physical model. The weight of a arterial branch and its distal connections, may also exert an additional force on a branching point further reducing its compliance. Manufactured rubber tubes may also have varying local compliance along their length because of localised variations in wall thickness.

For these reasons it is very difficult to obtain accurate mathematical representations of a multi-tube arterial system. This difficulty is further compounded when computer simulations are performed remotely from the physical model, because it becomes impossible to assess how much the factors described above have influenced the measured waveforms.

7.2 DESCRIPTION OF SEGERS MULTI-TUBE PHYSICAL MODEL

Data from the detailed multi-tube physical model built by Patrick Segers [Segers, 1997] was used to test the ability of the computer simulated forward model to simulate fluid dynamics waveforms. Mechanical data; Pressure and Flow waveforms from this physical model were provided courtesy of P.Segers.

The Segers Physical Model consisted of a series of custom made radially tapered elastic tubes. The tubes are similar in dimension to specific human arteries and are connected in a branching structure similar to the human arterial tree (Figure 7.1).

Terminal arteries were terminated with a parallel resistive and compliant chamber (analogous to a shunt resistor-capacitor electrical termination) . A water-glycerine mixture (viscosity = 0.028 poise; density = 1.07 g/cm^3) was used to simulate blood. The glycerine served to increase the viscosity of the solution thereby also decreasing the Reynold's number.

The fluid mixture was pumped through the system of tubes representing the arteries and was returned to the pump via another set of tubes representing the veins. A photograph of the Segers Model is shown in Figure 7.2

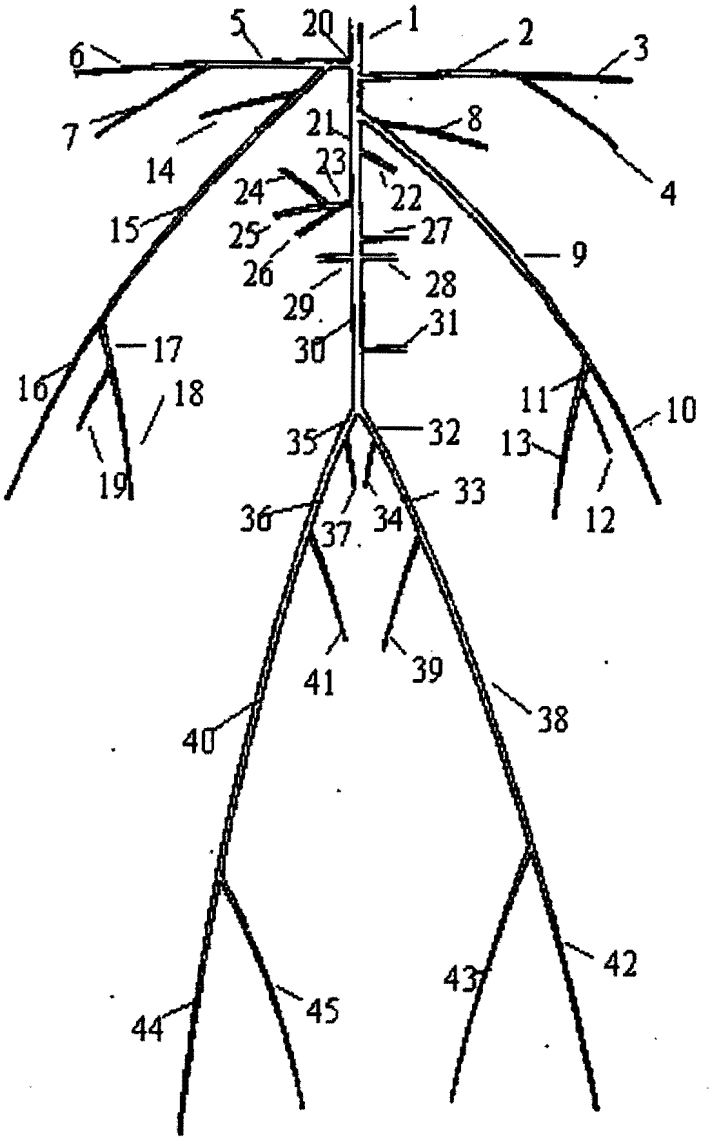

Figure 7.1 : Schematic of Seger's Physical Model . The arterial sections are numbered according to the scheme presented in Table 7.1 Segers P [1997]

Fluid-filled catheters were used to measure pressure waveforms from 16 *locations* [Figure 7.3] in the physical model. The measurement locations include points along the tube representing the aorta; the right arm and the right leg. The entry point of the catheters was at the level of the terminal impedance. Further details on the fluid-filled catheters are in Appendix X1.

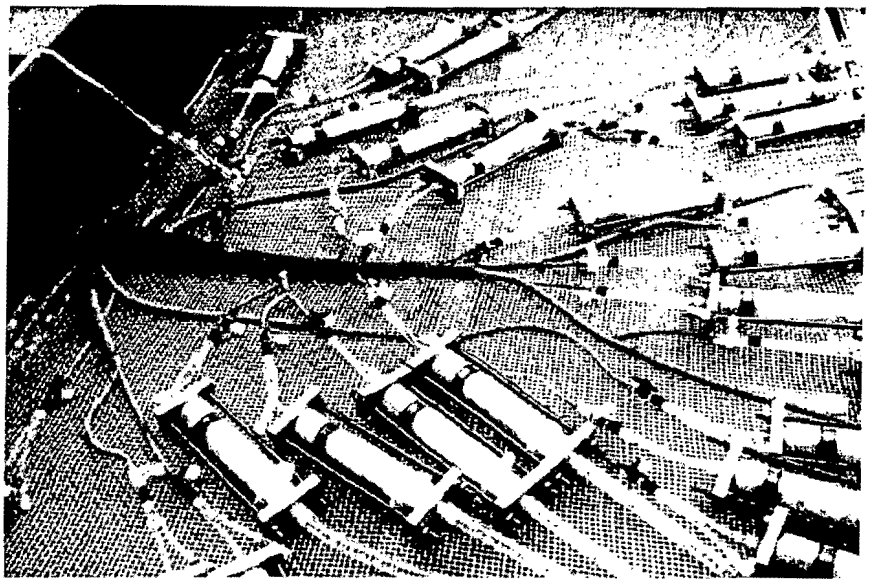

Figure7.2 : Segers physical model showing tapered tubes and terminal impedances (Segers P [1997].)

In addition the flow rate waveform, was obtained using Transonic™ Doppler probes at 6 locations. This waveform was also calibrated to the volume flow rates measured at the terminal branches. Appendix XI contains technical data on flow and pressure measurement . The 16 pressure measurement locations are illustrated in Figure 7.3

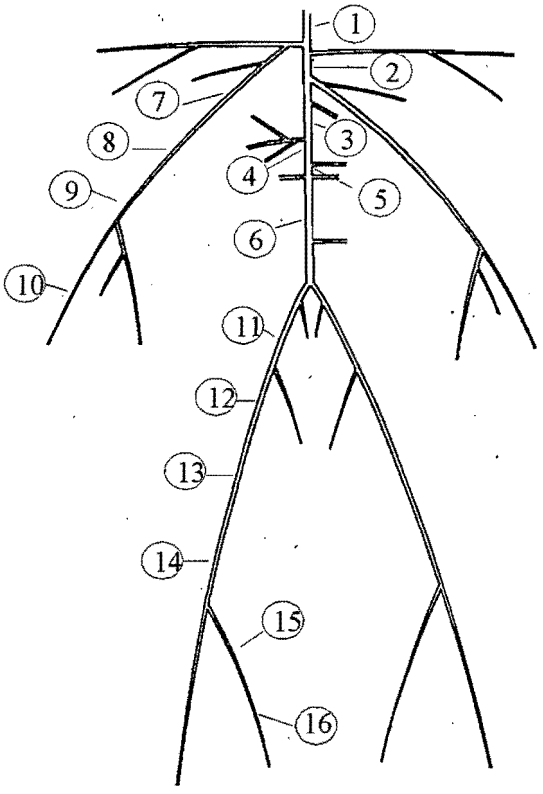

location	x (cm)	Δx (cm)
1	1	
2	10	9
3	20	10
4	30	10
5	36	6
6	48	12
7	19.5	
8	34	15
9	49	15
10	74	25
11	59	
12	76	17
13	91	15
14	106	15
15	126	20
16	146	20

Figure 7.3 : Segers physical model showing the 16 measurement locations. Note that the numbering of these measurement locations has no relation to the numbering of the arterial sections presented in Figure 7.1 and the "Artery, number" column of Table 7.1 . The 16 measurement locations are tabulated in the "Location " column of Table 7.1 (Segers P [1997])

The mechanical data of the Segers Model is tabulated in Table 7.1 below :

Artery , number	**radius R (cm)**	**Wall thickness h (cm)**	**Length x (cm)**	**E-modulus kPa**	**c m/s**	**Location**	**E**	**resistance mmHg/ml/ s**	**C ml/mmH g**
aorta **1,21,30**	1.470	0.143	1	587	6.02	1	_	_	_
	1.376	0.144	10	949	7.94	2	_	_	_
	1.145	0.136	20	1485	10.58	3	_	_	_
	0.935	0.119	30	2075	12.95	4	_	_	_
	0.851	0.110	36	2354	13.90	5	_	_	_
	0.620	0.079	45	3405	16.60	6	_	_	_
			49						
Anonymus	0.815	0.114	3	587	7.22	_	_	_	_
Intercostalis **22**	0.553	0.093	7.5	663	8.41	_	E21	13	0.0055
a.coeliaca **23**	0.285	0.049	3.7	1322	12.01	_	_		

a.lienalis **26**	0.203	0.053	5.5	863	11.96	_	E09	17	0.0055
a.hepatica **25**	0.155	0.037	6.2	944	11.96	_	E08	22	0.0055
a.gastrica **24**	0.245	0.039	5.3	1416	11.96	_	E07	19	0.0055
a.mesenterica sup. **27**	0.375	0.074	5.4	1444	13.45	_	E22	19	0.0055
l.a.renalis **28**	0.260	0.086	2.7	1001	14.50	_	E23	14	0.0055
r a.renalis. **29**	0.260	0.076	2.7	1133	14.50	_	E10	9	0.0055
a.mesenterica inf. **31**	0.195	0.047	4.4	1885	16.98	_	E24	32	0.0055
Rechterbeen **35,36,40**	0.374	0.048	9.67	2810	15.13	11	_	_	_
	0.330	0.046	27.01	2708	15.48	12	_	_	_
	0.283	0.044	42.01	2514	15.75	13	_	_	_
	0.244	0.043	57.01 65	2346	16.20	14	_	_	_
r.a.profundus **41**	0.193	0.029	11.2	2384	15.08	_	E12	21	0.0055
r. iliaca int. **37**	0.200	0.039	4	1930	15.46	_	E11	50	0.0055
r. a.tibialis ant. **44**	0.125	0.029	35.5	4352	25.32	_	E13	393	0.0055
r. a.tibialis post. **45**	0.125	0.034	12	3670	25.18	15	_	_	_
	0.125	0.034	32 35	3670	25.18	16	E14	38	0.0055
Linkerbeen **32,33,38**	0.374	0.051	9.67	2653	15.16	_	_	_	_
	0.330	0.045	27.01	2791	15.54	_	_	_	_
	0.283	0.039	42.01	2833	15.74	_	_	_	_
	0.244	0.034	57.01 65	2945	16.14	_	_	_	_
l. a.profundus **39**	0.193	0.037	11.2	1869	15.08	_	E26	144	0.0055
l. iliaca.int **34**	0.200	0.036	4	2075	15.40	_	E25	63	0.0055
l. tibialis ant. **42**	0.125	0.029	35.5	4277	25.10	_	E28	470	0.0055
l. a.tibialis post **43**	0.125	0.036	35.8	3465	25.17	_	E27	59	0.0055
Rechterarm **15**	0.391	0.066	10.5	1507	12.71	7	_	_	_
	0.328	0.059	25.5	1644	13.70	8	_	_	_
	0.261	0.053	40.5 42.5	1702	14.81	9	_	_	_
r. a.vertebralis. **14**	0.190	0.042	13.7	1073	12.27	_	E03	23	0.0055
r. a.radialis **16**	0.175	0.044	24	1317	14.50	10	E06	110	0.0055
r. a.ulnaris. **18**	0.175	0.033	14.9	1745	14.45	_	E04	58	0.0055
r. a.interosseus **19**	0.100	0.033	6.9	994	14.43	_	E05	180	0.0055
Linkerarm **9**	0.395	0.054	9.6	1810	12.53	_	_	_	_

	0.346	0.052	20.8	1886	13.42	_	_	_	_
	0.272	0.048	37.6 43.2	1911	14.63	_	_	_	_
l. a.vertebralis 14	0.190	0.040	13.7	1114	12.20	_	E17	58	0.0055
l. a.radialis 10	0.175	0.034	22.3	1725	14.59	_	E20	327	0.0055
l. a.ulnaris 13	0.175	0.045	22.25	1291	14.52	_	E18	201	0.0055
l. a.interosseus 12	0.100	0.028	7.2	1183	14.50	_	E19	1012	0.0055
r. a.carotis com 5	0.458	0.078	15.99	485	7.24	_	_	_	_
r. a.carotis ext 6	0.240	0.050	15.81	489	8.04	_	E01	42	0.0055
r. a.carotis int 7	0.240	0.048	15.81	509	8.04	_	E02	1009	0.0055
l. a.carotis com 2	0.458	0.082	20	524	7.72	_	_	_	_
l. a.carotis ext 3	0.240	0.056	15.81	436	8.04	_	E15	99	0.0055
l. a.carotis int 4	0.240	0.056	15.81	432	8.00	_	E16	58	0.0055

Table 7.1 : Mechanical data for Segers model. The artery numbers correspond to the numbers of the arterial sections of Figure 7.1 . The Location numbers correspond to the numbers of the measurement locations in Figure 7.3 (Segers P. [1997])

The Young's Modulus (E-modulus) values provided in Table 7.1 were calculated from the measured wave velocities (c) using the Bergel's 1960 modification of the Moens-Korteweg equation [Nichols & O'Rourke, 1990] :

$$c = \sqrt{\frac{E.h}{2.\rho.R.(1-\nu^2)}} \qquad \text{[Equation 7.1]}$$

where : c = wave speed, R = tube radius, E = elastic modulus,
ν = poisson's ratio, h = tube wall thickness

Young's Modulus data shown in Table 7.1 was calculated using Equation 7.1. When this data was included in a Forward Model simulation there was a distinct systematic error between the diastolic pressure level predicted by the Forward Model and the pressure waveforms measured from the physical model. This is an obvious indicator that the capacitance equation of the model was in error. Young's modulus has an influence on capacitance (see Equation 1.7) therefore the approach to calculating the Young's Modulus was re-examined.

While the Moens-Korteweg equation is well known and used by many authors , it's validity in the human arterial circulation has not been established [Nichols & O'Rourke, 1990]. Gow and Taylor modified this equation in 1968, to take into account thick walled tubes [Milnor, 1989].

Using $\nu = 0.5$, the Gow and Taylor wave speed equation is :

$$c = \sqrt{\frac{E.h}{3.\rho.R}} \qquad \text{[Equation 7.2]}$$

It is apparent that the square of the wave-speed for the thick walled tubes is 1/2 that of the thin walled tubes. Practically this means that if the Elastic Modulus is to be estimated from the wave-speed, then Equation 7.2 should provide a better estimate for thick walled tubes than Equation 7.1. Therefore the Elastic modulus has been recalculated using Equation 7.2 and this estimate has been used in the simulations that follow (i.e. the Elastic moduli provided by Table 7.1 were doubled for the computer simulation)

7.3 COMPUTER SIMULATED MODEL OF SEGERS PHYSICAL MODEL

Using the data provided in Table 7.1 (with the above-mentioned modification of the Elastic moduli) and the branching structure of Figure 7.1, the Segers Physical Model was simulated on computer. The purpose was to test the ability of the Computer Simulated Forward Model (Chapters 3 and 4) to simulate the fluid dynamics waveforms of a *physical* circulatory model.

The Matlab/Simulink simulation of the Segers model is illustrated in Figure 7.4.

Initial simulation of the Segers Physical Model used the original data (Table 7.1) and resulted in a poor fit of the diastolic pressure level. This level (in an electrical equivalent circuit) depends greatly on the transmission line capacitance. However using the proposed alternative equation (Gow and Taylor, Equation 7.2), for determining the Elastic Modulus resulted in an improved fit , the results of which are presented in this Chapter.

7.3 RESULTS OF COMPUTER SIMULATION OF SEGERS PHYSICAL MODEL

The computer simulated waveforms, were compared to the directly measured waveforms from the Segers Physical Model. Pressure waveforms were available from all 16 measurement locations of the Segers Physical Model (Figure 7.3), and Flow waveforms were available from 6 locations (Figure 7.3) of the Segers Physical Model . Comparisons between computer simulated and physical model waveforms, are illustrated in Figures 7.6 – 7.27.

Figures 7.6-7.13 (below): Computer simulated Pressure waveforms (blue solid lines) compared with measured (black dotted lines) from pressure locations 1-8 (see Figure 7.3) of Segers Physical Model

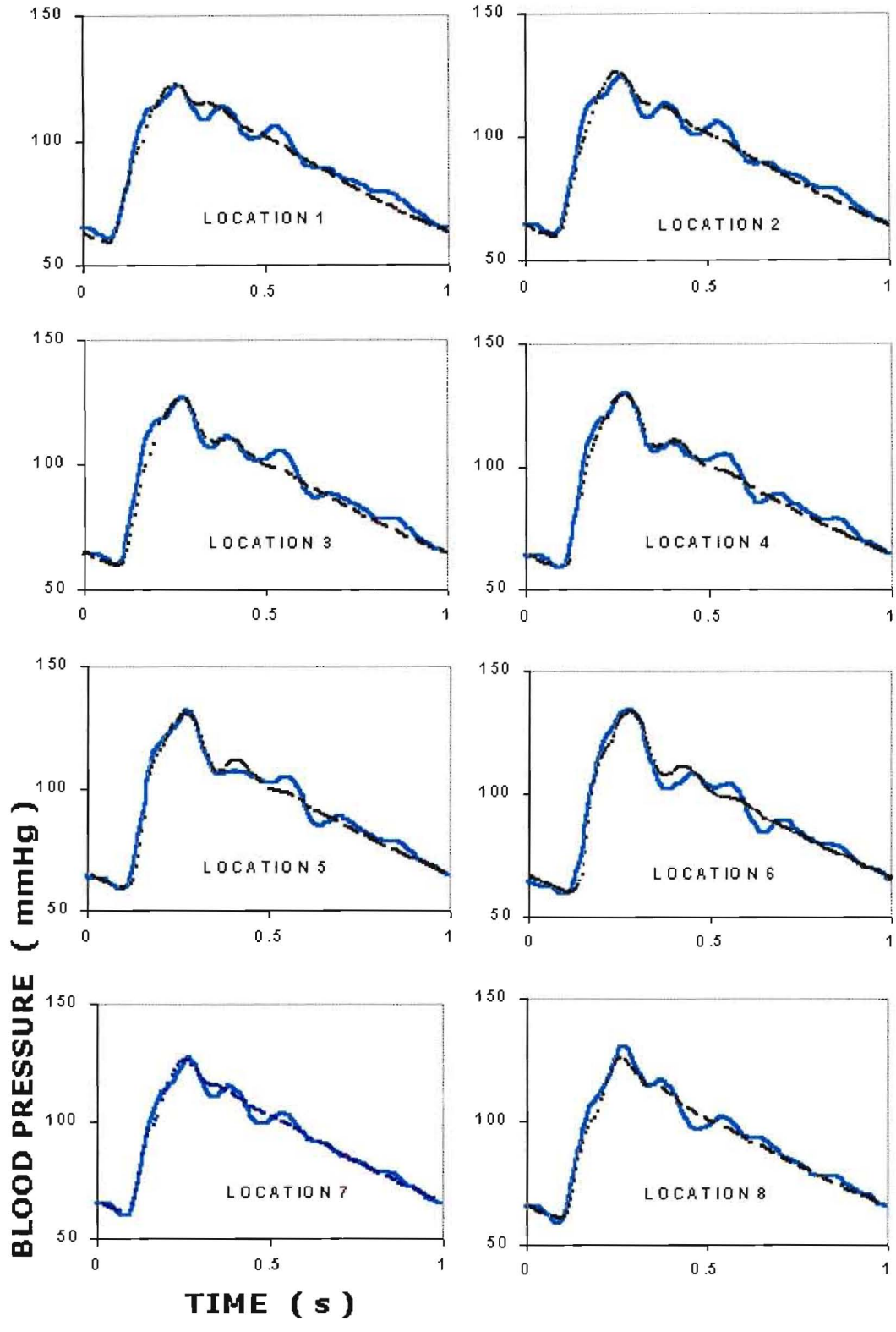

Figures 7.14-7.21 (below): Computer simulated Pressure waveforms (blue solid lines) compared with measured (black dotted lines) from pressure locations 9 - 16 (see Figure 7.3) of Segers Physical Model

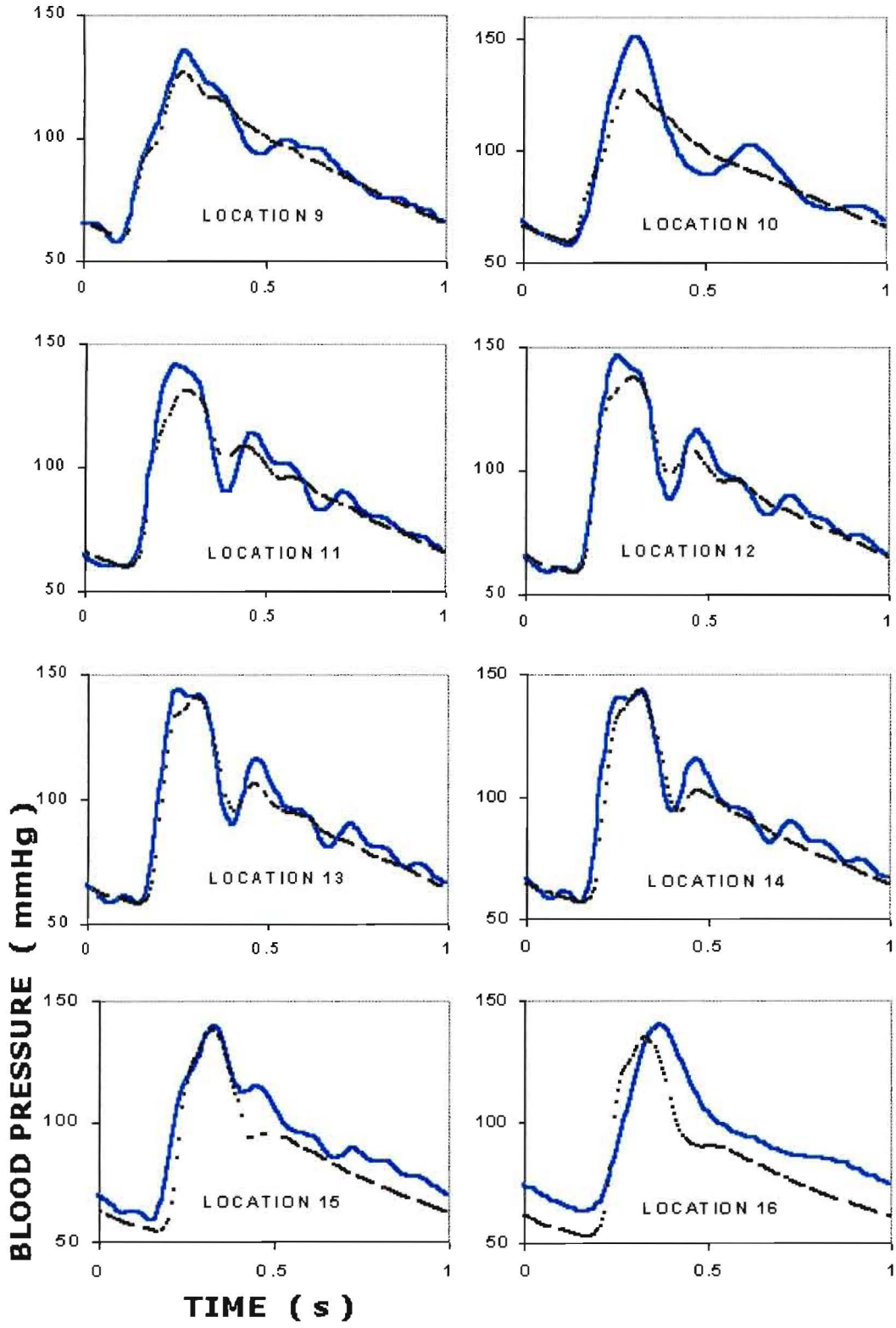

Figures 7.22 – 7.27 (below): Computer Simulated flow waveforms (solid lines) compared with measured waveforms (dotted lines) at flow locations 1-6 (see Figure 7.3) of the Segers Physical Model.

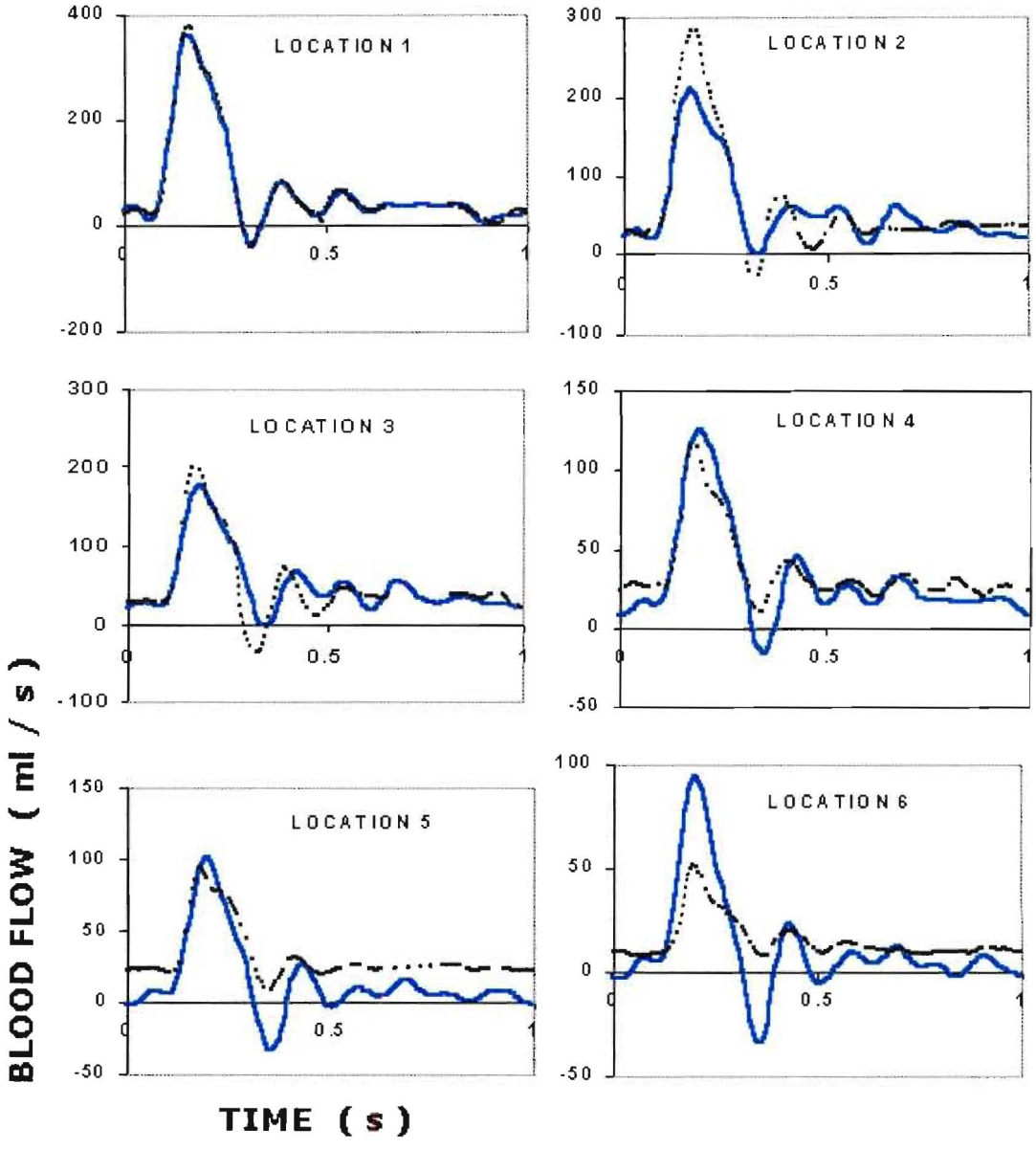

7.4 DISCUSSION

The waveform fits illustrated in Figures 7.6 –7.27 must be interpreted in the context of the discussion concerning artefacts present in physical models [Section 7.1.]. These artefacts are possibly the reason that similar studies have not been published despite the large number of physical models in existence. It is technically very difficult to computer simulate a complex multi-tube physical arterial model, indeed a detailed comparison between the two models is not available in the literature.

The comparison of pressure waveforms measured at 16 locations in the Segers Physical Model, to waveforms generated by the Matlab / Simulink implementation of the Forward Arterial Model (Figure 7.6-7.21) show them to be very similar , and this would seem to indicate that the transmission line model provides a very accurate representation of physical reality. The computer simulated pressure waveforms display less damping than the measured waveforms. The largest discrepancies between simulated and measured pressure waveforms (Figures 7.20 - 7.21), are present close to the termination locations (i.e. location 15 and 16). This implies some error in modelling the physical terminal impedance. The error may be due to a number of reasons including : the presence of air bubbles; movement artefact ; or theoretical modelling that does not accurately represent physical reality.

The comparison between computer simulated flow waveforms and flow waveforms measured from the Seger's physical model shows that they are similar at locations 1,3, and 4 but differ at locations 2, 5, and 6 . Many of the effects (discussed in Section 7.2) peculiar to physical circulatory models may result in these discrepancies. The poor fit at only some of the locations seems to imply that these errors may be due to un-modelled physical effects (longitudinal compliance; air bubbles; turbulence) . Because of the technical nature of the error sources in a physical model , further investigation of these discrepancies is not possible with remote computer analysis.

CHAPTER 8
INVERSE TRANSMISSION LINE MODEL

8.1 DEFINITION OF AN INVERSE MODEL

An Inverse transmission line model, is the mathematical inverse of a Forward transmission line model. The inputs of an Inverse model therefore correspond to the outputs of the Forward model, and vice versa. The inputs of the Inverse Transmission Line Model are the pressure and flow waveforms of the arterial system, and its outputs are the dimensions and physical properties of the arterial system. An Inverse model may be used for Clinical diagnosis of arterial disease, provided that the underlying Forward model adequately represents the human arterial system in both health and disease (Figure 8.1). By analogy, if a recipe for a cake represents a Forward Model, then the Inverse Model would be process of extracting the recipe, given only the cake.

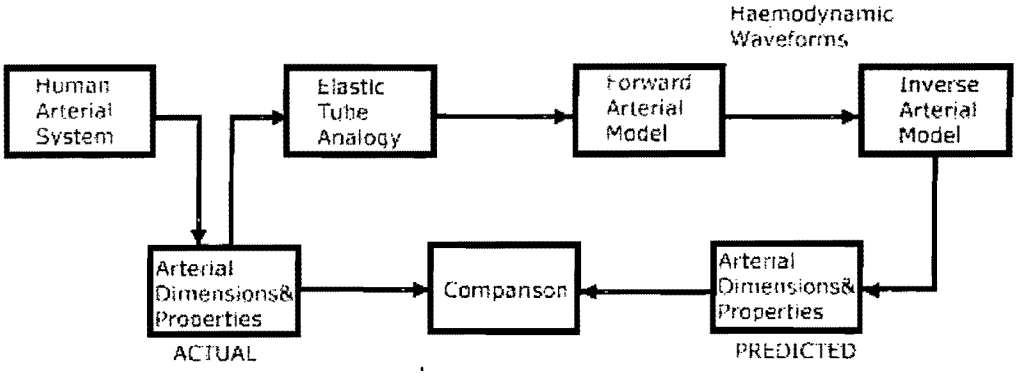

Figure 8.1 : Inverse Arterial Model in relation to a Forward Arterial Model

8.2 GENERAL REQUIREMENTS FOR INVERSION OF AN ARTERIAL MODEL

The *mathematical* requirement for inversion is that the underlying equation system of a model be critically or over-determined. A critically determined model has an equal number of *unknowns* and *equations.* An over-determined model

has more equations than unknowns. An underdetermined model has more unknowns than equations . If the equation system is underdetermined, then a unique solution cannot be guaranteed.

A *practical mathematical* requirement for inversion, is the existence of a numerical equation solving technique . The performance of a numerical technique depends on the mathematical characteristics of the equation system. For example, the presence of a large poorly scaled matrix may render it practically impossible to invert a model, even if it represented an over-determined system.

A *clinical constraint* for inversion of an arterial transmission line model, is the availability of spatially different waveforms (blood pressure and blood flow). These waveforms would correspond to equations, or the end-result of a series of multiple equations, in a model (e.g. blood pressure equation) . This constraint determines the number of *equations* available to the Inverse Model and hence also determines the number of unknowns that may be uniquely solved.

A clinically *invasive* implementation which uses an intra-arterial catheter to obtain blood pressure and blood flow waveforms from a subject may be employed in order to increase the number of *equations* . It is difficult to obtain multiple synchronous blood pressure and flow data from a human subject as this would require numerous catheters, with multiple sensors and complex data acquisition equipment. These measurements would have to be synchronous or 'pseudo-synchronous'. A 'pseudo-synchronous' method requires a steady heart rate with no significant change in cardiac and vascular states during the recording of data. This would allow for the timing of pressure and flow waveforms (at multiple sites using a single catheter) relative to the R-wave of an Electrocardiogram (ECG). The recorded Flow and Pressure waveforms may then be pseudo-synchronised offline (i.e. not in real time).

If a clinically *non-invasive* implementation of the inverse model is required, then the constraints are more severe. Non-invasive blood flow (via Doppler/Duplex Ultrasound) measurements cannot be recorded at all the areas of the arterial tree. Blood pressure can only be obtained non-invasively at 'pulse' points in the body (see Chapter 11).

For the preliminary development of an Inverse Transmission line model for the prediction of normal or stenotic arterial states in the lower limb, a non-invasive inverse model with a single haemodynamic measurement site (external iliac artery) implementation was chosen. For a preliminary clinical study, only the haemodynamic waveforms at the level of the external iliac artery were available non-invasively. Therefore only 2 equations were available.

8.3 GENERAL APPROACH TO THE INVERSION OF EXISTING FORWARD TRANSMISSION LINE MODELS

The Forward arterial model described in Chapters 2-5, has 126 arterial segments and 61 terminals loads. Each arterial segment has 4 unknowns (radius, wall thickness, Young's modulus, length); the AC component of each terminal impedance has 2 unknowns (the real and imaginary parts of terminal impedance at harmonic frequencies); and the DC component of terminal impedance has a single unknown (i.e. the terminal resistance). This results in a total of 126*4 + 61*2 + 61 = 687 mathematical unknowns. In addition the input waveform adds further unknowns. This 'problem' of an excessively large number of mathematical variables, is a typical 'problem' with all transmission line arterial models that has hampered the development of a unique Inverse solution.

8.4 RESTRUCTURING OF THE FORWARD MODEL INTO AN INVERTABLE FORM

It is therefore apparent that that the Forward model may be made invertable (critically-determined) using either one of two approaches. As a *first option*, it may be restructured in such a way that the number of equations *required* be reduced to equal the number of clinically available waveforms. This would inevitably also reduce the number of unknowns that may be uniquely solved. The proposed clinical implementation discussed in Chapter 9 provides only two equations (i.e. Blood Flow and Pressure) and hence only two unknowns may be uniquely solved.

The *second option* is to retain the larger number of unknowns, and attempt to make 687 haemodynamic waveforms clinically available. This would also result in a critically-determined system. Although theoretically invertable, this system would be very difficult to solve practically, because numerical techniques would

have to be implemented to solve this system. Numerical techniques do not guarantee a solution in such a large, non-linear system of equations. Even if a suitable numerical technique is located, or developed, the clinical implementation of such an inverse model would be difficult. Invasive catheter-based waveform acquisition would be necessary, in order to obtain 687 waveforms. This option, or even a reduced form thereof , is obviously impractical.

The *first option* was adopted. The Three Division Method described below presents a unique approach to the inversion of an electrical transmission line model of the entire human arterial system based on three non-invasive clinical measurements (ECG; Blood Flow; Blood Pressure).

8.5 CRITICALLY-DETERMINED TRANSMISSION LINE MODEL "THE THREE DIVISION METHOD"

In the Inverse Model , the arterial system was divided into 3 regions (Figure 8.2). These 3 regions were defined relative to the Right External Iliac artery. This was done because the clinical aspect of this thesis was confined to the lower limb arterial system. In order to investigate different arterial areas (e.g. carotid area), the 3 regions would have to be redefined, relative to the area under investigation.

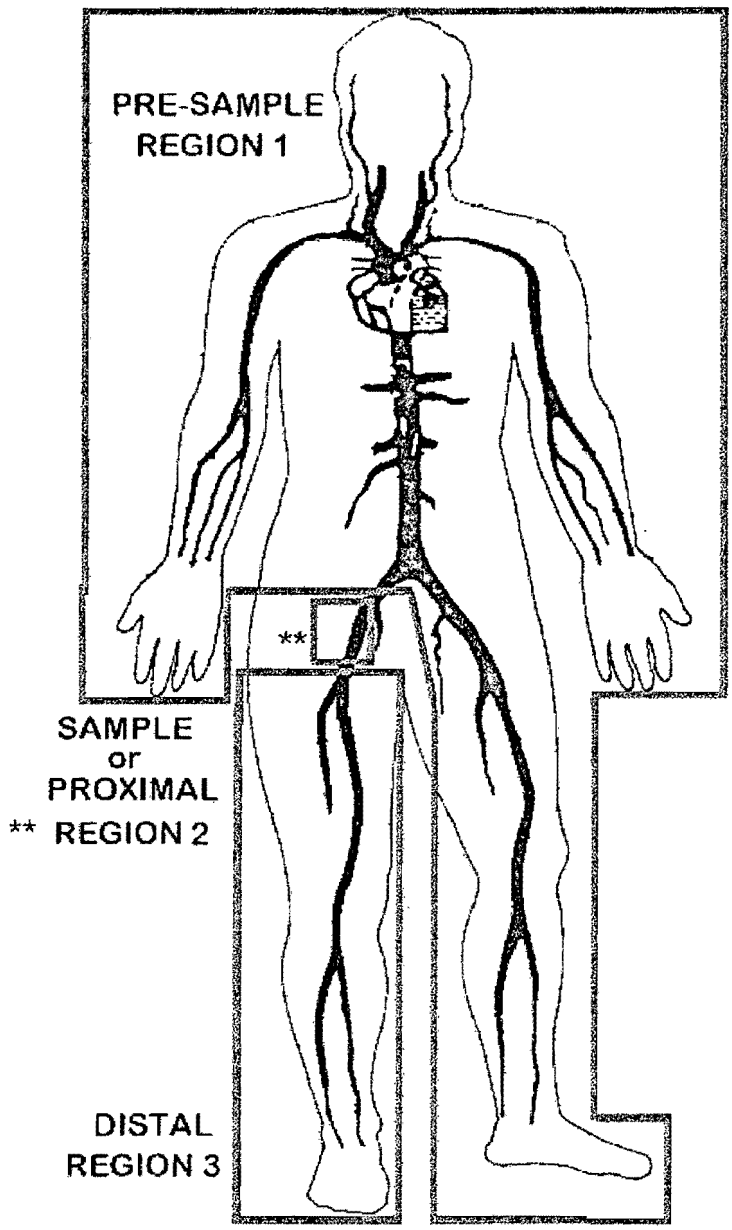

Figure 8.2 : The 3 Arterial Regions in the Inverse Model

8.5.1 REGION 1 : THE ARTERIAL PRESAMPLE REGION

This region includes all arterial segments *upstream* from the right external iliac artery. The carotids, arms, aorta as well as the left leg arterial segments are included. It is assumed that the physiological state of the Pre-Sample Region has a *lesser* effect on haemodynamics at the External Iliac region, than the physiological state of the External Iliac Region (i.e. Sample or Proximal Region), because of the latter's proximity to the sample site.

Therefore the Pre-Sample Region was assumed to be 'normal' for all subjects studied. This approximation may be improved if the effects of age, body dimensions, gender, state of fitness, and the presence of other arterial disease (see Chapter 6), as well as supplementary haemodynamic measurements (e.g. brachial artery, carotid artery waveforms) are included. However, for the purposes of this thesis the 'normal' approximation is used . If for example a subject was being investigated for stenotic external iliac disease, then his Pre-Sample Region would be modelled according to the data in Table 2.3, and Figure 2.3 . Although localised arterial disease (e.g. Iliac artery) is often associated with general arterial system disease (e.g. Carotid, Aortic, Coronary arteries), it is hypothesised that the effects of these co-existing diseases, on the External Iliac Artery waveforms, is much smaller than the effect of local External Iliac disease. This is a useful *first approximation*. Future and more advanced implementations of the Inverse Model may be able to take the effects of co-existing arterial disease, which often occurs with external iliac arterial disease, into account .

This process converts all the unknowns in the Pre-Sample Region into '*approximated knowns*'. Also included, amongst the 'approximated knowns' is the Aortic Flow Waveform (Figure 2.1) which is assumed to have the same shape for all subjects. Where any of these 'approximated knowns' may be clinically measured (e.g. cardiac stroke volume), the measured values in future implementations be used to replace the 'approximated knowns'.

8.5.2 REGION 2 : THE ARTERIAL SAMPLE or PROXIMAL REGION

This region is defined as the arterial region, *proximal* to the clinical measurement site i.e. the external iliac artery. It was modelled as a single transmission line segment i.e. as a tube with a known length, and a uniform, but unknown, radius. The predicted radius, relative to the 'normal' radius for that segment (Table 2.3) determines the predicted degree of stenosis. Obviously, this approach approximates a stenosis as an evenly distributed decrease in arterial radius. Actual arterial stenosis occurs with a variety of topologies . This uniformly distributed stenosis is therefore a first approximation that is sufficient for the purposes of this thesis.

Non-uniform stenoses may be modelled by dividing the stenotic region into a series of shorter uniform segments. However, this approach would require the acquisition of multiple haemodynamic waveforms. Very accurate modelling of stenosis haemodynamics must also include the effects of turbulence (which is often an early indicator of arterial disease) and non-uniform flow profiles. Electrical analogues are unable to model such effects. It may be possible, in future, to combine Electrical Inverse Models with local detailed Finite Element Models of stenoses.

The physiological state of the Sample region has the greatest effect on the haemodynamic waveforms measured at this site. This region was modelled as a single unknown i.e. Arterial Radius . Arterial Length was predefined according to the segment length defined in Table 2.3. Arterial Elasticity and Wall Thickness were also predefined according to Table 2.3. Although a stenotic tube would also have a decreased Elasticity, as well as an increased Wall Thickness, these factors affect only the capacitance of the electrical model . From the electrical analogue Equations 1.5-1.7 it is apparent that changes in Young's Modulus (E) and Wall thickness to Radius ratio (h) have similar effects on the electrical analogue. Tests carried out in Section 10.3 [Figure 10.6] indicate that large increases in local Young's Modulus have little effect on the predictions of the Inverse model in comparison to the larger effect of a small change in local arterial radius [Section 10.2.2 , Figure 10.4]. This justifies the use of Arterial Radius as the only unknown variable of an inverse model sample region for both the normal and stenotically diseased states of the external iliac artery.

Arterial segment lengths and elasticities may also be modified according to the subject's age and size using the techniques presented in Chapter 6. Such analysis has not been included in this Inverse Model but may be implemented in future Inverse Models.

8.5.3 REGION 3 : THE DISTAL REGION

This region is defined as the arterial region *downstream* from the Sample Region. With the Sample Region defined as the Right External Iliac Artery, the Distal region includes all the leg arteries below the Right External Iliac i.e. Common Femoral, Profunda Femorus, Popliteal, Peroneal, Posterior and Anterior Tibial.

In the Inverse Model this region was modelled as a steady state impedance spectrum. This impedance was obtained by transforming the clinically measured blood pressure and blood flow waveforms into the frequency domain, and calculating the ratio of their phasors at each harmonic frequency. The Distal Region therefore has no mathematical unknowns.

By using the Three-Division method, an entire 128 segment Forward Arterial Model (Chapters 2-5) has been converted into an Inverse form which requires only three clinical measured waveforms. The arterial radius of the Sample Region may thus be estimated. This approach retains the complexity (and accuracy) of a detailed Transmission Line Arterial Model, yet is simple enough to be applied clinically.

CHAPTER 9
COMPUTER SIMULATED IMPLEMENTATION OF THE INVERSE MODEL

The Inverse Arterial Model was implemented using Matlab and Simulink (Figure 9.1). Synchronous pressure and flow waveforms measured at the External Iliac Artery ('Clinical' Waveforms in Figure 9.1) were used as inputs to the Inverse Model. For computer simulated tests, these waveforms may be acquired from the Forward Arterial Model, whilst for clinical testing they may be acquired from Human Subjects.

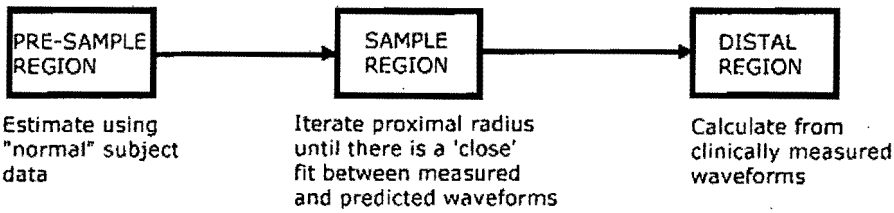

Figure 9.1 Three Division Inverse Arterial Model showing the Pre-Sample, the Sample, and the Distal Regions

Using the 'Three Division Method' , the first step was to define the *Distal* Region as a steady state impedance. This was done by calculating the frequency domain ratio of the 'Clinical' Pressure and Flow waveforms which were obtained using a Fast Fourier Transform.

The *Pre-Sample* Region was then estimated using 'normal' data from Table 2.3 and Figure 2.3. The subject's heart rate was calculated from either the measured flow or pressure 'clinical waveforms' or the ECG. The Aortic Flow Waveform (Figure 2.1) was then time-scaled to correspond to this heart rate. This involved either reducing or increasing the diastolic segment of the Aortic Flow waveform. More sophisticated techniques of adjusting the Aortic Flow waveform may be implemented in subsequent models.

In the *Sample* Region, the radius of the External Iliac Artery (Segment 92 in Figure 2.3) was then stepped from above its 'normal' radius (as defined by Table 2.3), through progressively larger stenoses. At each discrete radius new pressure and flow waveforms were generated. The mean squared error between these waveforms and the 'clinically' measured waveforms (Forward Model or Subject Data) was then plotted on three graphs i.e. Mean Squared Pressure Error, Mean Squared Flow Error, and Mean Squared Pressure + Mean Squared Flow Error

(Figures 9.4) . The sample region radius with the minimum mean squared error was the 'predicted' radius. The corresponding Flow and Pressure Waveforms for a normal subject were plotted in Figure 9.5 .

The *Software Flow Diagram* (Figure 9.2) shows the interface between Matlab Programs and the Simulink Inverse Model. Program Listings are in Appendix 3.14-3.17

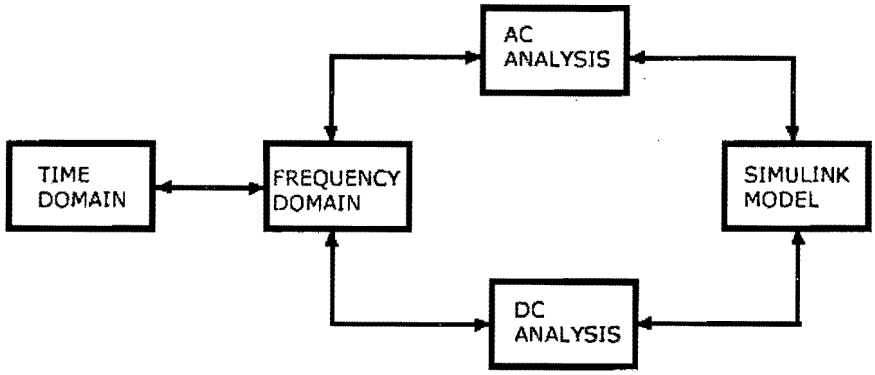

Figure 9.2 : Inverse Model Software Flow Diagram. All blocks except the Simulink Model, are implemented using Matlab. The Simulink model ('avoles5.m') is illustrated in Figure 9.3. The Time Domain block ('avoltes9.m'); the Frequency Domain Block ('simtim10.m'); the DC analysis block ('simavol6.m'); and the AC analysis block ('simavol5.m') are in Appendices 3.14-3.17 respectively

Time domain analysis with radius iteration and comparison of mean squared errors was carried out by the Matlab program 'Avoltes9.m'.

'Simtim10.m' (which is called by 'Avoltes9.m') contains a frequency loop. It calculates the DC output level (using 'Simavol6.m') and 10 AC harmonics (using 'Simavol5.m'). The frequency domain results were then converted into the time domain using the Inverse Fast Fourier Transform and sent to 'Avoltes9.m'.

Avoles5.m is the 'three-division' (see Chapter 8) Simulink representation of the Arterial System. It is similar to 'Avoles4.m', except in the Distal Region which is represented by the 'clinical' or 'measured' distal impedance spectrum . This model is valid for both DC and AC analysis. The Simulink model ('Avoles5.m') is illustrated in more detail in Figure 9.3.

The formula used to determine the error ('mean error' in Figure 9.4) between the *actual* (Clinical or Forward Model) waveforms and the *predicted* waveforms was :

$$\text{Error} = \frac{\text{Mean}\left(\sqrt{(\text{predicted}_i - \text{actual}_i)^2}\right)}{\text{Mean}(\text{actual})} \qquad \textbf{[Equation 9.1]}$$

The Error Formula (Equation 9.1) has not been optimised. It was used in conjunction with a qualitative visual analysis of the correspondence between the actual and predicted waveforms. Clinical investigators would favour the use of qualitative visual analysis, whilst mathematical scientists would favour the use of a minimum error formula. There are numerous other (and better) methods of statistically comparing two waveforms (e.g. statistical MLE analysis), however Equation 9.1 in combination with qualitative visual analysis (Figure 9.5) has been used for the purposes of this thesis as a simple and effective method of comparison. An optimised error function should be the subject of future study.

There are three Error Graphs (Figure 9.4). Ideally, the 'minimum error point' should be the same for the Flow and Pressure Error graphs. In practice this was found not to be true. An improved error formula could solve this problem. However qualitative analysis seems to be the best indicator of the minimum error point (Figure 9.5). From Figure 9.4, (which is an analysis of an actual normal subject) it is also apparent that the 'minimum error point' defines the start of a *minimum error region*. On the basis of the Error Graphs and the Waveform Graphs (Figure 9.5) any predicted radius within this 'minimum error region' would result in a similar waveform fit. The actual radius is therefore uncertain. However it is certain as long as the predicted radius remains within the minimum error region the predicted haemodynamic waveforms do not vary significantly. This is a well known characteristic of arteries with a sub-critical level of stenosis which are therefore considered *'physiologically normal'* .

Because of the presence of 'critical stenosis' (see Chapter 5), the *'effective'* radius rather than the *'actual'* radius was predicted. Stenoses below the level of critical stenosis have only a minor effect on the haemodynamic waveforms and therefore cannot be detected by haemodynamic waveform analysis. Therefore, the 'effective' sample region radius prediction of the Inverse Model may be divided into three areas:

1. Haemodynamically Normal ... below critical stenosis (e.g. Figures 9.4 & 9.5)
2. Mild Stenosis ... just above critical stenosis
3. Severe Stenosis

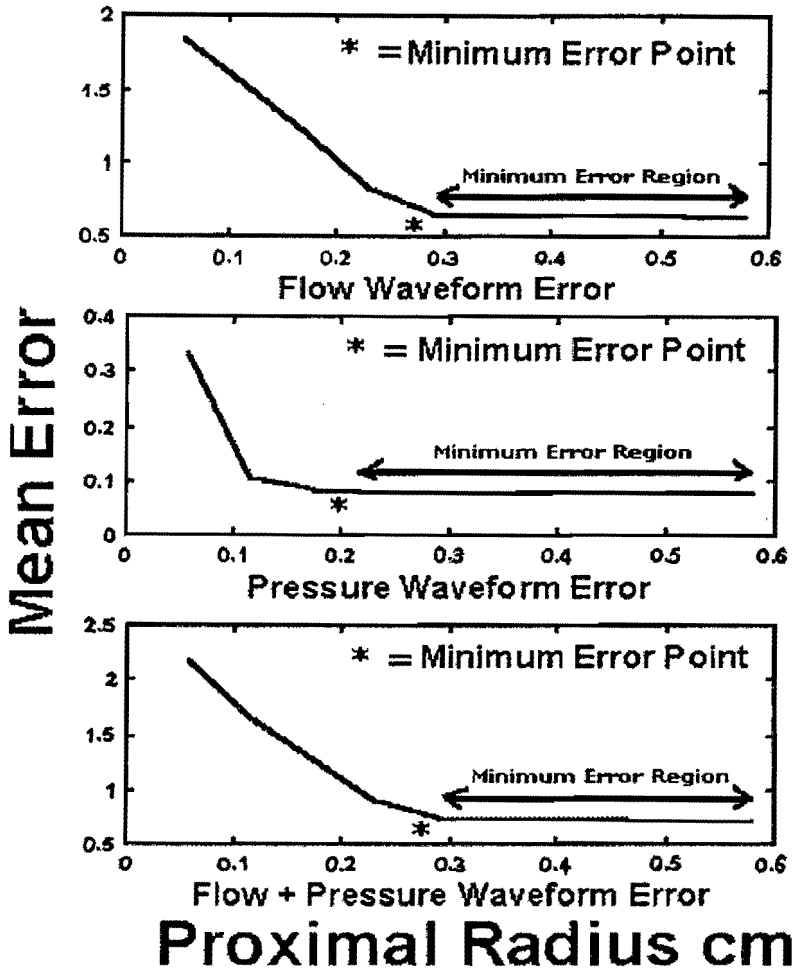

Figure 9.4: *Error Graphs* between Predicted and Actual Flow and Pressure waveforms for a normal human subject. The * represents the Minimum Error point (note that radii above 0.45 cm were not included in the determination of the Minimum Error Point because they were out of the normal physiological range for this simulation). The Minimum Error region is represented by the double arrowhead line.

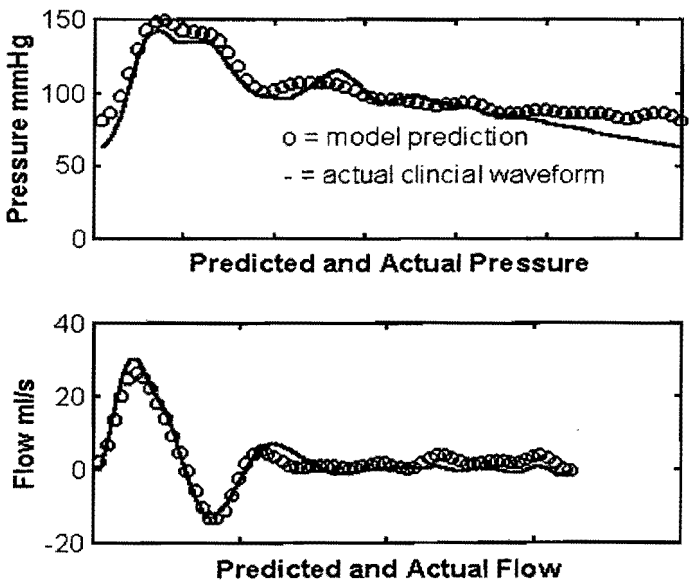

Figure 9.5 : Predicted and Actual *Waveform Graphs* of a normal human subject, plotted at the minimum error point (external iliac radius = 0.29 cm) of the Flow Error Graph shown in Figure 9.4

In addition to the sample region radius, the Inverse Model also provides information about the *distal arterial region*. This information is available in two forms :

1. Decomposition of total flow and pressure waves into their forward and reverse travelling (reflected) components [Figure 9.7-9.8]
2. The distal impedance spectrum. [Figure 9.6]

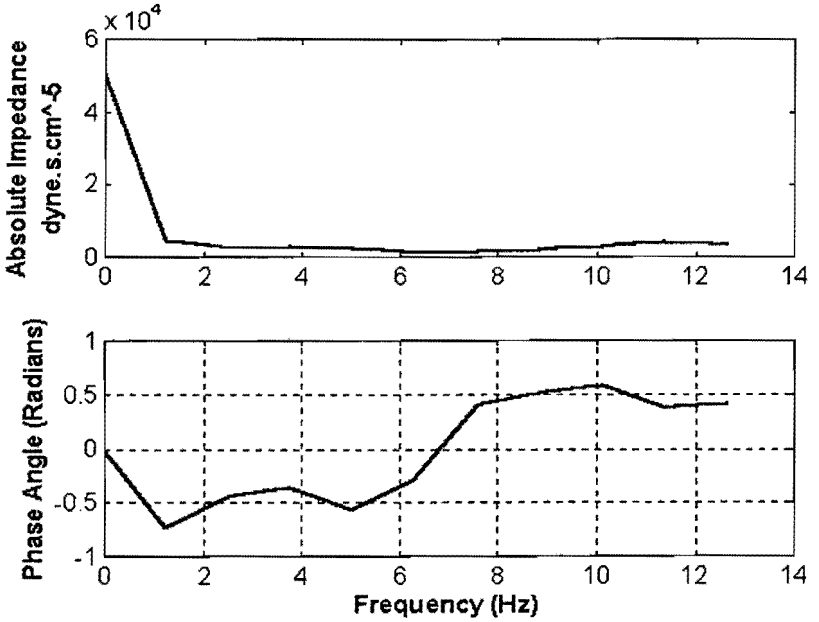

Figure 9.6 : Computer Simulated Normal External Iliac Artery Impedance Spectrum at a heart rate of 75 bpm.

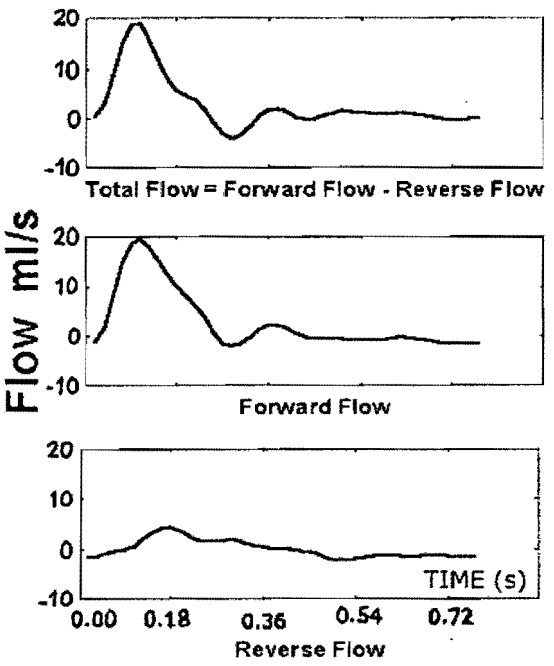

Figure 9.7 Computer Simulated Normal Ext.Iliac Flow Waveforms

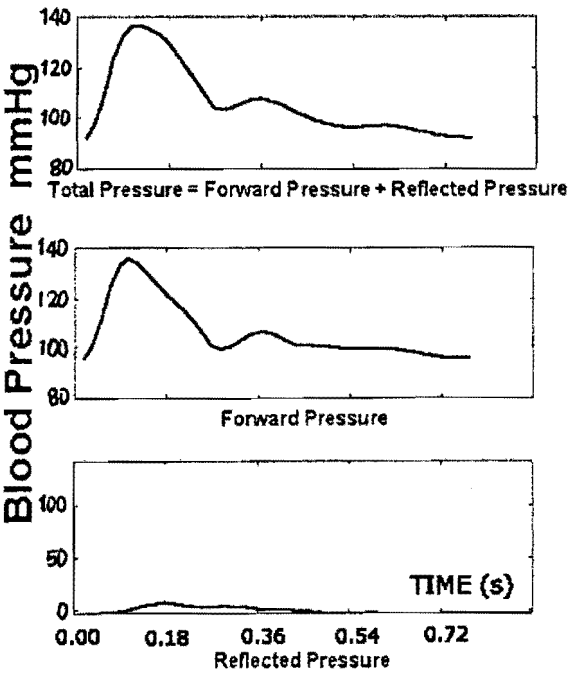

Figure 9.8 Computer Simulated Normal Ext.Iliac Pressure Waveforms

Some clinical information about the Pre-Sample Region is also available . The 'foot-to-foot' [Milnor, 1980] aortic wave time delay may be estimated by measuring the time difference between the aortic root waveforms, and the corresponding external iliac blood pressure or blood flow waveforms.

It is important to note that the 'foot to foot' method gives different results for pressure and flow waves. The time delays in Figures 9.10 and 9.11 illustrate this. In both these figures, the time resolution was limited to 18.5ms in order to correspond to the sample time of the data acquisition equipment that was used for the Preliminary Clinical Feasibility Study (Chapters 10-15). The Flow Wave Pulse delay was 130ms, whilst the same delay measured using Pressure waves was 93ms. The theoretical delay, using the Moens-Korteweg equation and Table 5.1, was 104ms.

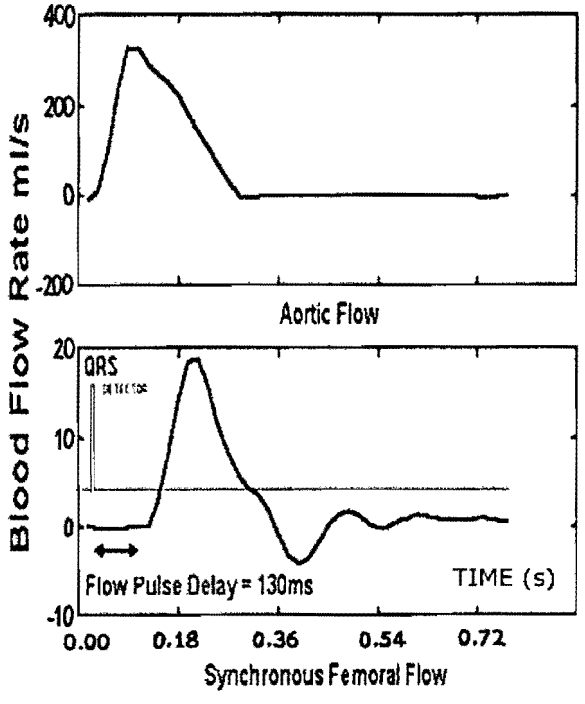

Figure 9.10 Computer Simulated Normal Aorta-to-Ext.Iliac Flow Pulse Arrival Time

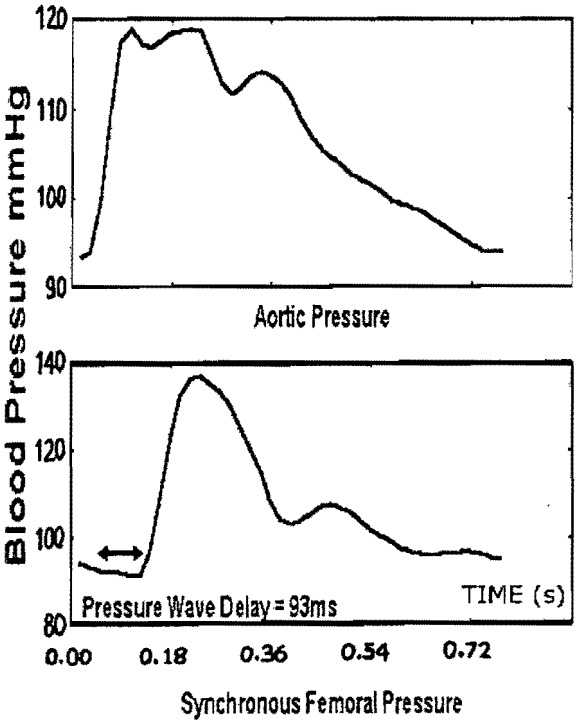

Figure 9.11 Computer Simulated Normal Aorta-to- Ext.Iliac Pressure Pulse Arrival Time

The time delay depends on the aortic and iliac artery length; compliance; and radius . The effects of age and height on arterial length were discussed in greater detail in Chapter 6 . 'Apparent time delay' depends on the method and the waveforms (i.e. pressure or flow) used.

The aortic wave velocity is discussed in Chapters 5 and 13. At this stage, it is important to note that clinically measured time delay information, may be used to improve on the estimation of the state of the Pre-Sample circulation and thereby improve the accuracy of the Inverse Model.

Whilst an accurate Error Function would be an important component of the Inverse Model, it is not a prerequisite of the Inverse Model. Waveform fits based on statistical criteria (e.g. MLE analysis) may yield a plausible solution to the error graph question. Indeed such statistical waveform fitting techniques may even provide a method of including spectral broadening (modelled as an increase in statistical variance) effects in an electrical analogy.

CHAPTER 10
COMPUTER SIMULATED VALIDATION OF THE INVERSION OF THE FORWARD MODEL

The Sample Region (external iliac artery) radius prediction of the Inverse Model was evaluated by using a computer simulated 'patient'. The 'patient' was represented by the Forward Arterial Model (Chapters 2-5). Atherosclerosis was simulated by reducing the arterial radius of various segments and increasing the sample region Young's Modulus. The simulated external iliac Flow and Pressure waveforms were then used as inputs to the Inverse Model. This procedure allowed a comparison of actual data to predicted data, in an ideal computer simulated situation.

The ability of the Inverse model to track variation in Sample Region radius; its sensitivity to the assumptions discussed in Chapter 9; and it's robustness in fitting waveforms which may have amplitude scaling 'noise' were investigated.

10.1 CHAPTER OBJECTIVES

The specific chapter objectives are presented according to their section numbers:

10.2 To investigate the sensitivity of the External Iliac radius prediction of the Inverse Model, to simulated arterial stenosis in three different regions of the human arterial tree.

- 10.2.1 Stenosis in the Pre-Sample Region
- 10.2.2 Stenosis in the Sample Region
- 10.2.3 Stenosis in the Distal Region

10.3 To investigate the sensitivity of the External Iliac radius prediction of the Inverse Model, to simulated variation in the External Iliac Young's Modulus.

10.4 To investigate the sensitivity of the External Iliac radius prediction of the Inverse Model, to simulated amplitude 'distortion' of the External Iliac flow and pressure waveforms.

10.2 ARTERIAL RADIUS DETECTION BY THE INVERSE MODEL

The pressure and flow waveforms from the Arterial Sample Region are affected, not only by the arterial properties within the Sample Region itself, but also by the arterial properties both upstream (the Pre-Sample Region) and downstream (the Distal Region) from the Sample segment.

It is an underlying assumption of the Three Division Inverse model that the Pre-Sample region may be treated as normal. Although the Inverse Model represents the Distal region as a clinically measured impedance spectrum, it is also possible that arterial stenosis in the Distal Region may influence the waveforms measured at the Sample Region, in such a manner that it mimics the effects of a Sample Region stenosis. The ability of the Inverse model to accurately predict the External Iliac radius in the presence of independent Pre Sample and Distal Region stenosis; combined Sample and Distal Region stenosis; as well as independent Sample Region stenosis, is a indication of its suitability for the clinical diagnosis of arterial disease.

If the Inverse Model is too sensitive to co-existing stenotic arterial disease, or variation, outside of the Sample Region then it would be unsuitable for Clinical application. If this is true then it would also indicate that the underlying assumptions of the Three Division Inverse Model are unrealistic. Clinical patients may have a variety of combinations of co-existing and widespread arterial disease, and may also present with a variety of different yet normal, arterial states.

10.2.1 STENOTIC DISEASE IN THE ARTERIAL PRESAMPLE REGION

OBJECTIVE : One of the assumptions of the *Three-Division* Inverse Model is that the Pre-Sample Region was normal. The *sensitivity* of the Inverse Model to this assumption, was tested by simulating stenotic disease in the Pre-Sample Region, and investigating the ability of the Inverse Model to resolve the Sample Region arterial State.

METHOD : The Forward Model was used to generate Pressure and Flow waveforms which were sampled from the External Iliac region in the Right leg. A stenosis was simulated in each of the 10 arterial segments [see Figure 2.3] that represent the aorta and common iliac artery, one at a time, and the Inverse Model was then used to predict the External Iliac arterial radius from the Pressure and Flow waveforms that were generated. (i.e. no sample region stenotic disease). As each block was stenosed, the preceding block was 'unstenosed'. This process has been termed 'sliding stenosis' . At each simulated instance of Pre-Sample Region stenosis, the Inverse Model was used to predict the corresponding External Iliac radius. Ideally, the External Iliac radius prediction should be independent of the stenoses in the Pre-Sample Region.

Sliding stenosis of 3 different radial severities were simulated (40%, 50%, and 60% diameter stenosis ... see Figure 10.1, 10.2, 10.3 respectively). The length of the stenoses corresponded to the pre-defined length of the stenosed segment [Table 2.3] so the 10 Pre-Sample Segments had different lengths. This non-uniformity of simulated stenosis length influences the results of the test, as the haemodynamic severity of a stenosis is determined by the degree of stenosis, as well as the *length* of the occlusion.

RESULTS : The results from inserting a stenosis in each segment of the aorta and the common iliac artery on the estimate of the External Iliac radius using the Inverse Model are illustrated in Figures 10.1 - 10.3.

The Inverse Model predicted a range of arterial diameters rather than one specific radius. The range of prediction was represented by error bars[1] which correspond to the Minimum Error Region illustrated in Figure 9.4.

---

[1] The error bars delimit a stable haemodynamic range. External iliac arterial radii within this range produce Pressure and Flow waveforms which are very similar to that produced by any other discrete radius within that same range. Therefore from a haemodynamic analysis viewpoint it is virtually impossible to distinguish between radii that exist in this stable region. It is important to note that this is not an artefact of the arterial model, but rather it is a phenomena of the human arterial system. Indeed for the clinical investigator the issue is not the actual physical radius of an arterial region, but rather the haemodynamic effect of a radius or range of radii. Therefore for the purpose of clinical diagnosis the accuracy of estimation of the arterial radius is unimportant compared to the estimation of the "effective haemodynamic radius". The effective haemodynamic radius in this context refers to any radius within a range of radii that produce the same haemodynamic effect. This is similar to the previously discussed concept of "critical stenosis".

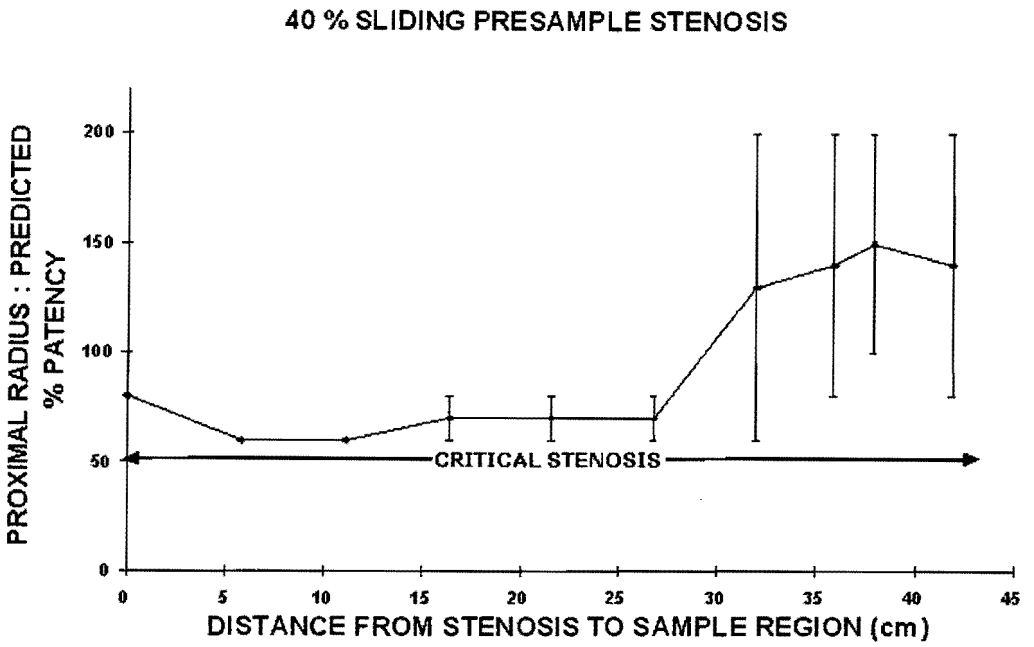

Figure 10.1 Sample Region Radius prediction with a 40% Pre-Sample Region stenosis (i.e. 60% patency) at various distances from the Sample Region. A predicted sample region patency of 100% refers to the radius predicted by the Inverse Model being equal to the actual simulated radius. Error bars $^{1 - P99}$ define a range of possible radii predicted by the Inverse Model. The critical stenosis line defines a theoretical radius above which an artery is considered to be physiologically normal, and below which is considered to be physiological stenosis.

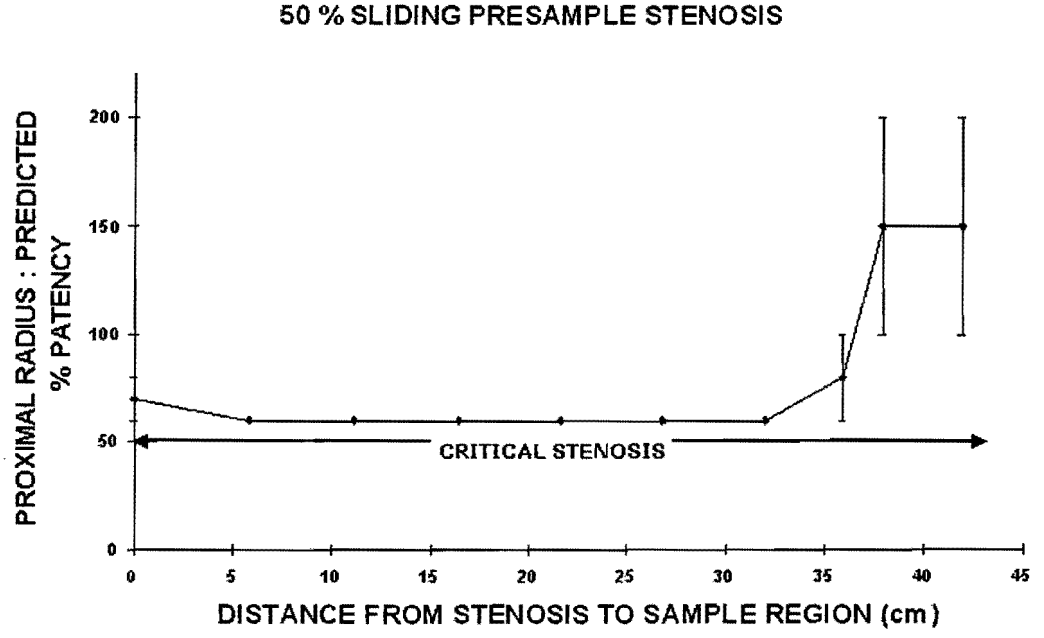

Figure 10.2 Sample Region Radius prediction with a 50% Pre-Sample Region stenosis (i.e. 50% patency) at various distances from the Sample Region. A predicted Sample Region patency of 100% refers to the radius predicted by the Inverse Model being equal to the actual simulated radius. Error bars $^{1 - P99}$ define a range of possible radii predicted by the Inverse Model. The critical stenosis line defines a theoretical radius above which an artery is considered to be physiologically normal, and below which is considered to be physiological stenosis.

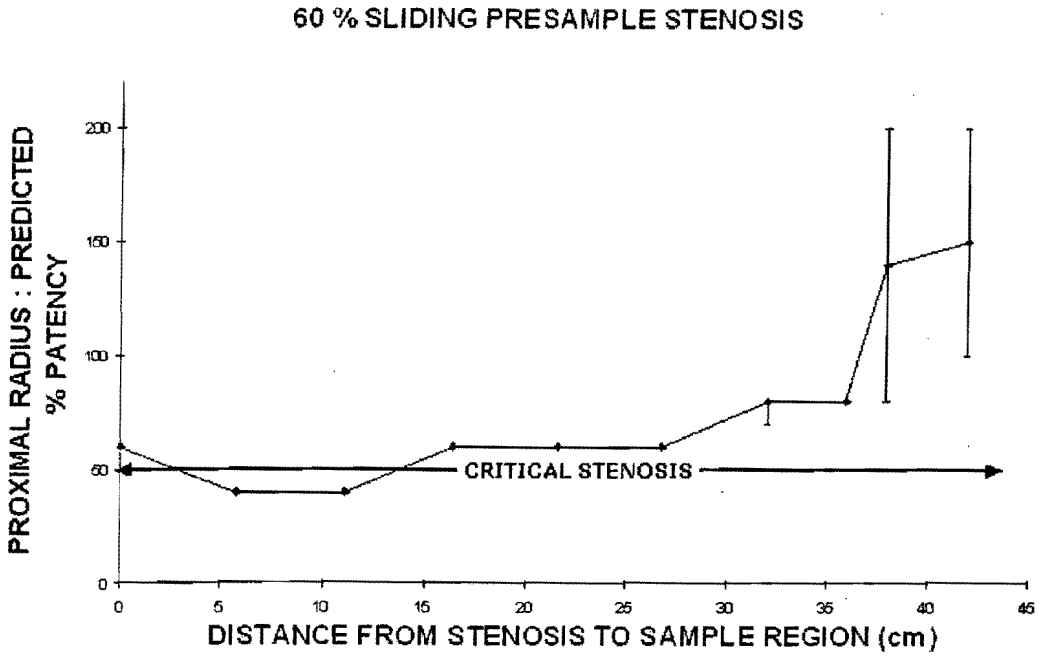

Figure 10.3 Sample Region Radius prediction with a 60% Pre-Sample Region stenosis (i.e. 40% patency) at various distances from the Sample Region. A predicted Sample Region patency of 100% refers to the radius predicted by the Inverse Model being equal to the actual simulated radius. Error bars $^{1 - P99}$ define a range of possible radii predicted by the Inverse Model. The critical stenosis line defines a theoretical radius above which an artery is considered to be physiologically normal, and below which is considered to be physiological stenosis.

DISCUSSION: The critical stenosis line drawn in all three graphs [Figures 10.1-10.3] provides a point of reference to the interpretation of the experimental results (Further discussion on the concept of critical stenosis is included in Appendix V). If the Inverse Model predicts a radius below this line as a result of the influence of an upstream stenosis, then this prediction may be considered to be in error. However if the upstream stenosis influences the Inverse Model prediction, but that prediction is still above the critical stenosis line, then the prediction is acceptable because it would still result in a correct classification of the Sample Region as "haemodynamically normal".

All three experimental graphs [Figure 10.1-10.3] illustrate the general trend, that the greater the distance a stenosis occurs upstream from the Sample Region, the lesser its influence on the prediction of the External Iliac artery radius by the Inverse Model. The exception to this trend is the region close to the aorto-iliac bifurcation, which is 5.8 cm upstream from the Sample Region (predefined to be Segment 92 in Figure 2.3, Table 2.3, and Figure 4.3). Of all the segments in the Pre-Sample Region , the aorto-iliac bifurcation appears to have the most influence on the Inverse Model.

It is apparent from Figures 10.1-10.3 that stenoses in the Pre-Sample Region do influence the predictions of the Inverse Model. However it is also apparent that as long as the Pre-Sample Region stenosis is sub-critical (i.e. less than 50 % diameter stenosis) it does not induce a false prediction by the Inverse Model (see Figures 10.1 – 10.2). A "false prediction" in this context refers to a false prediction of critical (or greater) Sample Region stenosis by the Inverse Model. If the Pre-Sample Region stenosis is critical [see Figure 5.3] then, depending on its physical location, it may induce a false prediction by the Inverse Model.

The Inverse Model therefore appears to be relatively insensitive to mild stenotic disease in the aortic or aortic-iliac region. However the Inverse Model may become unreliable in the presence of severe aorto-iliac disease .

10.2.2 STENOTIC DISEASE IN THE ARTERIAL SAMPLE REGION

OBJECTIVE :The Inverse Model has been designed to predict the External Iliac (Sample Region) arterial radius, therefore the ability of the Inverse Model to track variation in this radius was tested.

METHOD : A range of External Iliac arterial stenoses were simulated using the Forward Model. The arterial segment that was stenosed was the Right External Iliac artery corresponding to Arterial Segment 92 in Figure 2.3, Table 2.3, and Figure 4.3. The Pressure and Flow waveforms measured from this segment were then supplied to the Inverse Model for analysis. The actual radius (Forward Model) was compared to the predicted radius (Inverse Model). For these tests both the Pre-Sample and Distal regions were simulated as 'normal'.

RESULTS : The experimental results of External Iliac radius tracking by the Inverse Model are presented in Figure 10.4. Error bars $^{1\text{-}P99}$ delimit the range of predicted radii for each discrete actual radius.

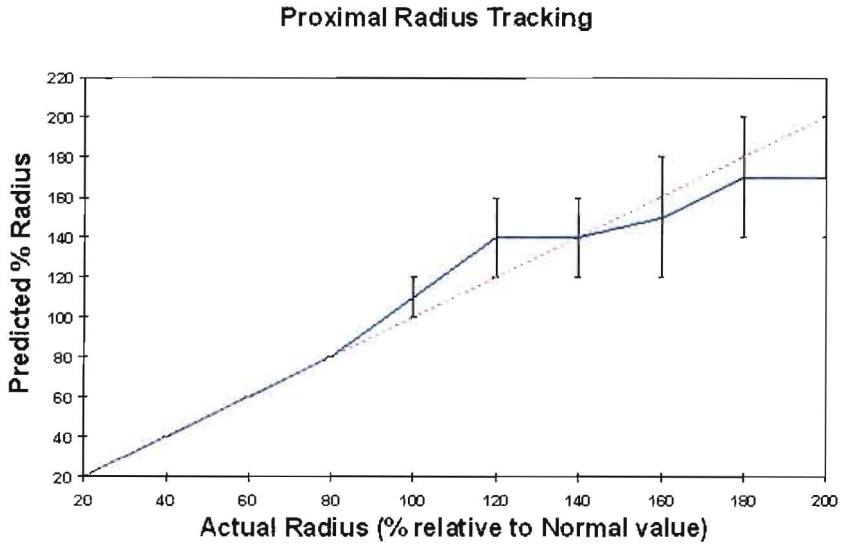

Figure 10.4 Sample Region Radius tracking by the Inverse Model. The solid line represents the predictions of the Inverse Model (i.e. the predicted radius), whilst the dashed line represents ideal tracking (i.e. where predicted radius = actual radius). Error bars $^{1 - P99}$ indicate that the Inverse Model has predicted a range of radii rather than a single radius. Radius was varied in discrete steps of 20%.

DISCUSSION : The point of reference for interpretation of the results presented in Figure 10.4 is the "ideal tracking" line (i.e. the dashed line). If the predicted discrete radius lies on this line or the predicted range of radii (delimited by error bars) includes this line, then is may be concluded that the predictions are correct. Any prediction of a range of radii or a discrete radius that excludes the ideal tracking line may be considered to be an incorrect prediction.

Therefore it is apparent from the experimental results that the Inverse Model is capable of accurately tracking changes in the External Iliac radius because none of its predictions exclude the ideal tracking line. Error bars, which indicate a haemodynamically stable region, are only present in experimental radii with a patency of 80% or more. For simulated radii with less than 80% patency the Inverse Model predicts a radius exactly equal to the simulated radius. This indicates that the Inverse Model is ideally suited to the tracking of an isolated stenosis in the External Iliac artery.

10.2.3 STENOTIC DISEASE IN THE DISTAL ARTERIAL REGION

The state of the Distal Region also affects the haemodynamic waveforms at the Sample Region. The Distal Region provides the load impedance for the Sample Region, and this impedance also includes the effects of reflected pressure and flow waveforms. Stenosis of arteries in the Distal Region results in changes in the Distal Impedance Spectrum, as well as the in the haemodynamic waveforms measured at the Sample Region.

Theoretically, distal disease cannot affect Sample Region predictions. This is because the distal region was modelled as a steady state impedance, defined using measured Sample Region flow and pressure waveforms. However it is theoretically possible that Distal stenoses may induce changes in the Sample Region haemodynamic waveforms that may be indistinguishable from changes induced by Sample Region stenoses.

OBJECTIVE : To confirm the ability of the Inverse Model to track the state of the Sample Region, independent of any variation in the Distal Region.

METHOD : A severe 80% diameter stenosis (i.e. 20% patency) was in turn , inserted into each of the 13 arterial segments in the Distal Region of the Forward Model. These distal segments correspond to the segments numbered : 99; 106; 107; 110; 112; 114; 117; 122; 118; 123; 127; 124; and 128 in Figure 2.3, Table 2.3, Figure 4.3, and Figure 10.5 . The simulated Pressure and Flow waveforms corresponding to an 80% stenosis at each of these segments were then analysed by the Inverse Model which predicted the External Iliac radius.

At each instance of Distal stenosis, the Sample region was also stenosed. This simulated co-existing Distal and Sample Region stenosis.

RESULTS : The effect of the sliding Distal stenosis on the External Iliac radius prediction is plotted in Figure 10.5. Note that for Figure 10.5 the simulated External Iliac (Forward Model) was 100% patent. Table 10.1 shows the same test repeated for 4 additional degrees (80%,60%,40%, 20% patency) of External Iliac stenosis.

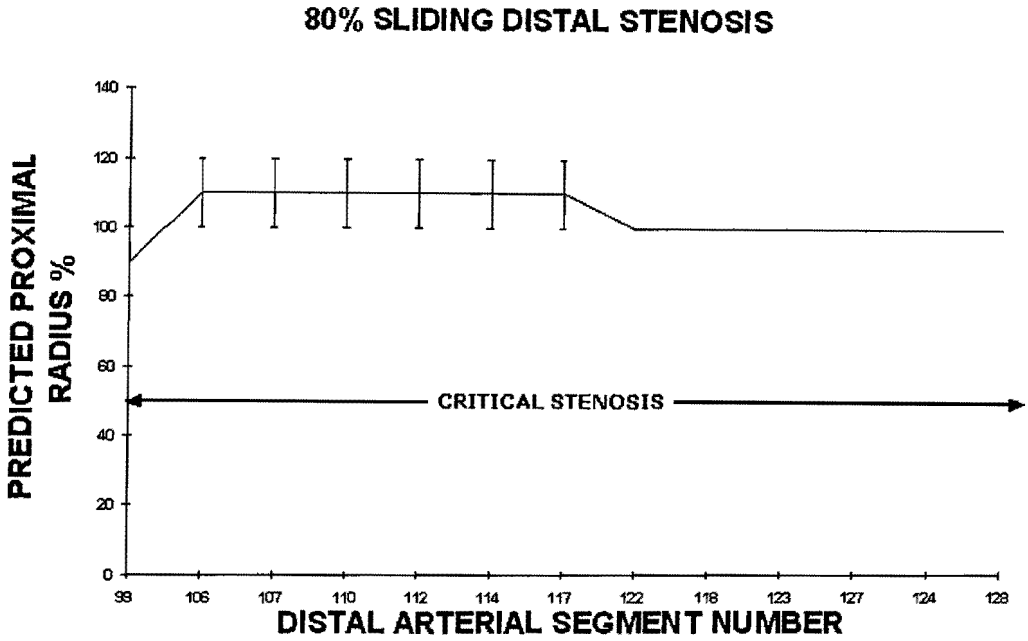

Figure 10.5 : Sample Region Radius tracking, with 80% distal stenosis inserted in turn into each of the 13 distal arterial segments. The abscissa lists the number of the distal arterial segment that was stenosed. These numbers correspond to the arterial segments in Figure 2.3, Table 2.3, Figure 4.3, and Figure 10.5 . The ordinate lists the predicted percentage patency of the External Iliac artery (i.e. arterial segment number = 92)

	External Iliac (Segment 92) Patency				
	100%	80%	60%	40%	20%
Distal Segment Number					
99	90%	40 -80 %	40 -60%	40 -60%	20%
106	100 -120 %	80 -120 %	60 -120%	40%	20%
107	100 -120 %	80 -120 %	60 -120%	40%	20%
119	100 -120 %	80 -120 %	60 -120%	40%	20%
112	100 -120 %	80 -120 %	60 -120%	40%	20%
114	100 -120 %	80 -120 %	60 -120%	40%	20%
117	100 -120 %	80 -120 %	60 -120%	40%	20%
122	100%	80 -120 %	60 -120%	40%	20%
118	100%	80 -120 %	60 -120%	40%	20%
123	100%	80 -120 %	60 -120%	40%	20%
127	100%	80 -120 %	60 -120%	40%	20%
124	100%	80 -120 %	60 -120%	40%	20%
128	100%	80 -120 %	60 -120%	40%	20%

Table 10.1 : Distal Region arterial stenosis (80% sliding stenosis) vs. Sample Region arterial stenosis. The rows represent the numbered distal segments which were each simulated with an 80% stenosis. The columns represent the simulated co-existing stenosis in the Sample Region tabulated as a patency (100% - 20% patency). The data represents the corresponding Sample Radius prediction of the Inverse Model written as a percentage patency. A range of predictions represents the "minimum error region". The case for a 100% Sample Region is also illustrated in Figure 10.5 with the error bars$^{1 - P99}$ used to represent a predicted range of radii.

DISCUSSION : The results presented in Figure 10.5 illustrate that the Inverse Model is able to accurately resolve the normal External Iliac radius under conditions of distal stenosis. The distal segment that has the most influence on the predictions of the Inverse Model is arterial segment number 99. This is the arterial region that is downstream-adjacent to the Sample Region, and is *also* called the External Iliac in Figure 2.3, Table 2.3, Figure 4.3, and Figure 10.5, but is more commonly referred to in the Medical Literature as the "Common Femoral" artery.

The results presented in Table 10.1 illustrate the performance of the Inverse model under various combinations of co-existing Distal and Sample Region disease. Note that whilst the severity of Distal disease is fixed at 80% stenosis and its location is varied, the location of the Sample Region disease is fixed but its severity is varied from 100% - 20% patency (i.e. 0% - 80% stenosis). It is apparent that the Inverse Model is able to accurately resolve the Sample Region radius under all simulated conditions of External Iliac stenosis provided that the severe co-existing Distal stenosis lies below the bifurcation of the Common Femoral artery (Segment 99) into the Profunda Femorus (Segment 106) and Superficial Femoral (Segment 106) arteries. Under conditions of severe stenotic disease (80% stenosis) downstream-adjacent from the External Iliac with mild (80%-60% patency, i.e. sub-critical stenosis) co-existing External Iliac stenosis, the Inverse Model would incorrectly predicts a range which includes and above-critical (ie. 40%-80% patency in Table 10.1) Sample Region stenosis. This specific type of false prediction is not a major flaw because it only occurs when there is severe stenotic disease directly adjacent to the site from which the Pressure and Flow waveforms are acquired. Therefore the Inverse Model still correctly predicts a critical stenosis but incorrectly predicts the precise location of that critical stenosis. However the location error is only between 0-6 cm directly downstream from the measurement site. Under conditions of severe External Iliac stenosis (40% - 20% patency) with severe co-existing Distal stenosis, the Inverse Model is able to accurately track the External Iliac radius.

Therefore the Inverse Model is robust in the presence of co-existing Sample Region and distal stenosis. The only condition that may 'confuse' the model is a severe downstream-adjacent stenosis which the Inverse Model confuses with Sample Region stenosis.

10.3 VARIATION IN SAMPLE REGION YOUNG'S MODULUS

One of the approaches to reducing the number of variables in the Transmission Line based Arterial Model was to convert the Sample Region Young's Modulus from an unknown to an *'approximated known'* , equal in value to the physiologically normal static Young's Modulus [Table 2.3].

Stenotic arterial disease results in an increased Young's Modulus (i.e. stiffer walls) and wall thickness (i.e. thicker walls), and a reduced arterial radius. For each arterial segment (of a predefined length) this results in 3 variables (unknowns) changing (i.e. Young's Modulus, Wall Thickness, and Radius). Young's Modulus and Wall thickness are only modelled by the Capacitive component of the Electrical Analogue [Equation 1.7]. In fact, because they are multiplied together , a stenosis with its corresponding increase in Young's Modulus *and* Wall thickness, may be modelled as a larger Young's Modulus with the same Wall Thickness, and vice versa. Therefore all test results , relating to a simulated increase in Young's Modulus, are also valid in identifying trends related to increased arterial Wall Thickness.

OBJECTIVE : To investigate the influence of computer simulated variations in the External Iliac Young's Modulus, on the External Iliac radius prediction of the Inverse Model.

METHOD : The Young's Modulus of the External Iliac (Segment 92) in the Forward Model was multiplied by a scaling factor, in order to simulate arterial wall hardening. Although the study of arterial aneurysms is not a focus of this thesis, a 90% decrease (i.e. scaling factor = 0.1) in Young's Modulus was also simulated. Twelve simulations were carried out :

aneurysm		scaling factor	=	0.1	(10%)
normal		scaling factor	=	1	(100%)
progressive	*stenosis*	scaling factors	=	2 - 10	(200-1000%)

RESULTS : The effects of varying the simulated External Iliac Young's modulus, in such a manner, on the predicted External Iliac radius are illustrated in Figure 10.6. Note that for Figure 10.6 the simulated External Iliac (Forward Model) was 100% patent. Table 10.2 shows the same test but also repeats this test for 4 additional degrees (80%,60%,40%, 20% patency) of External Iliac stenosis.

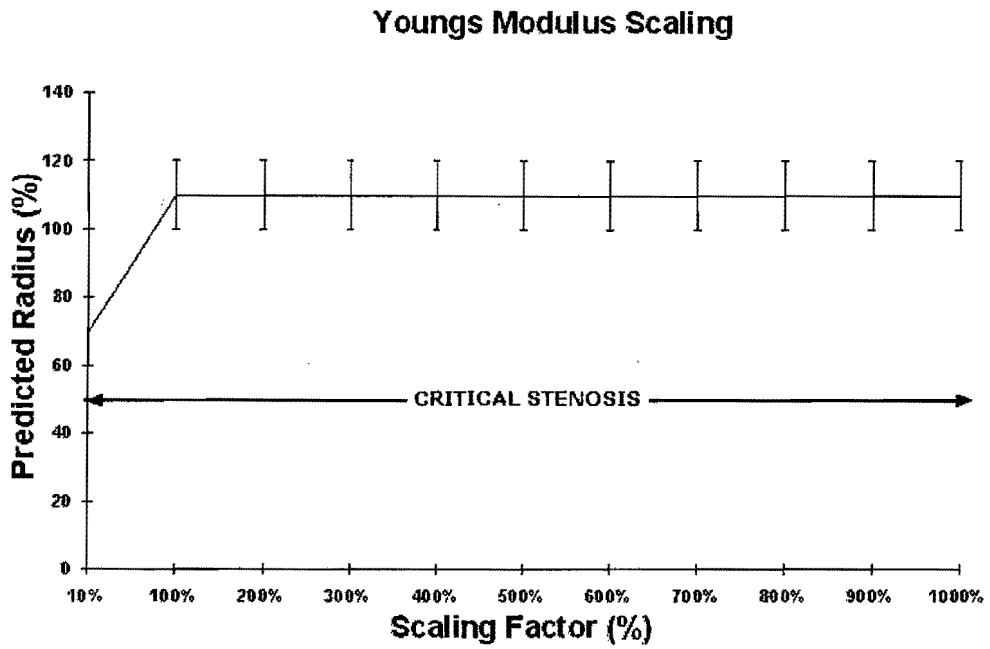

Figure 10.6 : The effect of variations in the Young's Modulus of the External Iliac artery on the predictions of the Inverse Model.

	External Iliac (Segment 92) Patency				
	100%	80%	60%	40%	20%
Scaling Factor in External Iliac (Segment 92)					
0.1	60 - 80 %	60 -80 %	60%	40%	20%
1	100 -120 %	80%	60%	40%	20%
2	100 -120 %	80%	60%	40%	20%
3	100 -120 %	80%	60%	40%	20%
4	100 -120 %	80%	60%	40%	20%
5	100 -120 %	80%	60%	40%	20%
6	100 -120 %	80%	60%	40%	20%
7	100 -120 %	80%	60%	40%	20%
8	100 -120 %	80%	60%	40%	20%
9	100 -120 %	80%	60%	40%	20%
10	100 -120 %	80%	60%	40%	20%

Table 10.2 : Sample Region Young's Modulus scaling factor vs Sample Region arterial stenosis. The rows represent the scaling factors applied to the Young's Modulus. The columns represent the simulated co-existing stenosis in the Sample Region tabulated as a patency (100% - 20% patency). The data represents the corresponding Sample Radius prediction of the Inverse Model written as a percentage patency. A range of predictions represents the "minimum error region". The case for a 100% Sample Region is also illustrated in Figure 10.6 with the error bars $^{1-P99}$ used to represent a predicted range of radii.

DISCUSSION : From Figure 10.6 and Table 10.2 , it is apparent that an increase in Young's Modulus (from normal or 100%, to 1000%) has no influence on the External Iliac Radius prediction of the Inverse Model when the External Iliac is either normal (100% patent) or progressively stenosed (80% - 20% patent). Therefore, under normal as well as stenotic disease conditions, the Young's Modulus of the External Iliac artery (i.e. common femoral artery), has no influence on the External Iliac Radius prediction (and indeed the Sample Region haemodynamic waveforms). Young's Modulus therefore, may be justifiably defined to be a physiological constant, without any negative influence on the accuracy of an electrical transmission line model of the arterial system.

It should be noted however, that decreasing the Young's Modulus (to 10% of its 'normal' value), for subjects with normal (100% - 80% patency) External Iliac arteries appears to have a some influence on the Inverse Model predictions. This implies that an aneurysm with a highly compliant wall, close to the site of measurement, may adversely influence the accuracy of the Inverse Model.

10.4 AMPLITUDE SCALING OF FLOW AND PRESSURE WAVEFORMS

Under computer simulated conditions the exact Flow and Pressure waveforms are always available. In the case of clinically measured waveforms however, the non-invasive techniques used may introduce a scaling error. For instance, if a Doppler technique is used, the Flow waveform may vary in amplitude depending on the angle between the Doppler probe and the arterial vessel. Incomplete insonation of an artery may also result in amplitude distortion (and probably also shape distortion). In addition the underdetermined version of the Inverse Model (Chapter 11.4) introduces amplitude distortion because it requires the estimation of waveform amplitudes (which could not be measured). The ability of the Inverse Model to handle this type of amplitude scaling error would be a good indicator of its suitability for clinical implementation, and would also indicate whether the underdetermined version of the Inverse Model is capable of producing meaningful results despite its obvious limitations. Therefore these tests also assess the sensitivity of the Inverse Model to waveform shape (rather than waveform amplitude).

OBJECTIVE : To test the performance of the Inverse Model, given amplitude scaled Flow and Pressure waveforms.

METHOD : Flow and Pressure waveform distortion was simulated by amplitude scaling the simulated waveforms from -50% to +50% in steps of 10%, prior to analysis of those waveforms by the Inverse Model. These tests were carried out for 6 levels of patency (100%; 80%; 60%; 40%; 20%) of the External Iliac.

Thus there were 22 simulations for each discrete External Iliac radius, 11 each for Flow as well as Pressure Waveforms. The results of these tests with a normal (100% patent) External Iliac artery are illustrated in Figures 10.7-10.8.

The test results for all levels of External Iliac patency are tabulated in Table 10.3–10.4.

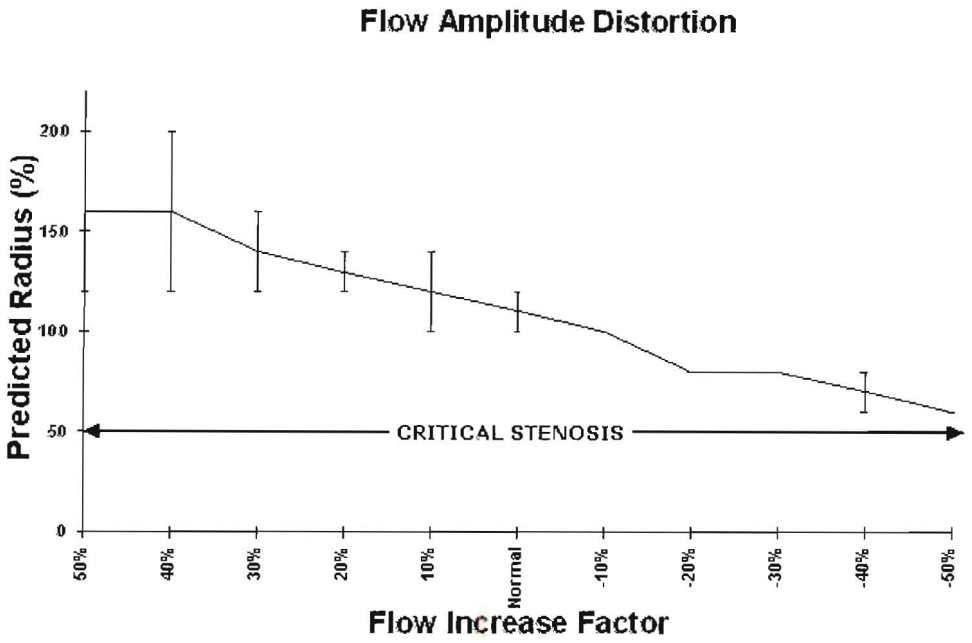

Figure 10.7 The effect of amplitude-scaling of simulated Flow Waveforms on the prediction of External Iliac Radius by the Inverse Model.

	External Iliac (Segment 92) Patency				
	100%	80%	60%	40%	20%
Flow Amplitude Scaling Factor					
+50%	120 - 200 %	120 - 200 %	80%	40%	20%
+40%	120 - 200 %	120 - 180 %	80%	40%	20%
+30%	120 -160 %	100 - 140 %	80%	40%	20%
+20%	120 -140 %	100 - 120 %	60 -80%	40%	20%
+10%	100 -140 %	80 -120 %	60%	40%	20%
normal	100 -120 %	80%	60%	40%	20%
-10%	100%	80%	60%	40%	20%
-20%	80%	80%	60%	40%	20%
-30%	80%	60%	60%	40%	20%
-40%	60 - 80 %	60%	60%	40%	20%
-50%	60%	60%	40%	40%	20%

Table 10.3 : Flow Amplitude scaling factor vs Sample Region arterial stenosis. The rows represent the scaling factors applied to the Blood Flow waveform. The columns represent the simulated co-existing stenosis in the Sample Region tabulated as a patency (100% - 20% patency). The data represents the corresponding Sample Radius prediction of the Inverse Model written as a percentage patency. A range of predictions represents the "minimum error region". The case for a normal (ie no amplitude distortion) Sample Region flow waveform is also illustrated in Figure 10.7 with the error bars $^{1\text{-}P99}$ used to represent a predicted range of radii. Note that the shaded results represent a predicted radius or range of radii that does not include the actual radius. The shaded results with dots represents a significant prediction error i.e. the actual and predicted radii lie on either side of the critical stenosis line.

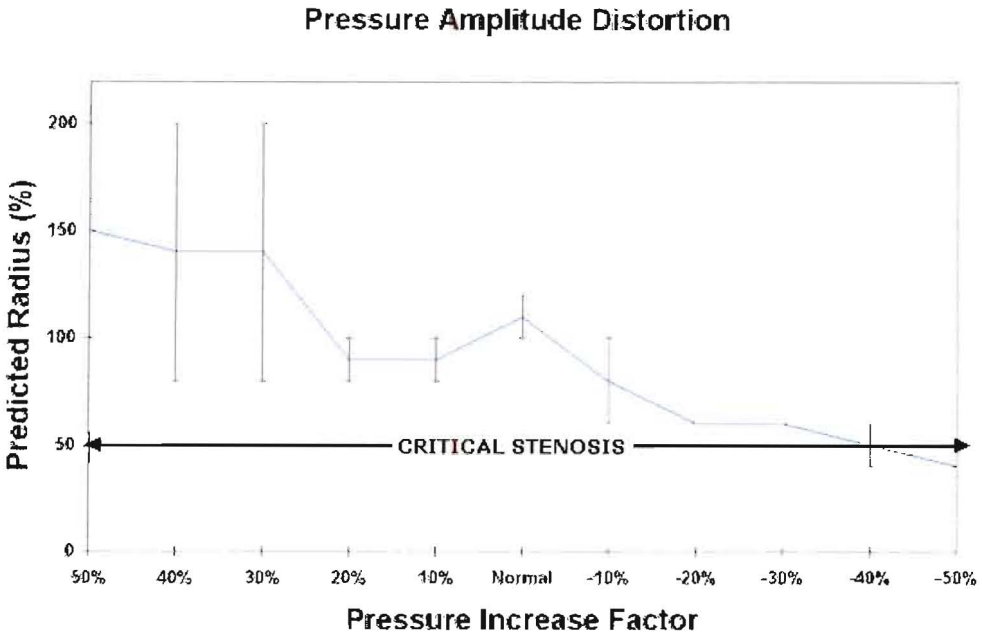

Figure 10.8 The effect of amplitude distortion of simulated Flow Waveforms on the predictions of Sample Region Radius

	External Iliac (Segment 92) Patency				
	100%	80%	60%	40%	20%
Pressure Amplitude Scaling Factor					
+50%	100 -200 %	80 - 200 %	60 -80%	60%	20%
+40%	80 - 200 %	80 - 200 %	60 -80%	40%	20%
+30%	80 - 200 %	80 - 200 %	60 -80%	40%	20%
+20%	80 - 100 %	80 - 200 %	60%	40%	20%
+10%	80 - 100 %	80 - 200 %	60%	40%	20%
normal	100 - 120 %	80%	60%	40%	20%
-10%	60 - 100 %	80%	60%	40%	20%
-20%	60%	60 - 80 %	60%	40%	20%
-30%	60%	60%	60%	40%	20%
-40%	40 - 60 %	40%	60%	40%	20%
-50%	40%	40%	40%	40%	20%

Table 10.4 : Pressure Amplitude scaling factor vs Sample Region arterial stenosis. The rows represent the scaling factors applied to the Blood Pressure waveform. The columns represent the simulated co-existing stenosis in the Sample Region tabulated as a patency (100% - 20% patency). The data represents the corresponding Sample Radius prediction of the Inverse Model written as a percentage patency. A range of predictions represents the "minimum error region". The case for a normal (i.e. no amplitude distortion) Sample Region flow waveform is also illustrated in Figure 10.8 with the error bars $^{1-P99}$ used to represent a predicted range of radii. Note that the shaded results represent a predicted radius or range of radii that does not include the actual radius. The shaded results with dots represents a significant prediction error i.e. the actual and predicted radii lie on either side of the critical stenosis line.

DISCUSSION :

For the case of a normal External Iliac artery, the critical stenosis line in Figures 10.7 - 10.8 provides a line of reference for interpretation of the results of the amplitude scaling tests. Whilst the Inverse Model's response to both Flow and Pressure amplitude distortion does follow a trend, it nonetheless still predicts a less than critical stenosis level for all levels of simulated flow amplitude distortion provided that the Sample Region is normal. Pressure amplitude distortion shows a similar trend but, in this case, if the pressure waveform is reduced by more than 40% (i.e. -40% scaling) a normal radius is incorrectly predicted as a critical stenosis. For the case of a normal External Iliac, the Inverse Model thus appears to be relatively insensitive to amplitude scaling of either the Flow or the Pressure waveforms except in the case of large reduction (>40% reduction) in the pressure amplitude. All other predicted radii (for the case of a normal External Iliac) do not cross the critical stenosis line. The Inverse Model does have a linear trend with respect to amplitude scaling in that the predicted radius is reduced if either the Flow or Pressure amplitudes are reduced, and increased if either of the Flow or Pressure Waveforms are increased.

In the case of pressure or flow amplitude distortion with co-existing External Iliac disease, the results are tabulated in Tables 10.3 – 10.4. The shaded regions indicate under what condition the Inverse Model predicts a radius (or range of radii) that excludes the actual radius.

For all the cases with a haemodynamically normal External Iliac (100%; 80%, 60% patency) flow or pressure amplitude distortion may result in a prediction error (i.e. shaded results in Table 10.3 -10.4). This prediction error is only significant in the case where a radius less than or equal to the critical radius stenosis (i.e. 50% patent and less) is predicted.

This situation (of a significant prediction error) only occurs when the flow or pressure waveforms are significantly reduced by amplitude distortion. In the case of the flow waveform this only occurs with amplitude distortion of -50% when the External Iliac is 60% patent. In the case of the pressure waveform this occurs with amplitude distortion of -40% to -50% for any of the haemodynamically normal ranges considered .

For both levels of stenosis (40% and 20% patency) greater than critical stenosis (50 % patent) the Inverse Model appears to be insensitive to flow amplitude distortion. The same is true for pressure amplitude distortion except in the case for a 40% patent External Iliac radius with the pressure waveform amplitude increased by 50%. In that case the Inverse Model incorrectly predicts a sub-critical radius (60% patent) where the actual radius (40% patent) is greater than critical stenosis.

These results indicate that severe flow or pressure amplitude distortion may result in normals being mis-diagnosed with stenotic disease, but rarely influences the cases for subjects with critical stenosis of the External Iliac. Furthermore it appears that the inverse model is more robust in the presence of positive amplitude distortion than it is in the presence of negative amplitude distortion. This implies that it would be better to over-estimate rather than under-estimate the amplitude of flow or pressure waveforms to be analysed by the Inverse Model.

Practically though, the Inverse Model may be considered to be relatively insensitive to amplitude distortion within 'reasonable' measurement limits. This is important not only because amplitude-scaling represents real clinical artefacts, but also because the underdetermined version of the Inverse Model (Chapter 11) that will be used for the preliminary clinical studies (Chapters 13) also introduces additional amplitude-scaling artefact.

Note that critical stenosis has been defined here in the context of the model. Clinical determination of critical stenosis is a point of much debate. Appendix V introduces the reader to the concept of clinically determining critical stenosis.

CHAPTER 11

A PROTOTYPE HAEMODYNAMIC DATA ACQUISITION SYSTEM FOR USE WITH AN UNDER-DETERMINED VERSION OF THE INVERSE MODEL

A Haemodynamic Data Acquisition System was developed by modifying an existing real time continuous wave Doppler ultrasound system. The system consisted of a Parks Medical Directional Doppler [5MHz and 9.5MHz] Unit; a single lead ECG from a Hellige Patient Monitor; and a non-invasive Millar arterial tonometer interfaced to an 80386 based PC via a Motorola DSP 56000 card. The DSP (Digital Signal Processing) card performs an AR (Auto-Regressive) spectral estimation of the blood velocity signal in addition to handling the tonometric blood pressure and the QRS complex of the ECG [Figure 11.3 and Figure 11.4]. Appendix IX –X provides more technical information.

For the preliminary clinical feasibility study , the External Iliac Artery Doppler Velocity signal as well as the External Iliac Artery Blood Pressure and a single lead ECG (Electrocardiogram) were required (Figure 11.1). A screen capture of the display of the prototype Data Acquisition is shown in Figure 11.2, and a photograph of the system in use is shown in Figure 11.4.

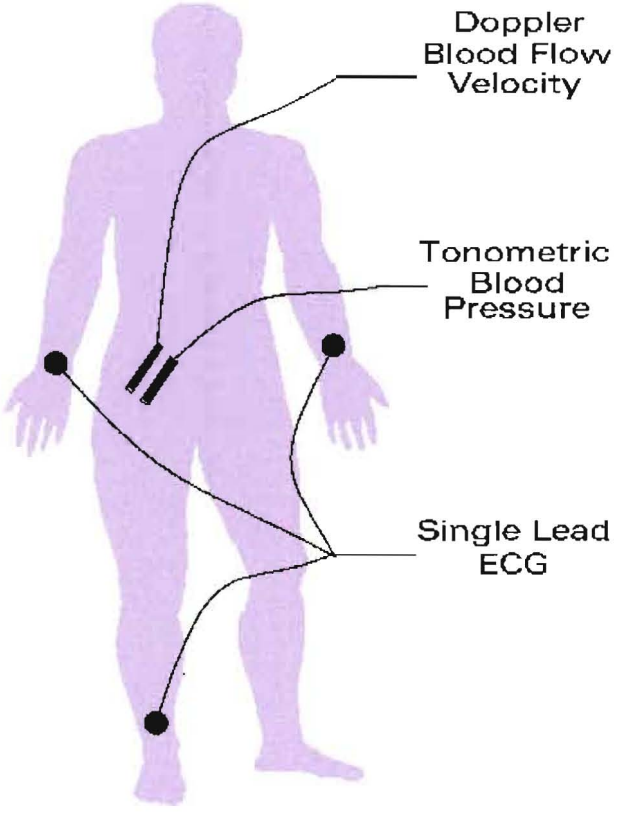

Figure 11.1 : Clinical Subject connected to the prototype Haemodynamic Data Acquisition System via non-invasive electrodes and transducers.

11.1 TRANSDUCERS FOR HAEMODYNAMIC MEASUREMENT

A continuous wave Doppler ultrasound transducer was used for non-invasive acquisition of the External Iliac blood velocity waveform. For subjects with deeper External Iliac arteries, a 5 MHz Doppler probe was used, and for subjects with more superficial arteries a 10MHz Doppler probe was used. Doppler ultrasound measurement is a well established clinical technique. Further details are provided in Appendix IX.

Arterial Tonometry may be used to non-invasively acquire a blood pressure waveform at an arterial pulse point [Drzewiecki et al, 1983; Kelly et al, 1989]. A Millar arterial tonometer was used for this purpose . Although the tonometer provides the shape of the blood pressure waveform, which contains important diagnostic information [Karamanoglu, 1997; O'Rourke et al, 1992] it is not commonly used clinically. However, there have been a number of research studies documenting the performance and use of arterial tonometers [Karamanoglu & Feneley, 1996; Chen et al , 1997]. Further details are provided in Appendix X.

Disposable ECG electrodes were used for the acquisition of a single lead ECG.

11.2 PSEUDO-SYNCHRONOUS DETECTION

Initial tests of the Data Acquisition System in a Clinical setting have highlighted the practical difficulties of non-invasively obtaining the synchronous Blood Pressure and Flow Velocity waveforms by using two separate probes. A custom-designed holder for both the Doppler Ultrasound and Tonometer probes was tested. This multi-probe holder, proved to be too cumbersome for Clinical use, especially with vascular-diseased patients who were already in a great deal of pain. Therefore the constraint of a strictly synchronous data acquisition system was relaxed, and a clinically feasible 'pseudo-synchronous' approach was adopted .

If a subject's heart rate and the state (e.g. peripheral vasodilation / vasoconstriction) of his vascular system do not vary significantly during the data-acquisition procedure, then pseudo-synchronous detection would produce waveforms equivalent to those produced by synchronous detection. Pseudo-synchronous detection, in the context of this study, refers to recording flow and pressure waveforms serially, instead of synchronously. Each waveform was however recorded synchronous with a single lead ECG QRS complex. The waveforms were then pseudo-synchronised offline using the synchronous QRS complex as a reference. Therefore the clinical operator needed to use only one probe at a time [Figure 11.4].

The subject's heart rate was easily assessed by calculating the time intervals between successive QRS complexes. It was, of course, impossible to assess changes in the systemic arterial state. However, for 5-20 minutes prior to testing, and for the duration of the test, the subject was allowed to rest in a supine position. The room temperature was stable and almost no movement was required of the subject. The duration of the test was 15 - 30 minutes per subject. Under such conditions, it is reasonable to assume that the subjects systemic arterial state did not change significantly.

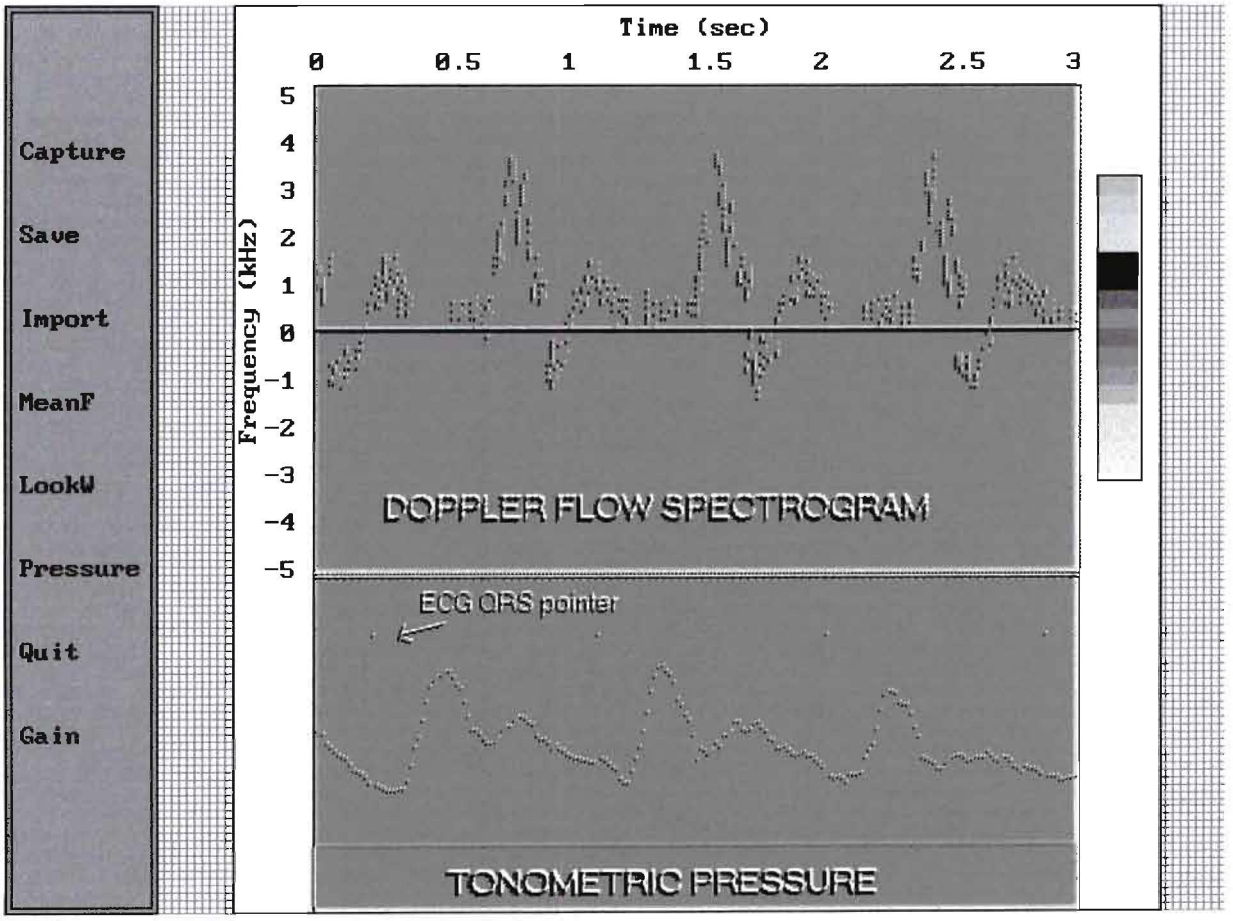

Figure 11.2 : Screen Capture of Normal Subject Waveforms, using the prototype Haemodynamic Data Acquisition System

11.3 QRS DETECTOR AND ANALOGUE ADDER

Relative timing of peripheral blood pressure or blood flow velocity waveforms may be determined by using the ECG R-wave as a reference. The time difference between the R-wave and the upstroke of either a peripheral pressure or blood flow waveform is a measure of the transit time of that waveform, from the Left Ventricle to the peripheral artery. This time difference is also referred to as the Pulse Arrival Time (PAT). Because of bandwidth limitations, the entire QRS complex was used instead of the R-wave. There is also a finite delay between the QRS complex and the start of aortic flow. This cardiac electro-mechanical delay is discussed further in Appendix XIII.

An analogue QRS detector was custom-designed and built [L.R John and M Kao-Wing, unpublished documents] for this purpose [see Figure 11.3]. Because of computational and bandwidth limitations of the existing DSP card, the entire ECG waveform could not be recorded . Therefore the output of the QRS detector was superimposed on the Blood Pressure Waveform [see Figure 11.2]. This combined signal was then sampled by the DSP card, and displayed on the computer monitor.

When no pressure signal was being recorded (e.g. during the first part of pseudo-synchronous data acquisition) the QRS complex was still recorded on the pressure channel.

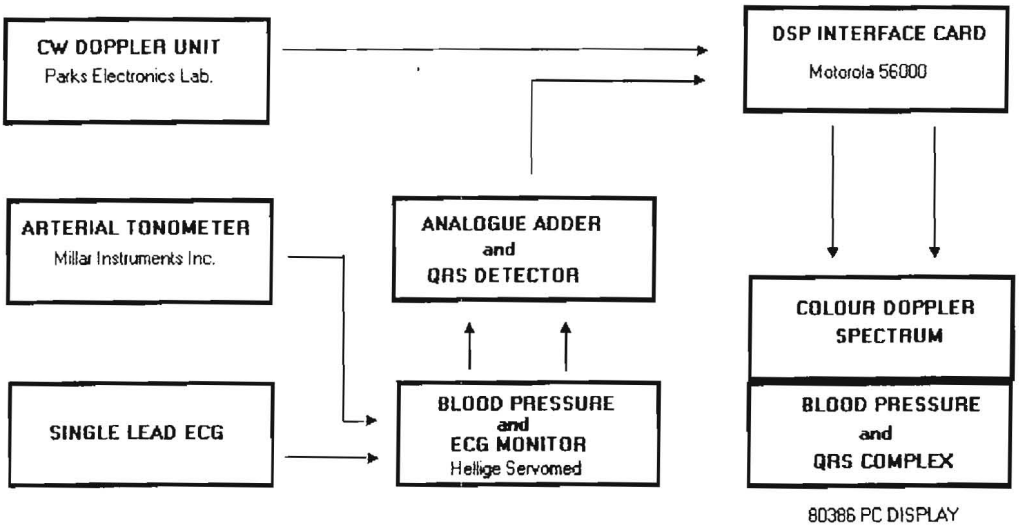

Figure 11.3 : Block Diagram of prototype Haemodynamic Data Acquisition System

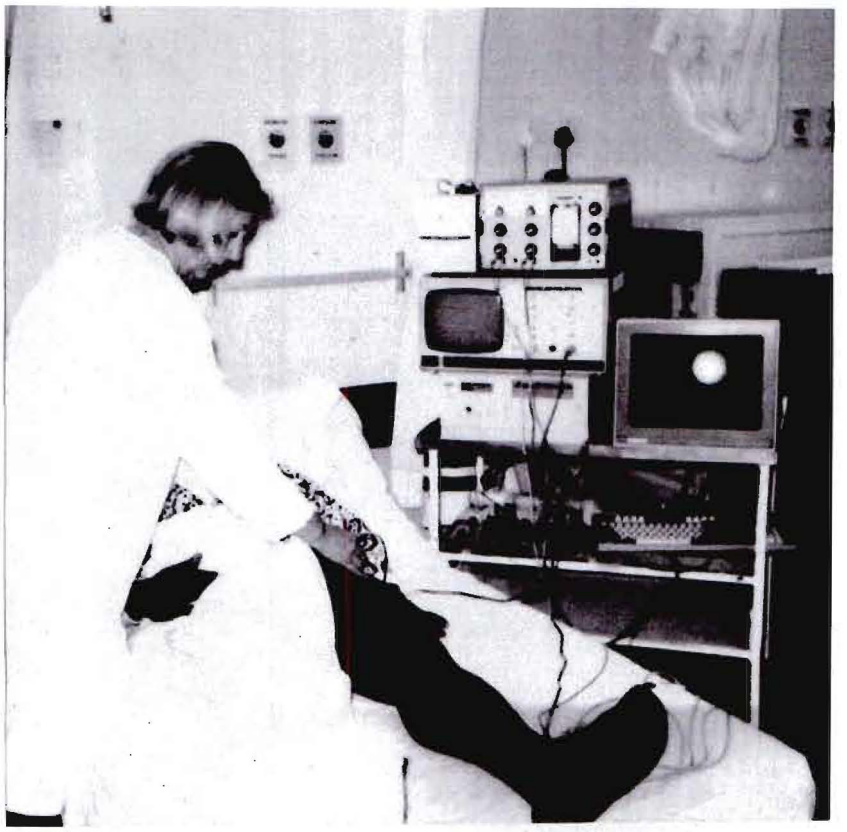

Figure 11.4: Clinical pseudo-synchronous measurement of the External Iliac Doppler Blood Velocity Waveform using the prototype Haemodynamic Data Acquisition System

11.4 TECHNICAL LIMITATIONS OF THE PROTOTYPE DATA-ACQUISITION SYSTEM AND AN UNDERDETERMINED VERSION OF THE INVERSE MODEL

The prototype system described thus far is not perfectly suited for full implementation of the Inverse Model which requires both the External Iliac Blood Flow (ml/s) signal as well as the External Iliac Blood Pressure signal synchronously. The prototype data acquisition system provides only the External Iliac Blood Flow Doppler Frequency Spectrum and the shape of the External Iliac Blood Pressure waveform. For this reason, an underdetermined version of the Inverse Model had to be implemented (for the preliminary studies : Chapters 13-15) rather of the critically determined implementation of Chapters 8 – 10.

Clinically, the volumetric Blood Flow signal may be estimated by using a Duplex Doppler System. Unfortunately, due to logistical reasons, the Duplex Doppler system was not always available for use. Therefore a scaling factor had to be estimated to convert the Doppler Flow Frequency Spectrum into an approximate Blood Flow Rate (ml/s). For Normal subjects under resting conditions , the volumetric External Iliac Blood Flow Rate is approximately 4.5% of the total Cardiac Output. Cardiac output may be estimated from Patient Size using methods described in Chapter 6 . Therefore the Doppler Flow waveforms of Normal subjects may be scaled using this relationship.

For subjects with Peripheral Arterial Disease, the External Iliac Arterial flow may be *less* than 4.5% of the cardiac output. An External Iliac Artery Flow scaling factor, for subjects with arterial disease was approximated using successive guesses (e.g. 4.5%-0.5% of cardiac output). The best curve fit between Predicted and scaled Clinically Measured flow waveforms, determines the approximate scaling factor.

The clinically acquired blood pressure waveform was also multiplied by a scaling factor, because Arterial Tonometry provides an accurate measure of only the shape of the pressure waveform. For Normal subjects the scaling factor may be estimated using sphygmanometry to measure Brachial Pressure limits, and then assuming that this is similar to the External Iliac Pressure Limits.

However for Patients with Peripheral Arterial Disease (PAD) such an approach cannot be adopted. The External Iliac pressures in such subjects vary greatly, depending on the state and location, of arterial disease. The Doppler Systolic Pressures in the Superficial Femoral and Popliteal arteries are routinely measured during the clinical assessment of PAD, however no technique exists at the present time, for measuring the External Iliac or the Common Femoral Artery Systolic Pressure. (A technique of measuring the External Iliac or Common Femoral Systolic Pressure has been proposed by this author, but the implementation of this technique is beyond the scope of this thesis) .

For PAD patients, the scaling of the Blood Pressure Waveform was implemented by using a process of successive guesses (with the Superficial Femoral Artery Systolic Pressures as a guide) until a good curve fit between Predicted (Inverse Model) and Actual (Clinical Measurements) was obtained.

These scaling procedures, in effect, add further mathematical unknowns to the Inverse Model . It is however important to note that these technical limitations are a feature of this prototype data acquisition system, rather than a feature of the Inverse Model. These limitations must be overcome and implemented in a more advanced data

CHAPTER 12
A PRELIMINARY CLINICAL FEASIBILITY STUDY OF THE INVERSE ARTERIAL MODEL

The prototype haemodynamic data acquisition system described in Chapter 11, was used to non-invasively acquire data from clinical subjects at the Vascular Laboratory of Groote Schuur Hospital (Cape Town, South Africa). This data was analysed using the under-determined version of the Inverse Arterial Model presented in Chapter 11.4 rather than the full Inverse Model [Chapters 8-10] because of the technical limitations of the prototype data acquisition system.

A comprehensive haemodynamic study, of all subjects (i.e. angiograms, arterial pull-through pressures and complete Duplex Doppler assessment) was not possible for logistical reasons.

Therefore the aims of this preliminary study were :

1. To assess the feasibility of implementing the full Inverse Transmission Line Model for the Clinical study of normal and diseased arterial systems, based on the results of the under-determined version of the Inverse Model.
2. To make recommendations concerning the prerequisites for a Clinical Pilot Study of the Inverse Arterial Model.

Whilst the *primary focus* of the Inverse Model lies in the prediction of the state of the Arterial Sample/Proximal Region (i.e. The External Iliac artery in this study), the remaining two arterial regions (i.e. Pre-Sample Region and Arterial Distal Region), as defined by the Three Division Method, were also investigated :

Chapter 13 : Pre-Sample Arterial Region [1]
Chapter 14 : Sample/Proximal Arterial Region [2]
Chapter 15 : Distal Arterial Region [3]

12. 1 CLINICAL SUBJECTS

Two broad groups of clinical subjects were selected. The "normal" group consisted of 6 healthy young persons (3 male, 3 female) with no history or symptoms of vascular disease. The "patient" group consisted of 12 persons (10 male, 2 female) selected from patients with vascular disease at the Vascular Laboratory in Groote Schuur Hospital. The "patients" had a variety of vascular disorders including hypertension, aortic disease (Pre-Sample Region), proximal disease (Sample Region : External Iliac), and distal disease (Distal Region : Common femoral artery, Superficial Femoral; Popliteal, Peroneal, Posterior and Anterior Tibials). Clinical data recorded from the Subjects is tabulated in Appendix 4.

Patients were chosen, subject to hospital staff and patient availability, in addition to patient's disease profile. From each subject limb, a Doppler ultrasound waveform and a tonometric pressure waveform, were acquired non-invasively. A synchronous QRS waveform marker (from a single lead ECG) was obtained with each haemodynamic waveform.

Subject heart rate was calculated by measuring the time intervals between successive QRS complexes. A stable heart rate (beat to beat variation not greater than one sample period i.e. 18.5 ms) allowed both the pressure (with synchronous ECG) and Doppler (with synchronous ECG) to be *pseudo-synchronised* offline. This was necessary for practical reasons, as it was difficult to use both the Doppler and the Tonometer probes simultaneously in a clinical setting.

In addition, the subjects age; height; weight; Brachial Systolic and Diastolic Pressures (using sphygmanometry) were recorded.

Figures 12.1 – 12.3 summarise the subject population data.

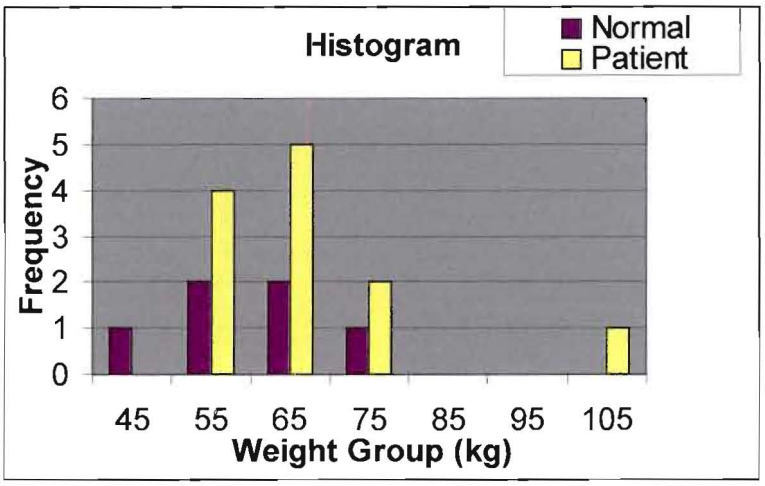

Figure 12. 1 : Weight Frequency of clinical subjects (n=18)

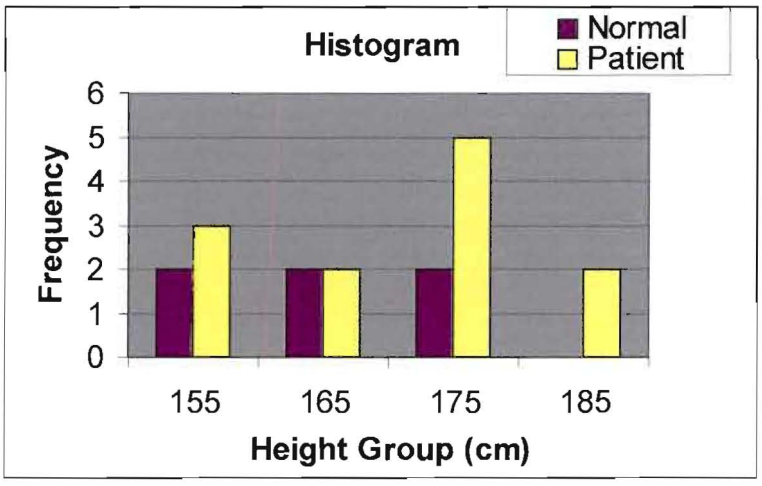

Figure 12.2 : Height Frequency of clinical subjects (n=18)

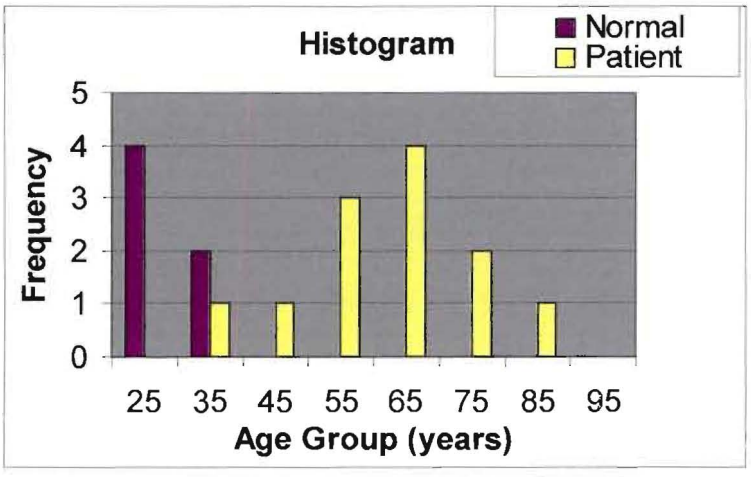

Figure 12.3 : Age Frequency of clinical subjects (n=18)

12.2 CLINICAL INVESTIGATORS

Doppler waveform acquisition and most of the Tonometric Pressure waveform acquisition was carried out by experienced staff at the Vascular Laboratory. ECG, Doppler, and Tonometric signals were stored in the data acquisition computer, and analysed offline using the underdetermined version of the Inverse Arterial Model. All analyses were carried using Matlab 4.2c.1 for Windows and Simulink 1.3c for Windows.

12.3 DURATION OF STUDY

Waveform acquisition from subjects required approximately between 10 and 20 minutes per limb. The entire study was carried out over the period between January 1998 and September 1998. Waveform measurements were taken subject to staff and patient availability.

12.4 CRITERIA FOR WAVEFORM ACCEPTANCE FOR ANALYSIS

Repeatability was the main criteria for waveform selection. If a repeatable signal could not be acquired, then the corresponding waveform was rejected and no analysis was carried out. Subject heart rate had to be stable in all the investigations (in order to allow for pseudo-synchronous waveform acquisition).

The first time that an arterial tonometer had been used by staff at the Vascular Laboratory, was for the purposes of this feasibility study. The use of an arterial tonometer requires a great deal of skill. Due to time constraints and inexperience with tonometric pressure measurement, a number of tonometric pressure waveforms that exhibited too much *baseline drift* (due to operator or subject movement and in some cases due to movement of the external iliac artery as a result of applied surface pressure) were rejected . Multiple sequential waveforms that were acquired were averaged to obtain a single representative waveform for analysis by the under-determined version of the Inverse Model.

12.5 SCALING OF FLOW AND PRESSURE WAVEFORMS

The Doppler Frequency Waveform differs from the Blood Flow Rate waveform by a *scaling factor* i.e. the waveform shapes are the same, but the amplitudes are different. The same is true for the tonometric Blood Pressure waveform. The tonometric Blood Pressure waveform has the same *shape* as the actual blood pressure waveform, but the systolic and diastolic limits are different. Actual blood pressure may be measured using invasive techniques.

Measured waveforms were multiplied by scaling factors (see Chapter 11.4) before analysis by the under-determined version of the Inverse Model. This required a trial and error process. The final scaling factors chosen were those which produced the best correspondence (i.e. curve fits) between the predicted (Inverse Model) and the clinically measured (scaling factor * actual measured) waveforms.

Scaling factors were chosen so that Flow Rates and Pressures were within reasonable physiological limits. The use of scaling factors results in this trial being categorised as a preliminary *feasibility study*, rather than a *pilot study*.

In order to carry out a pilot study the actual Pressures and Blood flow rates must be known and the full critically determined Inverse Model must be used. The hurdles that stand in the way of a pilot study are the availability of technical resources rather than genuine technical hurdles.

CHAPTER 13
PRELIMINARY CLINICAL FEASIBILITY STUDY 1 : THE PRE-SAMPLE REGION

The Pre-Sample Region of the Three Division Inverse model, was approximated as "normal" to reduce the number of mathematical unknowns. This is a *first approximation* approach to modelling the Pre-Sample Region. However, the Pre-Sample Region may also be abnormal in a clinical subject. Computer simulated tests, described in Chapter 10, concluded that *mild* Pre-Sample (Aortic) stenotic disease has a minimal effect on the accuracy of the estimation of Iliac artery radius.

Chapter 6, described a process, whereby the "normal" approximation may be improved by taking into account body dimensions, age, and gender. This allows the "normal" approximation to be adjusted for each individual subject, and is a *second approximation* approach to modelling the Pre-Sample region.

Clinically measured pressure or flow propagation times or velocities [Figure 13.1] can also be used to model the Pre-Sample Region and is a *third approximation* to modelling the Pre-Sample Region. Chapter 5 discussed pulse wave velocities in the computer simulated model, as well as published clinical study data.

13.1 OBJECTIVES

(1) To determine if a relationship exists between Aortic Disease and External Iliac (or Common Femoral) Pulse Arrival Time or Velocity

(2) Hence, to determine an approach to modelling the Pre-Sample Region

13.2 METHOD

The prototype Haemodynamic Data Acquisition System (Chapter 11) may be used to measure the time delay between the ECG QRS complex and both the blood flow and pressure waveforms of the external iliac artery.

The external iliac Pulse Arrival Time (P.A.T.) was clinically measured, by determining the time delay between the QRS complex of an ECG lead, and the upstroke of the

External Iliac Flow Velocity waveform .This PAT was then used to estimate the average Pulse Wave Velocity using the aorto-femoral length which is known to be proportional to height , with the proportionality constant increasing slightly with age. Both the subject age and height factors are therefore included in estimating a subjects' aorta-femoral length, and hence also PWV.

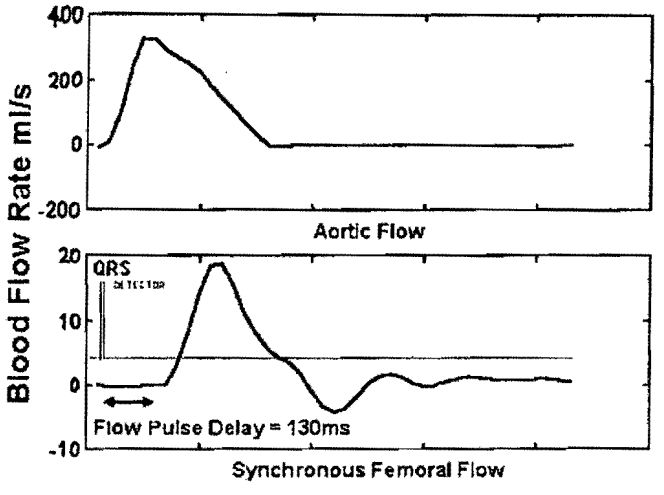

Figure 13.1 Pulse Arrival Time estimated using the time delay between the ECG QRS complex and the upstroke of the blood flow waveform measured at the defined transition point between the External Iliac and the Common Femoral artery.

13.3 THEORY

The time difference between the R-wave of the QRS complex and the arrival of a peripheral pulse is referred to in the literature as the 'pulse arrival time' (P.A.T) or the 'pulse wave transmission time' (P.W.T.T) [Atkinson & Woodcock, 1982; de Monchy & van der Hoeven, 1976 ; Geddes et al, 1981; Ward ,1980; Deshpande et al, 1990]. It is only an approximate measure of the pulse transit time because both the pressure and flow waves are also affected (either advanced or delayed) by wave reflections. [Milnor, 1980]

Pulse wave velocities vary along the normal arterial tree [Nichols & O'Rourke, 1990] as a result of radial and elastic taper. This is especially apparent in the aorta.

Pulse wave velocities vary along the normal arterial tree [Nichols & O'Rourke, 1990] as a result of radial and elastic taper. This is especially apparent in the aorta. Therefore this technique measures the *average* time-delay or pulse wave velocity of the Pre-Sample region.

13.3.1 CONVERSION BETWEEN PULSE ARRIVAL TIME AND PULSE WAVE VELOCITY

Converting a PAT into a PWV is possible, if the length of the arterial path is either known, or can be estimated. Chapter 6 describes the relationship between the length of the human aorta and a subject's height and age. Therefore, given a clinically measured PAT and the subject's height and age, the average PWV in the Pre-Sample region may be estimated :

Average Pulse Wave Velocity = Arterial Length / Pulse Arrival Time

[Equation 13.1]

13.3.2 EFFECT OF ARTERIAL PROPERTIES ON PULSE WAVE VELOCITY

Although the Moen's-Korteweg [Equation 7.1] and the Gow and Taylor equations, [Equation 7.2] for wave-speed have different constants, both show a direct relationship between wave velocity and Young's Modulus and wall thickness, and an inverse relationship between wave velocity and arterial radius.

Using those equations, the effect of four different arterial states on the pulse wave velocity may therefore be deduced :

13.3.2.1 NORMAL ARTERY

The "normal" artery may be used as a reference point for wave velocity measurements. By using e.g. the Moen's -Korteweg equation, the *'normal'* pulse wave velocity may be estimated f from the 'normal' Young's Modulus; arterial wall thickness, and arterial radius.

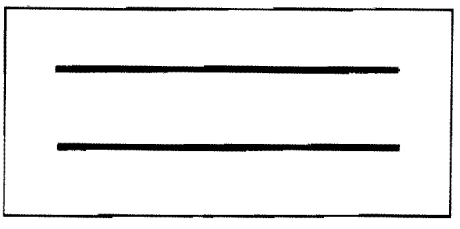

Figure 13.2 : Longitudinal-Section of Normal Artery

13.3.2.2 ARTERIAL ANEURYSM

An arterial *aneurysm* is a balloon-like malformation of the arterial wall. There is an increase in local arterial radius, a decrease in local arterial wall thickness, and a decrease in local Young's Modulus. Aneurysms may rupture, resulting in a haemorrhage.

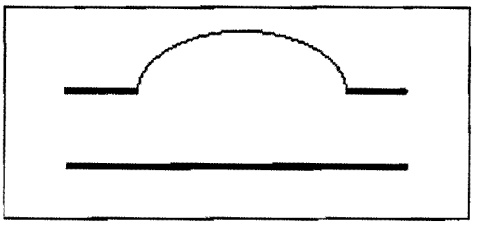

Figure 13.3 Longitudinal-Section of an Arterial Aneurysm

According to the Moen's-Korteweg equation, the pulse wave velocity would *decrease* in the presence of an arterial aneurysm.

13.3.2.3 ARTERIAL STENOSIS

Arterial stenosis results in narrowing of the arterial lumen. There is a decrease in local arterial radius; an increase in local arterial wall thickness; and an increase in local arterial Young's Modulus. Arterial stenoses may result in a loss of arterial pressure and downstream ischaemia.

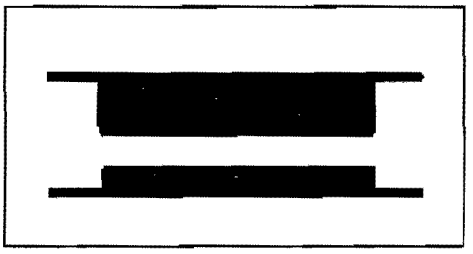

Figure 13.4 Longitudinal-Section of an Arterial Stenosis

According to the Moens-Korteweg equation, an arterial stenosis would result in an *increased* wave velocity. An arterial *aneurysm* may also result in the formation of a thrombus (blood clot). The presence of a thrombus may result in the physiological effect of the aneurysm being similar to that of a stenosis.

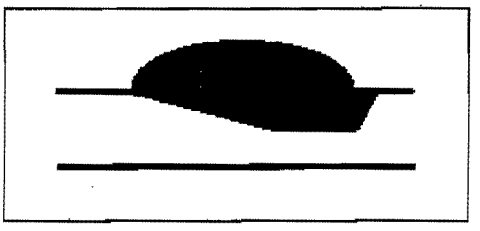

Figure 13.5 Longitudinal-Section of an Arterial Aneurysm, with Thrombus

13.3.2.4 ARTERIAL HYPERTENSION

Hypertension results in an increase in arterial radius, as well an increase in the Young's Modulus. The overall effect of hypertension is to increase the Pulse Wave Velocity [Dahan, et al , 1990].

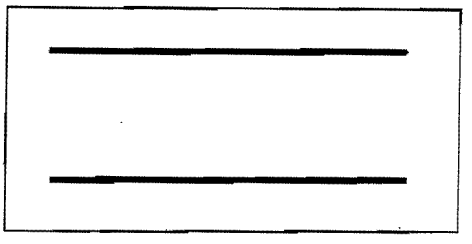

Figure 13. 6 Longitudinal-Section of a Hypertensive Artery

13.4 CLINICAL RESULTS IN THE PRESAMPLE REGION

Figure 13.7 shows the relationship between mean brachial pressure and age. Data from patients with known aortic disease (Patients 3,6,10) was plotted together with data from normals (Normals 1-6) and patients with no aortic disease (Patients 1,5,7,9). Note that Patients 2 and 8 were excluded because no brachial pressure was recorded and Patients 4, 11, and 12 were excluded because no ECG was recorded.

Figure 13.8 shows the relationship between mean brachial pressure and average pulse wave velocity. Because the average pulse wave velocity may differ in each limb of a subject, these results are categorised by limbs rather than subjects. Therefore there are 12 limbs representing the normals (normals 1-6 : both legs) ; 6 limbs representing patients with aortic disease (Patients 3,6,10 : both legs); and 5 limbs representing patients with no aortic disease (Patient 5 : both legs; Patient 1 : Right leg; Patient 7 : Left leg; Patient 9 : Left leg) . Note that Patients 2,4,8,11,12 were excluded for the same reasons they were excluded from Figure 13.7. No waveforms were recorded from Patient 9 : Right leg and Patient 1 : Left leg and Patient 7's : Right leg was previously amputated therefore they are also excluded from this graph. ***Figure 13.9*** shows the relationship between the Pulse Arrival Time (PAT) and subject age. Note that the plotted PAT's were averaged from multiple serial

waveforms recorded from individual subjects. Therefore whilst the time resolution of the serial measurements was 18.5ms, the averaged values plotted are not necessarily exact multiples of 18.5ms.

These results are categorised by limb rather than by subject for the same reason that this was done in Figure 13.8. There are 12 limbs representing the normal subjects (normals 1-6 : both legs); 8 limbs representing patients with aortic disease (Patients 3,6,8,10 : both legs); and 6 limbs representing patients with no aortic disease (Patient 1 : Right leg; Patient 2 : Right leg; Patient 5 : both leg; Patient 7 : Left leg; Patient 9 : Left leg).

Note that Patients 4,11, and 12 were excluded because no ECG was recorded, and Patient 7's Right leg had been previously amputated.

Figure 13. 10 shows the relationship between the calculated average Pulse Wave Velocity [using Equation 13.1] and age. These results are also classified by limbs rather than subjects. Because the PWV may be estimated from the PAT provided that subject height and age are known, exactly the same limb-subjects as those presented in Figure 13.9 are plotted here.

Note that Appendix 4 contains all the relevant data acquired from the Clinical Subjects.

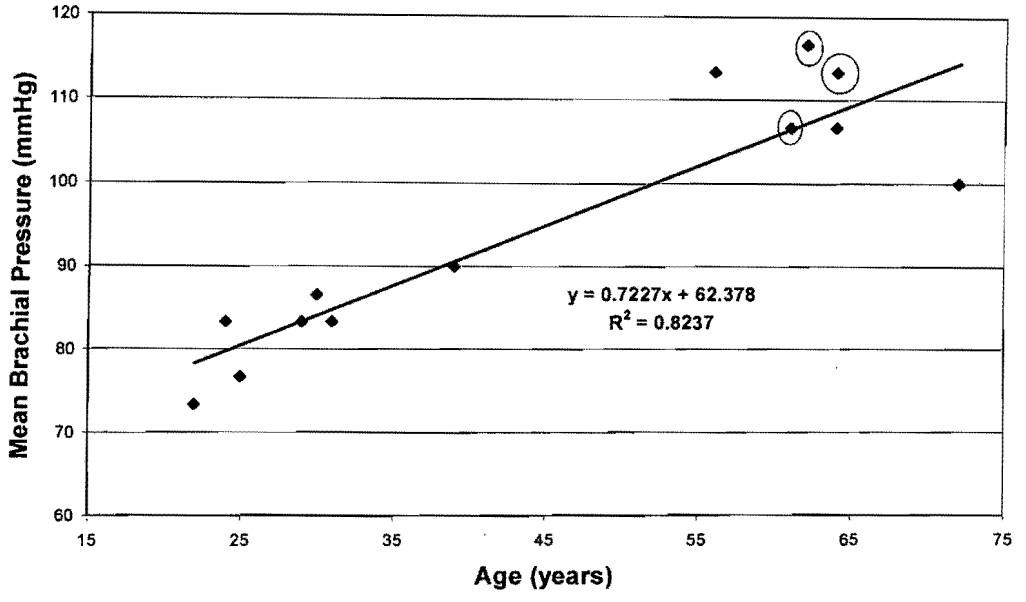

Figure 13.7 : Relationship between blood pressure, and age. Note that circled samples = patients with aortic disease, and un-circled samples = both normals and patients no aortic disease

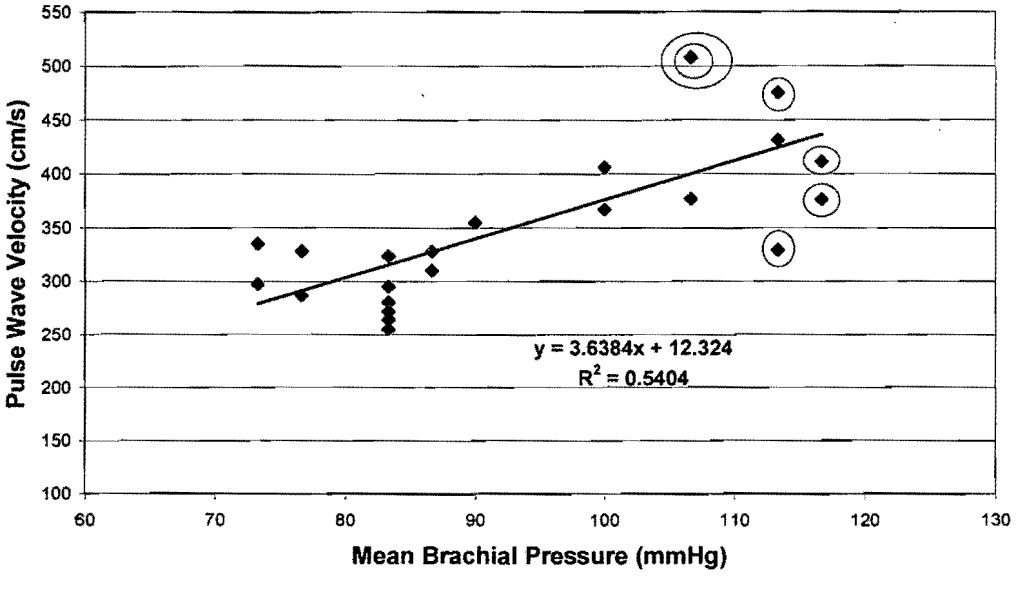

Figure 13.8 : Relationship between mean brachial pressure and pulse wave velocity. Note that circled samples = patients with aortic disease, and un-circled samples = both normals and patients with no aortic disease.

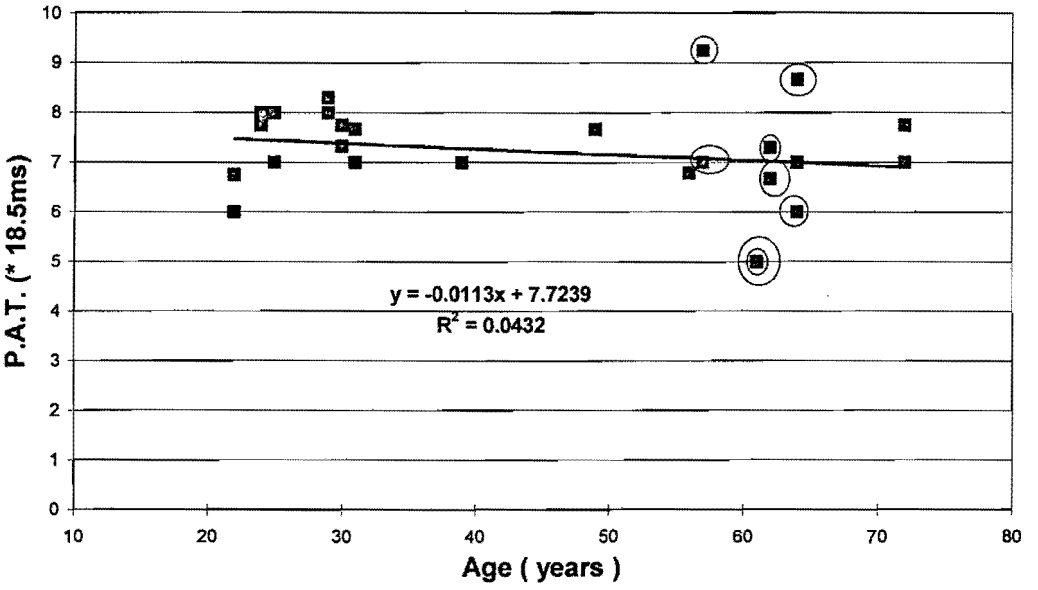

Figure 13.9 Relationship between Femoral/External Iliac Pulse Arrival Time and age. Note that circled samples = subjects with aortic disease; and un-circled samples = both normals and patients with no aortic disease

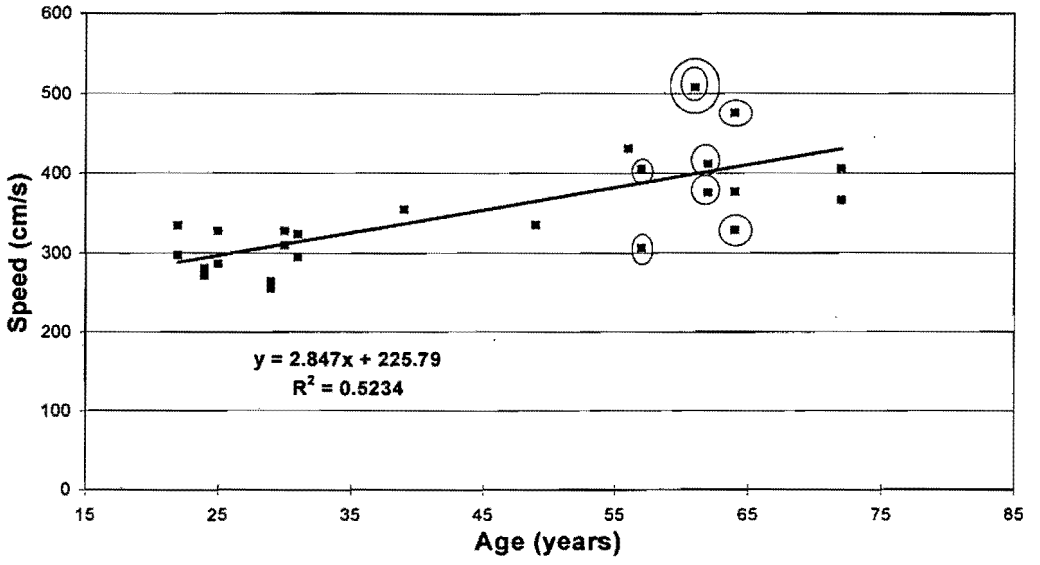

Figure 13.10 Relationship between Femoral/External Iliac Pulse Wave Velocity and age. Note that circled samples = subjects with aortic disease; and un-circled samples = both normals and patients with no aortic disease.

13.5 : DISCUSSION

The age-related scatter graphs (Figures 13.7 & 13.9 & 13.10) consists of two clusters (old and young subjects), because the subject population consisted of a young 'normal' sub-population, and an older sub-population with arterial disease.

For logistical reasons it was not possible to obtain age-matched normals, however aortic disease (represented by the circled samples in Figure 13.7 – 13.10) was not present in all of the older sub-population, thus allowing some of the older subjects to be categorised as, 'normal' with respect to aortic disease. These subjects are referred to in Figures 13.7-13.10 as "patients with no aortic disease". Despite the clustering effect, the distribution of samples follows a trend in all the graphs, except the age vs. PAT graph [Figure 13.9].

Subjects with aortic disease were chosen depending on their availability as well as staff and equipment availability. Aortic disease was not quantified. Patients 3, 8 and 6 were diagnosed with abdominal aortic aneurysms with Patient 6 also being diagnosed with iliac aneurysms. Patient 10 was diagnosed with ulcerated plaques in the aorta. Note that a diagnosis of an aneurysm does not necessarily imply a more compliant arterial wall [see Figure 13.5]

The well known correlation between age and blood pressure, is illustrated in Figure 13.7. The theory presented in Section 13.3.2.4, relates elevated blood pressure to increased Pulse Wave Velocity. This relationship is compatible with Figure 13.8.

Subjects with *aortic disease* may either have an increased PWV (stenosis or aneurysm with thrombus) or a decreased PWV (compliant aneurysm). It is therefore difficult to differentiate non-specific aortic disease , from PWV graphs (Figures 13.8 & 13.10) , on this basis alone. However, large positive or negative deviations from the expected linear trends may be an indicator of the presence of a significant aortic aneurysm or stenosis (Figures 13.8 & 13.10)

PAT appears to be poorly correlated to age [Figure 13.9] . The transformation of PAT to PWV shows an improved correlation between PWV and age. Both PWV and PAT graphs [Figures 13.9-13.10] show some of the limb-subjects with aortic disease

CHAPTER 14
PRELIMINARY CLINICAL FEASIBILITY STUDY 2 : THE UNDER-DETERMINED INVERSE MODEL APPLIED TO THE ARTERIAL SAMPLE REGION

The physiological state of the Arterial Sample Region has a significant effect on proximal Pressure and Flow waveforms. The reason for this, is that this region lies directly below the measuring probes. The ability of the Inverse Model to predict the state of this region is its primary function. Note that whilst the Inverse Model also has the potential to make assessments on the arterial states in the Pre-Sample Region (Chapter 13) and the Distal Region (Chapter 15), the primary focus of this thesis is assessment of the arterial Sample Region.

Technical limitations of the prototype Data Acquisition System (Chapter 11) require that Pressure and Flow waveforms are amplitude scaled. This process adds further mathematical unknowns to the Inverse Model, converting it into an Underdetermined System. Such a system raises the mathematical possibility of multiple solutions. Therefore the results presented in this Chapter must be interpreted within this context. The Inverse Model may only be properly clinically evaluated by using a Haemodynamic Data Acquisition System that measures both the shape and amplitude of the Pressure (mmHg) and Flow (ml/s) waveforms at the external iliac artery (or any other predefined arterial Sample Region).

Note that amplitude scaling is not the same as normalising. Normalised waveforms cannot be easily integrated into a transmission line based electrical circuit model. Whilst this process of amplitude scaling is bound to introduce some error into the predictive process, the results of computer simulated tests presented in Section 10.4 do suggest the Inverse Model to be fairly robust in the presence of amplitude scaling errors.

The preliminary clinical investigations carried out in this Chapter therefore relate to the Underdetermined Version of the Inverse Model. The predictive ability of this version would necessarily be less accurate than that of the Over-Determined Inverse Model. However if the underdetermined version is proved to have some clinical diagnostic potential, then it would be a reasonable assumption to make that the over-determined version would have even greater clinical diagnostic potential.

There are no prior studies in the literature that demonstrate the fitting of clinically acquired haemodynamic waveforms to waveforms generated by a transmission line representation model of the entire arterial system. Therefore an investigation of the ability of the underdetermined version of the Inverse Model to fit clinical waveforms to transmission line generated waveforms would be an important research step. Indeed, if the underdetermined version of the Inverse Model is able to reasonably fit clinical waveforms, this would suggest that the over-determined version would provide even better waveform fits.

14.1 OBJECTIVES

To investigate the ability of the underdetermined version of the Inverse Model to diagnose normal as well as stenosed arteries in the Sample Region, from clinically measured Pressure and Flow waveforms, based on *the analysis of the shapes* of the Pressure and Flow waveforms. In addition, to investigate the ability of the undetermined version of the Inverse Model to fit both normal and stenotic clinically acquired blood Pressure and Flow waveforms.

14.2 METHOD

Three normal subjects (six limbs), and three patients with known Sample Region stenotic disease (five limbs) were analysed using the underdetermined version of the Inverse Model. Note that the patients had co-existing distal disease in addition to Sample Region disease. Error Graphs were used to identify the predicted Sample Region radius which resulted in the closest fit between the pressure and flow waveforms generated by the under-determined Inverse Model, and waveforms measured from the external iliac arteries of the subject limbs.

The minimum error region of the Error Graphs corresponded to the External Iliac radius predictions of the under-determined Inverse Model. Note that any discrete radius within the minimum error region results in waveform predictions that are virtually identical to those predicted by any other discrete radius within the range defined by the minimum error region. A discrete radius nevertheless had to be selected to plot comparative waveforms. This discrete radius was selected from within the minimum error range using qualitative visual analysis in order to select the "best fit" from a range of "good fits".

Once a good waveform fit had been obtained, the predictions of the under-determined Inverse Model were compared to the results of independent clinical diagnoses. The model-predicted and actual-clinical flow and pressure waveforms, as well as the impedance spectra were plotted for each subject limb.

14.3 THEORY

According to the Three Division method that was introduced in Chapter 8, the arterial Sample Region could not be investigated without first defining the Pre-Sample and Distal arterial regions. The following 3 subsections therefore discuss the modified implementation of the Three Division method used by the under-determined version of the Inverse Model.

14.3.1 CLINICAL MODELLING OF THE PRESAMPLE REGION

Chapter 13 briefly discussed an approach to a *2nd or 3rd Approximation* of the Pre-Sample Region. By using those approaches the *1st Approximation* may have been improved upon. The adoption of a 2nd or 3rd approximation approach would have required extensive clinical research studies as well as equipment development. For the purposes of this preliminary Feasibility study the 1st Approximation to the Pre-Sample Region was considered to be sufficient. Accordingly, the Pre-Sample Region of all subjects presented in this Chapter was assumed to be 'normal' (as defined by Table 2.3 and Figure 2.3).

The chapter objective may therefore be alternatively stated as the answer to the question : Given the clinically measured Pressure and Flow waveforms, what Sample and Distal Region Arterial state would result in predicted waveforms of similar shape (to the measured waveforms) assuming that the subject's Pre-Sample Region is physiologically 'normal' ?

14.3.2 SAMPLE REGION vs. PROXIMAL REGION

The Sample Region (Three Division Inverse Model definition) and the Proximal (Clinical Definition) Arterial Region are 'almost analogous', with *one important difference* : In the Three-Division Inverse Model, the *border* between the Sample and Distal regions is defined as the part of the arterial tree downstream-distal to the point of measurement . In Clinical Vascular studies, the proximal region also *includes* the region just downstream from the measurement site [Figures 14.1, 14.2] whilst the distal region (e.g. profunda femorus and superficial femoral artery) is defined much further downstream. Referring back to Figure 2.3 and Table 2.3 with the external iliac segment 92 defined as the Sample Region, the downstream-adjacent arterial segment 99 would be defined as being in the Distal Region (or "just Distal") by the Three Division Method but as being in the Proximal Region by clinical definition.

Therefore clinically defined Proximal Disease may be classified as either Sample Region Disease [Figure 14.1] or just-Distal Region disease [Figure 14.2] by the Inverse Model, depending on the position of the probe relative to the Proximal Stenosis. As a result of this feature, the Inverse Model definition of sample region or distal disease does not correlate exactly with the clinical definitions of proximal or distal disease.

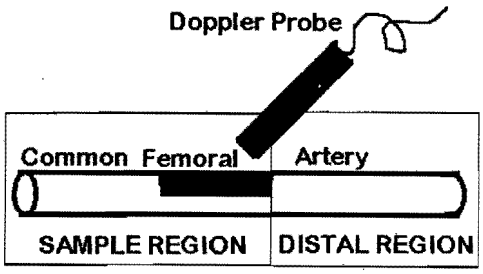

Figure 14.1: Proximal Arterial Disease defined as Sample Region Disease

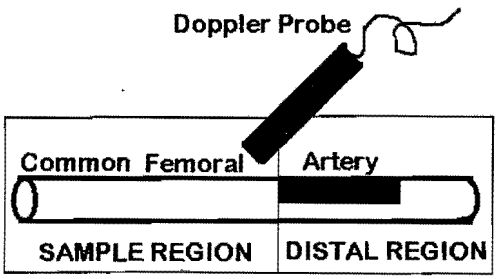

Figure 14.2: Proximal Arterial Disease defined as Distal Region Disease

The point of measurement of Flow and Pressure waveforms was not accurately known in this study because an Imaging Subsystem was not included in the Data Acquisition System. The position of the arterial probes and hence also the Sample / Distal Region border was approximated using surface anatomical landmarks.

The *Sample Region of the Inverse Model* , by definition, is the *segment* of the External Iliac Artery that begins 14.4 cm upstream from the femoral bifurcation (8.3cm in total length) and ends 6.1 cm upstream from the femoral bifurcation (i.e. segment 92 as defined by Figure 2.3 and Table 2.3). In clinical terms this is an 8.3 cm long segment of the External Iliac artery upstream-adjacent to the Common Femoral artery.

14.3.3 CLINICAL MODELLING OF THE DISTAL REGION

According to the Three-Division-Method, the Distal Region was defined by its steady state impedance spectrum. This impedance spectrum is a complex function that is frequency dependent. For a given harmonic frequency, the complex impedance is defined as the ratio of the harmonic Pressure phasor to the harmonic Flow phasor . Normalised Pressure and Flow waveforms could not be used in the definition of the Distal Region because the resultant normalised Distal Impedance would not have been suitable for use in an electrical Transmission Line Model. The measured Pressure and Flow Waveforms were instead amplitude scaled using a series of guesses until a good waveform fit was obtained.

14.4 NORMAL CLINICAL SUBJECTS

Pressure measurements from three (i.e. 3 young adult males) of the six normal subjects (Chapter 12) were stable and repetitive enough for Inverse Model analysis. Note that Appendix 4 provides more details on the clinical subjects. Measurements were taken from both legs of each subject, resulting in 6 sets of measurements. The normal measurements were therefore entitled : (see Figures 14.3-14.10)

Normal #4 : Right and Left Legs
Normal #5 : Right and Left Legs
Normal #6 : Right and Left Legs

14.4.1 UNDERDETERMINED INVERSE MODEL RESULTS for NORMAL SUBJECTS

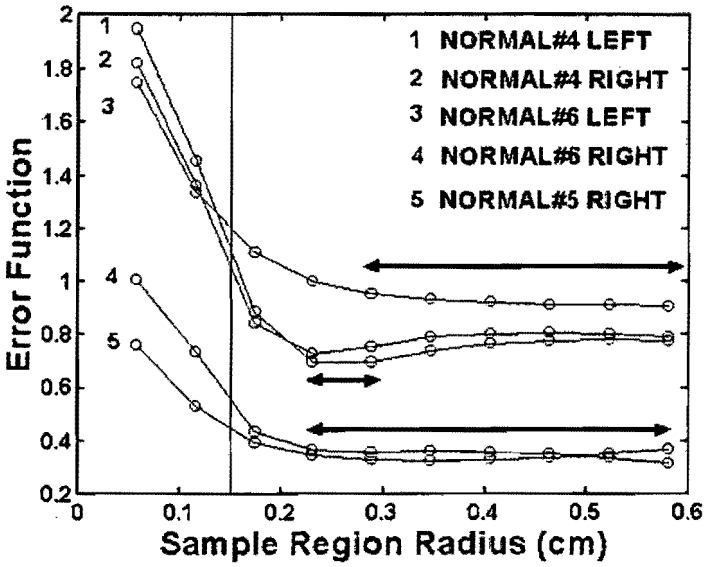

Figure 14.3 :Combined Flow Error Graphs for 5 Normal limbs. The double headed arrows define the 'minimum error regions'. The thin vertical line defines critical stenosis (estimated as 50% of 'normal' radius, with normal radius defined as 0.29cm))

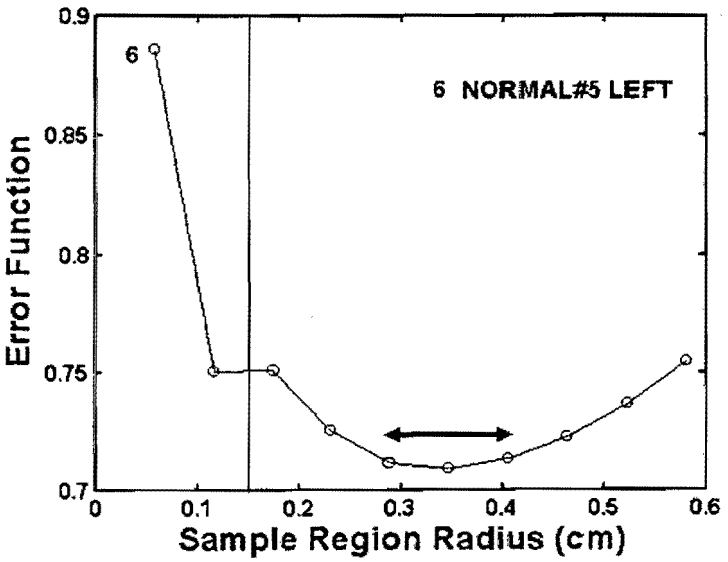

Figure 14.4 : Flow Error Graph for Normal 5, Left Leg. The double headed arrow defines the 'minimum error region'. The thin vertical line defines critical stenosis (estimated as 50% of 'normal' radius, with normal radius defined as 0.29cm)

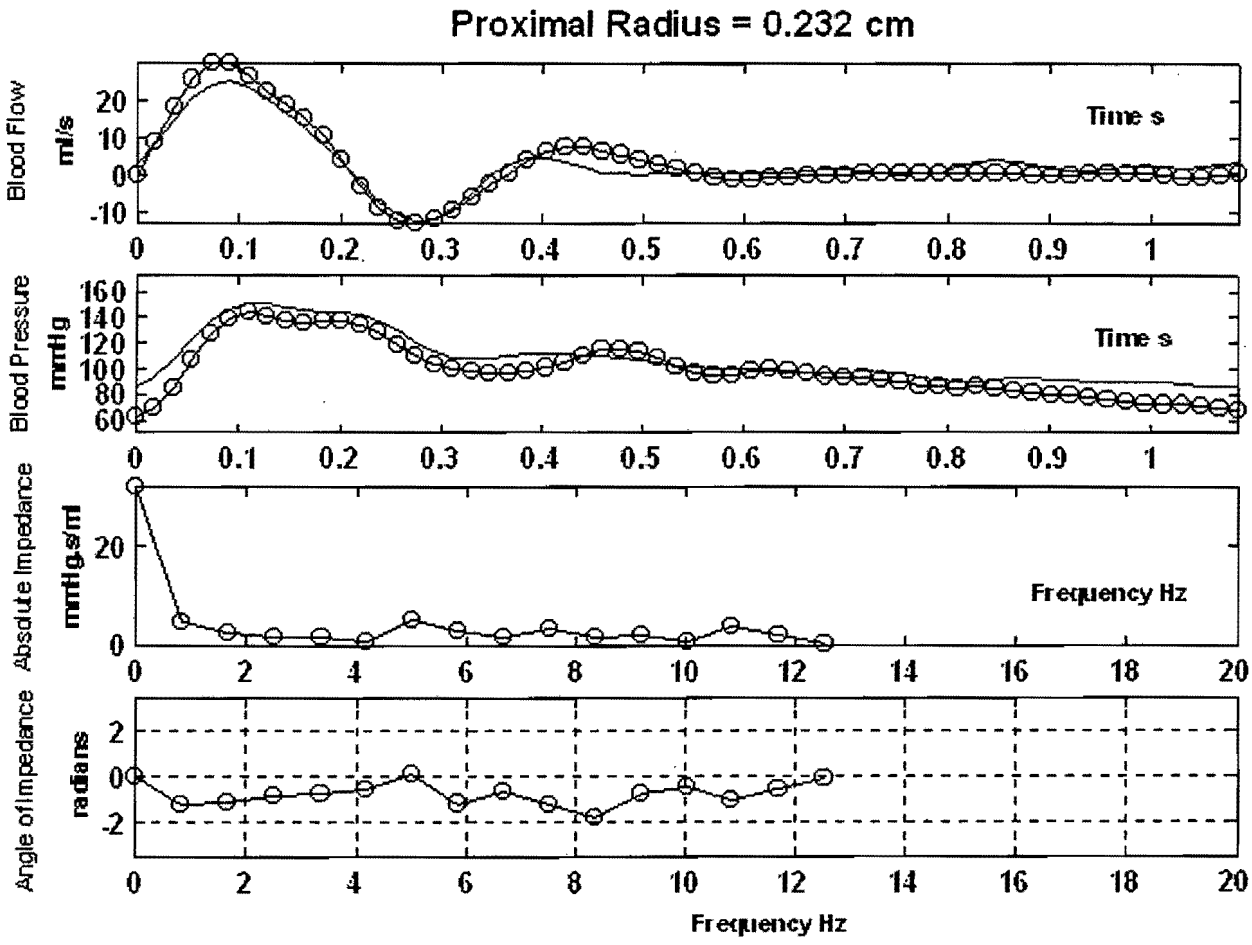

Figure 14.5 : Blood Flow and Pressure Waveforms as well as the Distal Impedance Spectrum for Normal # 4 Right Leg.

(lines with circles = actual clinical waveforms
straight lines = under-determined Inverse Model predicted waveforms)

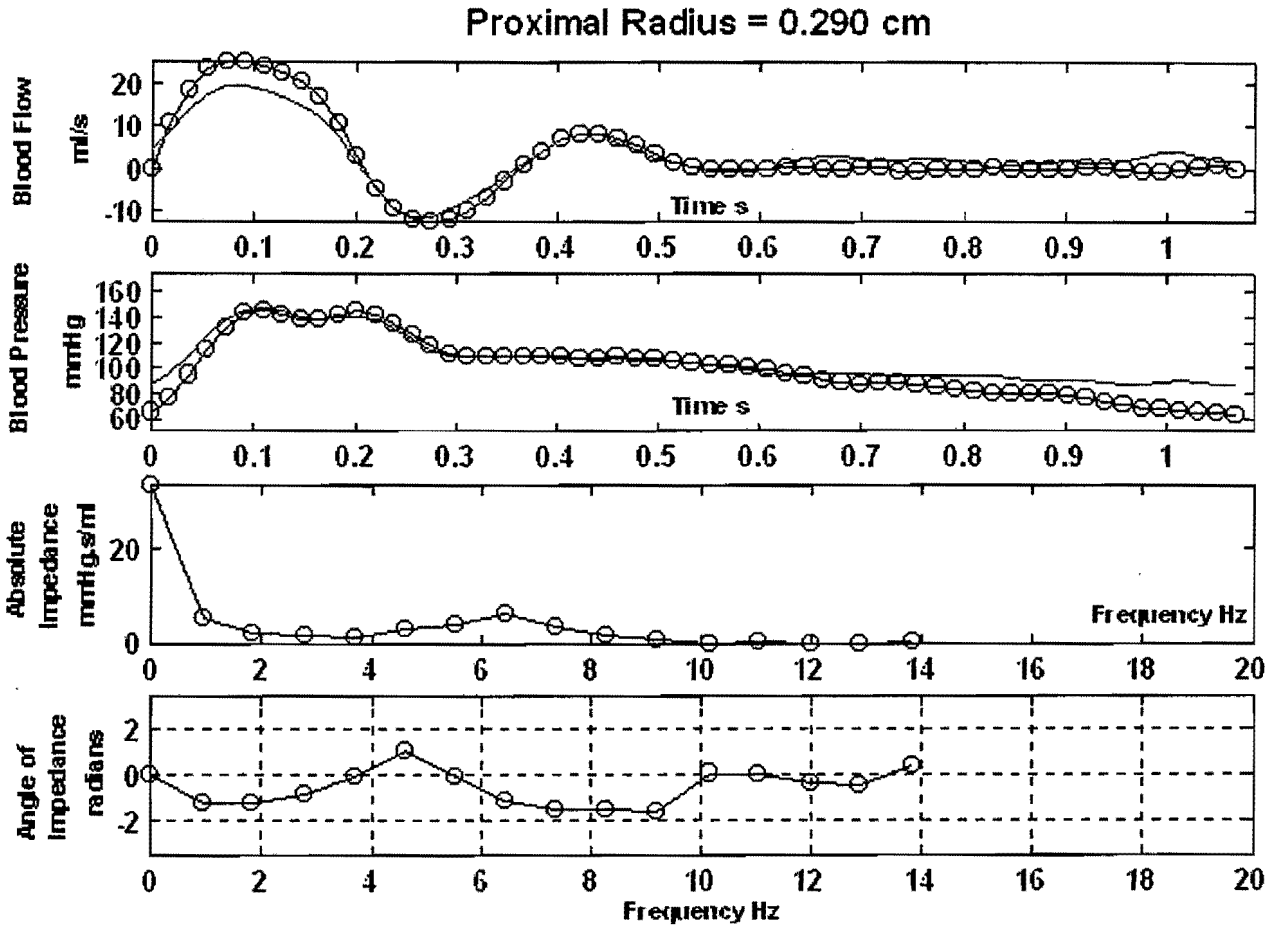

Figure 14.6: Blood Flow and Pressure Waveforms as well as the Distal Impedance Spectrum for Normal # 4 Left Leg

(lines with circles = actual clinical waveforms
straight lines = under-determined Inverse Model predicted waveforms)

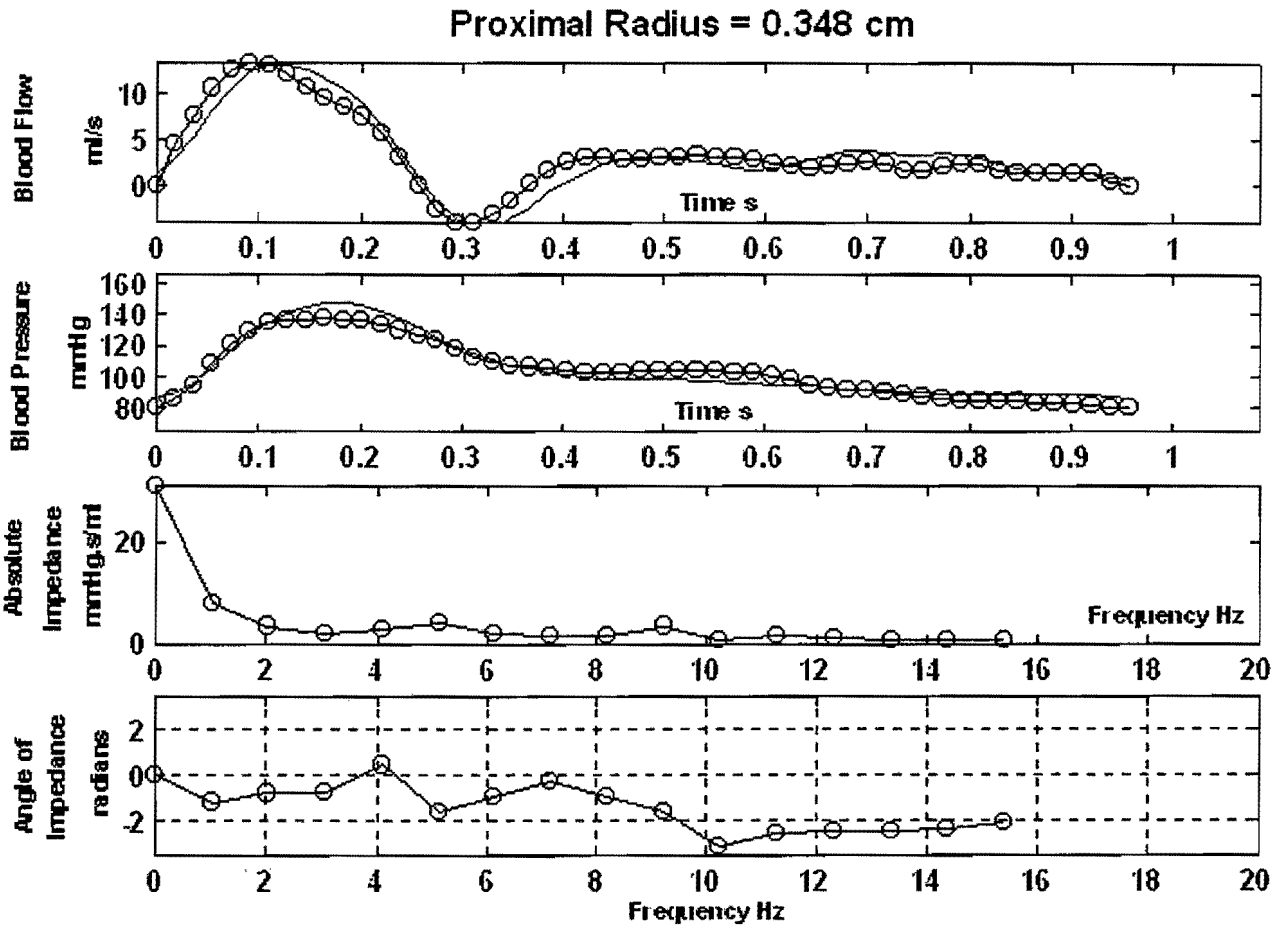

Figure 14.7 : Blood Flow and Pressure Waveforms as well as the Distal Impedance Spectrum for Normal # 5 Right Leg

(lines with circles = actual clinical waveforms
straight lines = under-determined Inverse Model predicted waveforms)

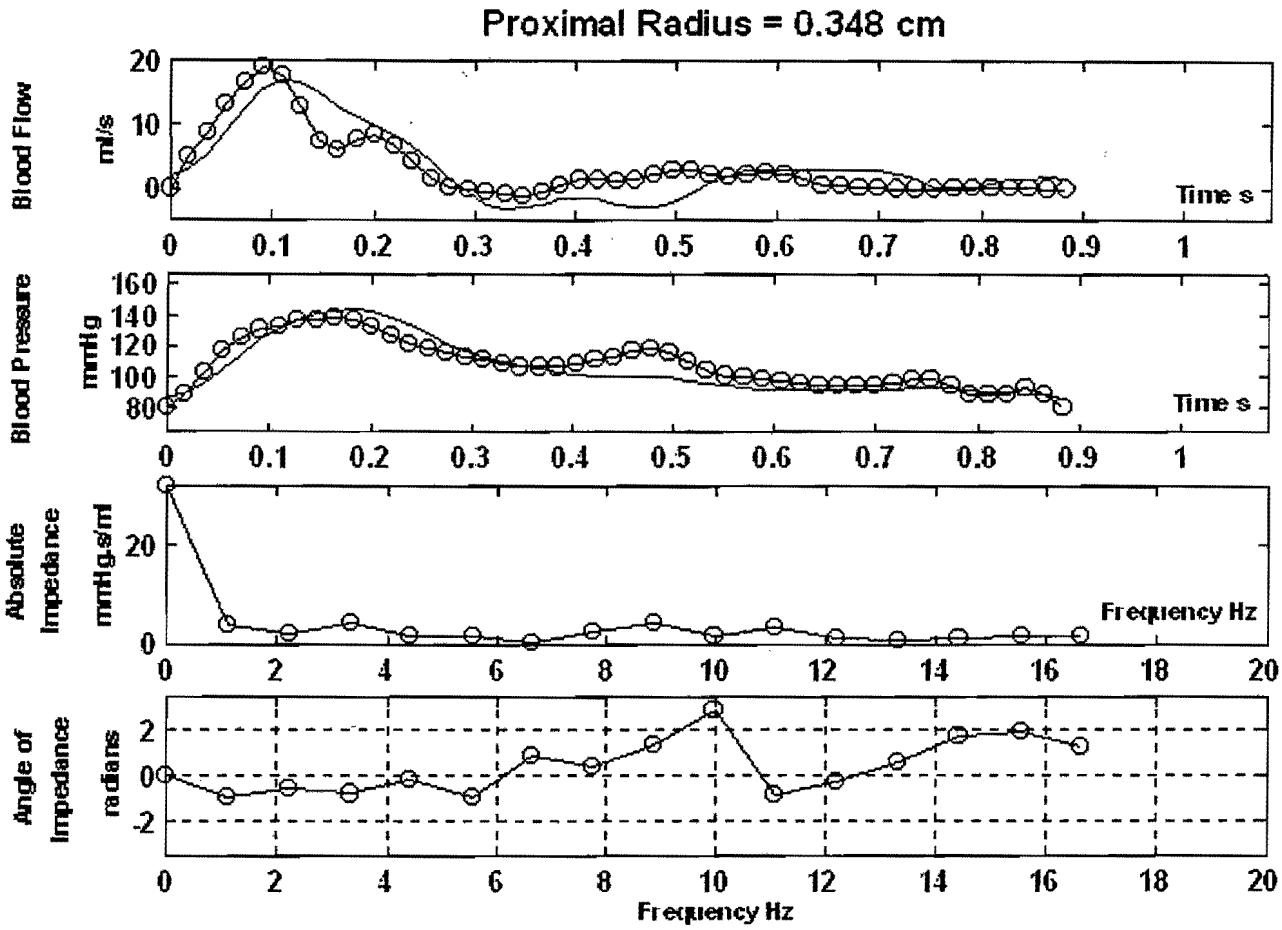

Figure 14.8 : Blood Flow and Pressure Waveforms as well as the Distal Impedance Spectrum for Normal # 5 Left Leg

(lines with circles = actual clinical waveforms
straight lines = under-determined Inverse Model predicted waveforms)

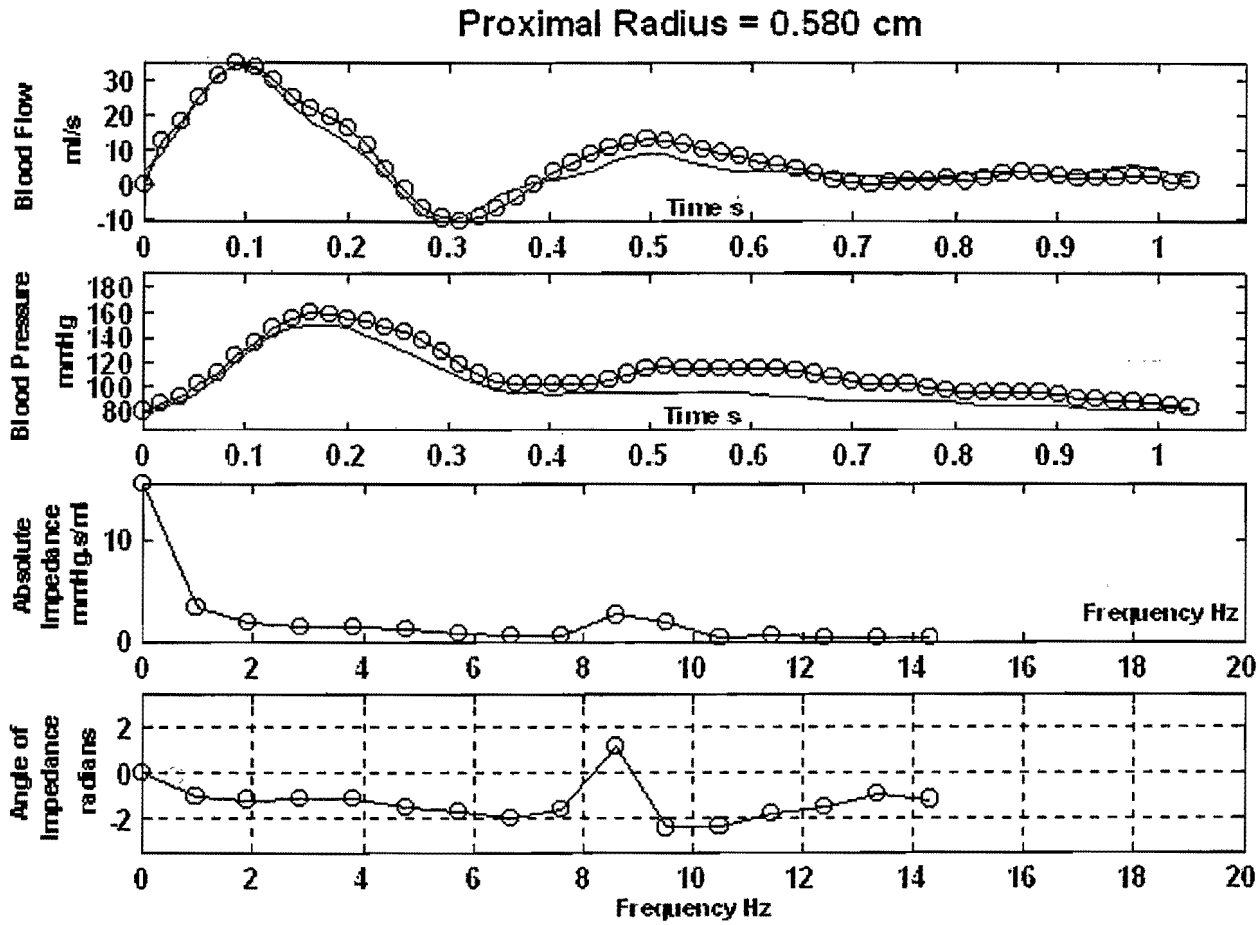

Figure 14.9 : Blood Flow and Pressure Waveforms as well as the Distal Impedance Spectrum for Normal # 6 Right Leg

(lines with circles = actual clinical waveforms
straight lines = under-determined Inverse Model predicted waveforms)

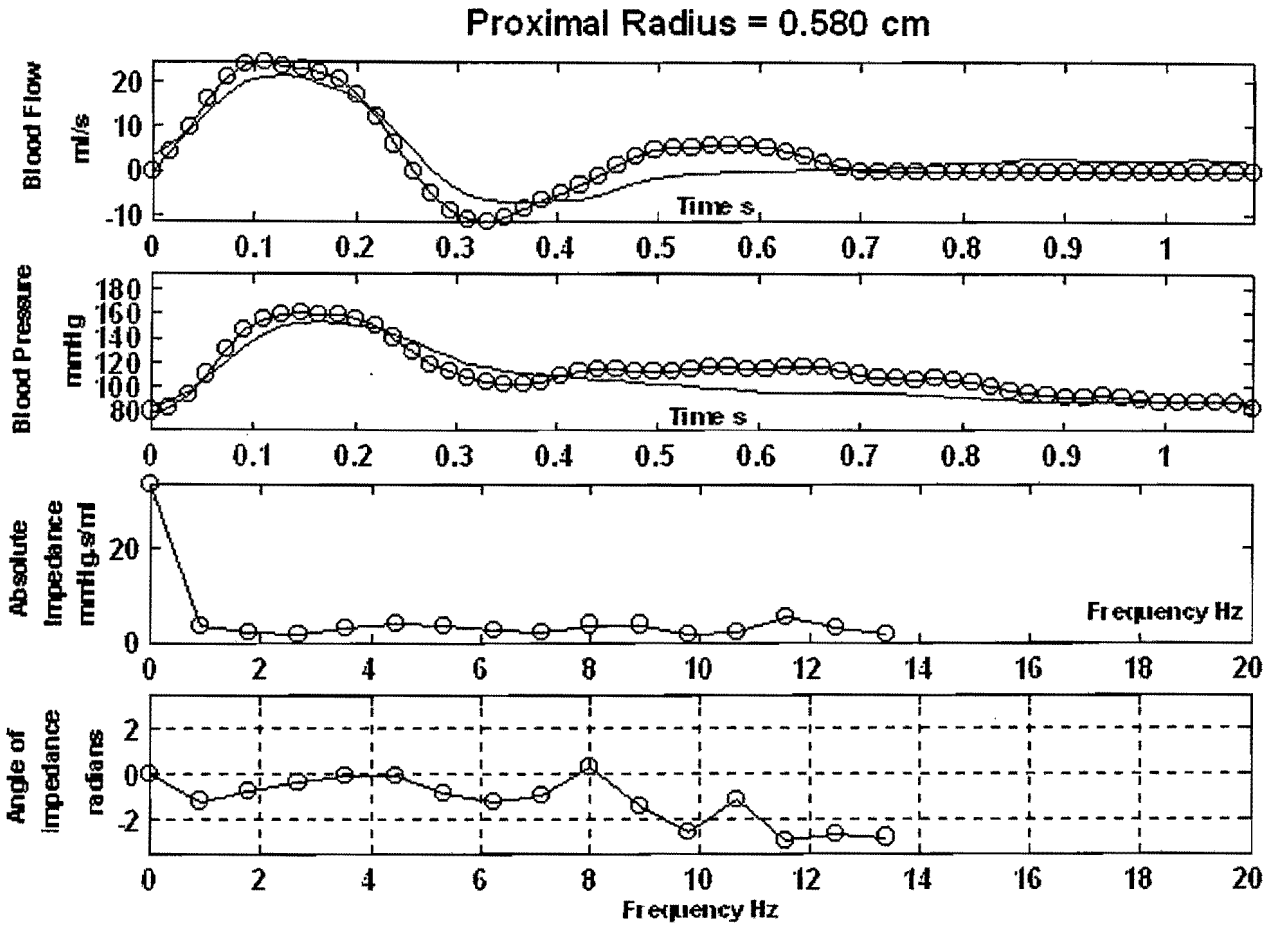

Figure 14.10: Blood Flow and Pressure Waveforms as well as the Distal Impedance Spectrum for Normal # 6 Left Leg

(lines with circles = actual clinical waveforms
straight lines = under-determined Inverse Model predicted waveforms)

14.4.2 DISCUSSION of the UNDERDETERMINED INVERSE MODEL RESULTS for NORMAL SUBJECTS

Error graphs : The error graphs (Figures 14.3 - 14.4) of all the normal subjects, indicate physiologically normal arterial Sample Regions because the minimum error regions are well above the defined critical stenosis radius. The minima extend over the normal range of radii for the external iliac artery. These normal error graphs are similar to the error graphs of a computer simulated normal subject [see Figure 9.4] .

Flow and Pressure Waveforms : All the normal flow waveforms (Figures 14.5 – 14.10) , except Figure 14.8 (due to a poorly insonated artery[1]) demonstrate the distinct triphasic nature of the external iliac Doppler waveform. The under-determined Inverse Model was able to achieve good waveform fits for both the Flow and Pressure waveforms of all the normal subjects.

Distal impedance spectrum : The distal impedance spectra, are discussed in Chapter 15.

The under-determined Inverse Model was therefore able to accurately diagnose the normal arterial state, and was also able to fit transmission line generated waveforms to normal clinically measured haemodynamic waveforms.

14.5 CLINICAL SUBJECTS WITH PROXIMAL ARTERIAL DISEASE

Three patients with Proximal Arterial Disease were analysed for this study (i.e. Patient #3, #10, #12 ... see Appendix 3). Patient #3 had Proximal disease only in the left leg. Patient #10 had Proximal disease in both legs. Patient #12 had Proximal disease in both legs. The waveforms measured from Patient #12's right leg were not suitable for analysis. The Proximal disease measurements were therefore entitled : (Figures 14.11-14.18)

Patient #3 : Right and Left Legs
Patient #10: Right and Left Legs
Patient #12: Left Leg only

[1] Doppler waveforms acquired using a Duplex Doppler system showed the waveform at this site to be triphasic. The prototype haemodynamic data acquisition system recorded a waveform at the same site that was not triphasic. This discrepancy is most likely due to a poorly insonated artery in the latter case.

14.5.1 UNDERDETERMINED INVERSE MODEL RESULTS for SUBJECTS WITH PROXIMAL ARTERIAL DISEASE

Patient 3 – Independent Clinical Details :

Patient #3 was a 61 year old male, with cellulitus and rest pain in the left foot. The patient experienced claudication in both legs, with greater pain in the left leg. Duplex Doppler Ultrasound was independently used to visualise the patient's arteries. No proximal disease was detected in the right common femoral artery which had a diameter of 0.78 cm . A plaque was detected in the left common femoral artery (arterial diameter in un-stenosed region = 0.81 cm; plaque diameter = 0.47cm; patent artery radius in stenosed region = (0.81-0.47)/2 = 0.17 cm). The independent Duplex Doppler tests were conducted a few minutes before this study.

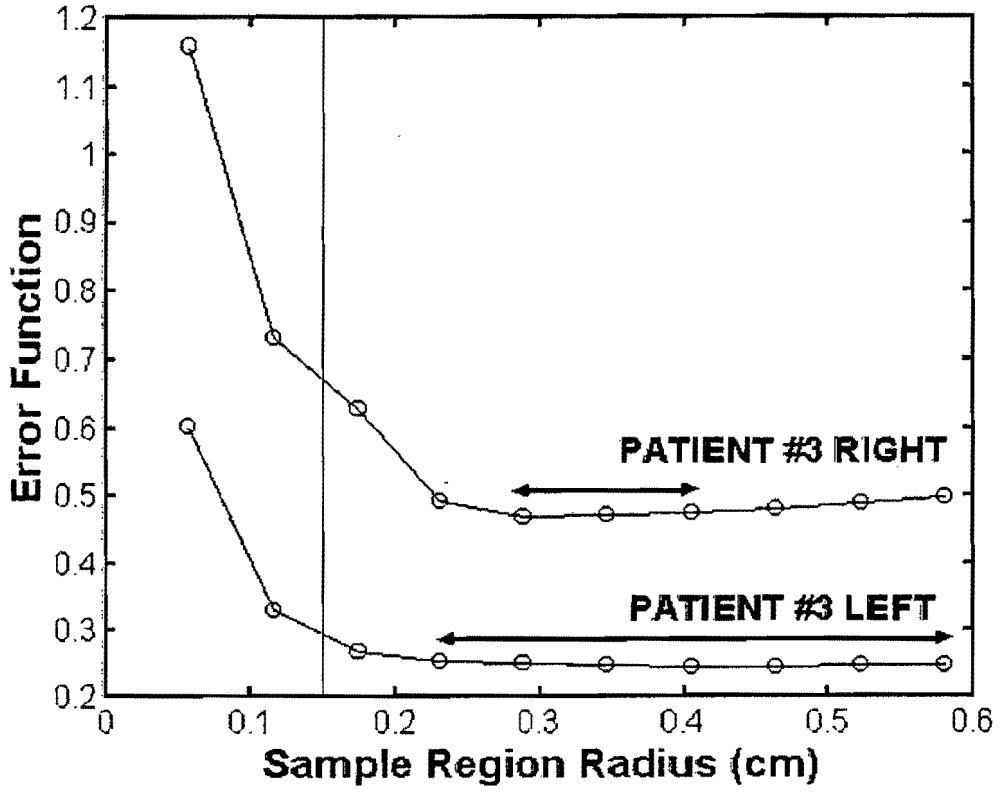

Figure 14.11: Flow Error Graphs for Patient #3, both limbs The double headed arrow defines the 'minimum error region'. The thin vertical line defines critical stenosis (estimated as 50% of 'normal' radius, where normal radius is defined as 0.29cm)

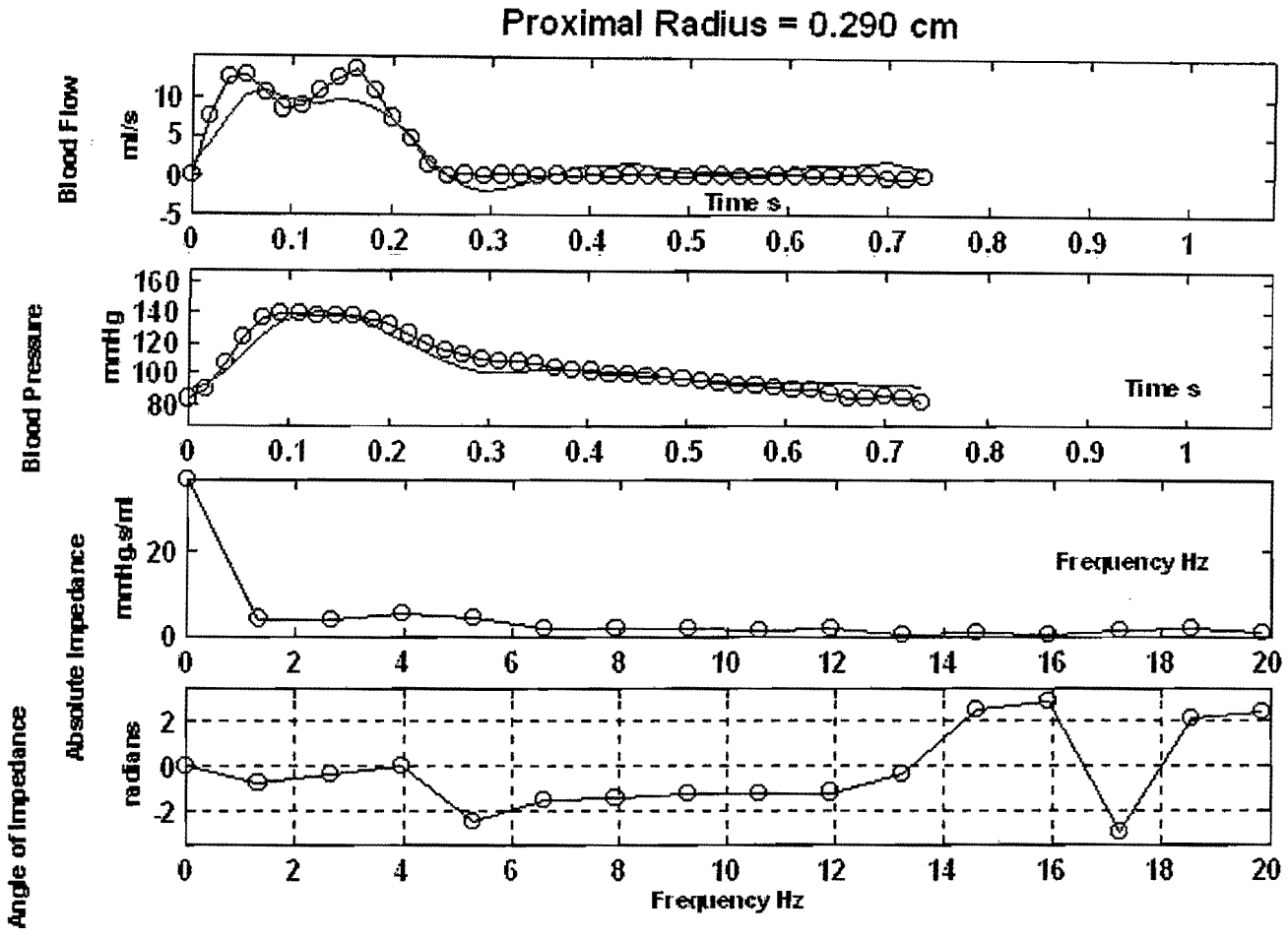

Figure 14.12 : Blood Flow and Pressure Waveforms as well as the Distal Impedance Spectrum for Patient #3 Right Leg

(lines with circles = actual clinical waveforms
straight lines = under-determined Inverse Model predicted waveforms)

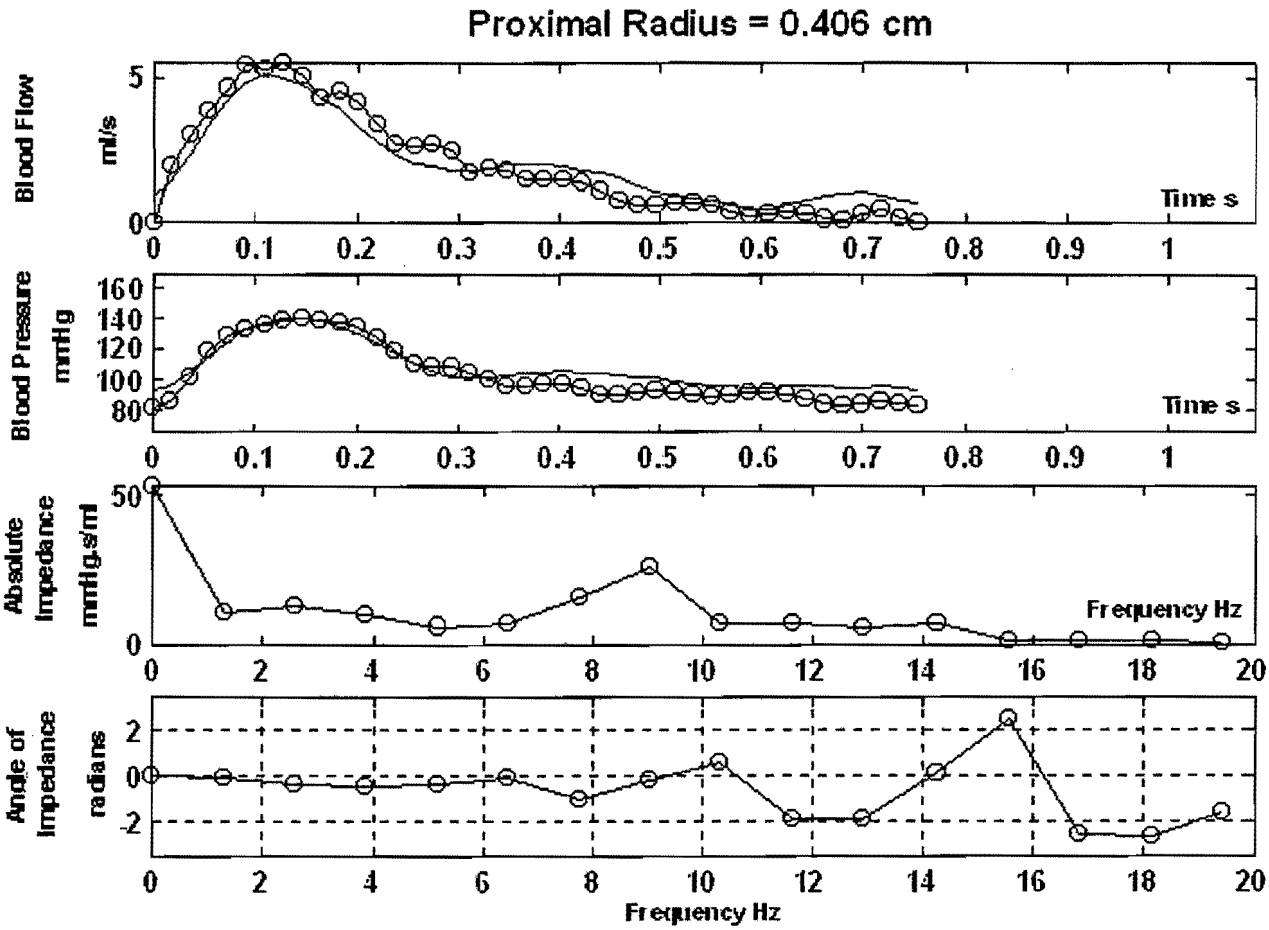

Figure 14.13 : Blood Flow and Pressure Waveforms as well as the Distal Impedance Spectrum for Patient #3 Left Leg

(lines with circles = actual clinical waveforms
straight lines = under-determined Inverse Model predicted waveforms)

Patient 10 – Independent Clinical Details

Patient 10 was a 64 year old male. The patient experienced rest pain in the right leg which was also swollen. His left leg had been similarly swollen and painful previously, but had recovered. A peripheral angiogram taken one day before this study showed widespread arterial disease, including aortic disease (multiple ulcerated plaques), bilateral proximal disease of the external iliac and common femoral arteries, as well as bilateral superficial femoral artery occlusion. Both the right peroneal and right posterior tibial arteries were occluded and the right anterior tibial was patent. There was no distal runoff in the leg.

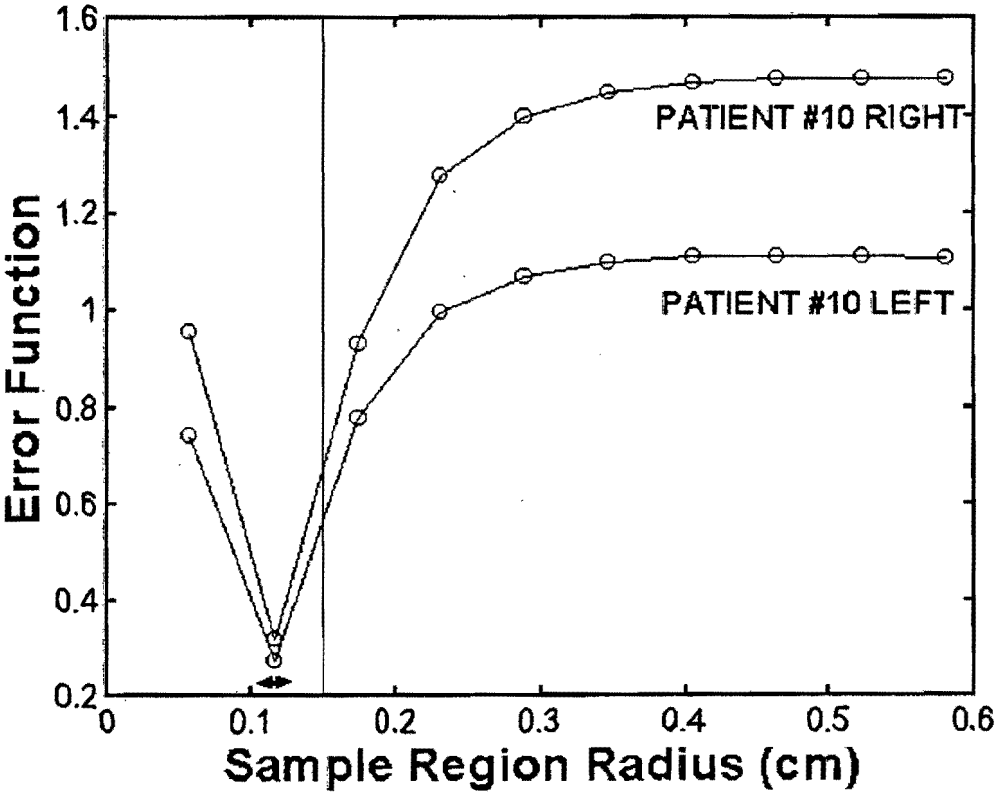

Figure 14.14 : Flow Error Graphs for Patient #10, both limbs The double headed arrow defines the 'minimum error region' which in both cases is the same as the 'minimum error point'. The thin vertical line defines critical stenosis (estimated as 50% of 'normal' radius, where normal radius is defined as 0.29cm)

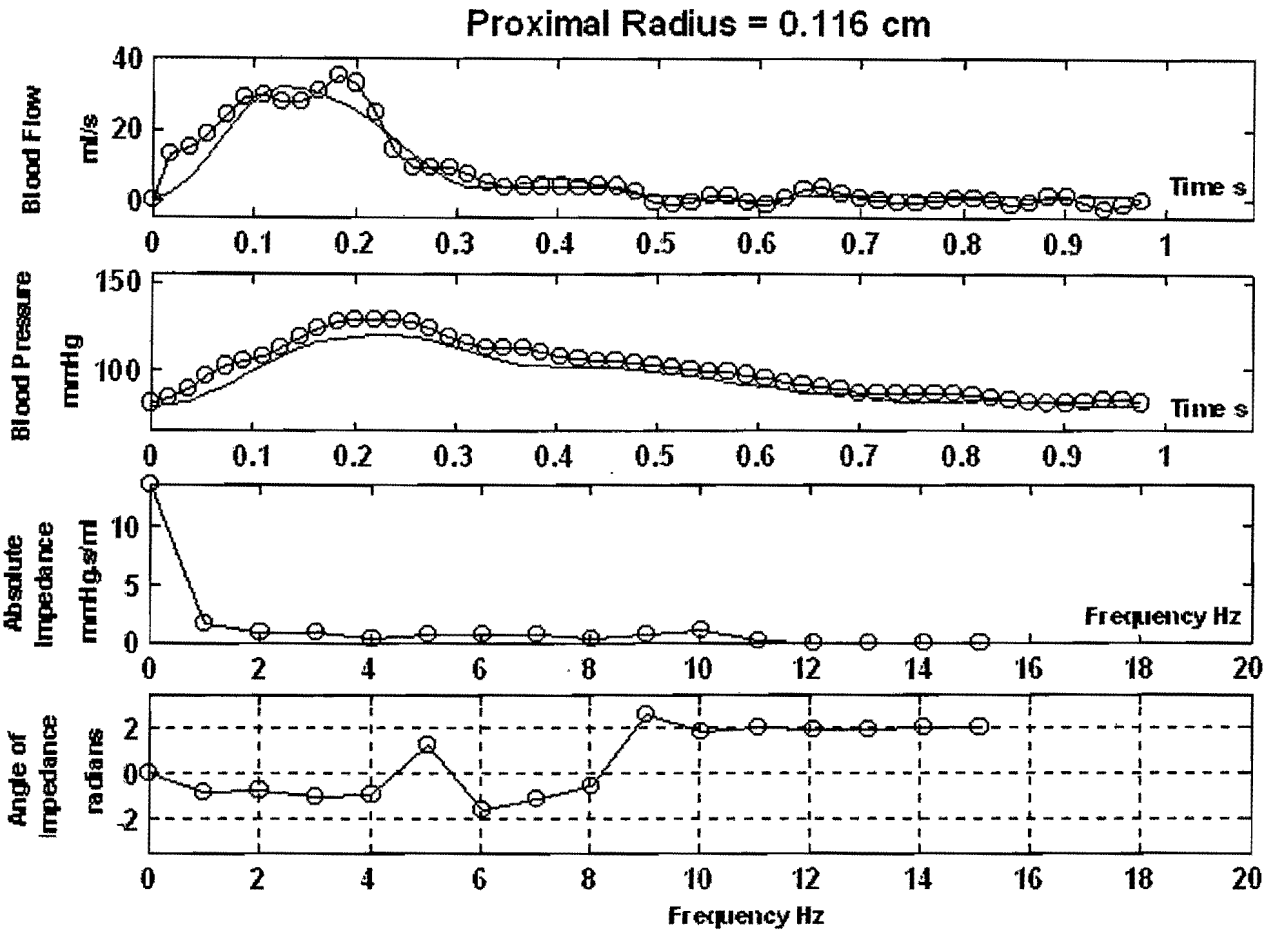

Figure 14.15 : Blood Flow and Pressure Waveforms as well as the Distal Impedance Spectrum for Patient #10 Right Leg

(lines with circles = actual clinical waveforms
straight lines = under-determined Inverse Model predicted waveforms)

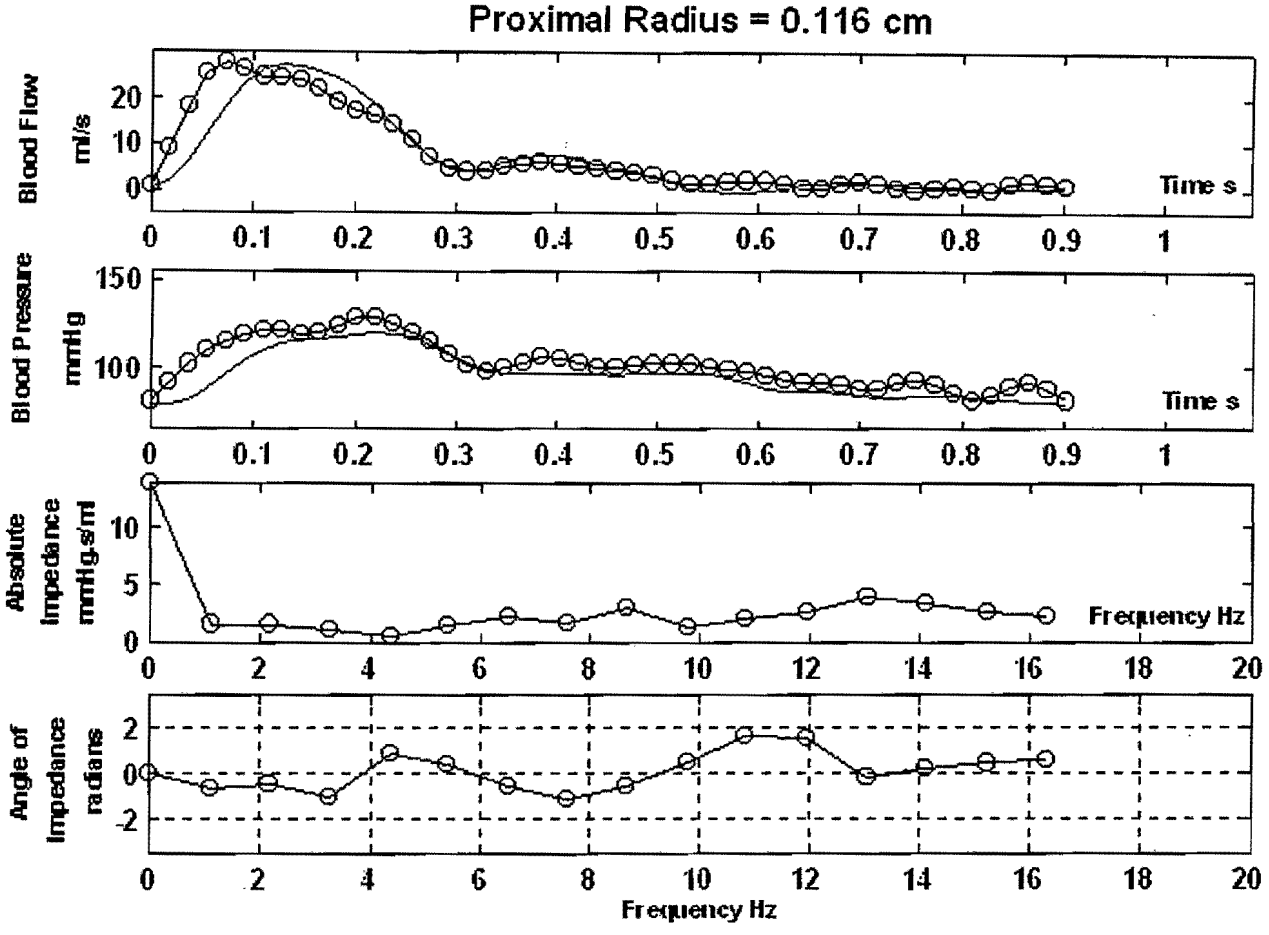

Figure 14.16 : Blood Flow and Pressure Waveforms as well as the Distal Impedance Spectrum for Patient #10 Left Leg

(lines with circles = actual clinical waveforms
straight lines = under-determined Inverse Model predicted waveforms)

Patient 12 – Independent Clinical Details

Patient 12 was a 72 year old female. The patient experienced rest pain in the right foot. A peripheral angiogram two months prior to this study showed bilateral superficial femoral artery occlusion, and distal disease. Duplex Doppler Ultrasound showed Proximal common femoral disease in both legs. The independent Duplex Doppler Ultrasound was conducted a few minutes before this study. Only waveforms from the patients left leg, were suitable (repeatable and low baseline drift in pressure waveform) for analysis by the Inverse Model.

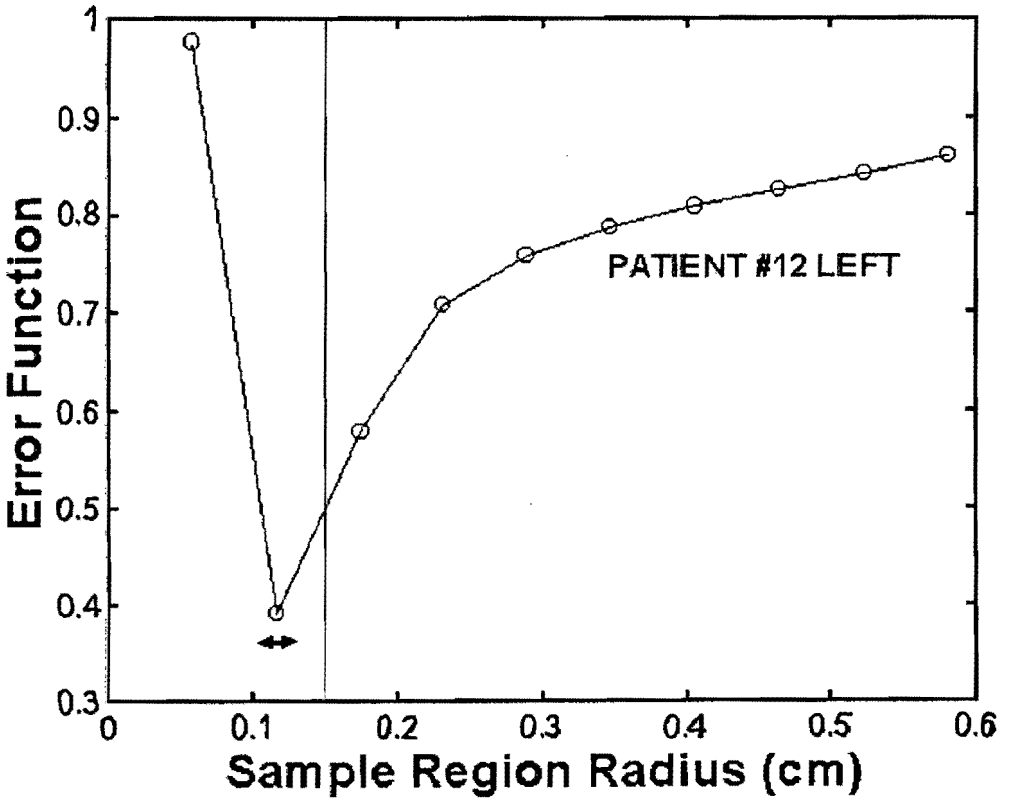

Figure 14.17 : Flow Error Graph for Patient #12, Left Leg The double headed arrow defines the 'minimum error region' which in this case is the same as the 'minimum error point'. The thin vertical line defines critical stenosis (estimated as 50% of 'normal' radius, where normal radius is defined as 0.29cm)

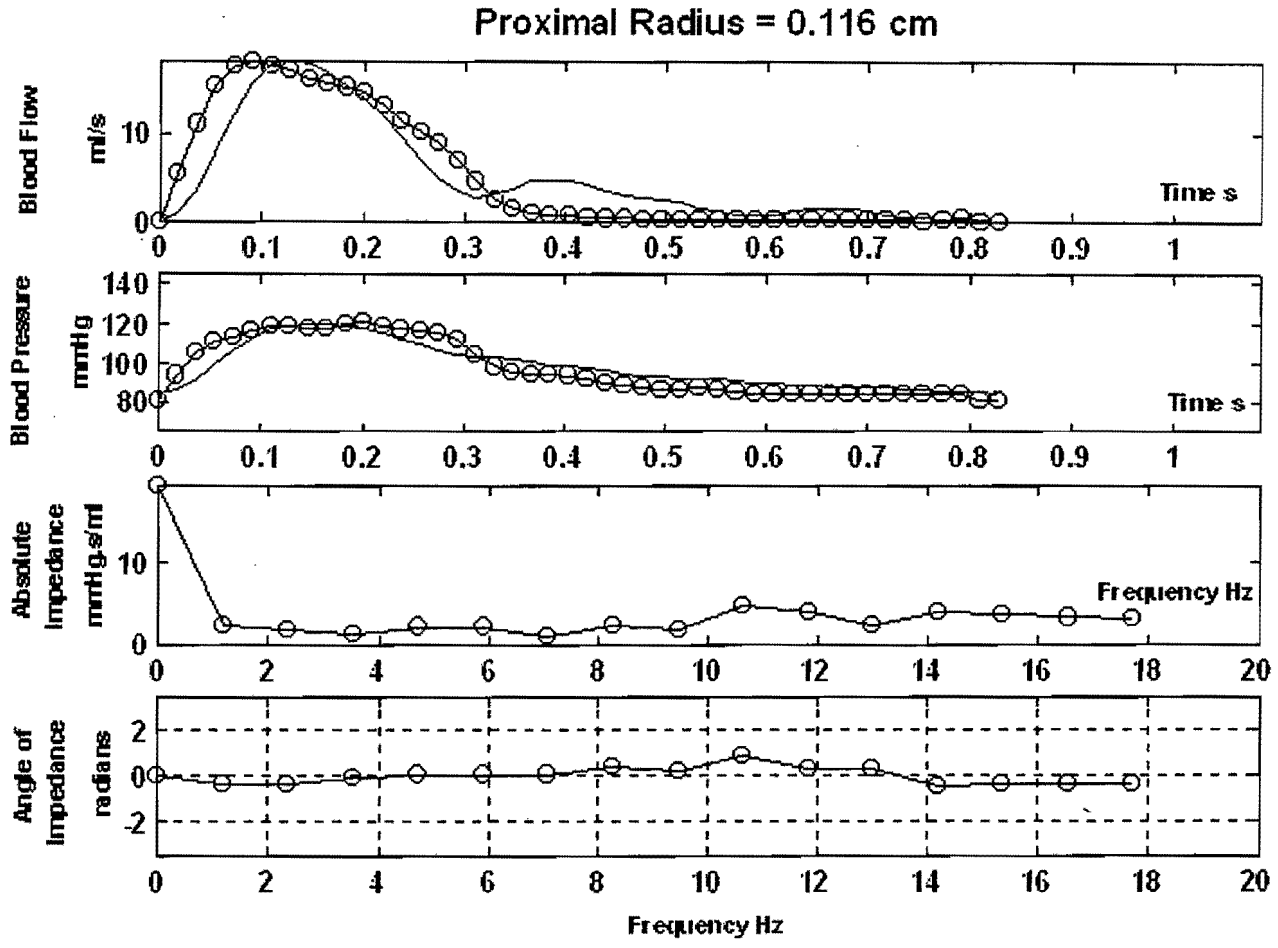

Figure 14.18 : Blood Flow and Pressure Waveforms as well as the Distal Impedance Spectrum for Patient #12 Left Leg

(lines with circles = actual clinical waveforms
straight lines = under-determined Inverse Model predicted waveforms)

14.5.2 DISCUSSION of the UNDERDETERMINED INVERSE MODEL RESULTS for SUBJECTS WITH PROXIMAL DISEASE

14.5.2.1 Patient # 3 :

Error Graphs : The error graphs (Figure 14.11) for both limbs of patient # 3, indicate normal arterial Sample Regions. Whilst the right leg was confirmed to be normal by independent clinical tests, left leg proximal disease was detected by independent Duplex Doppler ultrasound. For patient #3's left limb the under-determined Inverse Model appears to contradict independent clinical findings. This implies a possible *false negative* prediction by the Inverse Model. However it is possible that the clinically confirmed stenosis is present downstream from the measurement site which would not be classified as Sample Region disease by the Inverse Model. Further analysis of the Distal Impedance spectrum of Patient # 3, presented in Chapter 15, suggests that the under-determined Inverse Model concurs with clinical findings. The *apparent predictive error* appears to be due to the scenario described in Section 14.3.2

Flow and Pressure Waveforms : Patient #3's right limb flow waveform , whilst classified as normal by the under-determined Inverse Model is not a characteristic triphasic or biphasic waveform. The calculated PI was 4.7107 . Independent Duplex Doppler readings did however demonstrate a biphasic waveform at the same site, indicating that the Duplex Doppler system was technically superior to the continuous-Doppler based Data Acquisition system . Patient #3's left limb, shows damping which is qualitatively indicative of proximal disease, and has a calculated PI of 2.8447. The Inverse Model, achieved good fits, for all the Flow and Pressure waveforms (Figure 14.12-13) of Patient #3.

14.5.2.2 Patient # 10 :

Error Graphs : Both error graphs (Figure 14.14) for Patient #10, indicate the left and right Sample Regions are diseased. The minimum error regions are the same as minimum error points in both cases, and the under-determined Inverse Model predicts a radius that is smaller than the defined radius of a critical stenosis The Inverse Model is therefore in agreement with independent clinical diagnosis.

Flow and Pressure Waveforms : The monophasic flow waveforms (Figure 14.15-14.16) for both limbs are qualitatively indicative of proximal arterial disease. The calculated PI's are

8.3240 and 4.8706 for the right and left external iliac arteries respectively. Despite their monophasic nature both flow waveforms have a small mean flow component relative to their peak flows which results in large PI's. The under-determined Inverse Model predictions are in agreement with the angiogram tests, implying that the PI is not a good indicator of proximal disease in this case. The under-determined Inverse Model achieved good fits for all the Flow and Pressure waveforms of Patient #10.

14.5.2.3 Patient # 12 :

Error Graphs : The error graph (Figure 14.17) for patient # 12, is similar to those of patient #10. The position of the predicted minimum at an arterial radius less than the defined radius for critical stenosis , indicates stenotic arterial disease.

Flow and Pressure Waveforms : The damped flow waveform of patient #12's left limb (Figure 14.18) is qualitatively indicative of arterial stenosis. The calculated PI is 3.5902. The Inverse Model achieved good fits for both Flow and Pressure Waveforms, of patient # 12

CHAPTER 15
PRELIMINARY CLINICAL FEASIBILITY STUDY 3 : THE DISTAL ARTERIAL REGION

The Distal arterial region refers to the region of the arterial tree downstream from the measurement site. In the context of this study, this region has been defined as the distal arterial tree of the lower limb including profunda and superficial femoral; popliteal; peroneal; posterior and anterior tibial arteries (Figure 15.1).

For the Three-Division transmission line model of the arterial system, the distal arterial region is represented by the downstream load impedance that the Sample Region "sees".

The fully implemented Inverse Model provides two types of output, whereby the state of the Distal Arterial region may be studied :

1. The Distal Impedance Spectrum [Figure 9.6]
2. Decomposition of Total Flow and Pressure waveforms into Forward Travelling and Reverse Travelling (Reflected) components. [Figures 9.7-9.8]

It is difficult analyse the pressure and flow waveforms in order to obtain information about the Distal region, if their amplitudes are not known . Whilst amplitude scaling was a prerequisite for analysis of the Sample Region using the under-determined Inverse Model, this is not the case if the Distal Region is to be analysed separately. A normalised distal spectrum may be used for this purpose because it is not necessary to integrate this spectrum into an electrical model. Therefore a simpler clinical approach of using *normalised*[1] impedance spectra was adopted. This prevents errors introduced by amplitude scaling (in Chapter 14) from being carried over into Distal region analysis, but also results in the loss of important amplitude information.

This approach (which is a consequence of the technical limitations of the prototype haemodynamic data acquisition system) allowed for impedance spectra wave-shape analysis, but does not allow for decomposition of waveforms into their Forward-travelling and Reverse-travelling components.

---

[1] Note that a normalised spectrum is the result of a special form of amplitude scaling. Actual amplitudes have no meaning in a normalised impedance because only the relative amplitudes are important. Amplitude scaling, as implemented in Chapter 14 estimates "actual " amplitudes i.e. the actual amplitude does have a meaning

15.1 THEORY

Extensive research has been carried out on the characteristics of the arterial impedance spectrum. However because there are no existing data acquisition systems that are capable of obtaining the flow and pressure waveforms non-invasively, the impedance spectrum has found little clinical application. The invasive approach is used clinically primary for angiograms and pull-through pressures.

Forward Arterial Impedance Models : Chang et al [1995] discusses a 't-tube' forward model of arterial impedance, and Einav et al [1992] discusses a tapered forward transmission line model of arterial impedance.

Physiological Variation of Arterial Impedance : The effect of peripheral vasodilation, and vasoconstriction, on the arterial impedance spectrum was investigated by O'Rourke & Taylor [1966] . The effect of contraction of peripheral muscles on the impedance spectrum , was investigated by Lambert et al [1985].

Pathological Variation of Arterial Impedance : Ashe et al [1989] investigated canine clinical arterial impedance, in the presence of an aorto-femoral bypass graft. The effect of just distal arterial stenosis on the clinical canine impedance spectrum was studied by Farrar et al [1980]

Inverse Lumped Circuit Model of Arterial Impedance : A unique *lumped-circuit* approach, to an inverse model of the impedance spectrum of the peripheral vasculature was published by Bauer et al [1985]

In addition to the above mentioned studies , a number of textbooks Milnor [1989]; Nichols & O'Rourke [1990] , discuss arterial impedance, including qualitative changes .

Because only the shape of the distal impedance spectrum is known, a simple approach of comparing the shapes of computer simulated disease impedance spectra to clinically measured impedance spectra has been adopted.

The Forward model was used to simulate the effect of isolated distal disease on the pressure and flow waveforms in the Sample region. Whilst peripheral bed vasodilation in response to an upstream blockage, may also simulated using the Forward Arterial Model, it has not been included in the computer simulations because of insufficient clinical data to verify its' accuracy.

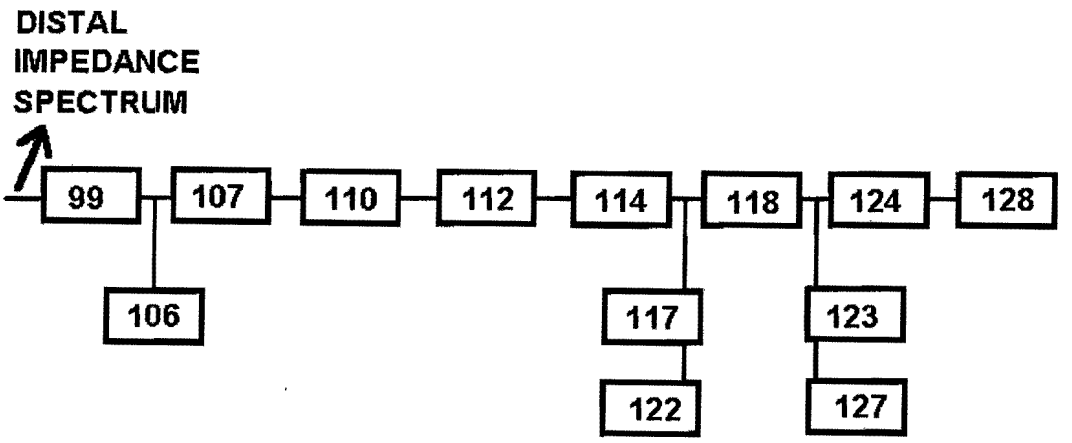

Figure 15.1 : Arterial segments in the right leg representing the Distal Arterial Region. Note that the numbering and position of these segments is identical to that of the arterial system presented in Figure 2.3 and Table 2.3.

Collateral vessels that are formed in response to an arterial blockage cannot be simulated in the Forward Model in it's existing form. The presence of these collateral vessels would also influence the Distal Impedance Spectrum. Age, hypertension, and other arterial diseases may also affect the Distal Impedance Spectrum to varying extents.

Multiple and distributed arterial disease is often present . Such disease may also be simulated using the Forward Model. However, the objective of this chapter was not to conduct an exhaustive and comprehensive study of impedance spectrum variation with distal arterial disease. The simpler simulations conducted here serve as a *starting point* for Distal Region disease investigation. Detailed clinical studies correlated with computer simulation of distal arterial disease are only feasible after the technical hurdle of a non-invasive, quantitative Haemodynamic Data Acquisition System has been overcome.

15.2 OBJECTIVE

The objective of this Chapter is to investigate whether the shape of the distal impedance spectrum of the lower limb may be analysed in order to predict a normal as well as a diseased distal arterial system.

15.3 METHOD

The state of the computer simulated distal arterial system was varied using the Forward Model. Each of the 13 modelled distal arterial segments (Figure 15.1) were progressively stenosed by reducing their radii . The absolute impedance spectra were then normalised, such that the DC level was equal to one.

The computer simulated distal impedance spectra are illustrated in Figures 15.2 – 15.13. The distal impedance spectra of 3 normal subjects (i.e. 6 normal limbs) are illustrated in Figures 15.15 - 15.17. The distal impedance spectra of a further 6 subjects with a variety of distal arterial disease profiles, are illustrated in Figures 15.18 – 15.23.

The shapes of the impedance spectra of the clinical subjects (normals and patients), were qualitatively compared to the shapes of the computer simulated spectra.

15.4.1 COMPUTER SIMULATED DISTAL REGION DISEASE

Computer simulated impedance spectra generated by the Forward Model are illustrated in Figures 15.2-15.14. The normal impedance spectrum (i.e. no simulated stenotic disease) is represented by the line with circles –o- . The colour scheme referenced to percentage stenosis presented in Figure 15.2 is continued in Figures 15.3 – 15.14.

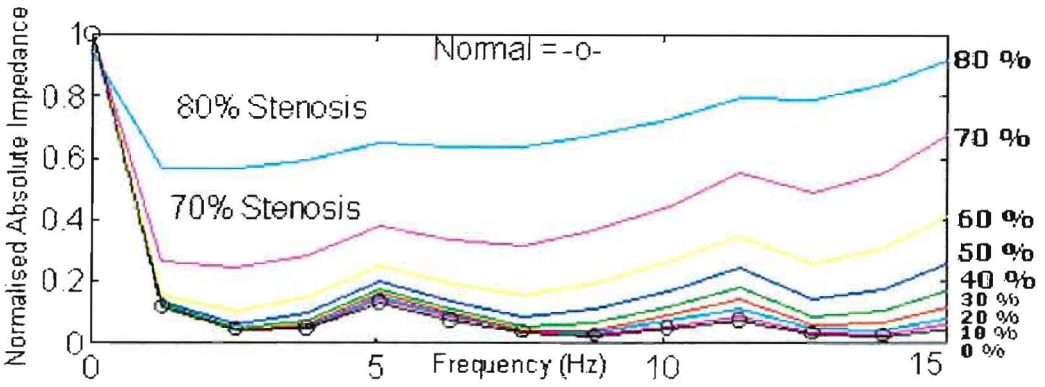

Figure 15.2 Progressive Stenosis in External Iliac (99)

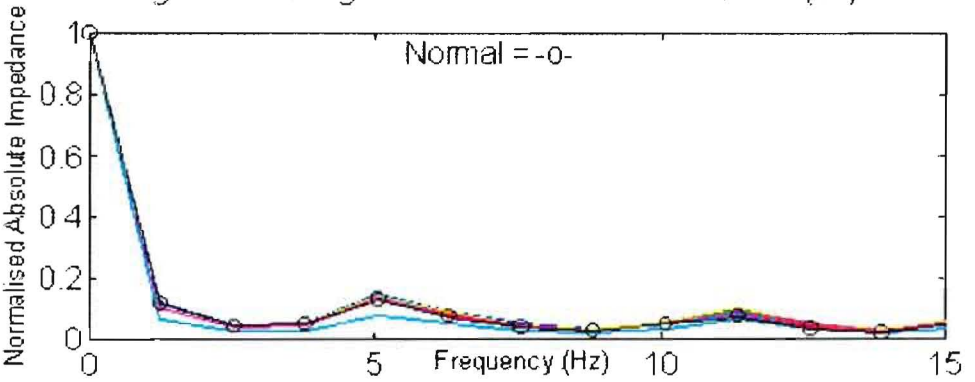

Figure 15.3 Progressive Stenosis in Profunda Femorus (106)

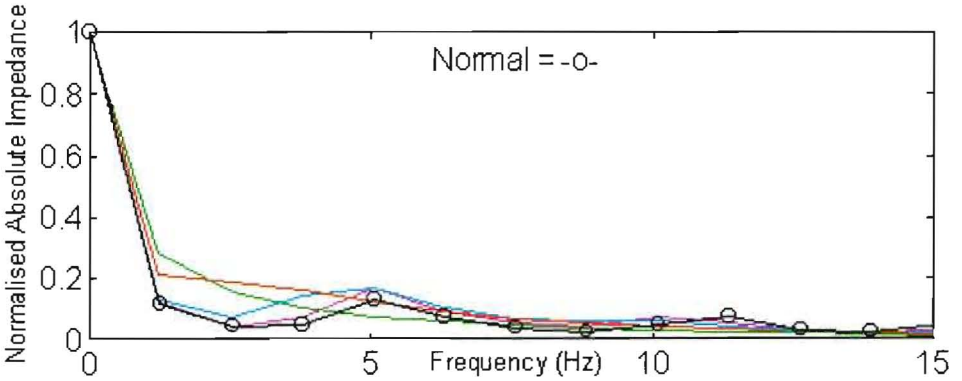

Figure 15.4 Progressive Stenosis in Superficial Femoral (107)

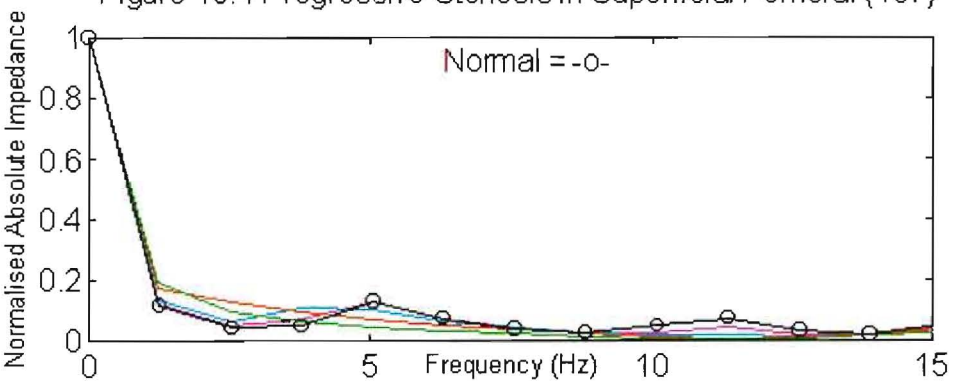

Figure 15.5 Progressive Stenosis in Superficial Femoral (110)

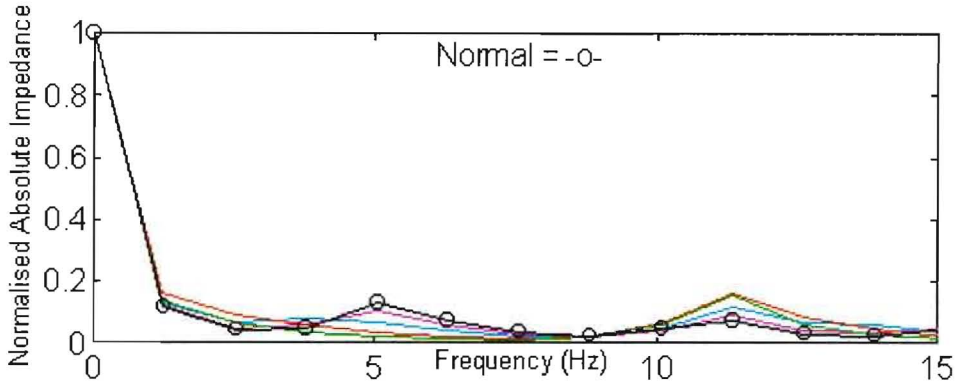

Figure 15.6 Progressive Stenosis in Popliteal (112)

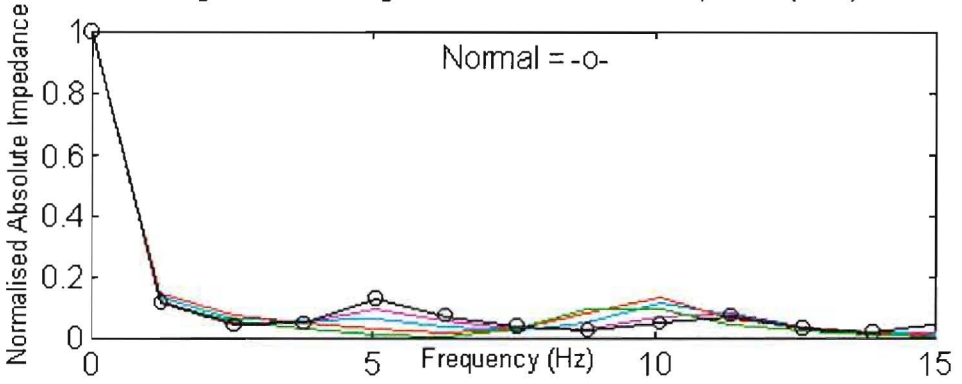

Figure 15.7 Progressive Stenosis in Popliteal (114)

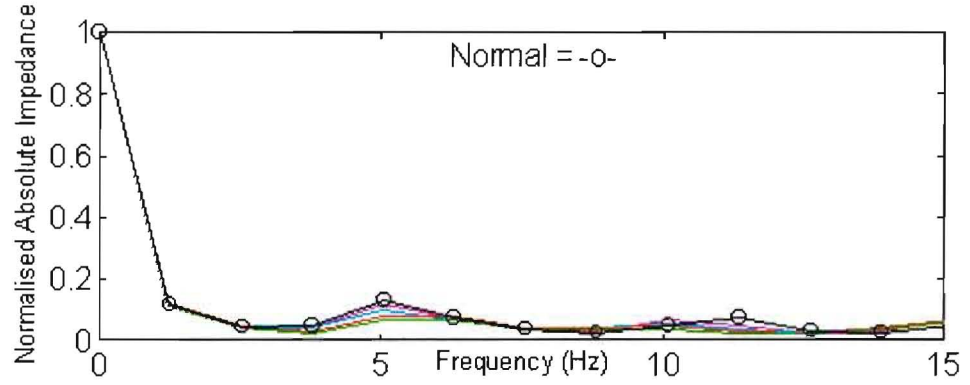

Figure 15.8 Progressive Stenosis in Posterior Tibial (117)

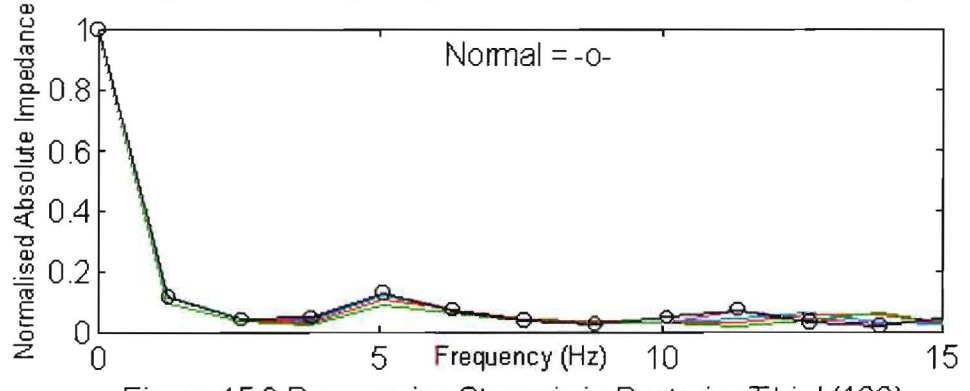

Figure 15.9 Progressive Stenosis in Posterior Tibial (122)

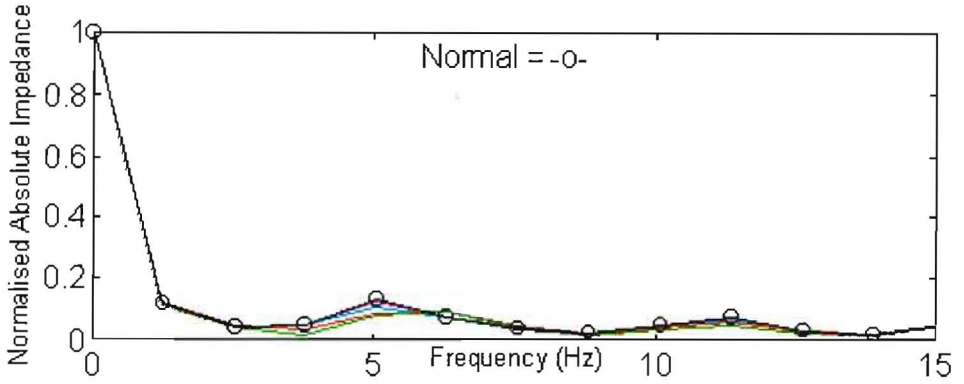

Figure 15.10 Progressive Stenosis in Anterior Tibial (118)

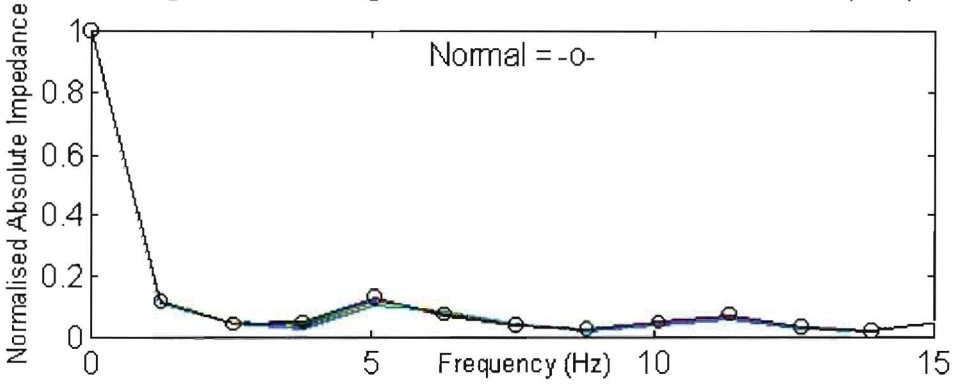

Figure 15.11 Progressive Stenosis in Peroneal (123)

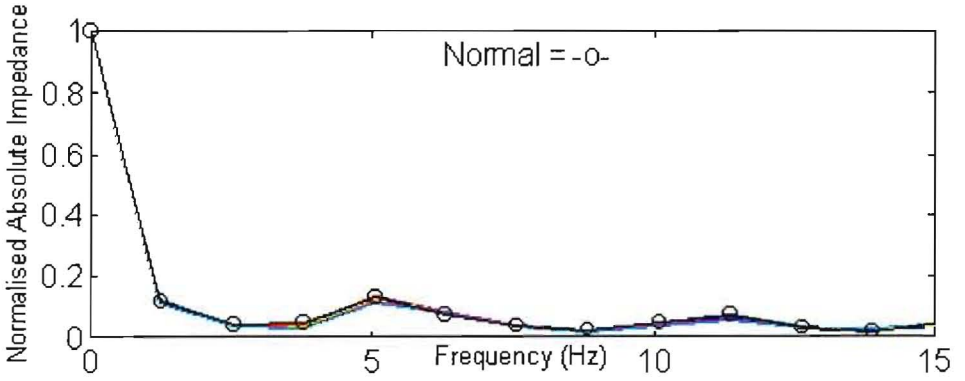

Figure 15.12 Progressive Stenosis in Peroneal (127)

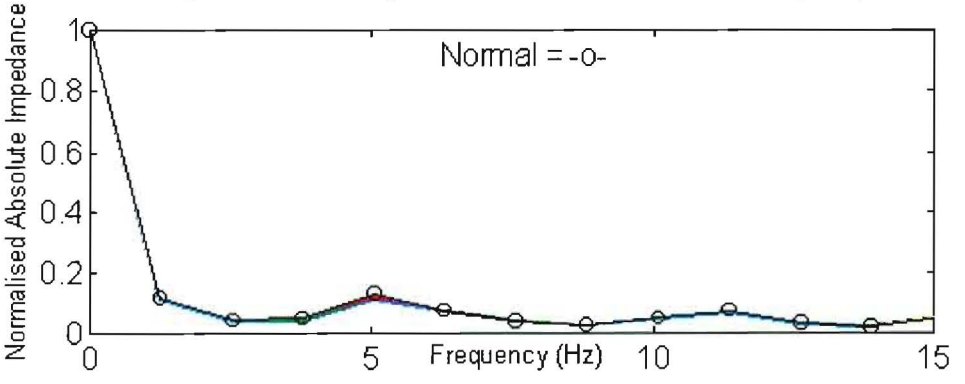

Figure 15.13 Progressive Stenosis in Anterior Tibial (124)

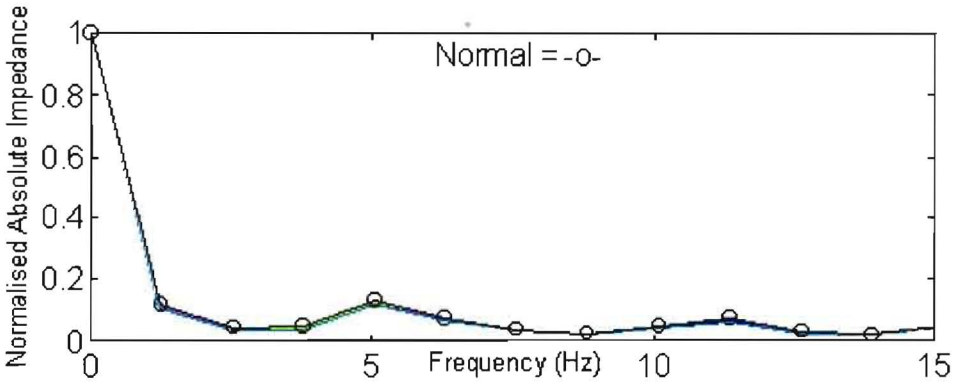

Figure 15.14 Progressive Stenosis in Anterior Tibial (128)

15.5.1 DISCUSSION OF COMPUTER SIMULATED IMPEDANCE SPECTRA

Figures 15.2 –15.14 present computer simulated distal arterial impedance spectra "seen" by the external iliac artery. It is immediately apparent from a study of these graphs, that the closer a stenosis is to the point of measurement, the greater its effect on the impedance spectrum.

A notable exception is computer simulated profunda femorus disease. Stenotic disease in the profunda femorus artery appears to have very little effect on the impedance spectrum at the external iliac artery (Figure 15.3), despite its close proximity. The superficial femoral artery is approximately the same distance (as the profunda femorus) from the external iliac artery, but when stenosed has a slightly greater effect on external iliac input impedance (Figure 15.4).

The arterial region just distal to the point of measurement has the most significant effect on the distal impedance spectrum (Figure 15.2). With progressive stenosis there is a notable increase, in the relative amplitudes of the higher harmonics. Such a characteristic deviation of a impedance spectrum from its normal value, would therefore be an indicator of 'just distal' stenosis. This region is defined to be proximal by clinical definition, but is defined to be 'just distal' by the Inverse Model definition (Chapter 14.3.2). Clinically induced 'just distal' stenosis in the canine femoral artery [Farrar et al, 1980] also shows a similar increase in the amplitudes (as well as relative amplitudes) of the higher harmonics of the impedance spectrum.

Single isolated superficial femoral artery stenosis, results in a subtle 'smoothening' of the normal impedance spectrum (Figures 15.4-15.5). Similar disease further downstream, in the popliteal artery, results in the reduction and eventual loss of the first 'normal' maximum at 5 Hz , and an increase in the second 'normal' maximum at 11 Hz (Figures 15.6 - 15.7). However it is important to note that these waveform changes are relatively small, and are only valid for single isolated arterial stenosis with no collateral artery formation.

Stenosis in the arteries below the knee (Figures 15.8 - 15.14) has very little effect on the normalised shape of the external iliac impedance spectrum.

15.4.2 DISTAL IMPEDANCE SPECTRA OF NORMAL CLINICAL SUBJECTS

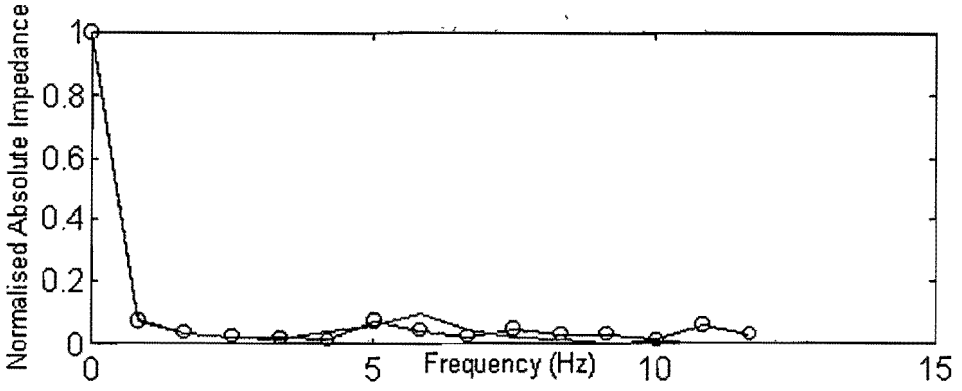

Figure 15.15 Normal 4 : Right Leg = o, Left Leg = -

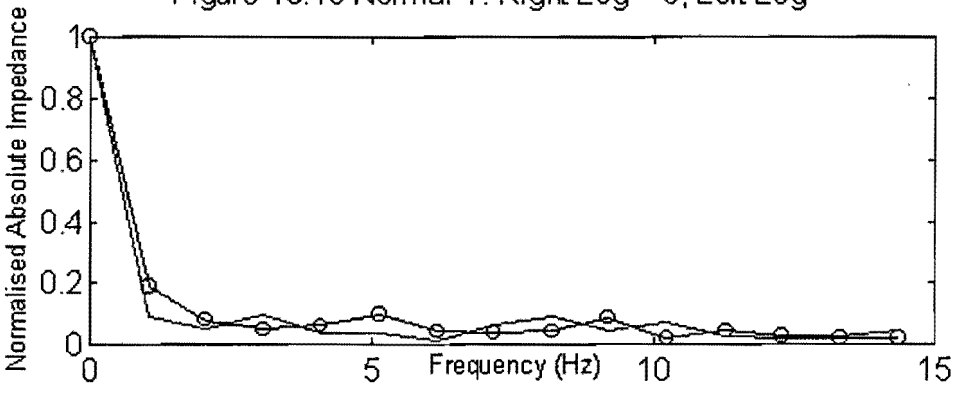

Figure 15.16 Normal 5 : Right Leg = o, Left Leg = -

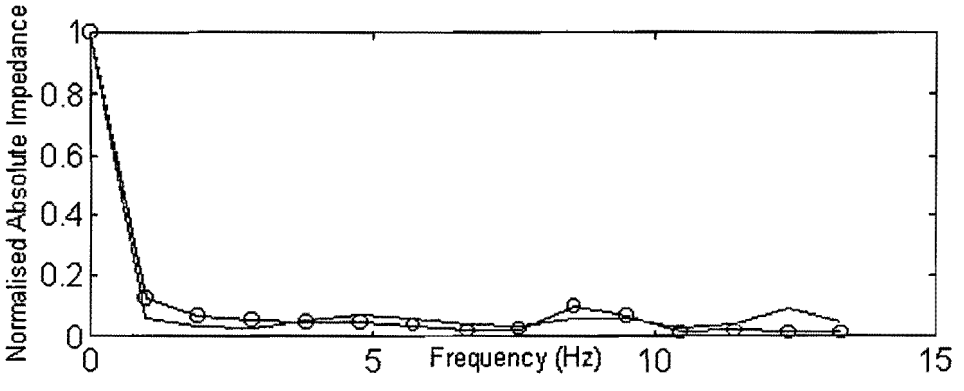

Figure 15.17 Normal 6 : Right Leg = o, Left Leg = -

15.3.2 SUBJECTS WITH DISTAL REGION DISEASE

Six subjects with distal region disease were chosen. A combination of radiographic and Duplex Doppler studies revealed the following clinical profiles for these patients :

Patient #3 : Male , 61 year old. Normal right leg. Proximal disease in left leg; possible left distal disease .
Patient #7 : Male, 39 year old .Buerger's disease. Previously amputated right leg. Left popliteal occlusion.
Patient #11: Male, 56 year old. Problematic arterial graft in right leg. Normal left leg.
Patient #4 : Female, 86 year old .Normal right leg. Critical ischaemia in left leg – below knee amputation after this study.
Patient #5 : Male, 72 year old. Right popliteal occlusion. Normal left leg.
Patient #9 : Male, 56 year old. No readings taken for right leg. Problematic left arterial graft
(Note that further details are in Appendix 4.)

The distal disease measurements were therefore entitled :

Patient #3 : Right and Left Leg
Patient #7 : Left Leg only
Patient #11 : Right and Left Leg
Patient #4 : Right and Left Leg
Patient #5 : Right and Left Leg
Patient #9 : Left Leg only

15.4.3 DISTAL IMPEDANCE SPECTRA OF SUBJECTS WITH DISTAL DISEASE

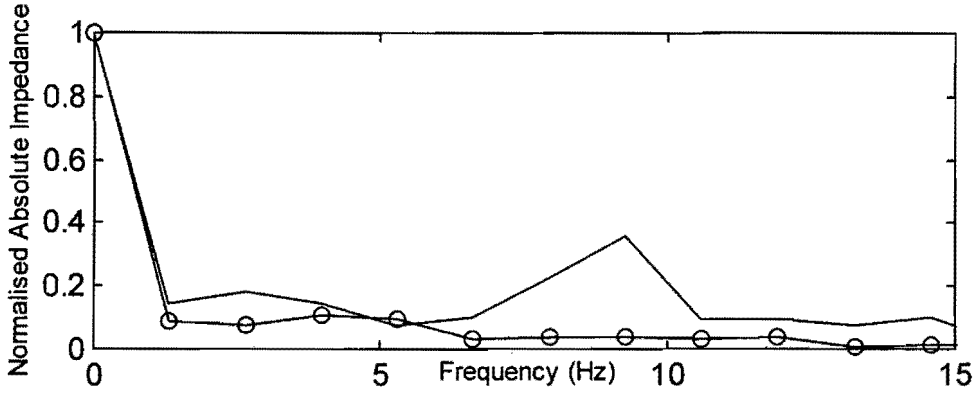

Figure 15.18 Patient 3 : Right Leg = o, Left Leg = -

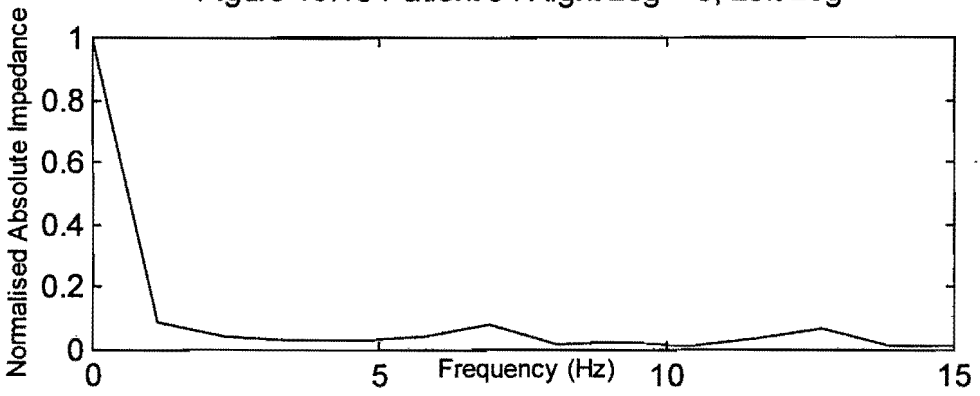

Figure 15.19 Patient 7 : Left Leg only

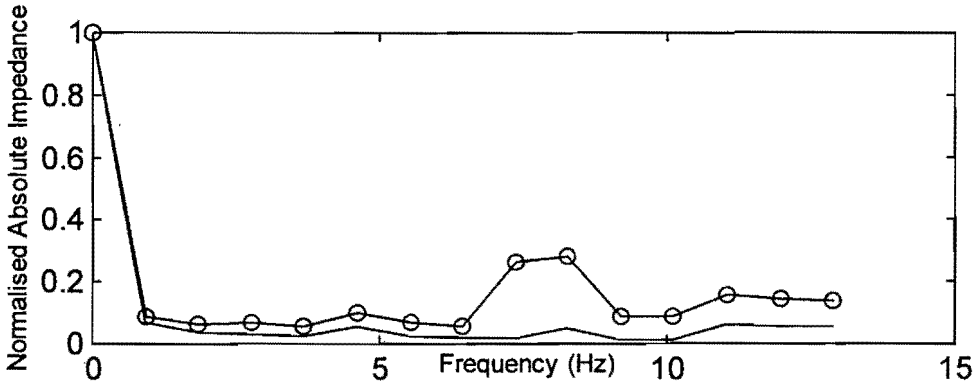

Figure 15.20 Patient 11 : Right Leg = o, Left Leg = -

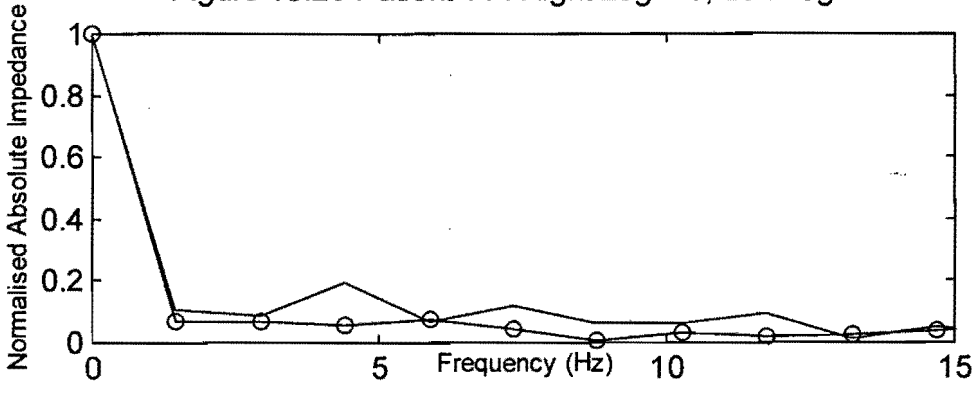

Figure 15.21 Patient 4 : Right Leg = o, Left Leg = -

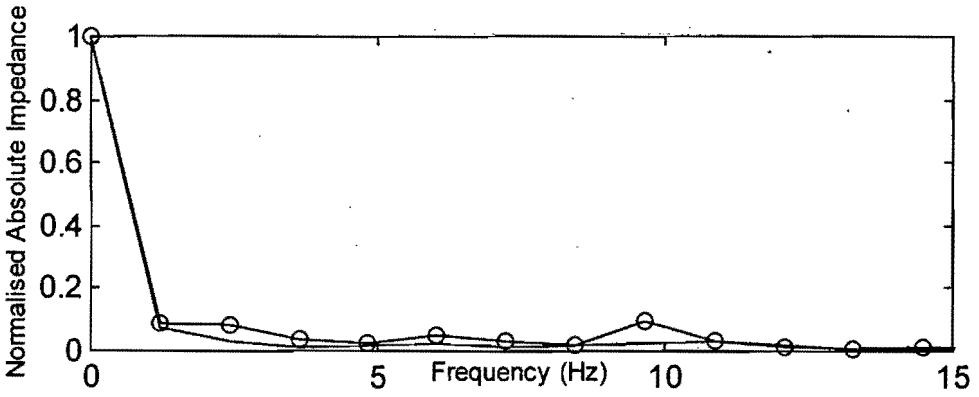

Figure 15.22 Patient 5 : Right Leg = o, Left Leg = -

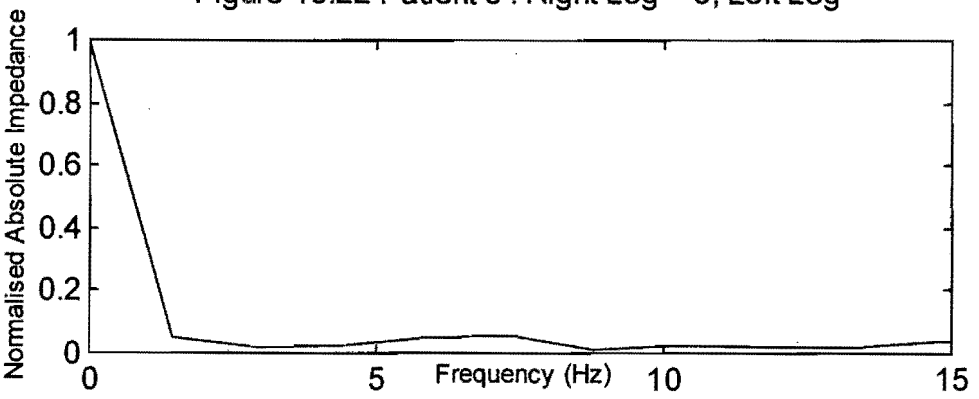

Figure 15.23 Patient 9 : Left Leg only

15.5.3 DISCUSSION OF PATIENT #3 IMPEDANCE SPECTRA

Patient #3 was investigated for Sample Region disease in Chapter 14. The Inverse Model predicted no Sample region disease, which appeared to contradict independent clinical diagnosis. However, inspection of the impedance spectrum of Patient #3 (Figure 15.18) reveals some important information. Firstly, there is a significant difference between the impedance spectra of the right and left legs. Clinical tests showed that the left leg of Patient #3 was problematic, whilst the right leg was normal. The impedance spectrum of the right leg does not indicate any deviation from the normal spectrum (whilst this does not rule out right 'very distal' disease, it does rule out right 'just distal' disease) . The left leg impedance spectrum shows a significant increase in the higher harmonics. Comparison of the left leg impedance spectrum to a computer simulated 'just distal' 60% stenosis (Figure 15.2) shows a similar characteristic increase in amplitude of the 2^{nd} maxima , but contrasting behaviour of the spectrum above the 2^{nd} maxima. Simulated popliteal stenosis (Figures 15.6-15.7) also shows and increase in the 2^{nd} maxima with a decrease in the 1^{st} maxima, but the 2^{nd} maxima is much smaller than it is for patient 3's left leg . The clinically measured distal impedance spectrum is most similar to the computer simulated 60% external iliac stenosis .

This suggests that Patient #3 has stenotic disease somewhere between the measurement site on external iliac artery, and the bifurcation of that artery into the superficial and deep (profunda) femoral arteries. Clinical terminology would classify this as proximal disease whilst the inverse model would classify this as 'distal' disease. Therefore the possible false negative mentioned in Chapter 14 may be due to this terminology difference (see Chapter 14.3.2). Impedance spectrum analysis suggests common femoral ('just distal') disease in the left limb of Patient #3 and is in agreement with the clinical diagnosis.

15.5.4 DISCUSSION OF CLINICAL DISTALLY-DISEASED PATIENT IMPEDANCE SPECTRA

Examination of impedance spectra for Patients #7, #4, #5. #9 did not reveal any distinguishing similarity with computer simulated, single isolated disease spectra. Indeed the spectra appear to be either normal or similar to the spectra of "very" distal disease. Of these patients (#7, #4, #5), with the exception of Patient #9, who had a possibly problematic arterial graft, all had independently confirmed very distal disease. There is little bilateral variation in impedance spectra for both patients #4 and #5 therefore the only possible conclusions for these patients (from a normalised impedance spectrum standpoint), are that they are either normal, or very distally diseased.

Patient #11 shows a significant difference between left and right impedance spectra (Figure 15.20). The problematic arterial graft in the right leg results in an impedance spectrum that bears some similarity to the 'just distal' disease in Figure 15.18. However, the computer simulated and clinical arterial graft spectra cannot be compared because of the difference between the physical properties of a normal artery and an artificial graft. The raised amplitudes in the 7Hz-8Hz band, appears to be qualitatively similar, to the scenario of input impedance of an occluded aorto-femoral graft ('AGCI') presented by [Ashe et al, 1989]. Note that even in the case of arterial occlusion arterial collaterals may still be present. However it is very difficult to reach any definite conclusions because of the unavailability of either detailed human clinical or theoretical arterial graft studies for comparison.

CHAPTER 16: DISCUSSION

The Inverse Arterial Model presented in this thesis is a unique addition to the vast and complex field of Human Arterial Modelling. It also introduces a shift from the paradigm that has driven theoretical arterial modelling for the last 35 years . The Inverse model allows complex electrical transmission line models to be used for clinical diagnosis and promises to spawn a new class of non-invasive vascular diagnostic machines. It not only provides solutions to problems that have not previously been tackled in the arterial modelling field, but like all research also raises further questions that would need to be answered by future research and development.

The development of Graphical Arterial Modelling Tools : A graphical approach has been chosen to implement both the Forward and Inverse models because this approach is particularly useful to the research process. This may also provide arterial researchers with a useful tool. Certainly a major hurdle in the arterial modelling field is the difficulty in setting up a detailed transmission line model. This difficulty is compounded if the researcher seeks to systematically modify this model to better represent clinical reality.

With a graphical model, the arterial researcher is not restricted by a predetermined model structure. For research purposes, an optimal model structure is often unknown. A variety of model structures may have to be implemented before the researcher is able to decide on the most suitable model. The graphical model introduced by this thesis, provides a model whose structure may be easily modified using a mouse driven user interface. Arterial sub-systems may be modelled in greater or less detail, according to specific research requirements. Arterial branches may be easily added or removed. Even the underlying mathematical equations used to represent a single tube element may be modified with relative ease.

The development of a language to implement this graphical model is a technical achievement of this thesis. Matlab and Simulink have been uniquely combined to form a new flowchart-based computer language. This is the ideal language for the implementation of any model algorithm because the logical relationship between the model equations, is represented visually in the form of a flowchart.

It would be reasonable to state that , without such a graphical model, it would be practically very difficult, if not virtually impossible to implement a complex Inverse model in a clinical setting. Therefore the graphical approach may be considered to be a further pre-requisite for an Inverse transmission model of the human arterial system.

The Forward Arterial Model : The accuracy and complexity of a state-of-the-art Forward arterial transmission line model has not been compromised in the development of an Inverse solution. Indeed, the strong point of the Inverse Model is its ability to retain a transmission line based representation of the human arterial system.

An Inverse model is, at best, as effective as its underlying Forward model. Therefore a lot of attention was paid to the development of a suitable Forward Model. The Forward arterial model has been shown to provide an accurate representation of the human arterial system under normal healthy as well as stenotically diseased conditions. The outputs from the Forward model compare favourably to outputs from equivalent computer simulated models, clinical research data, as well as a physical arterial model.

A drawback of this, and indeed every electrical circuit model, is its inability to include the effects of turbulence. A strong point of a transmission line model is its ability to quantitatively represent the effects of arterial propagation delays and wave reflections. A model which is able to take the effects of turbulence into consideration would be an improvement . Such a turbulence model may be able to be implemented as a 'hybrid' electrical circuit model which would retain the use of electrical circuit theory, whilst including non-linear effects such as turbulence as well.

The possible use of Arterial Allometry for Inverse Modelling purposes : The subject of cardiovascular allometry, and empirical clinical models has been introduced in Chapter 6. The results of allometric and clinical studies must be integrated into theoretical models, if these models are to be successfully used for clinical diagnosis. Forward arterial models have relied heavily on data for the physiologically 'normal' adult male subject. The use of allometry and empirical clinical models would allow the researcher to model the effects of age, gender, and body size on the state of the vascular system. The modelling of age-related cardiovascular variation is especially important because

stenotic arterial disease is prevalent amongst the elderly. Whilst arterial stenosis has been the focus of this thesis, it is also important to model the effects of co-existing arterial disease and other conditions such as hypertension and diabetes, which are often also present. Use of statistical General Linear Models may be a suitable approach to modelling the effect of multiple factors on the human arterial system.

Use of a Physical Arterial Model : The use of physical models to represent the arterial system was presented in Chapter 7. Whilst such models may be viewed as an intermediate step between an actual clinical subject and a computer simulation, there are some effects that are peculiar to physical arterial models. Despite this, there is good agreement between the presented physical model, and the computer simulated representation of that model. A physical model is not only useful for validation of a Forward arterial model, but it is also a very useful tool for the development and calibration of data acquisition equipment. The construction of a physical model is however a technically difficult and time consuming task. If the purpose of a physical arterial model is to validate a computer simulated model then it is recommended that existing data, such as the Segers [1997] physical model be used. If data acquisition equipment is being developed or calibrated or if haemodynamic effects such as flow profiles and turbulence are being studied, then a custom built physical model of the relevant complexity would be useful. Finite element computer models have not been included in this thesis, but may also prove to be useful to researchers investigating the Inverse Model.

The Computer Simulated Inverse Arterial Model : The Three Division Inverse model has been introduced and tested using a Forward computer model. Computer simulated tests have indicated the ability of this model to track variations in Sample Region radius, even under conditions of Pre-Sample or Distal Region disease. In addition, the Inverse model has been shown to be robust enough to handle 'reasonable' levels of amplitude distortion. The full over-determined Inverse Model could not be implemented in a clinical setting, because the prototype data acquisition system was unable to measure the absolute amplitudes of the blood flow and pressure waveforms. Therefore an under-determined version of this model was tested clinically. The objective of using the under-determined model was specifically to provide some clinical evidence that the over-determined Inverse Model could be useful for clinical diagnosis. Having

provided such evidence the next step would be a pilot clinical study using the full over-determined Inverse Model.

The Preliminary Clinical Feasibility Study : The clinical feasibility study has been presented in order to test the diagnostic potential of the Inverse Model, and to identify the prerequisites for its full clinical implementation. The ability of the under-determined version of the Inverse Model to accurately fit Flow and Pressure waveforms, as well as its success in predicting normal and diseased arterial states indicates that the full over-determined Inverse Model may perform even better. In addition to analysis of the Pre-Sample, Sample , and Distal regions, an important part of the feasibility study was a critique of the data acquisition equipment. Of the three arterial regions studied the most important region was the Arterial Sample region. The Pre-Sample and Distal regions, whilst they may assume greater importance in subsequent Inverse Models, have been presented more for the sake of completion. The predictions of the under-determined Inverse model were subject to the technical limitations of the data acquisition system. However the results of the feasibility study are promising enough, to warrant a pilot clinical study using the over-determined Inverse Model, provided the criteria for the data acquisition equipment have first been met. Because of the statistical nature of the Doppler Flow Velocity spectrum, it is important in future, to include a statistical criteria (e.g. Maximum Likelihood) in the selection of the 'best fit'. The 'best fit' selection criteria must also be developed further to include a single 'best fit' equation that would be a measure of the combined fits for flow as well as pressure waveforms. The development of a 'best fit' criteria is not as trivial as it may appear. It is an important area that needs to be investigated further, but its importance is directly correlated to the level of automation that would be expected of the Inverse Model. For the purposes of the feasibility study the simple flow error function combined with visual inspection was sufficient. The flow error function has been used for the preliminary clinical study simply because analysis of the doppler flow waveform is well established in clinical diagnosis of arterial disease. However an objective and statistically accurate error function is an additional prerequisite for a pilot clinical study.

Preliminary Clinical Feasibility Study of the Arterial Sample Region

The undetermined version of the Inverse Model has shown the ability to fit complex variations in waveform shapes of both normal and proximally diseased subjects studied. Predictions of the under-determined Inverse Model have shown

a good correlation with independent clinical diagnosis. Therefore it may be concluded that the full over-determined Inverse Model may be suitable for clinical usage. The suitability of the over-determined Inverse must be confirmed with a pilot study that would have as a prerequisite to its implementation the development of a haemodynamic data acquisition system capable of recording both the shapes and absolute amplitudes of the blood pressure and the blood flow waveforms.

Preliminary Clinical Feasibility Study of the Arterial Pre-Sample Region : Studies of the average aortic pulse wave velocity have been inconclusive. Aortic pulse wave velocity appears to be dependent on a number of factors (which may be inter-related) including age, hypertension, body size, and aortic disease. Therefore it is difficult to isolate the effects of aortic disease, without first quantifying the effects of the previously mentioned factors on the aortic pulse wave velocity. All the inter-related factors need to be first studied and modelled, before the information contained within the average aortic pulse wave velocity measurement may be critically analysed. Note that the pulse wave velocity is not measured, but is calculated from an estimated aortic length (and the measured pulse arrival time) and this is why the factors that influence aortic length must be studied and quantified. Furthermore the relationship between pulse wave velocity and the physical properties of an artery depend on Young's modulus, wall thickness, and arterial radius (according to the Moens-Korteweg : Equation 7.1) therefore the factors that influence these variables must also be studied and quantified. A model such as a statistical General Linear Model may prove to be useful approach to unravelling the multiple factors that influence the pulse wave velocity.

Aortic disease may either retard or advance the aortic pulse wave velocity. This makes it even more difficult to draw conclusions, especially from average aortic pulse wave velocity calculations. Disease may possibly also affect arterial length, and this should be researched further.

However an important conclusion of this aspect of the feasibility study, is that it is very easy to non-invasively estimate the *average* aortic pulse wave velocity. Ease and simplicity of measurement is an important factor in clinical tests. The Doppler velocity spectrum appears to be more suited to pulse wave time measurements, because the sharp systolic upstroke makes it easier to identify the waveform starting point. In contrast the upstroke of the pressure waveform has a lower

bandwidth, making it more difficult to accurately identify the waveform starting point.

Extreme deviations from expected velocities may indicate the presence of severe (aortic) Pre-Sample region disease. Measurements may also be taken at multiple accessible sites (e.g. common femoral , popliteal, etc) in order to determine a *local segmental* average pulse wave velocity.

Local pulse wave velocity measurements may be also carried out using a Duplex Doppler unit that provides a synchronous ECG lead. This would allow the measurement of *local* pulse wave velocities over short distances. Such measurements may provide much greater diagnostic information than the average aortic pulse wave velocity, which is measured over approximately 40cm.

Preliminary Clinical Feasibility Study of the Arterial Distal Region :
The feasibility study was limited to the analysis of haemodynamic waveforms, acquired at a single point i.e. External Iliac artery. Whilst the shape of the Distal Impedance spectrum has been shown to be sensitive to 'just distal' disease, it appears to be insensitive to very distal disease. This may be rectified by using the Inverse Model to analyse waveforms taken from a series of spatial measurements e.g. common femoral; popliteal; and dorsalis pedis arteries. The use of multiple spatial measurements would also allow the Three Division Model to be integrated with transfer function based models.

Distal analysis is able to detect distal stenotic disease that is close to the measurement point (i.e. above the knee), but is unable to separate a normal distal system from a system with very distal disease (i.e. below the knee).

An important feature that has been neglected is the modelling of *collateral circulation*. The existing forward model may be modified to allow the representation of collateral circulation. This would be a necessary prerequisite if the (diseased) distal arterial region is to be studied in further detail. The presence of collaterals would influence the distal impedance spectrum. If this spectrum is to be analysed then the effects of collaterals on it must be understood. In addition, a *closed loop circulatory model* may be necessary in order to automatically model the effect of peripheral vasodilation in response to upstream stenosis.

Prototype Haemodynamic Data-acquisition equipment used for the Preliminary Clinical Feasibility Study : Whilst the prototype haemodynamic data-acquisition has some unique features, it cannot be used in its current form with the full over-determined Inverse Model. A complex model such as the Three Division Inverse Model cannot be implemented without a suitable data acquisition system. The clinical feasibility study has demonstrated that a simple Continuous Wave Doppler Ultrasound system is not adequate to obtain flow velocity waveforms since the amplitude of the flow cannot be ascertained. For this reason a Duplex Doppler system is required. In addition the absolute pressure waveform is also required, and this is not available on commercially available equipment. If the Inverse Model is to be used on the clinical arena, then this hurdle must first be overcome by the development of custom equipment.

Whilst Duplex Doppler Ultrasound provides a relatively accurate measure of the blood flow velocity waveform, it must be integrated with real time arterial tonometry. This could be realised if an integrated tonometer and Duplex Doppler probe could be developed. Such an integrated probe would also allow for the synchronous measurement of flow and pressure, instead of the pseudo-synchronous measurements used thus far.

Arterial tonometry continues to be the subject of intensive research. Its lack of clinical application is due to the fact that clinicians have become reliant on other diagnostic technologies such as Doppler flow velocity measurement , advanced imaging technology, and sphygmanometric or invasive catheter-based pressure measurements. This preliminary study has illustrated the importance of measuring the entire blood pressure waveform, using a technique such as arterial tonometry, for the purpose of non-invasive Inverse arterial modelling.

Blood Pressure as well as Flow Velocity waveforms may be obtained *invasively*, with good accuracy, using catheter tip transducers. Whilst this may provide an alternative route to implementation of the Inverse Model, the author discourages this route in favour of the non-invasive approach. It is precisely techniques such as the Inverse Model, that may improve non-invasive diagnostic accuracy, to the extent that non-invasive diagnosis may even challenge established invasive approaches .

Because such development would be costly and time consuming, the scope of this thesis has been limited to the theoretical development of an Inverse Transmission Line Model, computer simulated testing of that model, and a preliminary clinical feasibility study that uses an under-determined version of the Inverse Model.

Further applications of the Inverse Model : The over-determined version of the Inverse Model may possibly be applied to the study of arterial aneurysms. In addition other arterial subsystems , such as the carotid or coronary arteries could be studied. An advanced implementation of the Distal Region model may prove to be of great importance in the study of the arteries within the cranium. The carotid artery provides a readily accessible site for non-invasive flow and pressure measurement. The downstream arterial system is not as accessible, and is often the site of stenotic or aneurysmal disease. Distal impedance spectrum analysis at the level of the carotid artery may therefore prove to be a very useful diagnostic tool.

The assumption that the arterial input waveform (at the level of the ascending aorta) had the same shape for all subjects, could be replaced by using a clinically measured aortic flow waveform. Furthermore the assumption that the Pre-Sample Region was normal for all subjects, could be replaced by using clinical measurements (e.g Duplex Doppler, CT scan, ect ..) of the Pre-Sample Region.
Both these assumptions were made for this thesis because of the unavailability of advanced arterial imaging and haemodynamic recording tools.

CHAPTER 17
CONCLUSION

In 1903 the Wright brothers tested the first engine-powered flying machine. The first flight lasted only 12 seconds, but served to demonstrate the practical potential of the theory of flying machines. The under-determined version of the Inverse Arterial Model, which was implemented in a clinical setting, serves the same role here. The results of the preliminary clinical feasibility study are promising but the study is not statistically rigorous and the under-determined model does not guarantee a unique solution. The under-determined model has been presented to draw attention to the clinical diagnostic potential of the underlying theory of a critically-determined or over-determined Inverse Transmission Model. The unique theory of an Inverse transmission line model has been rigorously presented and the complex problem of applying such a model to clinical diagnosis has been studied with more detail than has been previously done. Most of the major practical and theoretical hurdles have been overcome. Yet medical engineering research is an ongoing process and a few technical hurdles still need to be overcome before the Inverse Transmission Line Model may be used for routine clinical diagnosis.

WHAT HAS BEEN ACHIEVED :

1. A new visual algorithmic language has been developed using a unique combination of Matlab and Simulink.
2. Using this algorithmic language, a unique set a visual tools has been developed for the construction of Forward and Inverse arterial transmission line models.
3. A Forward transmission line model that is relatively accurate (compared to other arterial transmission line models) has been developed.
4. The outputs of the Forward Model have been compared to the outputs of a physical arterial model.
5. A unique prototype Haemodynamic Data-Acquisition system, that is able to non-invasively measure and record both the arterial flow velocity and blood pressure waveform shapes, has been developed.
6. A unique inverse solution to the electrical transmission line equations representing the human arterial system has been proposed and tested. This critically-determined inverse solution has been termed the 'Three Division' Inverse Transmission Line Model

7. An under-determined version of the Three Division Inverse Model has been developed and tested in a clinical setting. This was done in order to provide some insight into the potential clinical applicability of the over-determined Inverse Model (which cannot be clinically implemented without the development of custom haemodynamic data acquisition equipment)

PROPOSALS FOR FUTURE RESEARCH AND DEVELOPMENT :

1. The development of a haemodynamic data-acquisition system that would be able to non-invasively measure synchronous blood flow and pressure waveforms.
2. Further research into the application of arterial allometry to improve the clinical diagnosis of arterial disease.
3. A quantitative database recording synchronous arterial flow and pressure waveforms and an ECG together with clinically measured and quantified arterial data using e.g. quantitative Angiography and quantitative Duplex Doppler Ultrasound, from subjects with variety of normal and diseased arterial states.
4. Further development of both Forward and Inverse transmission line models to include the effects of arterial collaterals, local and global arterial feedback systems, and turbulence.
5. The Inverse Model is able to resolve Flow and Pressure waveforms into their Forward and Reflected components. This may prove to be a very useful Clinical tool. It's use is dependent on the development of custom haemodynamic data acquisition equipment.

WHAT CAN BE SUBSEQUENTLY ACHIEVED :

1. The development of a new class of medical equipment for the non-invasive diagnosis of arterial disease.
2. The further development of a new theoretical field of Inverse Transmission Line Theory.

REFERENCES

1. **Allard L, Cloutier G, Durand L-G** : Doppler velocity ratio measurements evaluated in a phantom model of multiple arterial disease, Ultrasound Med Biol, Vol 21 (4), pp 471-480, 1995

2. **Ashe JW, Marble AE, Swingler DN, Landymore RW, Kinley CE** : The measurement of afterload, vascular input impedance, and power distribution in aorto-femoral bypass, J Biomechanics, Vol 22 (5), pp 447- 453, 1989

3. **Atkinson P, Woodcock JP** : Doppler Ultrasound and its use in Clinical Measurement, Academic Press, London, 1982

4. **Avolio AP :** Multi-branched Model of the Human Arterial System, Med& Biol Eng & Comput, Vol 18, pp 709-718, 1980

5. **Bascom PAJ, Cobbold RSC, Routh HF, Johnston JW** : On the Doppler signal from a steady flow asymmetrical stenosis model : effects of turbulence , Ultrasound Med & Biol, Vol 19 (3), pp 197-210, 1993

6. **Bazett HC, Cotton FS, Laplace LB, Scott JC :** The calculation of cardiac output and effective peripheral resistance from blood pressure measurements with an appendix on the size of the aorta in man, Am J Physiol, Vol 113, pp 312-333, 1935

7. **Bauer RD, Busse R, Schabert A** : The Input impedance of the peripheral vascular termination in skeletal muscle, Pflugers Arch, Vol 403, pp 308 - 311, 1985

8. **Benetos A, Laurent S, Hoeks AP, Boutouyrie PH, Safar ME :** Arterial alterations with aging and high blood pressure, A noninvasive study of carotid and femoral arteries, Arteriosclerosis & Thrombosis, Vol 13, pp 90-97, 1993

9. **Brandfonbrener M, Landowne M, Schock NW** : Changes in Cardiac Output with Age, Circulation, Vol (12), pp 557-566, October 1955

10. **Bercu BB, Haupt R, Johnsonbaugh R, Rodbard D** : The pulse wave arrival time (QKd interval) in normal children, J. Pedriatrics, pp716-721, November 1979

11 **Bernstein A, Organ LW, Eisner LE, Smith KC, Rowe IH** : Measurements of the pre-ejection period during labor with the use of arterial pulse time, Am J Obstet Gynecol, Vol 126(2), pp 238-242, September 1976

12. **Cavalcanti S, Belardinelli E, Severi S** : Numerical Simulation of the Short-term Heart Regulation, in : Computer Simulations in Biomedicine, Editors Power H, Hart RT, Computational Mechanics Publications, Southampton, pp 115-122, 1995

13. **Chang KC, Tseng YZ, Kuo TS, Chen HI** : Impedance and wave reflection in arterial system : simulation with geometrical tapered T-tubes, Med & Biol Eng & Comput, Vol 33, pp 652 - 660, 1995

14. **Chen C-H, Nevo E, Fetics B, Pak PH, Yin FCP, Maughan WL, Kass DA** : Estimation of Central Aortic Pressure Waveform by Mathematical Transformation of Radial Tonometry Pressure , Circulation , Vol 95, pp 1827-1836, 1997

15. **Chen C-W, Shau Y-W R, Wu C-P** : Analog transmission line model for simulation of systemic circulation, IEEE trans biomed eng, Vol 44(1), January 1997

16. **Chipman RA** : Schaums Outline of the Theory an Problems of Transmission Lines McGraw Hill, New York, 1968

17. **Clifford PC, Skidmore R, Bird DR, Woodcock JP, Baird RN** : The role of Pulsatility Index in the clinical asssessment of lower limb ischaemia, J Med Eng Tech, Vol 5 (5), pp 237-240, 1981

18. **Corey PD , Wemple RR :** A combined left ventricle systemic arterial model, J Biomechanics, Vol 8, pp 9-15, 1975

19. **Dahan M , Paillole C, Ferreira B, Gourgon R** : Doppler echocardiographic study of the consequences of aging and hypertension on the left ventricle and aorta, European Heart Journal, Vol 11 (Supplement G), pp 39-45, 1990

20. **Dauzat M., Laroche J.-P., de Bray J.-M., Deklunder G., Winsberg F.** : Duplex and colour-coded Doppler examination for the diagnosis of lower limb veins and arteries, *in* Labs K.H., Jager K.A., Fitzgerald D.E., Woodcock J.P., Neuerburg-Heusler D. (Editors) : Diagnostic Vascular Ultrasound, Edward Arnold, London, 1992

21. **Deshpande AK, Jindal GD, Bapu IP, Nerurkar SN, Kelkar MD, Parulkar GB** : Diagnosis of Aortic Occlusive Diseases using Impedance Plethysmography, J of Postgraduate Medicine, Vol 36 (2), pp 80-82, 1990

22. **Diourte B, Siche JP, Comparat V, Baguet JP, Mallion JM** : Study of arterial blood pressure by a Windkessel-type model: influence of arterial functional properties. Comput Methods Programs Biomed; Vol 60(1), pp 11-22, July 1999

23. **Drzewiecki GM, Melbin J, Noordergraaf A** : Arterial Tonometry : Review and Analysis, J Biomechanics, Vol 16 (2), pp 141-152, 1983

24. **Einav S., Aharoni S., Manoach M.** : Exponentially Tapered Transmission Line Model of the Arterial System, IEEE Transactions on Biomedical Engineering, Vol. 35(5), pp 333-339, May 1988

25. **Einav S, Aharoni S, Manoach M** : Pulse transmission and impedance characteristics of a non-uniform circulatory model, J Biomed Eng, Vol 14, pp 390 - 396, September 1992

26. **Elad D, Sahar M, Avidor JM, Einav S** : Steady flow through collapsible tubes : measurements of flow and geometry , J Biomech Eng, Vol 114, pp 84-91, Feb 1992

27. **Evans, D.H.** : Principal Component Analysis applied to the Diagnosis of Arterial Disease, Chapter in : Diagnostic Vascular Ultrasound, Labs K.H., Jager K.A., Fitzgerald D.E., Woodcock J.P., Neuerburg-Heusler D. (Editors), Edward Arnold, London, 1992

28. **Farrar DJ, Malinzak GS, Johnson G** : Femoral Artery Input Impedance and Circulatory Reserve in Experimental Stenosis, J Surg Res, Vol 29, pp 31 - 39, 1980

29. **Ganong WF** : Review of Medical Physiology, 12th Ed, Los Altos California, 1985

30. **Geddes LA, Voelz M, James S, Reiner D** : Technical Note : Pulse arrival time as a method of obtaining systolic and diastolic blood pressure indirectly, Med & Biol Eng & Comput, Vol 19, pp 671-672, 1981

31. **Griffiths M** : Introduction to Human Physiology, 2nd Ed, Collier Macmillan Publishers, London, 1981

32. **Guha SJ** : Haemodynamics of the small arterial region in the femoral vascular bed , Med & Biol Eng, Vol 8, pp 291-299, 1970

33. **Guyton AC** : Physiology of the Human Body, 6th Ed, Saunders College Publishing, London, 1981

34. **Hasegawa M, Rodbard D, Kinoshita Y** : Timing of the Carotid Arterial Sounds in Normal Adult Men : Measurement of Left Ventricular Ejection, Pre-Ejection Period and Pulse Transmission Time, Cardiology, Vol 78, pp 138-149, 1991

35. **Helal M.A., Watts K.C., Marble A.E., Sarwal S.N.** : Theoretical Model for assessing Hemodynamics in arterial networks which include bypass grafts, Med Biol Eng Comput, 28, pp 465-473, 1990

36. **Helal M.A.**: Derivation of Closed-Form Expression for the Cerebral Circulation Models, Comp. Biol. Med., Vol 24(2), pp 103-118, 1994

37. **Helal MA, Watts KC, Marble AE** : Hydrodynamic smulation of arterial networks which include compliant and rigid bypass grafts, J Biomechanics, Vol 27 (3), pp 277-287, 1994

38. **Hoskins P** : Quantitative techniques in Doppler Ultrasound, Clin Phys Physiol Meas , Vol 11 (suppl A), pp 75-80, 1990

39. **Jager G.N., Westerhof N., Noordegraaf A** : Oscillatory Flow Impedance in Electrical Analog of Arterial System, Circulation Research, Vol 16 (Feb), pp 121-133, 1965

40. **Jensen OE** : Chaotic oscillations in a simple collapsible-tube model , J Biomech Eng, Vol 114, pp 55-59, Feb 1992

41. **Karamanoglu M, Gallagher DE, Avolio AP, O'Rourke MF :** Functional origin of reflected pressurewaves in a multibranched model of the human arterial system, Am J Physiol 267 (Heart Circ Physiol 36), H1681-H1688, 1994

42. **Karamanoglu M, Feneley MP** : Derivation of the Ascending Aortic-Carotid Pressure Transfer Function with an Arterial Model, Am J Physiol 271 (Heart Circ. Physiol. 40), H2399-H2404, 1996

43. **Karamanoglu M.** : A System for Analysis of Arterial Blood Pressure Waveforms in Humans, Computers & Biomedical Research, Vol(30), pp 244-255, 1997

44. **Kelly R, Hayward C, Ganis J, Daley J, Avolio A, O'Rourke M :** Noninvasive Registration of the Arterial Pressure Pulse Waveform using High-Fidelity Applanation Tonometry, J Vasc Med Biol, Vol 1, pp 142-149, 1989

45. **Krajewski L.P. , Olin J.W.** : Atherosclerosis of the Aorta and Lower Extremity Arteries, *in* : Peripheral Vascular Diseases, Young J.R. Graor R.A. Olin J.W. Bartholomew J.R. (Editors) , Peripheral Vascular Diseases, Mosby Year Book, London, 1991

46. **Labs K.H., Fitzgerald D.E.** : Quantification of pulsed Doppler spectra for the diagnosis of minor to moderate atherosclerotic lesions : experience from *in vitro* and *in vivo* models, *in* Labs K.H., Jager K.A., Fitzgerald D.E., Woodcock J.P., Neuerburg-HeuslerD. (Editors) : Diagnostic Vascular Ultrasound, Edward Arnold, London, 1992

47. **LaCourse J.R., Mohanakrishnan, Sivaprasad K.** : Simulations of Arterial Pressure Pulses using a Transmission Line Model, J. Biomechanics, Vol 19(9), pp 771-780, 1986

48. **Lambert CR, Gladden LB, Nichols WW, Pepine CJ** : Effects of muscle contraction on pulsatile pressure-flow relations in femoral bed , J Appl Physiol, Vol 58 (4), pp 1128-1135, 1985

49. **Law YF, Cobbold RSC, Johnston JW, Bascom PAJ** : Computer-controlled pulsatile pump system for physiological flow simulation, Med Biol Eng Comput, Vol 25, pp 590-595, 1987

50. **Law YF, Johnston KW, Routh HF, Cobbold RSC** : On the design and evaluation of a steady flow model for doppler ultrasound studies, Ultrasound Med Biol, Vol 15 (5), pp 505-516, 1989

51. **Learoyd BM, Taylor MG :** Alterations with age in the viscoelastic properties of human arterial walls, Circulation Research, Vol 18, pp 278-292, March 1966

52. **Li J K-J** : Comparative Cardiovascular Dynamics of Mammals, CRC Press Inc, Boca Raton USA, 1996

53. **Mainardi LT, Porta A, Acquino M, Monaco M, Lucini D, Pagani M, Cerutti S** A Transmission Line Model for the Non-Invasive Evaluation of the Vascular Mechanical Properties at the Level of the Brachial Artery, Computers in Cardiology Conference Proceedings, Indianapolis (USA), http://www.cinc.org/,1996

54. **McIlroy MB, Targett RC** : A Model of the Systemic Arterial Bed showing Ventricular-Systemic Arterial Coupling, Am J Physiol, Vol 254 (3Pt2), H:609-616, Mar 1988

55. **McIlroy MB, Seitz WS, Targett RC** : A Transmission Line Model of the Normal Aorta and its Branches, Cardiovasc Res, Vol 20 (8), pp 81-587, Aug 1986

56. **McVeigh GE, Bratteli CW, Morgan DJ, Alinder CM, Glasser SP, Finkelstein SM, Cohn JN** : Age-related abnormalities in arterial compliance identified by pressure pulse contour analysis: aging and arterial compliance. Hypertension ; Vol 33(6), pp 1392-8; June 1999

57. **Miller MA, Drakontides AB, Leavell LC** : Kimber-Gray-Stackpoles Anatomy and Physiology, 17th Ed, Macmillan Publishing Co. Ltd., New York, 1977

58. **Mills CJ, Gabe IT, Gault JH, Mason DT, Ross J, Braunwald E, Shillingford JP** : Pressure-flow relationships and vascular impedance in man, Cardiovascular Research, Vol 4, pp 405-417, 1970

59. **Milnor W. R** : Hemodynamics, 2nd Edition, Williams & Wilkinsm Baltimore, 1989

60. **Mohaiddin RH, Schoser K, Amanuma M, Burman ED, Longmore DB :** M.R. Imaging of age-related dimensional changes of thoracic aorta, J. Comput. Assist. Tomo., Vol 14(5), pp 748-752, Sep/Oct 1990

61. **De Monchy C, van der Hoeven GMA** : Pulse Wave Transmission Times in Central Aorta and Peripheral Arteries in Normal Children, Blood Vessels, Vol 13 (3), pp 129-138, 1976

62. **Moore KL** : Clinically Oriented Anatomy, 2nd Ed, Williams & Wilkins, Baltimore, 1985

63. **Nichols W.W, O'Rourke M.F.** (Editors) : McDonald's Blood Flow in Arteries, 3rd Edition, Lea & Febiger, Philadelphia, 1990

64. **Nicolaides A N** : Assessment of leg ischaemia, *in* : ABC of Vascular Diseases, Wolfe J.H.N. (Editor),British Medical Journal, London, 1992

65. **O'Rourke M.F., Avolio A.P.** : Pulsatile Flow and Pressure in Human Systemic Arteries, Studies in man and in a multibranched model of the human systemic arterial tree, Circulation Research, Vol. 46, pp 363 - 372, 1980

66. **O'Rourke MF, Kelly RP, Avolio AP** : The Arterial Pulse , Lea & Febiger, London, 1992

67. **O'Rourke MF, Taylor MG** : Vascular Impedance of the Femoral Bed, Circulation Research, Vol 18, February 1966

68. **Pearson AC, Guo R, Orsinelli DA, Binkley PF, Pasierski TJ :** Transesophageal echocardiographic assessment of the effects of age, gender, and hypertension on thoracic aorta wall size, thickness, and stiffness, Am Heart J, Vol 128, pp 344-351, 1994

69. **Pearce WH, Slaughter MS, LeMaire S, Salyapongse AN, Feinglass J, McCarthy WJ, Yao JST :** Aortic diameter as a function of age, gender, and BSA, Surgery, Vol 114 (4), pp 691-697, October 1993

70. **Plonus MA** : Applied Electromagnetics, McGraw Hill Kogakusha Ltd, Tokyo, 1978

71. **Raines J.K., Jafrin M.Y., Shapiro A.H.** : A Computer Simulation of Arterial Dynamics in the Human Leg, J. Biomechanics, Vol. 7, pp 77-91, 1974

72. **Remington RB, O'Brien LJ** : Construction of aortic flow pulse from pressure pulse Am J Physiol, Vol 218 (2), pp 437-447, Feb 1970

73. **Reul H, Tesch B, Schoenmakers J, Effert S** : Hydromechanical simulation of systemic circulation, Med Biol Eng, pp 431-436, July 1974

74. **Roller M.L., Clarke M.E. :** Precursor Cerebral Circulation Models, J. Biomechanics, Vol 2, pp 241-250, 1969

75. **Rutherford R.B. (Ed.) :** Vascular Surgery, 3rd Edition, W.B. Saunders Co., London, 1989

76. **Schlindwein FS, Evans DH** : A real-time autoregressive spectrum analyzer for Doppler ultrasound signals, Ultr. in Med. & Biol., Vol 15(3), pp 263-272, 1989

77. **Schlindwein FS, Evans DH** : Selection of the order of autoregressive models for spectral analysis of Doppler signals, Ultr. in Med. & Biol., Vol 16(1), pp 81-91, 1990

78. **Segers P.** : Biomechanische modellering van het arterieel systeem voor de niet-invasieve bepaling van de arteriale compliantie, PhD thesis, Hydraulics Laboratory, Institute of Biomedical Technology, University of Gent, Belgium, April 1997

79. **Semnani R., Smith R.E. :** Quantitative Evaluation of Arterial Pulsatile Flow and Pressure applying Impedance Plethysmography to a Human Arterial Model incorporating Anatomical Branching and Scale, Computer Methods and Programs in Biomedicine, Vol 25, pp 13-20, 1987

80. **Siebenhofer A, Kemp C, Sutton A, Williams B :** The reproducibility of central aortic blood pressure measurements in healthy subjects using applanation tonometry and sphygmocardiography. J Hum Hypertens; Vol 13(9): pp 625-9, September 1999

81. **de Simone G, Devereux RB, Daniels SR, Mureddu GF, Roman MJ, Kimbal TR, Greco R, Witt S, Contaldo F** : Stroke Volume and Cardiac Output in Normotensive Children and Adults, Circulation, assessment of relations with body size and impact of overweight, Circulation, Vol 95 (7), pp 1837-1843, April 1997

82. **Skidmore R.** : The use of the Transcutaneous Ultrasonic Flowmeter in the Dynamic Analysis of Blood Flow, PhD Dissertation, University of Bristol, UK, 1979

83. **Smith L** : A System for the Acquisition and Digital Analysis of Lower Limb Flow Waveforms , MScMed (Biomedical Engineering) Thesis, University of Cape Town, South Africa, March 1993

84. **Snyder M.F., Rideout V.C., Hillestad R.J.** : Computer Modelling of the Human Systemic Arterial Tree, J. Biomechanics, Vol. 1, pp 341-353, 1968

85. **Stergiopulos N, Young DF, Rogge TR :** Computer simulation of arterial flow with applications to arterial and aortic stenosis, J Biomechanics, Vol 25 (12), pp 1477-1488, 1992

86. **Strandness DE Jr**: Ultrasound in the study if atherosclerosis, Ultrasound in Med & Biol , Vol 12(6), pp 453-464, 1986

87. **Strandness D.E. Jr** , : Noninvasive Vascular Laboratory and Vascular Imaging ,Chapter in : Peripheral Vascular Diseases, Young J.R. Graor R.A. Olin, J.W. Bartholomew J.R. (Editors), Mosby Year Book, London, 1991

88. **Strandness D.E. Jr** : The gold standard in the diagnosis of vascular disease, *in* Labs K.H., Jager K.A., Fitzgerald D.E., Woodcock J.P., Neuerburg-HeuslerD. (Editors) : Diagnostic Vascular Ultrasound, Edward Arnold, London, 1992

89. **Sugimachi M, Kawada T, Shishido T, Matsumoto N, Alexander J Jr, Sunagawa K :** Estimation of arterial mechanical properties from aortic and tonometric arterial pressure waveforms. Methods Inf Med; Vol 36 (4-5), pp 250-3, December 1997

90. **Taylor DEM, Stevens AL (Editors) :** Blood Flow Theory and Practice, Academic Press, N.Y., 1983

91. **Thompson RS, Aldis GK, Linnett IW** : Doppler ultrasound spectral power density distribution : measurement artefacts in steady flow, Med. & Biol. Eng. Comput. , Vol 28, pp 60-88, 1990

92. **Toda T, Tsuda N, Nishimori I, Leszczynski DE, Kummerow FA :** Morphometrical analysis of the aging process in human arteries and aorta, Acta Anat, Vol 106, pp 35-44, 1980

93. **Tutty OR** : Pulsatile flow in a constricted channel, J Biomech Eng, Vol 114, pp 50-54, Feb 1992

94. **University of Natal Durban** : Lecture notes on Electrical Transmission Lines, 3rd Year, Durban , South Africa , 1989

95. **Ursino M** : A Mathematical Model of the Interaction between Arterial and Cardiopulmonary Baroreceptors during Acute Cardiovascular Stress, in : Computer Simulations in Biomedicine, Editors : Power H, Hart RT, Computational Mechanics Publications, Southampton, pp 139-146, 1995

96. **Ward AS** : Reactive hyperaemia recovery time, pulsatility index, and transit time in the diagnosis of aorto-iliac disease ,
Chapter in : *Baird RN, Woodcock JP* : Diagnosis and Monitoring in Arterial Surgery, John Wright & Sons Ltd, Bristol UK, 1980

97. **Westerhof N., Bosman F., DeVries C.J., Noordegraaf A.** : Analog Studies of the Human Systemic Arterial Tree, J. Biomechanics, Vol 2, pp 121-143, 1969

98. **Westerhof N, Elzinga G, Sipkema P** : An artificial arterial system for pumping hearts, J Applied Physiol, Vol 31 (5), pp 776-781, 1971

99. **Wilkinson IB, Cockcroft JR, Webb DJ** :
Pulse wave analysis and arterial stiffness. J Cardiovasc Pharmacol 1998;32 Suppl 3:S33-7

100. **Woodcock J (Ed.) :** Clinical Blood Flow Measurement , Sector Publishing, London, 1974

101. **Zhao SZ, Xu XY, Hughes AD, Thom SA, Stanton AV, Ariff B, Long Q :**
Blood flow and vessel mechanics in a physiologically realistic model of a human carotid arterial bifurcation. J Biomech; Vol 33(8), pp 975-84, August 2000

102. **Zorn EA, Wilson MB, Angel JJ, Zanella J, Alpert BS :**
Validation of an automated arterial tonometry monitor using Association for the Advancement of Medical Instrumentation standard. Blood Press Monit; Vol 2(4), pp 185-188, August 1997

ACKNOWLEDGEMENTS

The author wishes to acknowledge the following organizations and individuals for their assistance.

1. Thesis Supervision :
   1.1 Dr W.L. Capper : University of Cape Town, South Africa

2. Financial Assistance :
   2.1 Trust for Educational Advancement in South Africa (TEASA), South Africa
   2.2 Foundation for Research and Development (FRD), South Africa
   2.3 German Academic Exchange Service (DAAD), German Consulate in SA

3. Clinical Assistance :
   3.1 Prof E.J. Immelman, Sister G. Wheeler, Sister S. Casey, Ms G. Briggs, Ms Z. Behadien : Vascular Lab., Groote Schuur Hospital. South Africa

4. Academic material :
   4.1 Dr P. Segers : University of Ghent, Belgium

5. Medical Equipment :
   5.1 Millar Instruments Inc, USA : arterial tonometer
   5.2 Steve Bennett, UC Davis, USA : intra-arterial pressure catheter
   5.3 Groote Schuur Hospital, Cape Town, South Africa

6. Technical Assistance :
   6.1 Mr M. Price : Department of Biomedical Engineering, University of Cape Town, South Africa
   6.2 Dr ECS Naidu : University of Natal Durban, South Africa

7. Moral support from friends and family.

APPENDIX 1
GLOSSARY

1. **Electrical Transmission Line Model** : a mathematical representation of propagating voltage and current waveforms in an electrical transmission line analogous to propagating pressure and flow waveforms in an arterial system.

2. **Forward Arterial Model** : mathematical model of the arterial circulation where the inputs are arterial dimensions and properties, and the outputs are haemodynamic waveforms.

3. **Inverse Arterial Model** : mathematical model of the arterial circulation where the inputs are haemodynamic waveforms, and the outputs are arterial dimensions and properties. The mathematical inverse of a Forward Arterial Model.

4. **Under-determined Equation System** : a system of equations that has more unknowns than equations. A unique solution cannot be guaranteed.

5. **Critically-determined Equation System** : a system of equations that has the same number of unknowns and equations. A unique solution is guaranteed.

6. **Over-determined Equation System** : a system of equations that has more equations than unknowns. A unique solution is guaranteed.

7. **Three Division Arterial Model** : the type of Inverse arterial model introduced in this thesis, that divides the arterial system into 3 regions : Pre-Sample, Sample, and Distal.

8. **First Approximation to the Pre-Sample Region** : the arterial Pre-Sample Region is assumed to be normal.

9. **Second Approximation to the Pre-Sample Region** : the arterial Pre-Sample region is modified using allometric data.

10. **Third Approximation to the Pre-Sample Region** : the arterial Pre-Sample Region is modified using clinically measured data.

11. **Error Graph** : a function of arterial radius, which shows the error between predicted and actual waveforms at each discrete predicted radius.

12. **Minimum Error Point of an Error Graph** : the predicted radius which results in the absolute minimum of an Error Graph

13. **Minimum Error Region of an Error Point:** a range of predicted radii that span a broad minima of an Error Graph.

14. **Haemodynamically Normal Region** : A range of arterial radii, where each discrete radius results in corresponding haemodynamic waveforms that do not vary significantly from those produced by a predefined "normal" radius.

15. **Critical stenosis** : A degree of arterial stenosis (50% diameter or 75% area stenosis) above which there is a marked decrease in flow. Any artery that has a sub-critical (ie < 50% diameter or < 75% area stenosis) stenosis may still be considered to be "haemodynamically normal"

16. **Physical Arterial Model :** a physical representation of the arterial system constructed using fluid-filled elastic tubes.

17. **Pseudo-synchronous measurement** : a technique where two asynchronous waveforms are synchronised to each other by using a common repetitive third waveform as a reference. The third waveform is always measured synchronous to each of the other two waveforms, and must not vary significantly in frequency.

18. **Triphasic**: A positive phase followed by a negative phase followed by another positive phase. Used to qualitatively categorise a normal Doppler blood flow velocity waveform.

19. **Biphasic** : A positive phase followed by a negative phase. Used to qualitatively categorise a normal Doppler blood flow velocity waveform.

20. **Monophasic** : A single positive phase only. Used to qualitatively categorise a Doppler blood flow velocity waveform from a stenosed artery.

Electrical Transmission Line Terms

ρ_{INPUT} : Steady state voltage reflection coefficient between the source and the input impedance.

ρ_s : bounce diagram voltage reflection coefficient between the source and the adjacent transmission line. Note that this is not the same as ρ_{INPUT}

Z_0 : Characteristic impedance of electrical transmission line . Used either to indicate a single line or, in the case of a system of multiple lines, to designate the line directly adjacent to the source. (dyn.s/cm^5)

$Z_1, Z_2, Z_{3,...}$: Characteristic impedance of discrete transmission lines in a multiple transmission line system. The subscript is an index representing a discrete line. (dyn.s/cm^5)

Z_{input} : Input impedance of an electrical transmission line, looking from the source towards the load .
(dyn.s/cm^5 using flow rate , or dyn.s/cm^3 using flow velocity)

Z_s : Source impedance

Z_L : Load impedance

γ_0 : Complex Propagation constant of an electrical transmission line .

Used either to indicate a single line or, in the case of a system of multiple lines, to designate the line directly adjacent to the source.
$\gamma_0 = \alpha + j.\beta$

α : Attenuation Coefficient. real part of the complex propagation constant. (nepers/cm).

β : Phase Coefficient. Imaginary part of the complex propagation constant (rad/cm).

$\gamma_0, \gamma_1, \gamma_2$: Propagation constant of discrete transmission lines in a multiple transmission line system. The subscript is an index representing a discrete line.

Vro : Reverse travelling or Reflected voltage waveform in an electrical transmission line-0

Vfo: Forward travelling voltage waveform in electrical transmission Line-0

Vt:	Total voltage waveform in electrical transmission line-0 i.e. $Vf + Vr$
Iro:	Reverse travelling or Reflected current wave in transmission line-0
Ifo:	Forward travelling current wave in transmission line-0
It :	Total current waveform in a transmission line i.e. $If + Ir$

Electro-mechanical analogies

E :	Young's Modulus (dyn/cm^2)
h:	Arterial wall thickness (cm)
μ :	Viscosity of blood (poise = $dyn.s/cm^2$)
ρ :	Density of Blood (g/cm^3)
R :	Poiseuille Resistance ($dyn.s/cm^5$)
L :	Fluid Inertance or Inductance per unit length (g/cm^5)
C :	Wall Compliance or Capacitance (cm^5/dyn)

Hydraulic quantities

P :	Pressure (mmHg or cm H_2O or dyn/cm^2)
Q :	Flow Rate (ml/s or cm^3/s)
v :	Flow Velocity (cm/s)

APPENDIX 2 : Simulink System Diagrams

2.1 Arterial Segment Blocks : 5 Types

Arterial Input Block
Arterial PreSample Block
Arterial Sample Block
Arterial Distal Block
Arterial Terminal Block

2.2 Arterial Connectors : 3 Types

Arterial Bifurcation
Arterial Trifurcation
Arterial Quadfurcation

2.3 Arterial SubSystem Blocks : 8 plus 1 SubSubSystem Block

Left Carotid SubSystem
Right Carotid SubSystem
Right Arm SubSystem
Left Arm SubSystem
Left Leg SubSystem
Right Leg SubSystem
Right Leg Distal SubSubSystem
Coeliac Artery SubSystem
Renal, Superior Mesenteric, Gastric SubSystem

2.1.1 ARTERIAL SEGMENT BLOCK icons:

ARTERIAL INPUT BLOCK
one input, one output

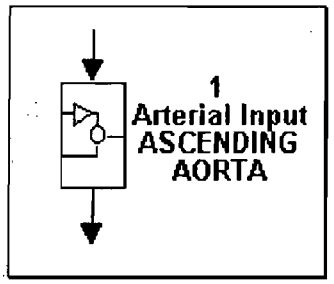

ARTERIAL PRESAMPLE BLOCK
two inputs, two outputs

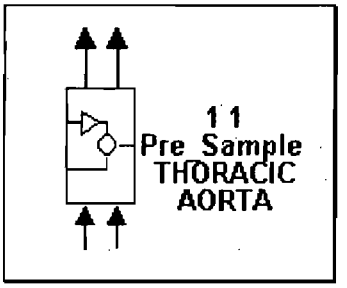

ARTERIAL SAMPLE BLOCK
two inputs, one output

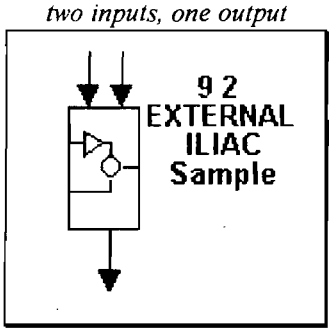

ARTERIAL DISTAL BLOCK
one input, one output

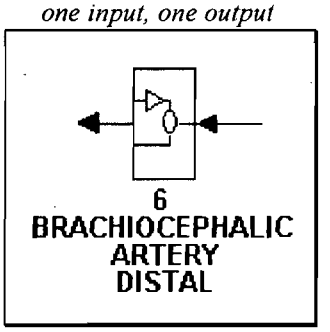

ARTERIAL TERMINAL BLOCK
one output

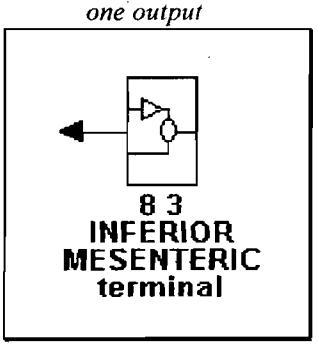

2.1.2 ARTERIAL SEGMENT BLOCKS detail:

ARTERIAL INPUT BLOCK *one input, one output*

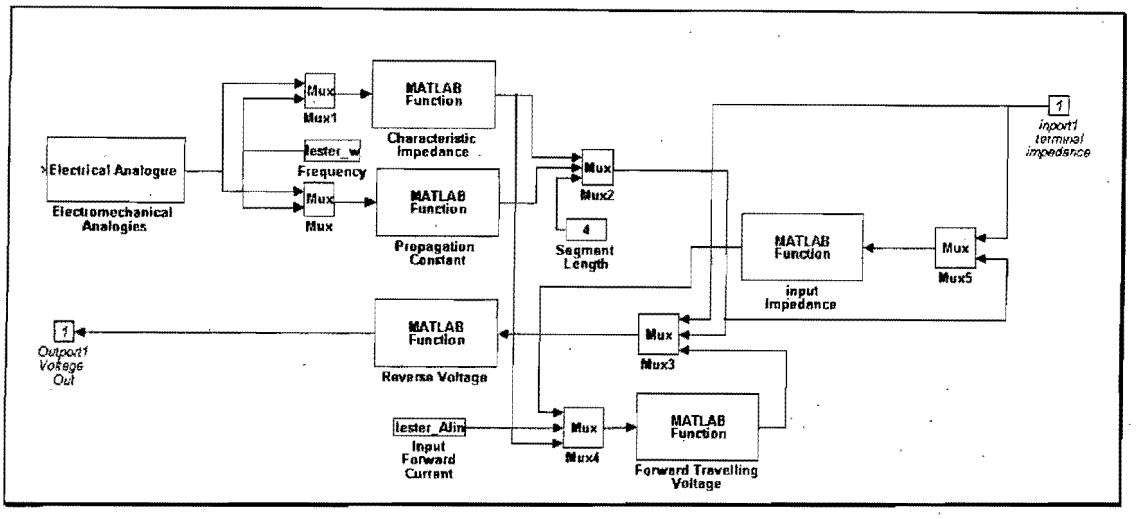

* Electrical Analogue Block see Appendix 3.1

ARTERIAL PRESAMPLE BLOCK *two inputs, two outputs*

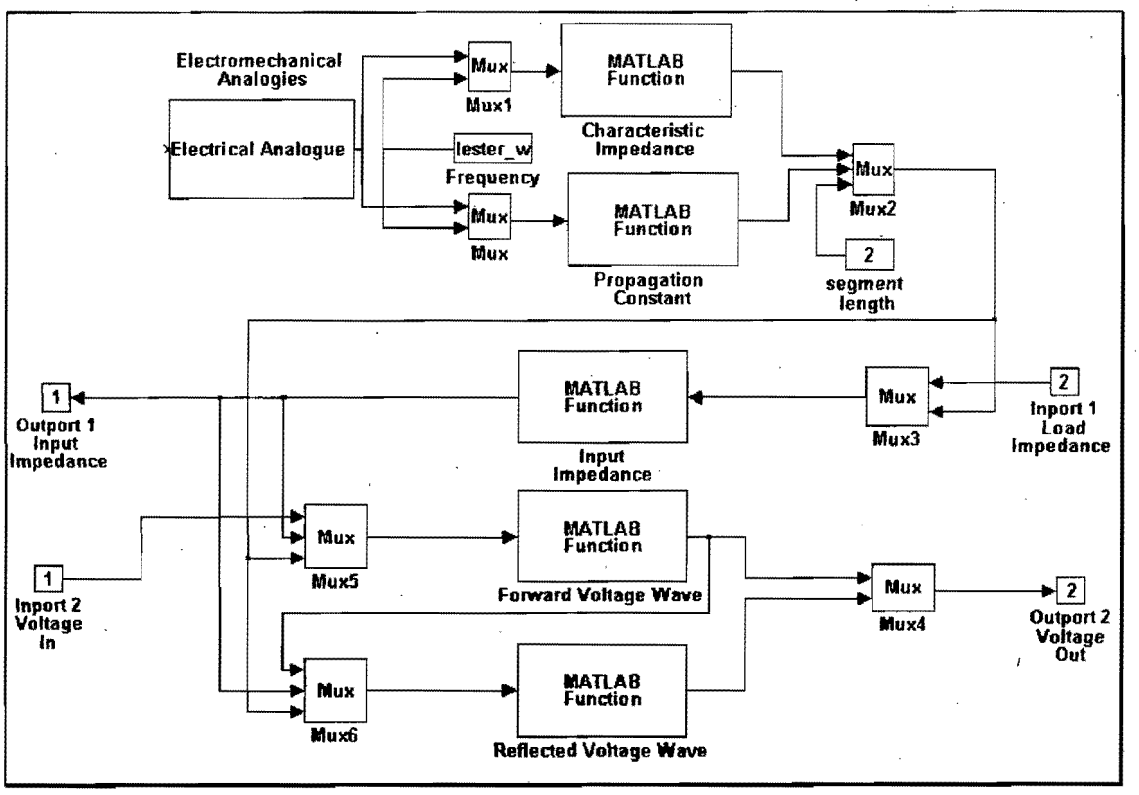

ARTERIAL SAMPLE BLOCK *two inputs, one output*

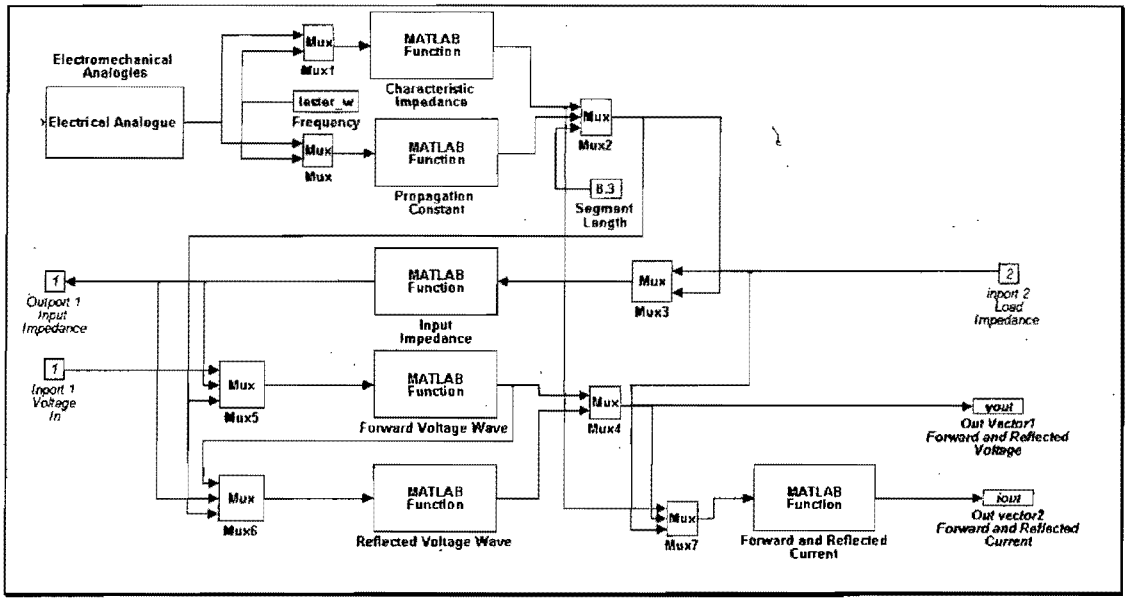

ARTERIAL DISTAL BLOCK *one input, one output*

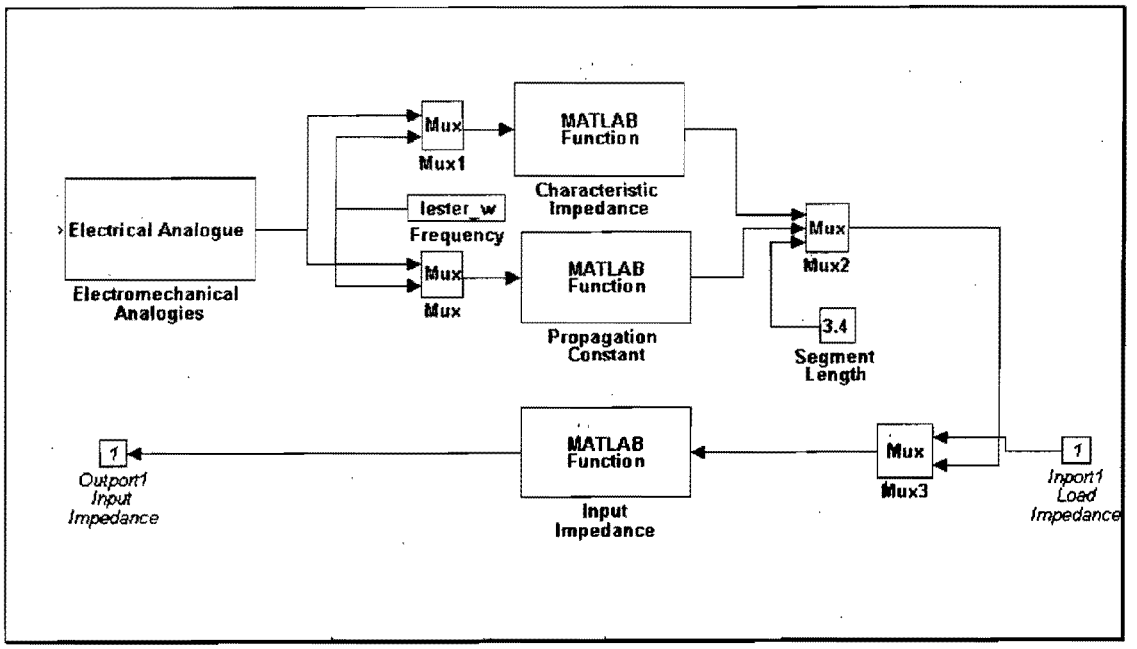

ARTERIAL TERMINAL BLOCK *one output*

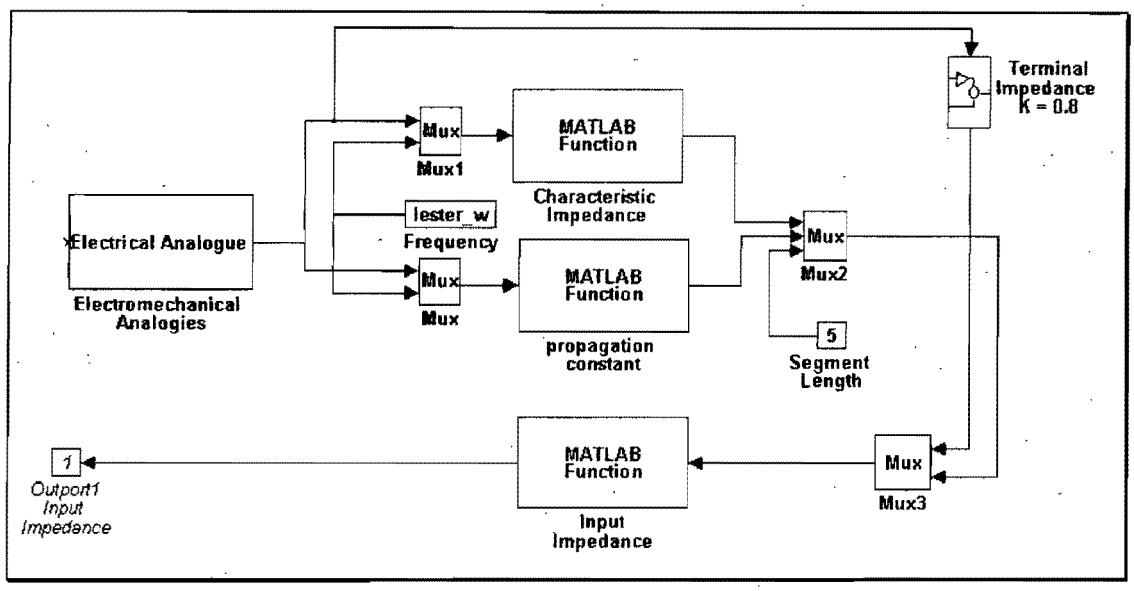

Terminal Impedance Block detail

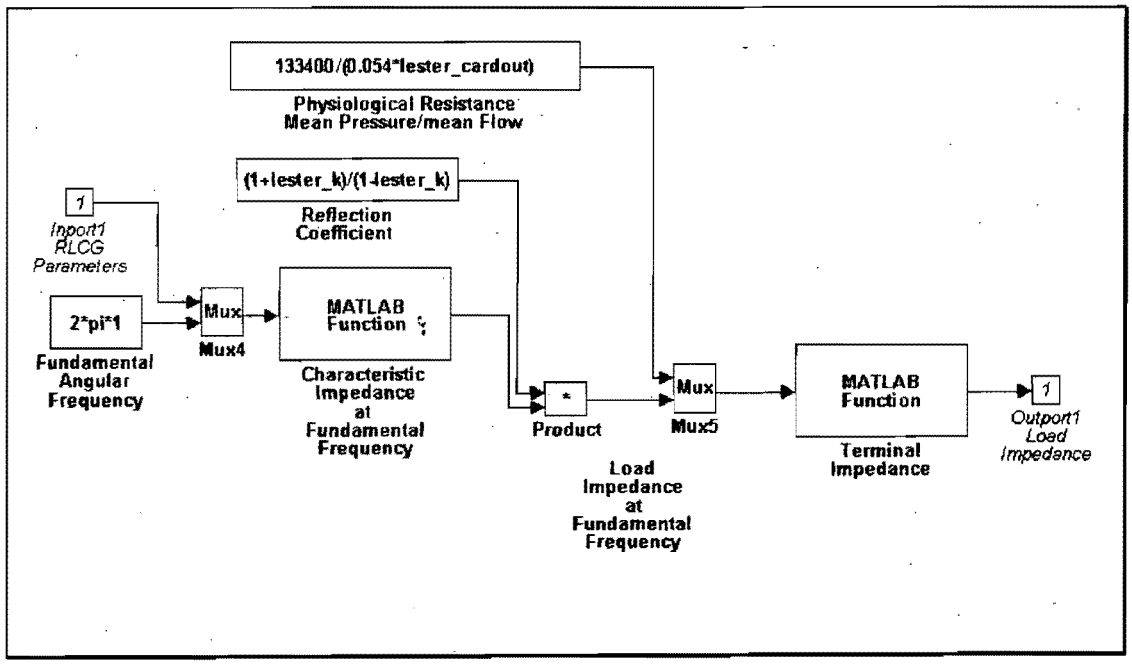

2.2 ARTERIAL CONNECTORS : sim19.bmp

Arterial Bifurcation : * for function underlying Matlab Function Block see Appendix ***** (txsimpll.m)

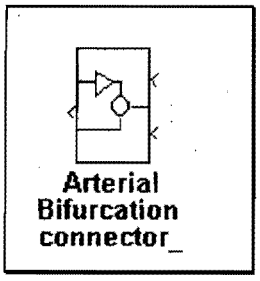

icon

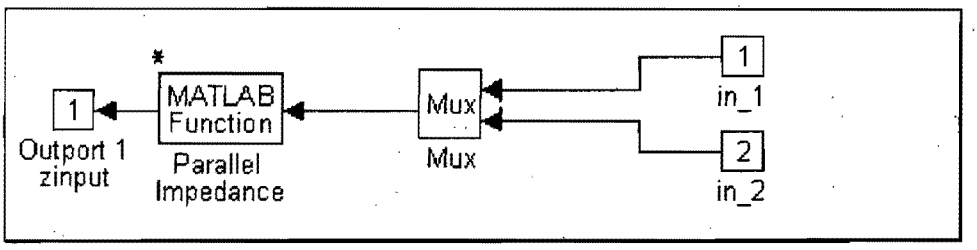

detail

Arterial Trifurcation :

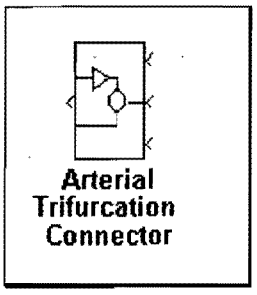

icon

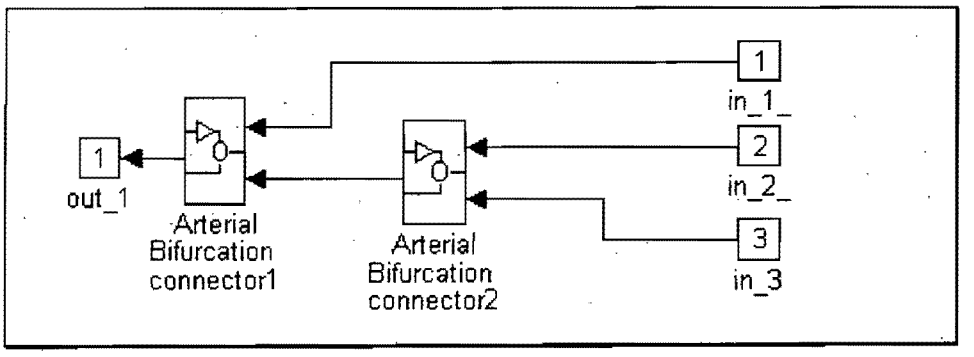

detail

Arterial Quadfurcation :

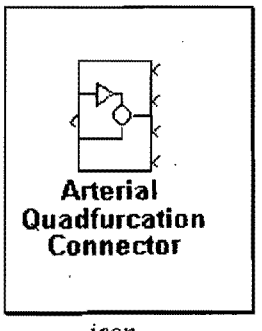

icon

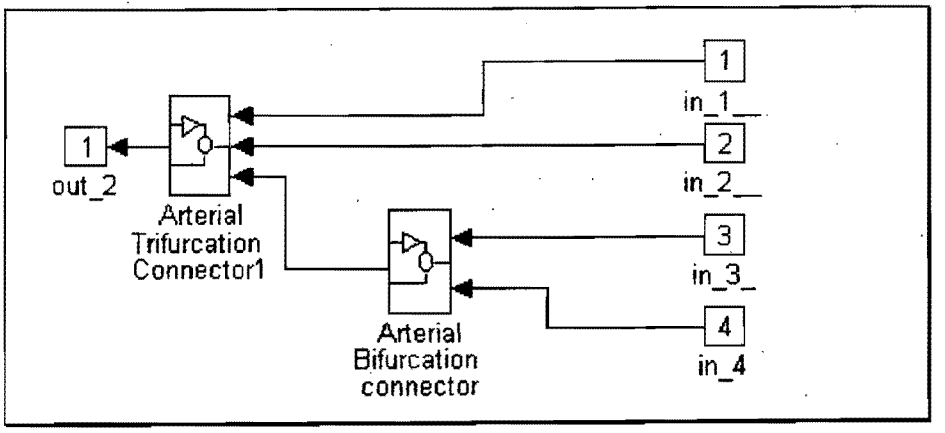

detail

2.3.1 ARTERIAL SUBSYSTEM BLOCKS : icons

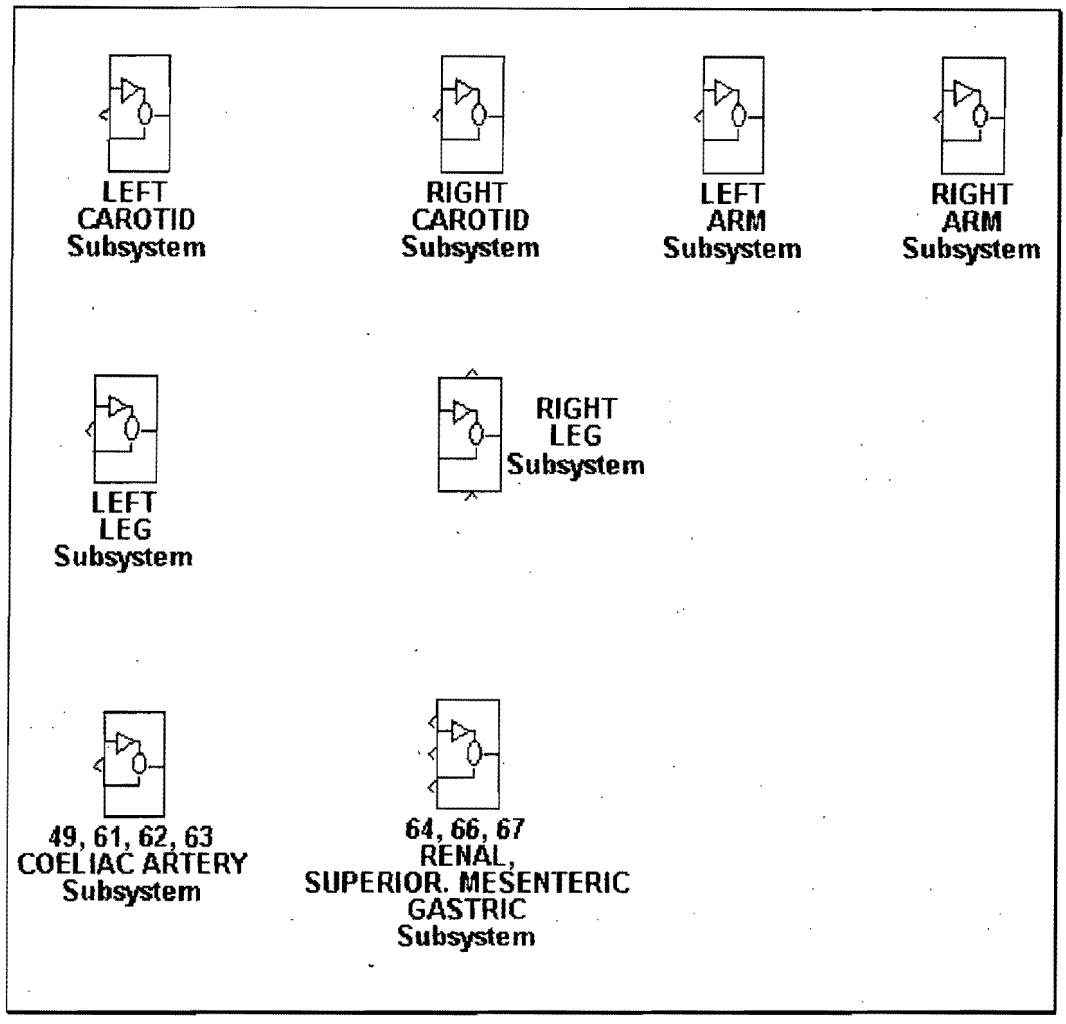

2.3.2 ARTERIAL SUBSYSTEM BLOCKS : detail

LEFT CAROTID SUBSYSTEM sim10. bmp

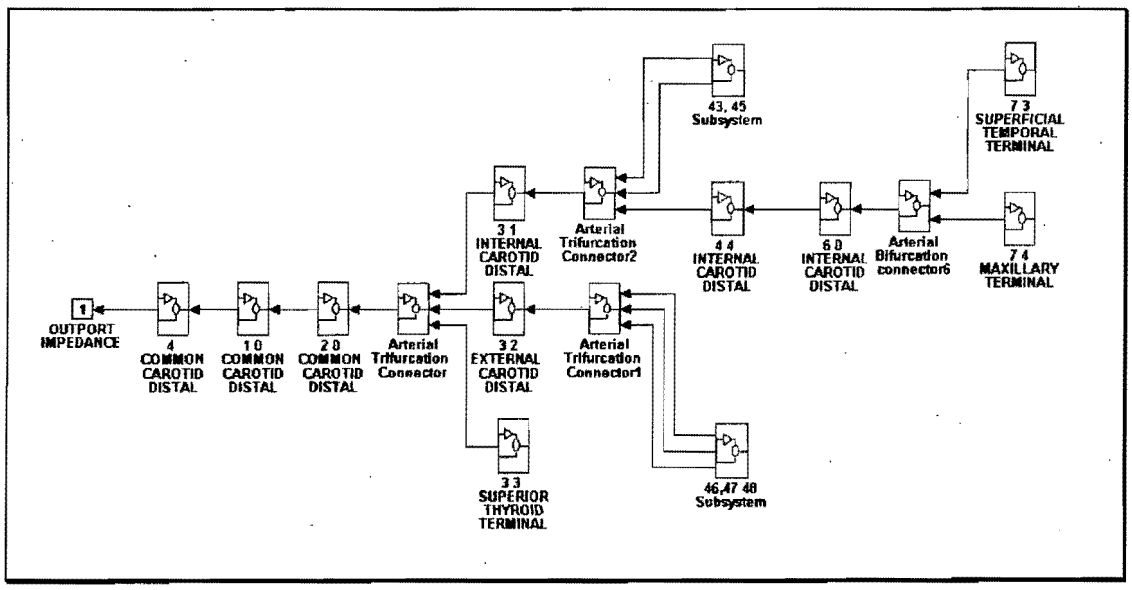

RIGHT CAROTID SUBSYSTEM sim11. bmp

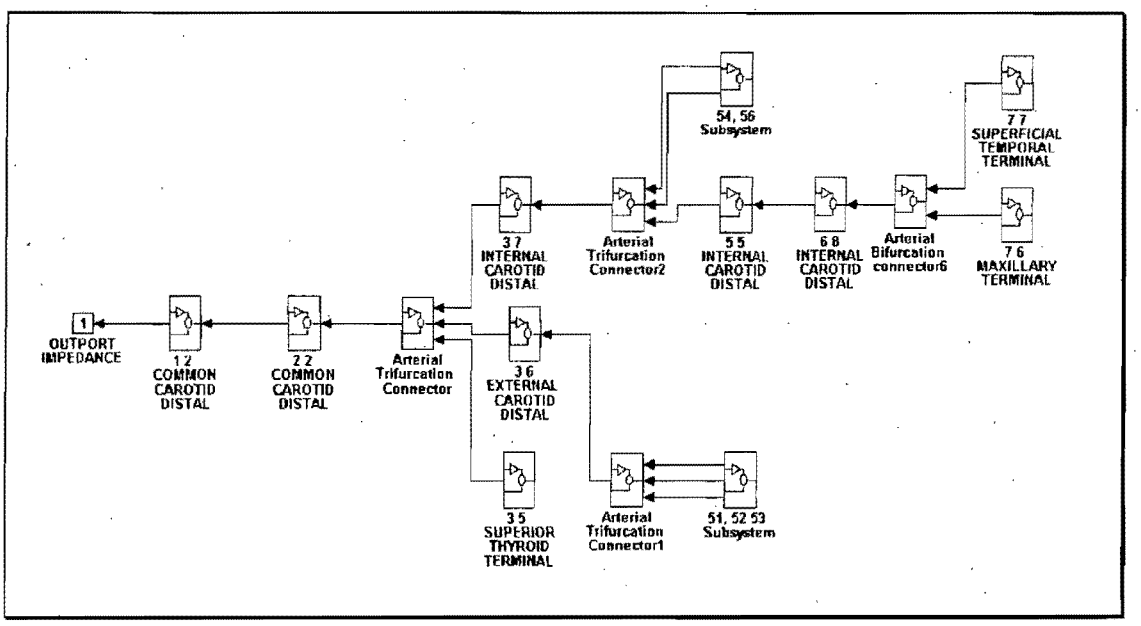

LEFT ARM SUBSYSTEM sim12 bmp

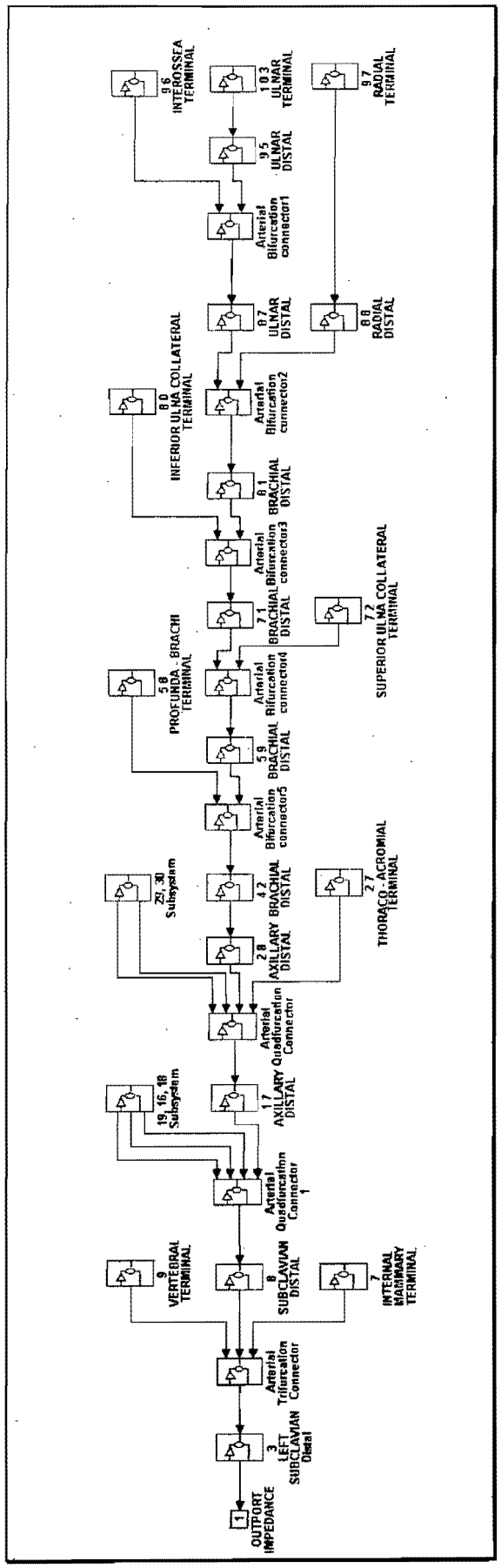

RIGHT ARM SUBSYSTEM sim13 bmp

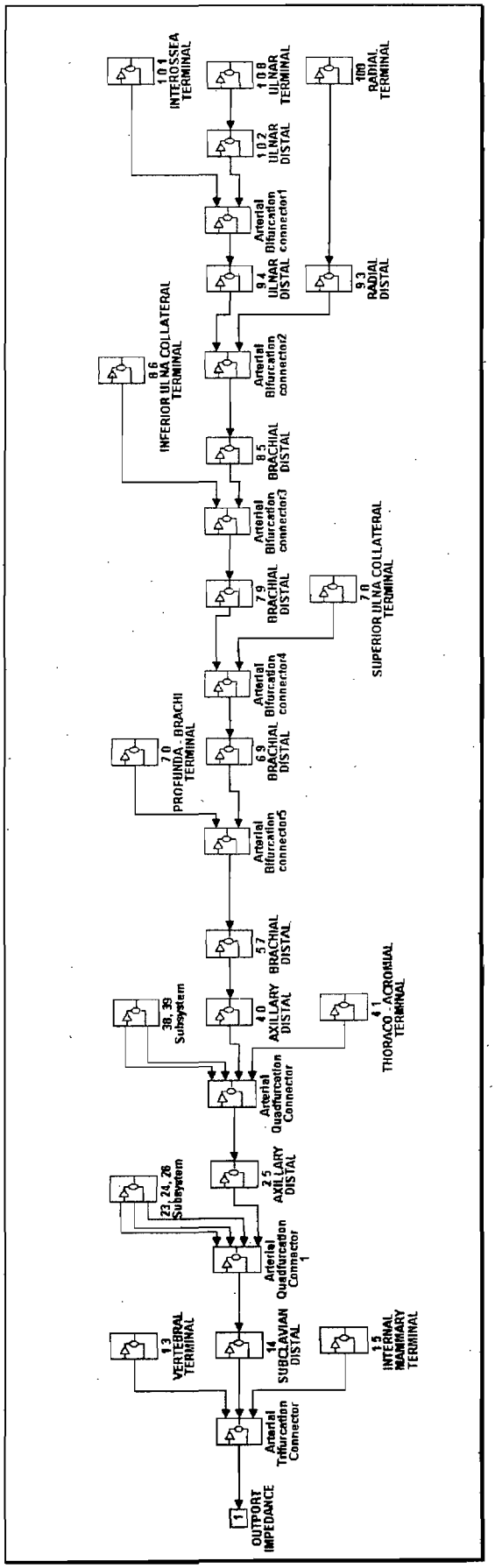

LEFT LEG SUBSYSTEM sim14 bmp

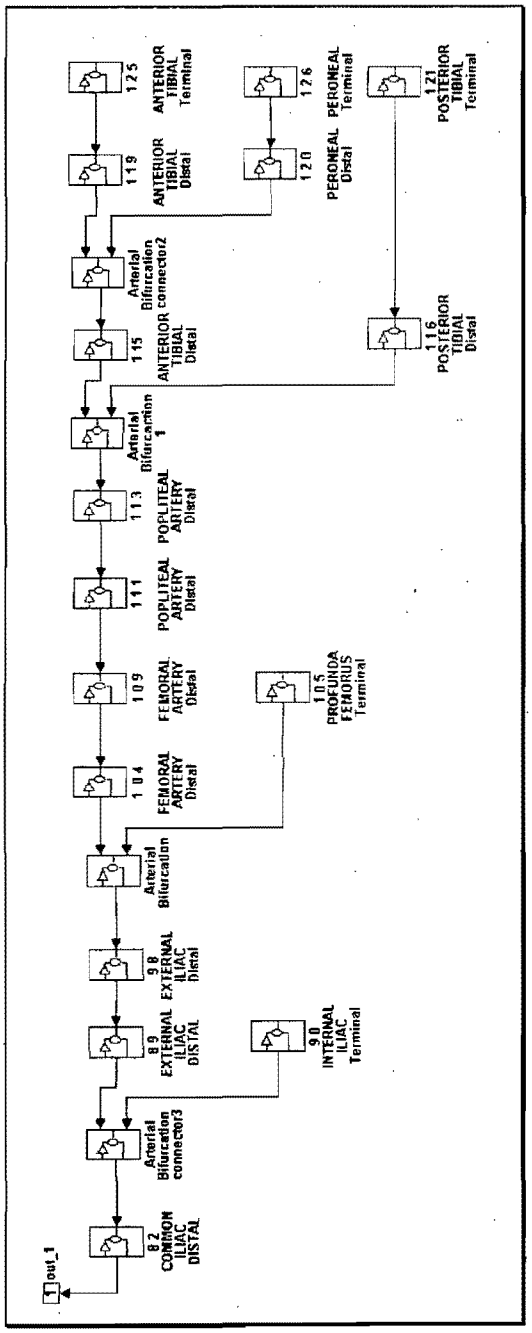

RIGHT LEG SUBSYSTEM sim15 bmp

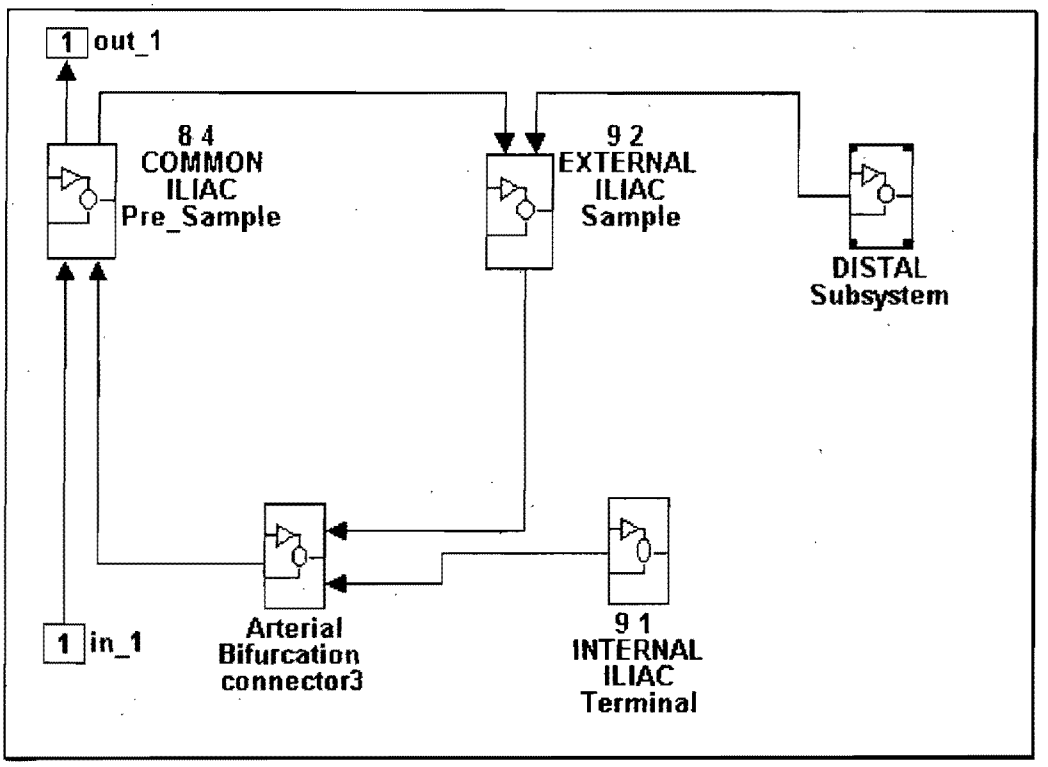

RIGHT LEG DISTAL SUBSYSTEM sim16 bmp

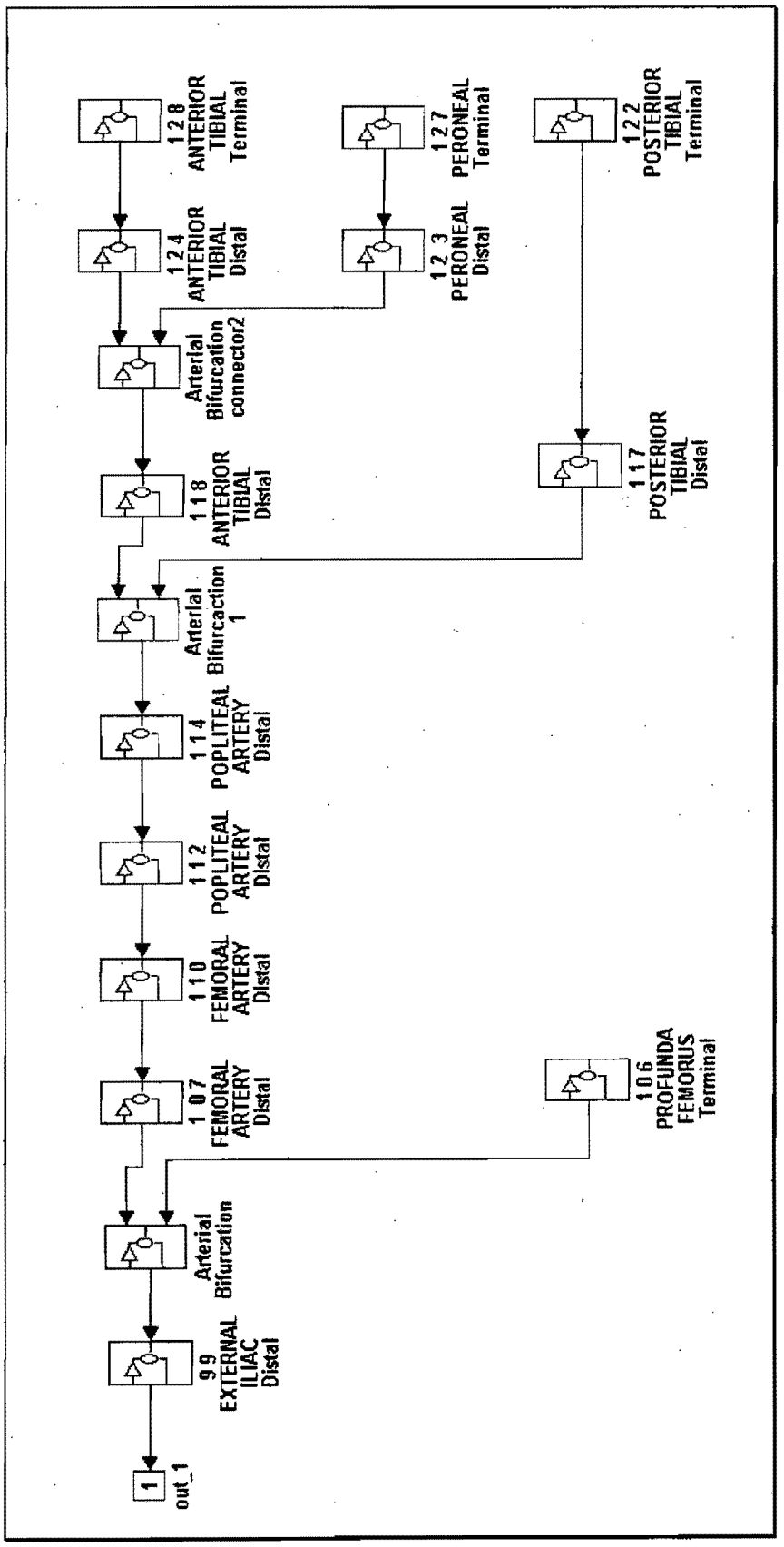

COELIAC ARTERY SUBSYSTEM sim17 bmp

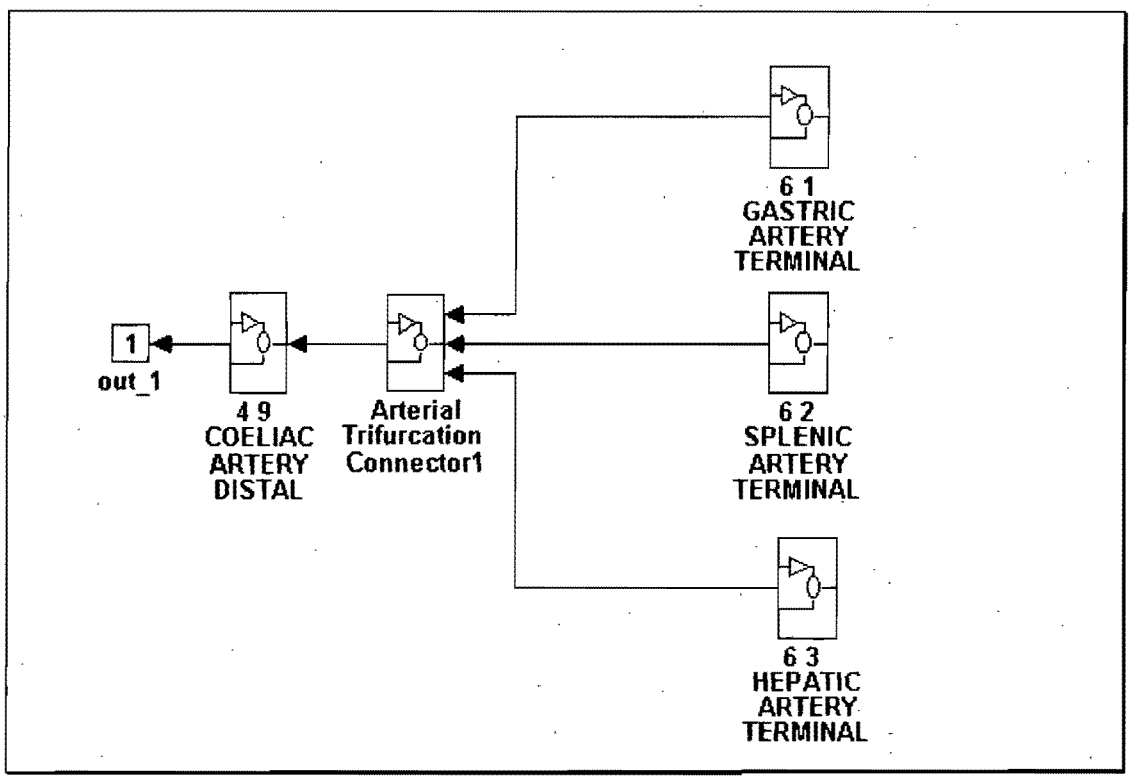

RENAL, SUPERIOR MESENTERIC, GASTRIC SUBSYSTEM sim18. bmp

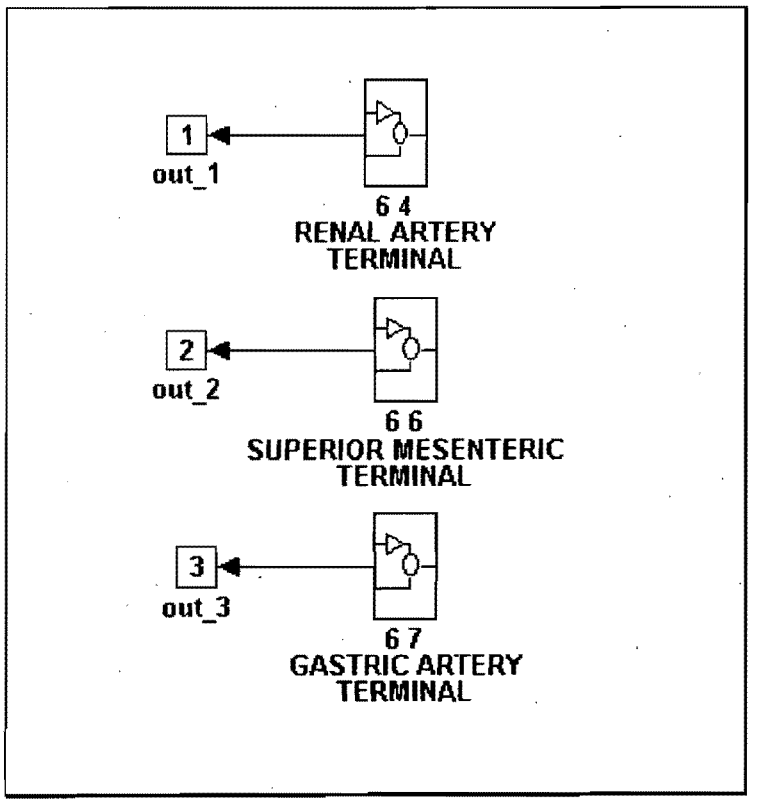

COELIAC ARTERY SUBSYSTEM sim17 bmp

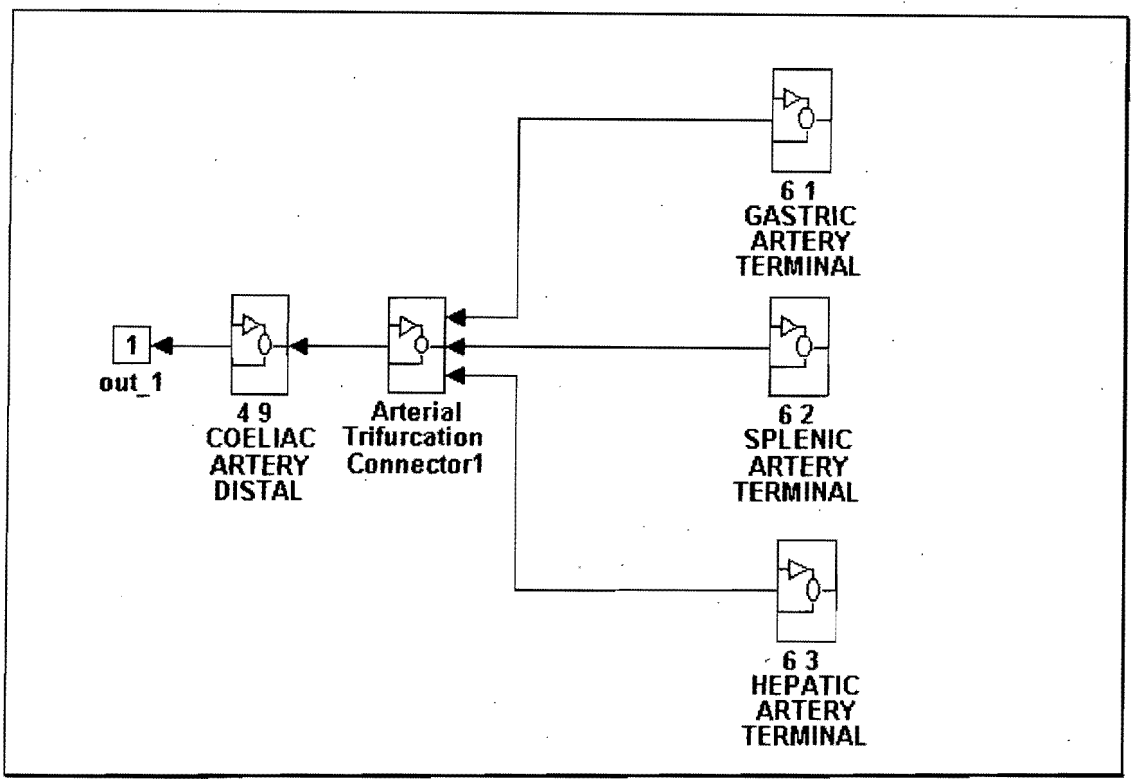

RENAL, SUPERIOR MESENTERIC, GASTRIC SUBSYSTEM sim18. bmp

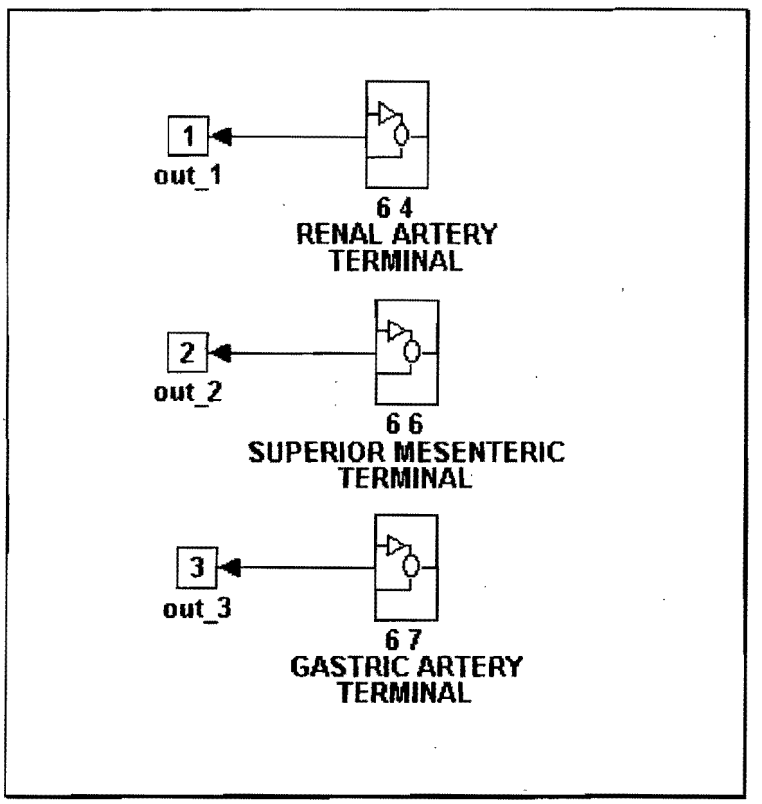

APPENDIX 3 : Matlab Program and Function files

3.1. Functions called by Simulink Block **Electromechanical Analogies :**

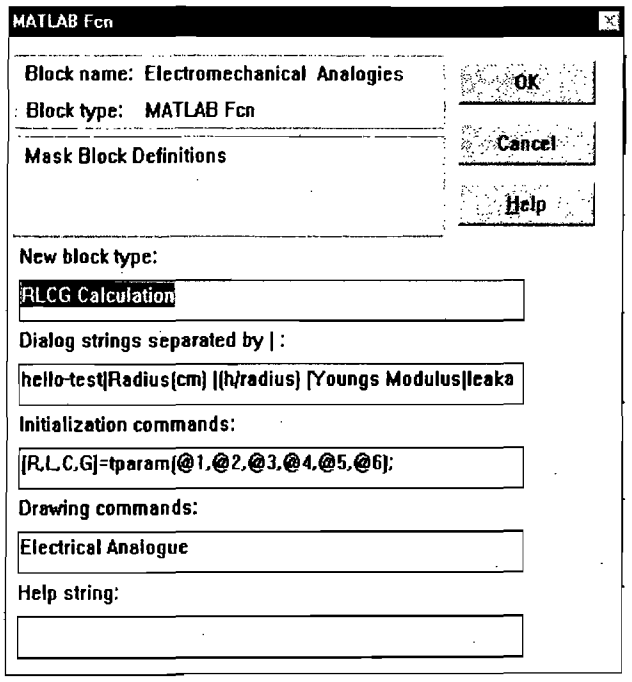

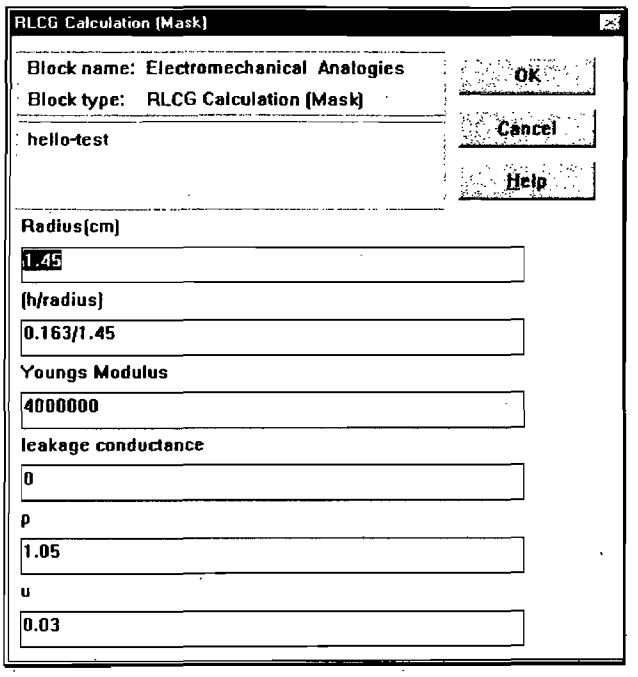

function paramout = **tvals**(R,L,C,G)

% This function converts RLCG output variables
% into a single vector form
%
% This forms part of the Simulink
% Block Masking Procedure
% This function takes the output of
% **tparam.m** and outputs it from the simulink
% mask as a 4 element vector

global lester_aortalength;
global lester_aortaelastic;
global lester_aortaradius;

paramout(1,1) = R;
paramout(2,1) = L;
paramout(3,1) = C;
paramout(4,1) = G;

function [R,L,C,G] = **tparam**(rad,hhr,EE,Gin,p,u);

% This function calculates the RLCG parameters
% from the input box of the electromechanical
% analogies simulink mask
%
% rad = radius
% hhr = wall thickness/radius
% EE = static Youngs Modulus
% Gin = leakage conductance
% p = blood density
% u = blood viscosity
%
% R = electrical resistance
% L = electrical inductance
% C = electrical capacitance
% G = electrical conductance

global lester_w;
global lester_p;
global lester_u;
global lester_aortaelastic;
global lester_legelastic;

G = Gin;
R = **txsimr**(rad,p,u);
L = **txsiml**(rad,p,u);
C = **txsimc**(rad,EE,hhr,p,u);

3.1.1 Resistance Function (**txsimr.m**) called by **tparam.m**

```
function resistance = txsimr(radius,p1,u1)
global lester_w;
global lester_p;
global lester_u;
global lester_aortalength;
global lester_aortaelastic;
global lester_aortaradius;

% Function to calculate fluid resistance using
% Poiseuilles equation
%
% This function is called by tparam.m

p          = lester_p;
u          = lester_u;
resistance = (8*lester_u)/(pi*radius^4);
```

3.1.2 Inductance Function (**txsiml.m**) called by **tparam.m**

```
function inductance = txsiml(radius,p1,u1);
global lester_w;
global lester_p;
global lester_u;
global lester_aortalength;
global lester_aortaelastic;
global lester_aortaradius;

% Function to calculate Fluid Inductance
%
% This function is called by tparam.m

p          = lester_p;
u          = lester_u;
inductance = lester_p/(pi*radius^2);
```

3.1.3 Capacitance Function (**txsimc.m**) called by **tparam.m**

```
function capacitance = txsimc(radius,EE,hhr,p1,u1);

global lester_w;
global lester_p;
global lester_u;
global lester_aortalength;
global lester_aortaelastic;
global lester_aortaradius;

% Function to calculate Arterial Wall Capacitance
%       p       = blood density
%       u       = blood viscosity
%       radius  = arterial radius
%       hhr     = wall thickness to radius ratio
%       EE      = arterial static Youngs Modulus
%
% This function is called by tparam.m

p          = lester_p;
u          = lester_u;
```

3.2.1 Function **tchar.m** called by Simulink Block **Characteristic Impedance :**

```
function zo = tchar(u);
global lester_w;

%     Calculation of Characteristic Impedance (zo)
%
%     for DC analysis the resistance (R) is used instead
%     of characteristic impedance.
%
%     for Harmonic analysis, the RLCG equivalent
%     impedance  at the given angular frequency (w) is
%     used
%
%     RLCG   = resistance,inductance,capacitance,
%                conductance per unit length
%     lester_w = w = angular  frequency

R = u(1);
L = u(2);
C = u(3);
G = u(4);
w = u(5);

if lester_w==0,
        zo(1) = R;
        zo(2) = 0;
else
        zo(1) = real  (txsimzo(R,L,C,G,w));
        zo(2) = imag (txsimzo(R,L,C,G,w));
end
```

3.2.2 Function **txsimzo.m** called by **tchar.m** for Harmonic analysis only :

```
function zo = txsimzo(r,l,c,g,w);

% Function to calculate characteristic impedance
% of a transmission line at angular
%  frequency = w
%

i       =       sqrt(-1);
zo      =       sqrt((r+i*w*l)/(g+i*w*c));
```

3.3.1 Function (**tprop.m**)called by Simulink Block **Propagation Constant :**

```
function go = tprop(u);
global lester_w;

% Calculation of propagation constant (go)
% given the electrical parameters RLCG and angular
% frequency w.
%
% Propagation constant is set to 0 for DC analysis

        R       = u(1);
        L       = u(2);
        C       = u(3);
        G       = u(4);
        w       = u(5);

if lester_w == 0,
% for DC analysis the propagation constant has no meaning so its set to zero
        go(1)   = 0;
        go(2)   = 0;
else
% AC analysis
        go(1)   = real(txsimgo(R,L,C,G,w));
        go(2)   = imag(txsimgo(R,L,C,G,w));
end
```

3.3.2 Propagation Constant function (**txsimgo.m**) called by **tprop.m** for Harmonic analysis only:

```
function go = txsimgo(r,l,c,g,w);

% Function to calculate characteristic
% impedance of a transmission line (RLCG)
% at angular  frequency = w
%
% This function is called by tprop.m

i       =       sqrt(-1);
go      =       sqrt((r+i*w*l)*(g+i*w*c));
```

3.4.1 Function **timped.m** called by Simulink Block **Input Impedance**

```
function zin = timped(u);

global lester_w;

% Calculation of input impedance (zin)

zlr             = u(1);  % real part of load
zli             = u(2);  % imaginary part of load
zor             = u(3); % real part of characteristic impedance
zoi             = u(4); % imag part of characteristic impedance
gor             = u(5); % real part of propagation constant
goi             = u(6); % imag part of propagation constant
ll              = u(7);   % length of line (cm)

% DC analysis .. zor*ll = R*ll is the total series resistance of the segment
if lester_w==0,
        zin(1)  = zlr+zor*ll;
        zin(2)  = 0;
% AC analysis
else
        zl      = zlr+sqrt(-1)*zli;
        zo      = zor+sqrt(-1)*zoi;
        go      = gor+sqrt(-1)*goi;
        zin(1)  = real(txsimz(zo,zl,go,ll));
        zin(2)  = imag(txsimz(zo,zl,go,ll));
end
```

3.4.2 Characteristic Impedance Function (**txsimz.m**) called by **timped.m**

```
function zinput = txsim(zo,zl,go,ll)

% Input Impedance at the source of a transmission line of :
%  Characteristic Impedance  = zo
%  Load                      = zl
%  Propagation constant :    = go
%  Length :                  = ll
%

num     = (zl-zo)*
          exp(-go*ll)+(zl+zo)*exp(go*ll);

den     = (zo-zl)*
          exp(-go*ll)+(zo+zl)*exp(go*ll);

zinput  = zo*num/den;
```

3.5 Function (**tvf11.m**) called by Simulink Block Forward Travelling Input Voltage

note: this function is only used by the first arterial segment (ascending aorta) in order to calculate the forward travelling voltage at the input to the arterial system

```
function vf = tvf11(u);

% This function calculates the
%  Forward Travelling Aortic Pressure Waveform (vfc),
% given the Total Aortic Flow waveform (Iin) with the intermediate
% step of calculating the Total Aortic Pressure waveform (vt)
%
% z1    = input impedance
% zo    = characteristic impedance
% Iin   = total input current
% vt    = total input voltage
% rho   = voltage reflection coefficient at input (source)

global lester_w;

z1      =       u(1)+sqrt(-1)*u(2);
Iin     =       u(3)+sqrt(-1)*u(4);
zo      =       u(5)+sqrt(-1)*u(6);

rho     =       (z1-zo)/(z1+zo);
vt      =       Iin*z1;
vfc     =       vt/(1+rho);

if (lester_w==0)
% DC analysis ... note z1 is the total DC resistance seen by the source for DC analysis
        vfc     = Iin*z1;
end
vf(1)           = real(vfc);
vf(2)           = imag(vfc);
```

3.6 Function **tainput.m** called by Simulink Block Reverse Travelling Input Voltage

note: this function is only used by the first arterial segment (ascending aorta) in order to calculate the reverse travelling voltage at the input to the arterial system

```
function vr = tainput(u);
global lester_w;

% This function calculates the reverse voltage
% at the input to the arterial system
% and then calculates the  reverse and forward
% voltages at the load end of the transmission
% line segment
%
% The result is output in a single vector
%
% zldd  = input impedance
% zo    = characteristic impedance
% go    = propogation constant
% llo   = line length
% Vf11  = forward voltage at the source

zldd          =     u(1)+sqrt(-1)*u(2);
zo            =     u(3)+sqrt(-1)*u(4);
go            =     u(5)+sqrt(-1)*u(6);
llo           =     u(7);
Vf11          =     u(8)+sqrt(-1)*u(9);

% Load end voltages

vr11d         =     Vf11*exp(-go*llo)*(zldd-zo)/(zldd+zo);
vf11d         =     Vf11*exp(-go*llo);

if lester_w == 0,
% DC result
        vr(1)   =     real(vf11d);
        vr(2)   =     imag(vf11d);
        vr(3)   =     0;
        vr(4)   =     0;
else
% AC result
        vr(1)   =     real(vf11d);
        vr(2)   =     imag(vf11d);
        vr(3)   =     real(vr11d);
        vr(4)   =     imag(vr11d);
end
```

3.7.1 Function (**tforward.m**) called by Simulink Block **Forward Voltage Wave**

note: this function is used by all segments except the first arterial segment (ascending aorta) in order to calculate the forward travelling segmental voltage

```
function vf = tforward(u);
global lester_w;

vf11d          = u(1)+sqrt(-1)*u(2);
vr11d          = u(3)+sqrt(-1)*u(4);
zld            = u(5)+sqrt(-1)*u(6);
zo             = u(7)+sqrt(-1)*u(8);
go             = u(9)+sqrt(-1)*u(10);
llo            = u(11);

if lester_w == 0,
% DC analysis
        vfi    = real(vf11d);
        vfo    = real(vfi*real(zld)/(real(zld)+real(zo)*llo));      % for DC real(zo) = R, see tchar.m
        vf(1)  = real(vfo);
        vf(2)  = imag(vfo);
else
% AC analysis
        vfi    = tsimvfi(vf11d,vr11d,zld,zo);
        vfo    = tsimvfo(vfi,go,llo);
        vf(1)  = real(vfo);
        vf(2)  = imag(vfo);
end
```

3.8.2 Source End Forward Voltage function (**tsimvfi.m**) called by **tforward.m**

```
function vfi = tsimvfi(Vf11o,Vr11o,Zli,ZO);

% This function calculates the forward travelling voltage at the %input of a steady state
% transmission line given forward and reflected voltages of the preceding line; input
% impedance at the junction of the two lines; and the characteristic impedance of the
% line under investigation.
%
% Vf11. and Vr11o  = forward and reflected voltages of preceding segment
% Zli              = input impedance of current segement
% ZO               = characteristic impedance of current segement

vfi          =        (Vf11o+Vr11o)/(1+(Zli-ZO)/(Zli+ZO));
```

3.8.3 Load End Forward Voltage Function (**tsimvfo.m**)called by **tforward.m**

```
function vfo = tsimvfo(Vfi,Go,llo);

% This function calculates the forward travelling voltage at the output (load end )of a steady state
% transmission line given input (source end) forward voltage ; propogation constant; and length of the
% line under investigation.
%
% Vfi  =      source end forward voltage
% Vfo  =      load end forward voltage
% Go   =      propagation constant
% llo  =      length (cm) of transmission line

Vfo          =              Vfi*exp(-Go*llo);
```

3.8.1 Function (**treverse.m**) called by Simulink Block Reflected Voltage Wave

note: this function is all segments except the first arterial segment (ascending aorta) in order to calculate the reverse travelling segmental voltage

```
function vr = treverse(u);
global lester_w;

% Function to calculate load end reverse voltage
%
% vf21d = load end forward voltage
% zld   = load impedance
% zo    = characteristic impedance
% go    = propagation constant
% llo   = line length (cm)

vf21d          =      u(1)+sqrt(-1)*u(2);
zld            =      u(3)+sqrt(-1)*u(4);
zo             =      u(5)+sqrt(-1)*u(6);
go             =      u(7)+sqrt(-1)*u(8);
llo            =      u(9);

if lester_w ==0,
% DC analysis
        vr(1)  =      0;
        vr(2)  =      0;
else
% AC analysis
        vro    =      tsimvro(vf21d,zld,zo,go,llo);
        vr(1)  =      real(vro);
        vr(2)  =      imag(vro);
end
```

3.8.2 Reflected Voltage function (**tsimvro.m**) called by treverse.m

```
function vro = tsimvro(Vfo,Zli,ZO,GO,llo);

% This function calculates the reverse travelling voltage at the output of a steady state
% transmission line given output forward voltage ; propogation constant; characteristic
% impedance , input impedance and length of the line under investigation.
%
% Vfo  =      load end forward voltage
% vro  =      load end reverse voltage
% Go   =      propagation constant
% ZO   =      characteristic impedance
% Zli  =      input impedance of segment
% llo  =      length of line (cm)

vro            =           Vfo*exp(+2*GO*llo)*(Zli-ZO)/(Zli+ZO);
```

3.9 Function **(tsimpll.m)** called by Simulink Block Arterial Bifurcation

note: this function is used at (bifurcation) branching points in the arterial tree. for multiple branches (trifurcation, bifurcation) this function is called more than once.

```
function ZLeq = tsimpll(u);

% This function calculates the equivalent input impedance at
% a transmission line bifurcation given the input impedance at
% both branch lines.

zl1             =       u(1)+sqrt(-1)*u(2);
zl2             =       u(3)+sqrt(-1)*u(4);

zl              =       (zl1*zl2)/(zl1+zl2);

ZLeq(1)         =       real(zl);
ZLeq(2)         =       imag(zl);
```

3.10 Function **tcurrent.m** called by Simulink Block Forward and Reflected Current

note: this function is only used by the arterial sample block. This is so, because all analysis is done using a voltage analysis approach. The forward and reflected current is only required at the segment where the pressure and flow are to be sampled.

```
function Iout = tcurrent(u);

global lester_w;

% This function calculates the electrical current in a
% a transmission line given the forward and reverse voltage
% and characteristic impedance.

z2              =       u(1)+sqrt(-1)*u(2);
Vf21            =       u(3)+sqrt(-1)*u(4);
Vr21            =       u(5)+sqrt(-1)*u(6);
zload           =       u(7)+sqrt(-1)*u(8);

if lester_w == 0,
        If21    =       Vf21/zload;
        Ir21    =       0;
else
        If21    =       Vf21/z2;
        Ir21    =       Vr21/z2;
end

Iout            =       [real(If21) imag(If21) real(Ir21) imag(Ir21)];
```

3.11 Function **tperiph.m** called by Simulink Block Peripheral Impedance

note: this function is only used by the arterial terminal block. It calcultes the peripheral impedance at the terminal end of a transmission line. Different methods are used to calculate the impedance for harmonic and mean analysis.

```
function peripheral = tperiph(x);

% This function switches the terminal impedanceof an artery from its DC value of
%  mean pressure/mean flow to its AC value which depends on the selected reflection coefficient

global lester_w;
global lester_fundamental;

i                       =       sqrt(-1);
dc_termination          =       x(1);
ac_termination          =       x(2)+i*x(3);

if lester_w == 0,
% DC analysis
        peripheral(1)   =       dc_termination;
        peripheral(2)   =       0;
else
% AC analysis
        fundamental_load_impedance      = x(2)+i*x(3);
        ac_resistor                     = 1/(real(1/fundamental_load_impedance));
        ac_capacitor            = imag(1/fundamental_load_impedance)/(2*pi*lester_fundamental);
        load_impedance                  = ac_resistor/(1+i*lester_w*ac_resistor*ac_capacitor);
        peripheral(1)                   = real(load_impedance);
        peripheral(2)                   = imag(load_impedance);
end
```

3.12.1 Matlab Program (**Simavol.m**) that controls the Simulink Model (**avoles4**) by harmonic analysis

```
% Simavol.m     Forward Simulink Model.
%
% Lester John
% Department of Biomedical Engineering
% University of Cape Town Medical School
% Anzio Road
% Observatory, 7925
% Cape Town, South Africa
%
% 1. lester_test is an impedance probe
% 2.          is a pressure probe
% 3.          is a flow rate (ml/s) probe
%
% Define global variables
% Use of global variables allows more fexibility in the Matlab - Simulink interface
% All global variables are prefixed with lester_ so that the variable names are not
% the same as any local variables that may be used by User or Matlab funtion files.

global lester_w;
global lester_AIin;
global lester_p;
global lester_u;
global lester_cardout;
global lester_n;
global lester_test;
global lester_test2;
global lester_lbrachial;
global lester_rbrachial;
global lester_lccarotid;
global lester_rccarotid;
global lester_lfemoral;
global lester_rfemoral;
global lester_probe1;
global lester_probe2;
global lester_probe3;
global lester_probe4;
global lester_probe5;
global lester_probe6;
global lester_aortalength;
global lester_aortaelastic;
global lester_aortaradius;
global lester_k;
global lester_fundamental;

% Start simulation by defining Input Waveform (current) in the frequency domain.

tic;
[Iin,f2,f3]          =      heart(43,6);

% Scale input waveform to predefined stroke volume eg. 60ml per stroke

stroke_vol           =      60;
Iin_scale            =      stroke_vol/(Iin(1)/length(Iin));
Iin                  =      Iin*Iin_scale;
```

```
% Anatomical scaling factors : default = 1
% This is used as a multiplication factor for the length, elasticity, and radius
% of the aorta

lester_aortalength          =       1;
lester_aortaelastic         =       1;
lester_aortaradius          =       1;

% Load Voltage Reflection Coefficient : default = 0.2
%  note Avolio et al , 1980 uses 0.8 (nominal) however, for the model
%  used here a value of 0.2 gives a closer simulation of physiological waveforms

lester_k                    =       0.2;

% Define Blood Viscosity and Density

lester_u                    =       0.04;
lester_p                    =       1.05;

% Cardiac Output

lester_cardout              =       Iin(1)/length(Iin);

% Set up null vectors
doppler                     =       zeros(size(Iin));
fdoppler                    =       zeros(size(Iin));
rdoppler                    =       zeros(size(Iin));
tonometer                   =       zeros(size(Iin));
ftonometer                  =       zeros(size(Iin));
rtonometer                  =       zeros(size(Iin));
freq_vec                    =       [];
lester_aorta1               =       [];
lester_aorta2               =       [];
lester_aorta5               =       [];
lester_aorta11              =       [];
lester_aorta21              =       [];
lester_aorta34              =       [];
lester_aorta50              =       [];
lester_aorta65              =       [];
lester_aorta75              =       [];
lester_iliac84              =       [];
lester_iliac92              =       [];

flen                        =       15;
IIstart2                    =       real(ifft(Iin));
Nmaxl                       =       length(Iin);
f_sample                    =       54.3478;
t_sample                    =       1/f_sample;
lester_fundamental          =       1/(t_sample*Nmaxl);
```

```
% Set up loop to perform DC (n=1) and AC analysis (n=2:15)

for n =1:flen,

        lester_n                =       n;
        w                       =       2*pi*(n-1)*f_sample/Nmaxl;
        freq_vec(n)             =       w/(2*pi);

% Adjust input vector to Current Phasor form

        Aiin                    =       [real(Iin(n)) imag(Iin(n))]/Nmaxl;
        lester_w                =       w;
        lester_AIin             =       AIin;

% Call Simulink Model 'avoles4'
        options                 =       [1e-3 1 1 0 3 0];
        sys                     =       'avoles4';
        rk23('avoles4',0,[],options);

% Test sampling probe in Femoral sample point : block 92
% Note: sample format is [real imaginary]

% store output variables of the forward model
        qqq                     =       [qqq;lester_test(1)+sqrt(-1)*lester_test(2)];

% store impedance spectrum at various points in the arterial system
        lester_lbrachial        =       [lester_lbrachial;lester_probe1];
        lester_rbrachial        =       [lester_rbrachial;lester_probe2];
        lester_lccarotid        =       [lester_lccarotid;lester_probe3];
        lester_rccarotid        =       [lester_rccarotid;lester_probe4];
        lester_lfemoral         =       [lester_lfemoral;lester_probe5];
        lester_rfemoral         =       [lester_rfemoral;lester_probe6];

% store time delay(s) and phase velocity (cm/s) values along the aorta
        lester_aorta1           =       [lester_aorta1;lester_test1];
        lester_aorta2           =       [lester_aorta2;lester_test2];
        lester_aorta5           =       [lester_aorta5;lester_test5];
        lester_aorta11          =       [lester_aorta11;lester_test11];
        lester_aorta21          =       [lester_aorta21;lester_test21];
        lester_aorta34          =       [lester_aorta34;lester_test34];
        lester_aorta50          =       [lester_aorta50;lester_test50];
        lester_aorta65          =       [lester_aorta65;lester_test65];
        lester_aorta75          =       [lester_aorta75;lester_test75];
        lester_iliac84          =       [lester_iliac84;lester_test84];
        lester_iliac92          =       [lester_iliac92;lester_test92];

% Convert values from phasor form to FFT form prior to
% implementing the IFFT

        iout                    =       iout*Nmaxl;
        yout                    =       yout*Nmaxl;

% Convert received values in pressure and flow waves

        flow                    =       (iout(1)+sqrt(-1)*iout(2))-(iout(3)+sqrt(-1)*iout(4));
        pressure                =       (yout(1)+sqrt(-1)*yout(2))+(yout(3)+sqrt(-1)*yout(4));
```

```
% Resolve Forward and Reverse Flow vectors

        fflow           =       iout(1)+sqrt(-1)*iout(2);
        rflow           =       iout(3)+sqrt(-1)*iout(4);

% Resolve Forward and Reverse Pressure vectors

        fpressure       =       yout(1)+sqrt(-1)*yout(2);
        rpressure       =       yout(3)+sqrt(-1)*yout(4);

        doppler(n)      =       flow;
        fdoppler(n)     =       fflow;
        rdoppler(n)     =       rflow;
        tonometer(n)    =       pressure;
        ftonometer(n)   =       fpressure;
        rtonometer(n)   =       rpressure;

% Aortic input impedance

        InZ(n)          =       azin(1)+sqrt(-1)*azin(2);

end


% Reformat phasors into format suitable for IFFT

doppler(length(Iin):-1:length(Iin)-flen+2)      =       conj(doppler(2:flen));
tonometer(length(Iin):-1:length(Iin)-flen+2)    =       conj(tonometer(2:flen));

% use this for a roving sample block

InZ(length(Iin):-1:length(Iin)-flen+2)          =       conj(InZ(2:flen));
InT                                             =       real(ifft(InZ));
InT(length(InT)+1:length(InT)+length(InT))      =       InT;
InT(length(InT)+1:length(InT)+length(InT))      =       InT;

% Extract time domain waveform

dopflow                                         =       real(ifft(doppler));
tonpres                                         =       real(ifft(tonometer));

% Plot Input Flow , Output Pressure and Output Flow waveforms (time domain) at the sample point

figure(1);
set(1,'Position',[7 38 272 375]);
subplot(3,2,3);
plot(dopflow);
title('      Doppler Flow Velocity Waveform');

subplot(3,2,5);
plot(tonpres/1334);
title(' mmHg            Blood Pressure Waveform');

subplot(3,2,1);
plot(IIstart2);
title('          Input Blood Flow Waveform');
```

```
% repeat the same waveforms over larger time frames ... easier to visualise

figure(2);
set(2,'Position',[285 38 343 375]);

tflow                                                   =       dopflow;
tflow(length(tflow)+1:length(tflow)+length(dopflow))   =       dopflow;
tflow(length(tflow)+1:length(tflow)+length(dopflow))   =       dopflow;
tflow(length(tflow)+1:length(tflow)+length(dopflow))   =       dopflow;
tflow(length(tflow)+1:length(tflow)+length(dopflow))   =       dopflow;

tpres                                                   =       tonpres;
tpres(length(tpres)+1:length(tpres)+length(tonpres))   =       tonpres;
tpres(length(tpres)+1:length(tpres)+length(tonpres))   =       tonpres;
tpres(length(tpres)+1:length(tpres)+length(tonpres))   =       tonpres;
tpres(length(tpres)+1:length(tpres)+length(tonpres))   =       tonpres;

tinflow                                                 =       IIstart2;
tinflow(length(tinflow)+1:length(tinflow)+length(IIstart2)) =   IIstart2;
tinflow(length(tinflow)+1:length(tinflow)+length(IIstart2)) =   IIstart2;
tinflow(length(tinflow)+1:length(tinflow)+length(IIstart2)) =   IIstart2;
tinflow(length(tinflow)+1:length(tinflow)+length(IIstart2)) =   IIstart2;

subplot(3,1,2);
plot(tflow);
title('      Doppler Flow Velocity Waveform');

subplot(3,1,3);
plot(tpres/1334);
title('  mmHg          Blood Pressure Waveform');

subplot(3,1,1);
plot(tinflow);
title('            Input Blood Flow Waveform');
toc

% Convert pressure from cgs units to mmHg

tpres_mmhg                                              =       tpres/1334;

% Plot impedance spectrum at the Sample point

figure(3);
plot(freq_vec(1:11),abs(qqq(1:11)));
title('Impedance Spectrum')
xlabel('Absolute Impedance');

% store results in an output file : tempavol

save tempavol dopflow tonpres Iin lester_rbrachial lester_lbrachial lester_rfemoral lester_lfemoral
lester_rccarotid lester_lccarotid
```

3.12.2 Function (**heart.m**)called by simavol.m ... Generate Input waveform

```
function [IIstart_1,IIstart_2,IIstart_3]=heart(Nmax,Nshift);

% This function generates the FFT of the Aortic Flow  Waveform corresponding to
%  figure 2.1- given the heart rate
%
% Three waveforms are generated for test purposes.  Only the first ouput waveform
%  (IIstart_1) is used by simavol.m
%
% Nmax   = size of waveform in samples  (ie. vector size)
% Nshift   = representation of time shifting of input waveform
% Ipeak - Peak of waveform - systole1
% a     - fraction of peak - systole2
%                       n1

if ~(exist('Nshift')),
        Nshift          =       9       ;
end

t_sample                =       1/54.3478;              % same value used by simavol.m
Ipeak                   =       720;

% Input vector length
% Nmax*t_sample  =  seconds per beat
% Heart_rate         = beats per minute

Heart_rate              =       60/(Nmax*t_sample);
Nmax                    =       round(Nmax);

% Systole 1 (approx 60ms)
% Ipeak is the peak of the LV waveform systole1
% Systole 1 represents the upstroke of the flow waveform, from zero flow to it's peak value (Ipeak)
% note: although a peak is specified here, simavol.m rescales the waveform in terms of a
%       a chosen stroke volume (ie. 60ml per stroke)


n1                      =       4;
t1                      =       (n1-1)*t_sample;
IIin(1:n1)              =       Ipeak/t1)*t_sample*[0 1 2 3];


% Systole2
% Systole 2 represents the downstroke of the flow waveform to 64% of it's peak value
%

a                       =       0.64;
t2                      =       (-528e-6)*(Heart_rate-60)+0.095;
n2                      =       t2/t_sample;

% truncate n2
if ( round(n2) - n2 ) > 0,
        n2              =       round(n2) - 1;
else
        n2              =       round(n2);
end
```

```
% Generate systole 3
for n = 1:n2,
        Iin(n1+n)       =       (Ipeak*(a-1)/t2)*(n*t_sample)+Ipeak;
end


%  Systole3 represents the second part of the downstroke of systole, with a
%  different gradient to systole 2.
t3                      =       0.5*((-1.714e-3)*(Heart_rate-60)+0.23);
n3                      =       t3/t_sample;

% truncate n3
if ( round(n3) - n3 ) > 0,
        n3              =       round(n3) - 1;
else
        n3              =       round(n3);
end

% generate systole 3

for n = 1:n3,
        Iin(n1+n2+n)    =       (-Ipeak*a/t3)*(n*t_sample)+a*Ipeak;
end

%* Diastole

IIin(n1+1+n2+n3:Nmax) =         zeros(size(1:Nmax-n1-1-n2-n3+1));

% Shift the input waveform to simulate delays
% This shift was used, so that the output waveforms would start at approximately
%  time=zero. This was accomplished by shifting the input waveform back in time
% so that the input to output time (phase) delay would be compensated for.

IIin                    =       vecshift (IIin,Nshift);

% Band limit the signal to 10 harmonics. ie Low Pass Filter

Iin                                     =       fft(IIin);
Iin(Nmax/5+1:Nmax/2+1)                  =       zeros(size(1:3*Nmax/10+1));
Iin(Nmax/2+1:Nmax/2+1+3*Nmax/10+1)      =       zeros(size(1:3*Nmax/10+2));

% Final output waveform

Iistart_1               =       Iin;
IIstart_2               =       Iin;    % used for testing purposes only
Iistart_3               =       Iin;    % used for testing purposes only
```

3.12.3 Function (**vecshift.m**) called by **heart.m** ... Time Shift Input waveform

```
function xout=vecshift(xin,n);

% This functions time shifts an input vector (xin) by (n times)
% by rotating the vector to the right or left depending on
% the sign of n. For use with repetitive signals
%
% note: -  = lag/delay   waveform
%       +  = lead/advance waveform

if n >=1,
        xtemp                                   =       xin(1:n);
        xout                                    =       xin(n+1:length(xin));
        xout(length(xout)+1:length(xout)+n) =   xtemp;
end

if n == 0,
        xout                                    =               xin;
end;

if n < 0,
        n                                                       = -n;
        xout                                                    = xin(length(xin)-n+1:length(xin));
        xtemp                                                   = xin(1:length(xin)-n);
        xout(length(xout)+1:length(xout)+length(xtemp))         = xtemp;
end
```

3.13. Program (**degraph.m**) used to capture data values from a scanned graph :

```
% Degraph.m
%
% This program be used to capture data  from a scanned graph
% in Matlab format ... results in vectors new_xin, new_yin
%
% Modified version 1.0b ... allows for non-zero origin of axes
%
% Edit the first line to include the path name format of
% the image file to be 'degraphed'
%
% To change the mouse pointer, edit the Matlab function
% 'ginput.m' The 'arrow' pointer looks better than
% the default 'crosshair'
%
% Options are
%
%       1. Rotate button .... rotates graph according
%                             to the value in the rotate box
%                             (degrees)
%       2. Set XY-axis button .... click on 4 points in the graph
%                                  according to the prompt
%                                     in the graph title
%                                     ie. Xstart,Xend,Ystart,Yend
%       3. Read Data button ... read  vectors new_xin, new_yin
%                                  from graph.
%                                  terminate reading with the 'Enter'
%                                  key
%       4. Rotate box       ... set angle of rotation in degrees
%                                  for skewed graphs
%
%
%       5. Xmin,Xmax,Ymin,Ymax boxes ... set actual xy limits
%                                        of the graph
%
%     note: modify the image reading function according to the
%           format of the image file.
%           The method used here is for .bmp files
%
%           some preprocessing using a graphics program
%           may be necessary eg. to sharpen the image,
%           select only the graph part of an image,
%         rotate the image , ect..
%
%           results are output in the Matlab vectors
%           xin, yin ... plotted in figure (2)
%
% Lester John
% LJOHN@anat.uct.ac.za
% October 1998
%
% Department of Biomedical Engineering
% University of Cape Town Medical School
% Anzio Road
% Observatory, 7925
% Cape Town, South Africa
% http://www.bme.uct.ac.za/
```

```
% First read and plot the graphics file
% 70K seems to be a suitable file size

load ch5f01;
super_x=freq_vec(1:9);
super_y=InZ(1:9);


[xx,map]=bmpread('c:\angio\t5fig1.bmp');
%[xx,map]=bmpread('c:\psp\files\g22.bmp');
figure(1);
set(gcf,'Position',[40 32 716 520]);
colormap(map);
image(xx);
%axis('xy');
axis('ij');
set(gcf,'Name','    Graph Reader 1.0b for Matlab,    Lester John 1998,    LJOHN@anat.uct.ac.za  ');

% Preset Variables

rot_angle       =       0;
new_xstart      =       0;
new_ystart      =       0;
new_xend        =       10;
new_yend        =       3200;


% Set 4 Push buttons

% Rotate

pbxy = uicontrol(gcf,...
                'Style','push',...
                'Position',[10 5 40 15],...
                'String','Rotate',...
                'CallBack', [...
                                'xx=imrotate(xx,-rot_angle,"nearest","crop");,',...
                                'image(xx);,',...
                                'axis("xy");']);

% Set XY

pbxy2 = uicontrol(gcf,...
                'Style','push',...
                'Position',[60 5 40 15],...
                'String','Set XY',...
                'CallBack', [...
                                'title("Click on START and END of X-AXIS");,',...
                                '[x,y]=ginput(2);,',...
                                'xstart=x(1);,',...
                                'xend  =x(2);,',...
                                'title("Click on START and END of Y-AXIS");,',...
                                '[x,y]=ginput(2);,',...
                                'title("                        ");,',...
                                'ystart = y(1);,',...
                                'yend   = y(2);,']);
```

```
% Read Data

pbxy3 = uicontrol(gcf,...
                  'Style','push',...
                  'Position',[120 5 40 15],...
                  'String','Read',...
                  'CallBack',       [...
                                    'title("Read DATA with left mouse button.  Press ENTER to end");,',...
                                    'xunit = (xend-xstart)/(new_xend-new_xstart);,',...
                                    'yunit = (yend-ystart)/(new_yend-new_ystart);,',...
                                    '[xin,yin]=ginput;,',...
                                    'title("                                    ");,',...
                                    'hold on;,',...
                                    'plot(xin,yin,"ko");,',...
                                    'hold off;,',...
                                    'new_xin = new_xstart+(xin-xstart)/xunit;,',...
                                    'new_yin = new_ystart+(yin-ystart)/yunit;,',...
                                    'figure(2);,',...
                                    'plot(new_xin,new_yin);,',...
                                    'axis([new_xstart new_xend new_ystart new_yend]);,',...
                                    'title("New DATA Vector");,',...
                                    'xlabel("new_xin");,',...
                                    'ylabel("new_yin");']);

% Superimpose existing matlab data on image

pbxy4 = uicontrol(gcf,...
                  'Style','push',...
                  'Position',[180 5 40*3 15],...
                  'String','Superimpose',...
                  'CallBack',       [...
                                    'title("Superimposing Matlab XY vector with image");,',...
                                    'xunit = (xend-xstart)/(new_xend-new_xstart);,',...
                                    'yunit = (yend-ystart)/(new_yend-new_ystart);,',...
                                    'xout=super_x*xunit+xstart;,',...
                                    'yout=abs(super_y)*yunit+ystart;,',...
                                'hold on;,',...
                                    'plot(xout,yout,"b");,',...
                                    ]);



% Exit
pbxy4 = uicontrol(gcf,...
                  'Style','push',...
                  'Position',[320 5 40 15],...
                  'String','Exit',...
                  'CallBack', [...
                                'end;']);

% Create Editable text boxes

% Y-end
pbed = uicontrol(gcf,...
                  'Style','edit',...
                  'String',int2str(new_yend),...
                  'Position',[10 100 50 15],...
                  'Max',1e6,...
                  'CallBack', [...
                                'new_yend=str2num(get(pbed,"String"));']);
```

```
tpbed = uicontrol(gcf,...
                  'Style','text',...
                  'String','Ymax',...
                  'Position',[10 120 50 15]);


% Y-start
pbed2 = uicontrol(gcf,...
                  'Style','edit',...
                  'String',int2str(new_ystart),...
                  'Position',[10 150 50 15],...
                  'Max',1e6,...
                  'CallBack', [...
                        'new_ystart=str2num(get(pbed2,"String"));']);

tpbed2 = uicontrol(gcf,...
                  'Style','text',...
                  'String','Ymin',...
                  'Position',[10 150+20 50 15]);

% X-end
pbed3 = uicontrol(gcf,...
                  'Style','edit',...
                  'String',int2str(new_xend),...
                  'Position',[10 200 50 15],...
                  'Max',1e6,...
                  'CallBack', [...
                        'new_xend=str2num(get(pbed3,"String"));']);

tpbed3 = uicontrol(gcf,...
                  'Style','text',...
                  'String','Xmax',...
                  'Position',[10 200+20 50 15]);

% X-start
pbed4 = uicontrol(gcf,...
                  'Style','edit',...
                  'String',int2str(new_xstart),...
                  'Position',[10 250 50 15],...
                  'Max',1e6,...
                  'CallBack', [...
                        'new_xstart=str2num(get(pbed4,"String"));']);

tpbed4 = uicontrol(gcf,...
                  'Style','text',...
                  'String','Xmin',...
                  'Position',[10 250+20 50 15]);

% Angle of Rotation
pbed5 = uicontrol(gcf,...
                  'Style','edit',...
                  'String','0000',...
                  'Position',[10 350 50 15],...
                  'Max',2,...
                  'CallBack', [...
                        'rot_angle=str2num(get(pbed5,"String"));']);

tpbed5 = uicontrol(gcf,...
                  'Style','text',...
                  'String','Rotate',...
                  'Position',[10 350+20 50 15]);
```

SCREEN CAPTURE OF PROGRAM 'DEGRAPH.M' being used to capture aortic input impedance data that has been redrawn in Figure 5.1

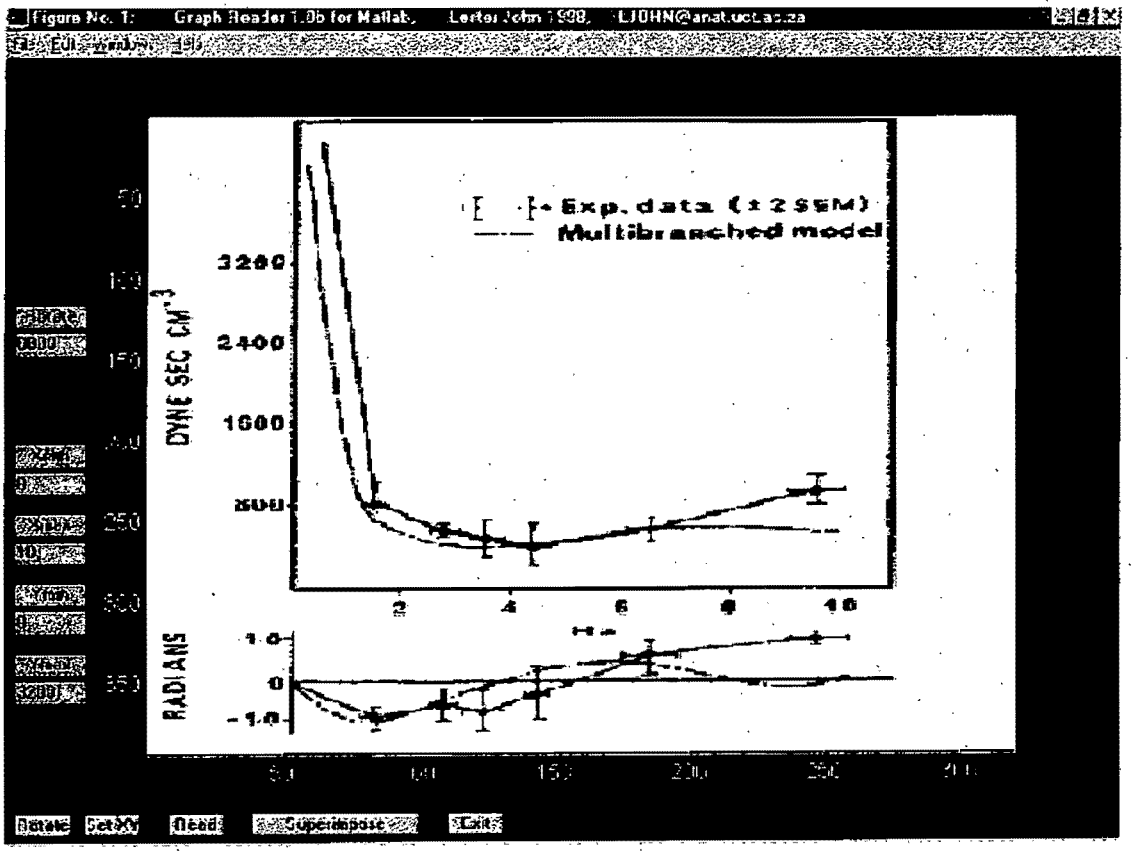

3.14 Inverse Model Main Program (**avoltes9.m**) which sets up the proximal radius iteration.
This program calls the inverse model function_ called **simtim10.m** . It stores the waveforms and error graphs at each discrete proximal radius. The final output is a set of error graphs and waveform graphs.

```
% Time domain implementation of inverse model

% Define Global Variables
global lester_test2;
global lester_k;
global lester_w;
global lester_AIin;
global lester_Iin;
global lester_flow;
global lester_pressure;
global lester_fflow;
global lester_fpressure;
global lester_rflow;
global lester_rpressure;
global lester_Nmaxl;
global lester_param;
global lester_p;
global lester_u;
global lester_cardout;
global lester_lbrachial;
global lester_rbrachial;
global lester_lccarotid;
global lester_rccarotid;
global lester_lfemoral;
global lester_rfemoral;
global rfemoral_spectrum;
global lfemoral_spectrum;
global rbrachial_spectrum;
global lbrachial_spectrum;
global rccarotid_spectrum;
global lccarotid_spectrum;
global lester_modelflow;
global lester_modelpres;
global lester_expflow;
global lester_exppres;
global lester_aortalength;
global lester_aortaelastic;
global lester_aortaradius;
global lester_legelastic;
global lester_fundamental;

% Global Scaling Factors for the Aorta

lester_aortalength      =       1;
lester_aortaelastic     =       1;
lester_aortaradius      =       1;

% Blood Viscosity and Density.
% Adjust viscosity to increase damping

lester_u =      0.04;
lester_p =      1.05;


% Global Scaling factor for the Leg Elasticity

lester_legelastic = 1;
```

```
% Peripheral Reflection Coefficient
% Note : [Avolio AP, 1980] used a value of 0.8, but for this simulation 0.2 resulted in better waveforms

lester_k        =       0.2;

% Load Clinical Data from Patient Files
% Forward Model data may also be loaded instead as a  computer simulated 'Patient'
% Two waveforms are loaded ie Femoral Pressure (tonpres) and Femoral Flow (dopflow),
% The Frequency Domain Input Waveform (Iin) is calculated from the time length of
% the Femoral Flow waveform, using the function heart.m

load c:\matlab\clinical\normal4;
dopflow                         =       doppler_wmean_rm;
tonpres                         =       pressure_qrs_rm;
tonpres                         =       tonpres-min(tonpres);
tonpres                         =       tonpres-2;
[heart_1_rm,heart_2_rm,heart_3] =       heart(length(doppler_wmean_rm),5,15);
Iin                             =       heart_1_rm;

% Set sampling frequency and hence sample time. The sampling frequency corresponds to the
% sampling frequency of the Data Acquisition System

f_sample                        =       54.3478;
t_sample                        =       1/f_sample;


% Scale Femoral Pressure Waveform according to measured or estimated Systolic and Diastolis values
%**** normal4: Brachial Blood Pressure =110/70,  Pulse Pressure (PP) = 40mmHg
% Conversion to Femoral Levels
%SYSfem  = 1.3*SYSTOLIC_brachial
%DIASfem = 0.9*DIASTOLIC_brachial
% note: estimated  mean BP  = 1/3(SP-DP) + DP
%

SYSfem                          =       1.3*110;
DIASfem                         =       0.9*70;
PPfem                           =       SYSfem-DIASfem;

tonpres                         =       tonpres*PPfem;
tonpres                         =       tonpres+DIASfem;


%Convert Pressure from mmHg to cgs units

tonpres                         =       tonpres*1334;

% Now scale input waveform to stroke_volume
% Use DuBois Formula, 1934  to calculate BSA(m^2)
% Use deSimone et al,1997   to calculate SV(ml)

height                          =       1.65;
weight                          =       61;
BSA                             =       (height^0.725)*(weight^0.425)*0.2025;
stroke_volume                   =       35.38*(BSA^1.19)
stroke_scale                    =       1.0;
stroke_volume                   =       stroke_volume*stroke_scale;
Iin_temp                        =       real(ifft(Iin));
Iin_temp                        =       Iin_temp*stroke_volume/mean(Iin_temp);
Iin                             =       fft(Iin_temp);
```

```
% Scale Doppler Ultrasound Waveform to convert to Volume Flow Rate Waveform.
% Flow Rates may be estimated using a Duplex Doppler
% For a 'normal resting' state,  the mean Common Femoral Flow is about 4.6% of the cardiac output

flow_scale                      =       1.0;
dopflow                         =       dopflow/mean(dopflow);
dopflow                         =       dopflow*flow_scale*0.046*lin(1)/length(lin);

% For computer simulated tests add amplitude distortion of flow and pressure.
% This feature is disabled (=1) for Clinical Tests.

dopflow                         =       1.0*dopflow;
tonpres                         =       1.0*tonpres;

% Rename Haemodynamic Data using global variables

lester_expflow                  =       dopflow;
lester_exppres                  =       tonpres;
lester_lin                      =       lin;

% Store initial values since simtim10 modifies lester_expflow/exppres;

lester_expflow_init             =       lester_expflow;
lester_exppres_init             =       lester_exppres;

% Frequency Domain Flow and Pressure

pdata                           =       fft(dopflow);
pf                              =       fft(tonpres);

% set up terminal impedance data in at sample .
%  note: this is volume flow rate data **not** flow velocity
% This sets up Region 3: Distal Region of the Three-Division Inverse Model
% Region3 is set to correspond to the distal circulation of the Right Leg

lester_rfemoral                 =       [];
lester_rfemoral(1:10,1)         =       real(pf(1:10)./pdata(1:10))';
lester_rfemoral(1:10,2)         =       imag(pf(1:10)./pdata(1:10))';


%

lester_cardout                  =       lin(1)/length(lin);
lstart2                         =       real(ifft(lin));
lester_Nmaxl                    =       length(lin);
lester_fundamenta       1       =       1/(t_sample*lester_Nmaxl);

% call the FSOLVE function
% This code section has been disabled. It was used when a numerical technique instead of an iterative technique
% was implemented by the Inverse Model
%
% Initial Values for Proximal Radius and Proximal Ypungs Modulus
% note : The iteration of Youngs Modulus has been disabled for reasons discussed in the text.
%       xx(1,1)                   =       0.29;
%       xx(2,1)                   =       4e6;
%
%       scale = [1e6 1]';
%       fvectol = eps^(1/3);
%       mintol  = eps^(2/3);
%       maxstepi = 3e10*eps^(2/3);
%       maxitns = 15*4/4;
```

```
%       options = [1 1 0 0 0 maxitns 0 fvectol eps^(2/3) mintol 1e8*maxstepi -log10(eps) 0 0 0 2]';
%
%       2 variable FSOLVE
%       [qq,termcode]=fsolve('simtim10',xx(:,1),options)
%
%       1 variable FSOLVE
%       [qq,termcode]=fsolve('simtim10',xx(1,1),options)
%       ff = simtim10(xx);


% Initial Values for Proximal Radius and Proximal Youngs Modulus
% Youngs Modulus iteration has been disabled for reasons discussed in text
% Radius is iterated

xsum                    =       [];
radstart                =       0.29*2;
radstep                 =       10;
radend                  =       radstart/radstep;

estart                  =       4e6;
estep                   =       1;
eend                    =       estart/estep;

xsum                    =       1e6*ones([radstep estep]);
radrad                  =       [];

% Begin Proximal Radius Iteration.
% Note: Proximal Youngs Modulus Iteration has been disabled by setting estep = 1.
%       At each discrete Proximal Radius, the Function simtim10.m is called to generate the predicted
%       waveforms and the corresponding error (xsum) graphs .

for radloop     =       radstep:-1:1
        radloop         =       radloop
        for eloop       =       estep:-1:1
                eloop           =       eloop
                radnow          =        radstart*(radloop/radstep)
                radrad          =       [radrad;radnow];
                enow            =       estart*(eloop/estep);
                xx(1,1)         =       radnow;
                xx(2,1)         =       enow;
                lester_expflow  =       lester_expflow_init;
                lester_exppres  =       lester_exppres_init;
                ff              =       simtim10(xx);
                xsum(radstep-radloop+1,1:4)=ff';
        end
end

% Plot the Error Flow and Pressure Error Graphs (xsum).
% xsum(:,3) is the Flow Error and  xsum(:,4) is Pressure Error

figure(21);
hold off;
plot(radrad,xsum(:,3),radrad,xsum(:,4));
hold on;
plot(radrad,xsum(:,3),'o',radrad,xsum(:,4),'o');
grid on;
zoom on;
xlabel('Radius cm');
ylabel('Xsum value ');
title('Patient3 - Right Leg - Inverse model - error relative to MEAN');
hold off;
```

```
% Convert from Phasor format into format suitable for Inverse Fast Fourier Transform

doppler(length(lester_Iin):-1:length(lester_Iin)-flen+2)      =      conj(doppler(2:flen));
tonometer(length(lester_Iin):-1:length(lester_Iin)-flen+2)    =      conj(tonometer(2:flen));

% Generate Time Domain Waveforms

dopflow                       =      real(ifft(doppler*lester_Nmaxl));
tonpres                       =      real(ifft(tonometer*lester_Nmaxl));

% Extract maximum and minumum data for setting limits of graphs

ton_max                       =      num2str(max(tonpres)/1334,6);
ton_min                       =      num2str(min(tonpres)/1334,6);
ton_mean                      =      num2str(mean(tonpres)/1334,6);

dop_max                       =      num2str(max(dopflow),6);
dop_min                       =      num2str(min(dopflow),6);
dop_mean                      =      num2str(mean(dopflow),6);
dop_perc                      =      num2str(100*mean(dopflow)/(lester_Iin(1)/length(lester_Iin)),6);;


% Rename Predicted Flow and Pressure Waveforms as global variables

lester_modelflow              =      dopflow;
lester_modelpres              =      tonpres;


% Error Equations : Calculate Error between Predicted and Actual Waveforms
% Note only the last 2 are used for analysis purposes
% If a different is to be used, then it must be inserted here.

ff(1,1)   = mean(sqrt(((dopflow - lester_expflow)).^2))/max(lester_expflow);
ff(2,1)   = mean(sqrt(((tonpres - lester_exppres)).^2))/max(lester_exppres);
ff(3,1)   = mean(sqrt(((dopflow - lester_expflow)).^2))/mean(lester_expflow);
ff(4,1)   = mean(sqrt(((tonpres - lester_exppres)).^2))/mean(lester_exppres);


mean_diff_flow=num2str(ff(1,1),6);
mean_diff_pres=num2str(ff(2,1),6);


% Plot Predicted and Actual Waveforms, including some waveform parameters

figure(20);

% scale axes

y_max                         =      max(max([dopflow;lester_expflow]));
y_min                         =      min(min([dopflow;lester_expflow]))*4;
x_min                         =      0;
x_max                         =      length(dopflow);

subplot(2,3,1);
rad_text                      =      num2str(xx(1,1));
rad_title                     =      'Iterative Comparisons ';
rad_str                       =      rad_title;
rad_str(length(rad_str)+1:length(rad_str)+length(rad_text))   =      rad_text;
plot(dopflow);
axis([x_min x_max y_min y_max]);
title(rad_str);
```

3.15 Function (**simtim10.m**) that is called by the main inverse model program (**avoltes9.m**).
This functioncalculates the haemodynamic time domain waveforms corresponding to a given proximal radius. It also calculates the error between the predicted and actual waveforms. The function performs frequency domain analysis by calling **simavol6.m (DC)** and **simavol5.m(AC)**. Results are converted into the time domain before being sent to **avoltes9.m**

```
function ff = simtim10(xx);
% Time/Frequency domain function for Inverse Model

% Define global variables

global lester_test2;
global lester_k;
global lester_w;
global lester_AIin;
global lester_Iin;
global lester_flow;
global lester_pressure;
global lester_fflow;
global lester_fpressure;
global lester_rflow;
global lester_rpressure;
global lester_Nmaxl;
global lester_param;
global lester_p;
global lester_u;
global lester_cardout;
global lester_lbrachial;
global lester_rbrachial;
global lester_lccarotid;
global lester_rccarotid;
global lester_lfemoral;
global lester_rfemoral;
global rfemoral_spectrum;
global lfemoral_spectrum;
global rbrachial_spectrum;
global lbrachial_spectrum;
global rccarotid_spectrum;
global lccarotid_spectrum;
global lester_modelflow;
global lester_modelpres;
global lester_expflow;
global lester_exppres;
global lester_aortalength;
global lester_aortaelastic;
global lester_aortaradius;
global lester_fundamental;

% Define Data Acquisition Constants

flen        = 10;
f_sample    = 54.3478;
t_sample    = 1/f_sample;
```

```
% Set up Distal Region ie. Femoral Impedance Spectrum in limb under investigation
% note: This spectrum is defined in terms of  the Measured or Clinical Waveforms

lester_rfemoral                 =       [];
lrf_complex                     =       fft(lester_exppres)./fft(lester_expflow);
lester_rfemoral(1:10,1)         =       real(lrf_complex(1:10))';
lester_rfemoral(1:10,2)         =       imag(lrf_complex(1:10))';


% Set up frequency loop to carry out analysis from DC to 10 Harmonics

for n           =       1:flen,

                w               =  2*pi*(n-1)*f_sample/lester_Nmaxl;
                Aiin            = [real(lester_Iin(n)) imag(lester_Iin(n))]/lester_Nmaxl;
                lester_w        = w;
                lester_AIin     = AIin;

% note: conversion between FFT and Voltage Phasor format , divide by lester_Nmaxl



% Set measured distal impedance data as global variables for use by avoles5

        rfemoral_spectrum = [lester_rfemoral(n,1) lester_rfemoral(n,2)];


% For DC analysis call simavol6.m. For Ac analysis call simavol5.m
% Note : Results are received via global variables rather than function return vectors

        if lester_w == 0,
                simavol6(xx(1,1));
        else
                simavol5(xx(:,1));
        end


% ***********************************************
% remember conversion between FFT and Phasor form
% ***********************************************
%
% Extract Total, Forward, and Reverse Flow and Pressure vectors
% Note : The global variables below were generated by the simavol6.m and simavol5.m functions

        doppler(n)              =       lester_flow;
        fdoppler(n)             =       lester_fflow;
        rdoppler(n)             =       lester_rflow;
        tonometer(n)            =       lester_pressure;
        ftonometer(n)           =       lester_fpressure;
        rtonometer(n)           =       lester_rpressure;

end
```

```
xlabel('model flow');
subplot(2,3,2);
plot(lester_expflow,'w');
axis([x_min x_max y_min y_max]);
xlabel('measured flow')

subplot(2,3,4);
y_max=max(max([tonpres/1334;lester_exppres/1334]));
y_min=min(min([tonpres/1334;lester_exppres/1334]));
plot(tonpres/1334);
axis([x_min x_max 0 y_max]);
xlabel('model pressure');
subplot(2,3,5)
plot(lester_exppres/1334,'w');
axis([x_min x_max 0 y_max]);
xlabel('measured pressure');

% Now plot the values of some constants;

subplot(2,3,6)
axis([0 100 0 100]);
axis('off');
text(0,90,mean_diff_pres);
text(80,90,'Mean Error');
text(0,70,ton_max);
text(80,70,'mmHg Max');
text(0,50,ton_min);
text(80,50,'mmHg Min');
text(0,30,ton_mean);
text(80,30,'mmHg Mean');
title('PRESSURE PARAMETERS')

subplot(2,3,3)
axis([0 100 0 100]);
axis('off');
text(0,90,mean_diff_flow);
text(80,90,'Mean Error');
text(0,70,dop_max);
text(80,70,'ml/s Max');
text(0,50,dop_min);
text(80,50,'ml/s Min');
text(0,30,dop_mean);
text(80,30,'ml/s Mean');
text(0,10,dop_perc);
text(80,10,'% Output');
title('VOLUME FLOW PARAMETERS');
```

3.16 Function (**simavol6.m**) that calculates the DC or Mean Pressure & Flow levels of the Inverse Arterial Model This function is called by **simtim10.m**

```
function ff = simavol6(xin);

% Note : this function is only used for DC analysis
%        for Harmonic (AC) analysis use simavol5.m
%        The output variables are stored in global variables

global lester_test2;
global lester_k;
global lester_w;
global lester_Alin;
global lester_flow;
global lester_pressure;
global lester_fflow;
global lester_fpressure;
global lester_rflow;
global lester_rpressure;
global lester_Nmaxl;
global lester_param;
global lester_u;
global lester_p;
global lester_cardout;
global lester_lbrachial;
global lester_rbrachial;
global lester_lccarotid;
global lester_rccarotid;
global lester_lfemoral;
global lester_rfemoral;
global rfemoral_spectrum;
global lfemoral_spectrum;
global rbrachial_spectrum;
global lbrachial_spectrum;
global rccarotid_spectrum;
global lccarotid_spectrum;
global lester_aortalength;
global lester_aortaelastic;
global lester_aortaradius;
global lester_fundamental;


% Proximal Radius String ... note 30 digit accuracy

        proxrad                 =       num2str(xin(1,1),30);

% Call Simulink Model : Avoles5.m

        options                 =       [1e-3 1 1 0 0 0];
        mask_str                =       proxrad;
        mask_str(length(mask_str)+1:length(mask_str)+14) =      'V0.055/0.29V';
        mask_str(length(mask_str)+1:length(mask_str)+3)  =      '4e6';
        mask_str(length(mask_str)+1:length(mask_str)+17) =      'V0V1.05V0.03V';
        mask_str                =       mask_str;
        sys                     =       'avoles5';
        set_param([sys,'/',[",13,'RIGHT',13,'LEG/',13,'9 2
        ',13,'EXTERNAL',13,'ILIAC',13,'Sample',13,",13,'/electromechanical ',13,'analogies']],....
        'Mask Entries',mask_str,...
        'position',[55,127,175,193])
```

```
rk23('avoles5',0,[],options);


% True output values .
% Convert received Simulink values into  pressure and flow wave variables
% Note: these global values are received by the calling function simtim10.m
%       for DC the reverse Flow and Pressure is set to zero

    lester_flow          =     iout(1);
    lester_pressure      =     yout(1);
    lester_fflow         =     iout(1);
    lester_rflow         =     0;
    lester_fpressure     =     yout(1);
    lester_rpressure     =     0;

% Dummy Output Equations: not used by the calling function

    ff(1,1)              =     lester_flow;
    ff(2,1)              =     lester_pressure;
```

3.17 Function (**simvol5.m**) that calculates the AC or Harmonic levels of the Inverse Arterial Model
This function is called by **simtim10.m**

```
function ff = simavol5(xin);

% Harmonic Analysis Function
% The output variables are stored in global variables

global lester_test2;
global lester_k;
global lester_w;
global lester_Alin;
global lester_flow;
global lester_pressure;
global lester_fflow;
global lester_fpressure;
global lester_rflow;
global lester_rpressure;
global lester_Nmaxl;
global lester_param;
global lester_u;
global lester_p;
global lester_cardout;
global lester_lbrachial;
global lester_rbrachial;
global lester_lccarotid;
global lester_rccarotid;
global lester_lfemoral;
global lester_rfemoral;
global rfemoral_spectrum;
global lfemoral_spectrum;
global rbrachial_spectrum;
global lbrachial_spectrum;
global rccarotid_spectrum;
global lccarotid_spectrum;
global lester_aortalength;
global lester_aortaelastic;
global lester_aortaradius;
global lester_fundamental;


% Proximal Radius and Youngs Modulus string ... note 30 digit accuracy

        proxrad         =       num2str(xin(1,1),30);
        proxEy          =       num2str(xin(2,1),30);

% Call Simulink Model

        options         =       [1e-3 1 1 0 0 0];
        mask_str        =       proxrad;
        mask_str(length(mask_str)+1:length(mask_str)+14) =      '\0.055/0.29\';
        mask_str(length(mask_str)+1:length(mask_str)+length(proxEy))    =      proxEy;
        mask_str(length(mask_str)+1:length(mask_str)+17) =      '\0\1.05\0.03\';
        mask_str=mask_str;
        sys='avoles5';
```

```
        set_param([sys,'/',['',13,'RIGHT',13,'LEG/',13,'9 2
        ',13,'EXTERNAL',13,'ILIAC',13,'Sample',13,'',13,'/electromechanical ',13,'analogies']],...
        'Mask Entries',mask_str,...
        'position',[55,127,175,193])

        rk23('avoles5',0,[],options);

% True output values
% Convert received Simulink values in complex pressure and flow phasors
% These global variables are accessed by the function simtim10.m

        lester_flow       =    (iout(1)+sqrt(-1)*iout(2))-(iout(3)+sqrt(-1)*iout(4));
        lester_pressure   =    (yout(1)+sqrt(-1)*yout(2))+(yout(3)+sqrt(-1)*yout(4));
        lester_fflow      =    iout(1)+sqrt(-1)*iout(2);
        lester_rflow      =    iout(3)+sqrt(-1)*iout(4);
        lester_fpressure  =    yout(1)+sqrt(-1)*yout(2);
        lester_rpressure  =  yout(3)+sqrt(-1)*yout(4);

% Dummy Return Vector of this function :
% This vector is not used because the results are returned using the global variables above

        ff(1,1)           =    real(lester_flow);
        ff(2,1)           =    imag(lester_flow-);
```

APPENDIX 4 : SUBJECT DATA RECORDED FOR THE PRELIMINARY CLINICAL FEASIBILITY STUDY

Normal Subject Number	Gender	Age (y)	Height (cm)	Weight (kg)	Doppler Waveforms	Tonometer Waveforms	ECG Waveforms	Pulsatility Index
Normal 1	Female	29	156	41	R: Doppler recorded L: no Doppler recorded	R: Pressure recorded L: Pressure recorded, baseline drift	R: ECG recorded L: ECG recorded	R= 4.7026 L= 6.5298
Normal 2	Female	24	165	55	R: Doppler recorded L: Doppler recorded	R: Pressure recorded, baseline drift L: Pressure recorded, baseline drift	R: ECG recorded L: ECG recorded	R= 5.3721 L= 8.3180
Normal 3	Female	22	154	50	R: Doppler recorded, noisy waveforms L: Doppler recorded	R: Pressure recorded, baseline drift L: Pressure recorded	R: ECG recorded L: ECG recorded	R= 4.0403 L= 5.7824
Normal 4	Male	31	165	61	R: Doppler recorded L: Doppler recorded	R: Pressure recorded L: Pressure recorded	R: ECG recorded L: ECG recorded	R= 14.2896 L= 12.6474
Normal 5	Male	30	176	71	R: Doppler recorded L: Doppler recorded	R: Pressure recorded L: Pressure recorded	R: ECG recorded L: ECG recorded	R= 5.2590 L= 6.0753
Normal 6	Male	25	173	61	R: Doppler recorded L: Doppler recorded	R: Pressure recorded L: Pressure recorded	R: ECG recorded L: ECG recorded	R= 6..4038 L= 10.8210

Normal Subject Number	Brachial Systolic BP(mmHg)	Brachial Diastolic BP (mmHg)	Estimated Mean BP (mmHg)	Measured Average Pulse Arrival Time (ms)	Estimated Body Surface Area (m^2)	Estimated Aortic Length at 21 years (cm)	Estimated Aortic Length now (cm)	Estimated average Aorto-Femoral Pulse Wave Velocity (cm/s)
Normal 1	110	70	83	R= 148 L=154	1.355	37.44	39.24	R=265.12 L=255.53
Normal 2	110	70	83	R=143 L=148	1.599	39.6	40.31	R=281.17 L=272.38
Normal 3	100	60	73	R=111 L=125	1.460	36.96	37.18	R=334.97 L=297.75
Normal 4	110	70	83	R=130 L=142	1.671	39.6	41.98	R=324.14 L=295.82
Normal 5	120	70	87	R=136 L=143	1.876	42.24	44.52	R=328.31 L=310.52
Normal 6	110	60	77	R=148 L=130	1.729	41.52	42.52	R=287.27 L=328.31

Table I : Data recorded from Normal Subjects

Patient Subject Number	Gender	Age (y)	Height (cm)	Weight (kg)	Doppler Waveforms	Tonometer Waveforms	ECG Waveforms	Pulsatility Index
Patient 1	Male	64	162	55	R: Doppler recorded, noisy waveforms L: no Doppler recorded	R: Pressure recorded L: no Pressure recorded	R: ECG recorded L: no ECG recorded	R= 12.5860 L= no Doppler
Patient 2	Male	49	170	65	R: Doppler recorded L: no Doppler recorded	R: Pressure recorded, small signal L: no Pressure recorded	R: ECG recorded L: no ECG recorded	R= 9.8884 L= no Doppler
Patient 3	Male	61	158	62	R: Doppler recorded L: Doppler recorded	R: Pressure recorded L: Pressure recorded	R: ECG recorded L: ECG recorded	R= 4.7107 L= 2.8447
Patient 4	Female	86	150	52	R: Doppler recorded L: Doppler recorded	R: Pressure recorded L: Pressure recorded, small signal	R: no ECG recorded L: no ECG recorded	R= 4.8084 L= 3.8924
Patient 5	Male	72	168	68	R: Doppler recorded L: Doppler recorded	R: Pressure recorded L: Pressure recorded, very small signal	R: ECG recorded L: ECG recorded	R= 7.9511 L= 16.4246
Patient 6	Male	62	170	76	R: Doppler recorded L: Doppler recorded	R: no Pressure recorded L: no Pressure recorded	R: ECG recorded L: ECG recorded	R= 14.7812 L= 16.6156
Patient 7	Male	39	173	55	R: Doppler recorded L: no Doppler, amputated	R: Pressure recorded L: no Pressure, amputated	R: ECG recorded L: no ECG, amputated	R= 8.3452 L= no Doppler, amputated
Patient 8	Male	57	180	110	R: Doppler recorded L: Doppler recorded	R: no Pressure recorded L: no Pressure recorded	R: ECG recorded L: ECG recorded	R= 15.3673 L= 34.5578
Patient 9	Male	56	187	68	R: no Doppler recorded L: Doppler recorded	R: no Pressure recorded L: Pressure recorded	R: no ECG recorded L: ECG recorded	R= no Doppler L= 10.8212
Patient 10	Male	64	175	65	R: Doppler recorded L: Doppler recorded	R: Pressure recorded L: Pressure recorded	R: ECG recorded L: ECG recorded	R= 8.3240 L= 4.8706
Patient 11	Male	56	173	78	R: Doppler recorded L: Doppler recorded	R: Pressure recorded L: Pressure recorded	R: no ECG recorded L: no ECG recorded	R= 5.4744 L=10.4090
Patient 12	Female	73	158	56	R: no Doppler recorded L: Doppler recorded	R: no Pressure recorded L: Pressure recorded	R: no ECG recorded L: no ECG recorded	R= no Doppler L= 3.5902

Table II : Data recorded from Patient Subjects

Patient Subject Number	Brachial Systolic BP(mmHg)	Brachial Diastolic BP (mmHg)	Estimated Mean BP (mmHg)	Measured Average Pulse Arrival Time (ms)	Estimated Body Surface Area (m^2)	Estimated Aortic Length at 21 years (cm)	Estimated Aortic Length now (cm)	Estimated average Aorto-Femoral Pulse Wave Velocity (cm/s)
Patient 1	140	90	107	R= 130 L= not recorded	1.578	38.88	48.91	R=377.69 L=not estimated
Patient 2	no BP recorded	no BP recorded	no BP recorded	R=142 L=not recorded	1.754	40.80	47.65	R=335.84 L=not estimated
Patient 3	140	90	107	R=92.5 L=92.5	1.630	37.92	47.02	R=508.3 L=508.3
Patient 4	170	70	103	R=not recorded L=not recorded	1.457	not estimated	not estimated	R=not estimated L=not estimated
Patient 5	140	80	100	R=143 L=130	1.773	40.32	52.66	R=367.27 L=406.62
Patient 6	170	90	117	R=135 L=123	1.874	40.80	50.84	R=376.4 L=412.0
Patient 7	130	70	90	R = not recorded L = 130	1.654	41.52	46.00	R=not estimated L=355.24
Patient 8	no BP recorded	no BP recorded	no BP recorded	R=130 L=171	2.286	43.20	52.53	R=405.6 L=307.0
Patient 9	160	90	113	R=not recorded L=126	1.916	44.88	54.30	R=not estimated L=431.68
Patient 10	160	90	113	R=160 L=111	1.791	42	52.84	R=329.4 L=476.0
Patient 11	170	90	117	R = not recorded L = not recorded	1.919	not estimated	not estimated	R=not estimated L=not estimated
Patient 12	180	90	120	R = not recorded L = not recorded	1.561	not estimated	not estimated	R=not estimated L=not estimated

Table II : Data recorded from Patient Subjects

Patient Subject Number	Arterial Pre-Sample Region (aorta, common & internal iliac)	Arterial Sample Region (both external iliac and common femoral included here)	Arterial Distal Region (profunda femorus, superficial femoral,popliteal, posterior and anterior tibials, peroneal)	General comments
Patient 1	normal aorta, L: mild common iliac disease	R: small common femoral plaque	R: mild disease in SFA and popliteal; diseased trifurcation L: occluded SFA, popliteal and trifurcation	This patient readings were taken using the experimental combined tonometer + doppler probe holder. This holder was not used for any of the other subjects.
Patient 2	normal aorta	normal	R: mild disease below trifurcation	Diabetes. Arterial hardening. R: Gangrenous toes
Patient 3	infra-renal abdominal aortic aneurysm, R: possible internal iliac artery occlusion	R: normal L: 60% stenosed by plaque	R: reduced pedal pulse L: no pedal pulse	L:Cellulitus in the foot & middle toe
Patient 4	normal aorta	R: normal L: 75% stenosed	R: normal L: critical ischaemia	L:gangrene in the 3rd & 4th toes
Patient 5	normal aorta	normal	R: mid SFA to peroneal arterial bypass graft (occlusion from distal popliteal to below trifurcation)	NIDDM, Gout, high cholesterol R: leg ulcers and early rest pain
Patient 6	multiple aortic aneurysms, previous aneurysms in both common iliacs which have been treated with stents	L : mild 35% stenosis due to a plaque	R: severe SFA disease, patent popliteal, diseased trifurcation ,anterior tibial patent up to mid-calf region L: moderate disease of SFA, mild disease of popliteal & trifurcation	
Patient 7	normal aorta	normal	L: severely diseased trifurcation	Smoker, Buergers disease, R: leg previously amputated L: non-healing toe , popliteal - peroneal bypass procedure one day after these readings were taken
Patient 8	large infra-renal abdominal aortic aortic aneurysm			Hypertension. Not always in sinus rhythm
Patient 9	normal aorta	L: normal doppler	L: reduced ankle pulse	Hypertension. Patient in continuous pain
Patient 10	infra-renal aortic disease with multiple ulcerated plaques.	R: external iliac stenosis L: early disease of external iliac	R: occluded SFA, reconstituted popliteal,occluded peroneal & posterior tibial L: occluded SFA, reconstituted but diseased popliteal, no distal run-off for anterior tibial	smoker, painfull swollen right leg
Patient 11	mild distal abdominal aortic disease	R: External Iliac to popliteal arterial graft (occluded common femoral) L: mild disease	R: reconstituted SFA and profunda. Possible distal arterial stenosis or distal graft stenosis	R: common femoral trauma due to previous stab wound.
Patient 12	normal distal aorta and iliac vessels	R&L: diseased common femoral	R: severe SFA & popliteal disease with distal popliteal reconsituted via collaterals. Severe trifurcation disease with reconsituted anterior tibial & dorsalis pedis via collaterals L: severe proximal SFA disease with distal SFA reconstituted via collaterals	Diabetes, Hypertension

Table II: Data recorded from Patient Subjects

APPENDIX V :
SHORT REVIEW OF CRITICAL STENOSIS IN AN ARTERY

1. Critical Stenosis :

Progressive atherosclerosis results in the narrowing of the arterial lumen. Anatomical classification of that narrowing would include the location, degree, geometry and length of the affected region. Physiological classification of a stenosis would include the degree of pressure drop and flow reduction caused by that stenosis.

A critical stenosis is clinically defined as : *the stenosis level beyond which a small reduction in the arterial lumen would cause drastic reductions in flow and pressure.*

There is no single accepted criteria for defining the point of critical stenosis, and there are even some contradictory opinions [Woodcock J, 1976]. Some approaches to determining critical stenosis include :

1.1 Percentage Reduction of Arterial Lumen Area
1.2 Absolute cross-sectional area of the stenosis
1.3 Measurement of peripheral resistance
1.4 Measurement of blood velocity in the unstenosed area

For the purposes of the Inverse Transmission Line Model a simple evenly distributed circular model of stenosis has been used. Using this approach a 50% arterial diameter reduction would result in a 75% area reduction. Experimentally determined levels of critical stenosis indicate that a 75% area reduction or greater would result in critical stenosis [Rutherford RB, 1989] . Computer simulations of stenosis in Chapter 5 , Figures 5.11 – 5.12 concur with this, as they indicate an increasing reduction in pressure and flow at a circular-symmetric level of 50% diameter (i.e. 75% area stenosis).

2. Circular Symmetric Stenosis

Consider a circular symmetric stenosis as illustrated in Figure V.I

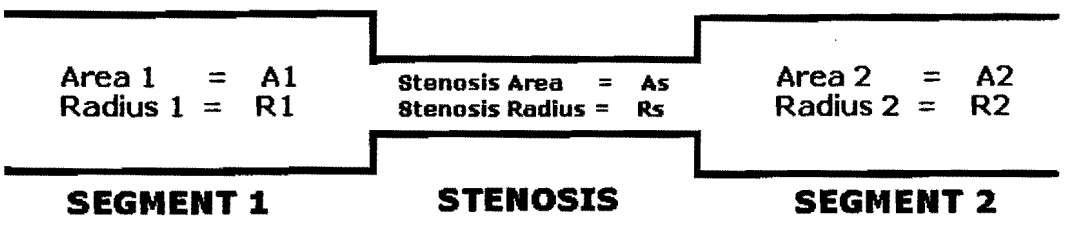

Figure V.I : An abrupt-symmetrical Stenosis

The Poiseuille Equation [Equation 1.5] may be used to predict a DC pressure drop across the stenosis, if the flow rate is known. This is the viscous Pressure Drop, which depends on both the severity of the stenosis and the length of the stenosis. Because the resistance of the stenotic segment is inversely proportional to the 4th power of the patent radius, and directly proportional to the length, the radius of the stenosis is considered to be more significant than it's length. Furthermore the pressure drop increases as blood flow increases. Exercise for example, results in increased blood flow to skeletal muscle. If a stenosis is present, the increased blood flow as a result of exercise, would also result in a greater pressure loss across the stenosis.

$$\Delta P_{VISCOUS} = Q.\frac{8.\mu.L}{\pi.r_s^4} \qquad \text{[Equation A5.1]}$$

Where :
- Q = blood flow
- μ = blood viscosity
- r_s = radius of the stenotic segment
- L = length of stenotic region

However the Poiseuille equation is not the only predictor of pressure drop across the stenosis. There are inertial losses at both the entrance and the exit of the stenotic region. These losses depend on the shape of the entrance and exit, being lesser when there is a gradual area change compared to an abrupt (eg. Figure V.I) area change. Furthermore, there are greater losses if the stenosis is asymmetrical, compared to a symmetrical (eg. Figure V.I) stenosis .

Energy losses are usually greater at the exit of a stenosis [Sumner DS in : Vascular Surgery 3rd Ed, Rutherford RB (Ed.), 1989].

The pressure loss as a result of energy "losses" at the exit of the stenosis may be represented by :

$$\Delta P_{INERTIAL\ EXIT} = k\frac{\rho}{2}.v^2.\left[\left(\frac{r}{r_s}\right)^2 - 1\right]^2 \qquad \text{[Equation A5.2]}$$

[Sumner DS in : Vascular Surgery 3rd Ed, Rutherford RB (Ed.), 1989]

Where :
- v = velocity of the blood in the vessel downstream to the stenosis
- r_s = radius of the stenotic segment
- r = radius of the segment downstream to the stenosis
- k = constant. 1.0 for an abrupt stenosis; <0.2 for a 6 degree angle.
- P = blood density

3. Non-symmetrical stenosis :

Clinical stenoses are rarely symmetrical. An asymmetrical stenosis results in greater inertial losses than a symmetrical stenosis.

4. The Inverse Model and Critical Stenosis :

The definition of critical stenosis is : *the stenosis level beyond which a small reduction in the arterial lumen would cause drastic reductions in flow and pressure*

This definition is based only on variations in flow and pressure waveforms. However , the corresponding anatomical and physiological criteria for defining critical stenosis is the subject of much debate. The reason for this is simple : the arterial parameters of an actual clinical subject cannot be adjusted to determine the individual degree and geometry of stenosis that would mark the point beyond which any increase in stenosis would result in drastic reductions in flow and pressure. Furthermore, there may exist different combinations of blood flow (e.g. at rest or at exercise); and degree , length, and geometry of stenosis that would determine critical stenosis for a particular individual.

As a starting point for investigation of the Inverse Model, the level of critical stenosis was elected to be a 50% diameter stenosis. Arteries were modeled as uniform tubes with symmetrical stenoses. Therefore this degree of stenosis also corresponded to a 75% area stenosis.

For computer simulated tests (Chapter 10), inspection of the changes in the flow and pressure waveforms were sufficient to reasonably elect a 50% diameter reduction as corresponding to critical stenosis.

For clinical subjects however, the issue of stenosis geometry, degree, length, and blood flow rate becomes much more important. The choice of a 50% diameter reduction as a predefined critical stenosis may be criticized under such circumstances. It is however important to note that this 50% level was used as a first approximation starting point. The approach of simplifying assumptions is a legitimate scientific approach when initially tackling a very complex problem using a completely new technique such as the Inverse Model. This approach enables different theoretical and practical problems to be prioritized and researched further, and allows for successive improvements in a model.

The issue of the manner in which a complex stenosis geometry may be represented in a mathematically invertable transmission model is not easily resolved. However with regard to critical stenosis, the Inverse Model provides a very elegant solution by virtue of its inversion process.

The pressure and flow waveforms at a single point, serve as inputs to the Inverse Model. The frequency domain ratio of pressure and flow characterizes the distal circulation in the form of an electrical impedance spectrum. The Inverse model attempts to fit predicted waveforms to clinically measured waveforms by variation of the arterial radius in the sample region, and by determining the closest fit between predicted and measured waveforms.

Therefore the Inverse Model is actually able to also detect the level of critical stenosis. This is because the Inversion process varies the radius, and the pressure and flow waveforms are therefore available at every discrete radius (that the model has been designed to step through) . Hence the level of simulated stenosis which marks the point beyond which further stenosis results in marked reductions in pressure and flow is available to the Inverse Model.

By its very definition, critical stenosis is characterized by noticeable reductions in flow and pressure waveforms. Therefore any waveform fit in the region beyond critical stenosis would be for a very specific discrete radius. In terms of the Error Graph (Figure 9.4) a radius match at a level beyond critical stenosis would be indicated by a sharp distinct minimum (see Figures 14.14; 14.17), and a match at a "normal" radius would be indicated by a flat minimum region (see Figures 14.3; 14.4; 14.11).

Therefore the shape of the minimum error function may serve as a very useful indicator of critical stenosis. This feature is compatible with the results in Chapter 14.

5. Pressure Upstream and Downstream to a symmetrical stenosis :

The External Iliac artery (Segment 92, in Figure 2.3 and 4.3) of the Forward Arterial Model was progressively stenosed, and the corresponding upstream and downstream pressures were plotted. This was carried out under conditions of 100% radial patency – 20% radial patency, in steps of 20%.

The comparative pressures are plotted in Figures V.II – V.VI .

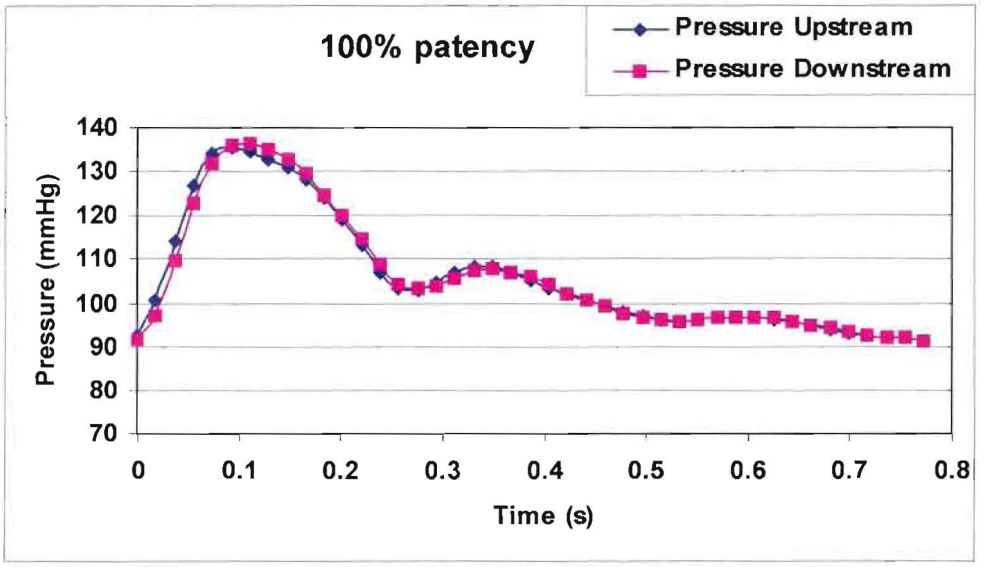

Figure V.II : Computer simulated synchronous Pressure waveforms upstream and downstream from a 100% (radial) patent External Iliac artery.

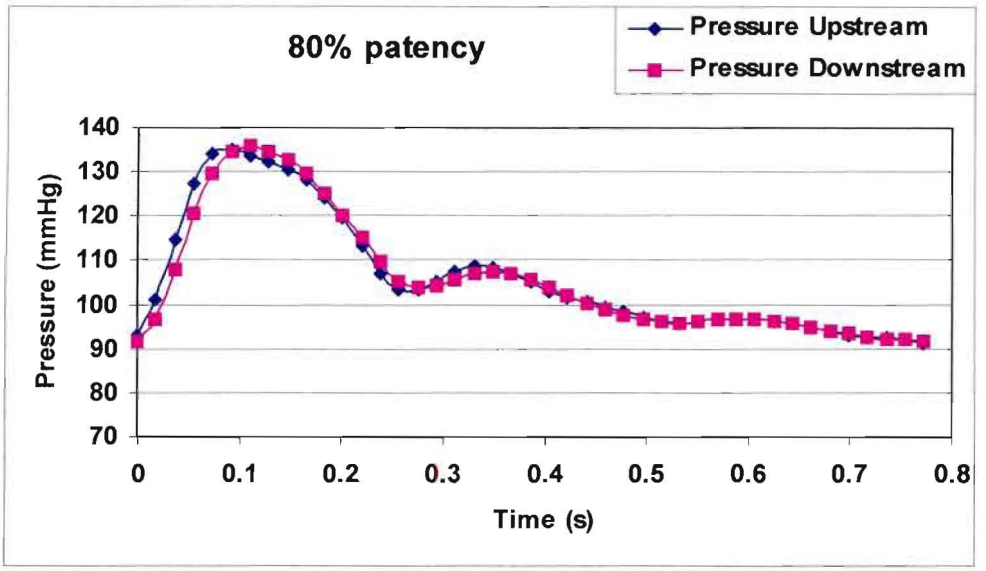

Figure V.III : Computer simulated synchronous Pressure waveforms upstream and downstream from a 80% (radial) patent External Iliac artery.

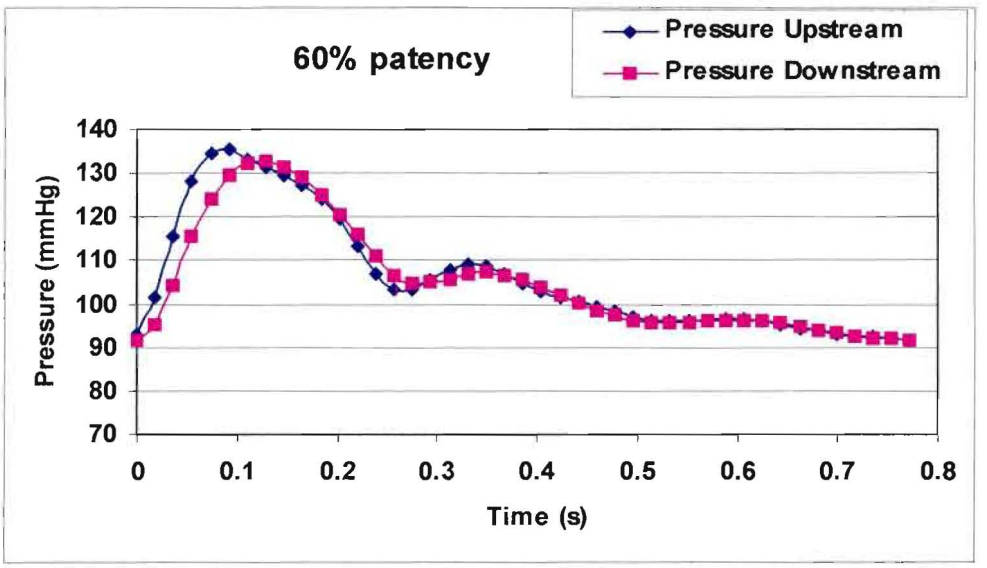

Figure V.IV : Computer simulated synchronous Pressure waveforms upstream and downstream from a 60% (radial) patent External Iliac artery.

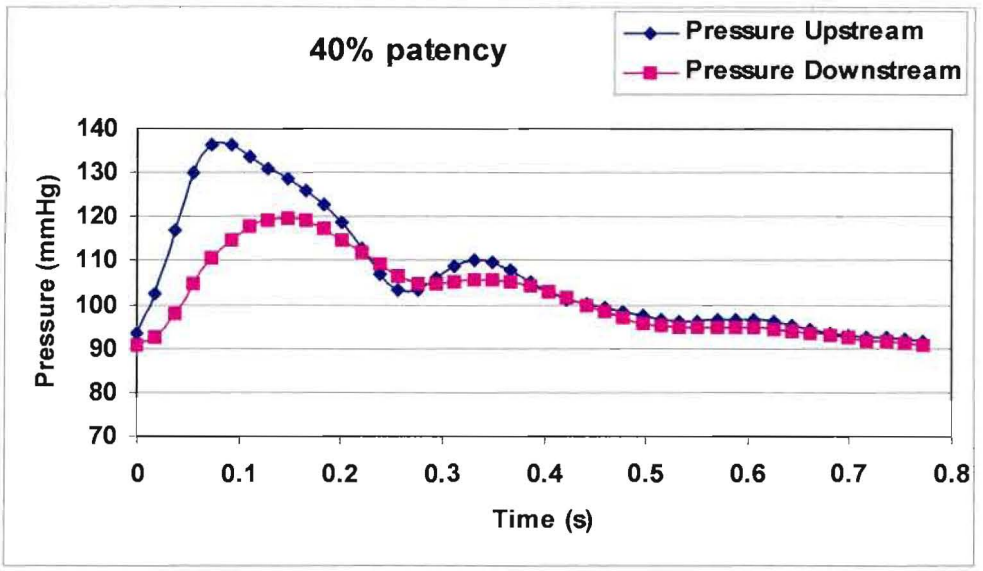

Figure V.V : Computer simulated synchronous Pressure waveforms upstream and downstream from a 40% (radial) patent External Iliac artery.

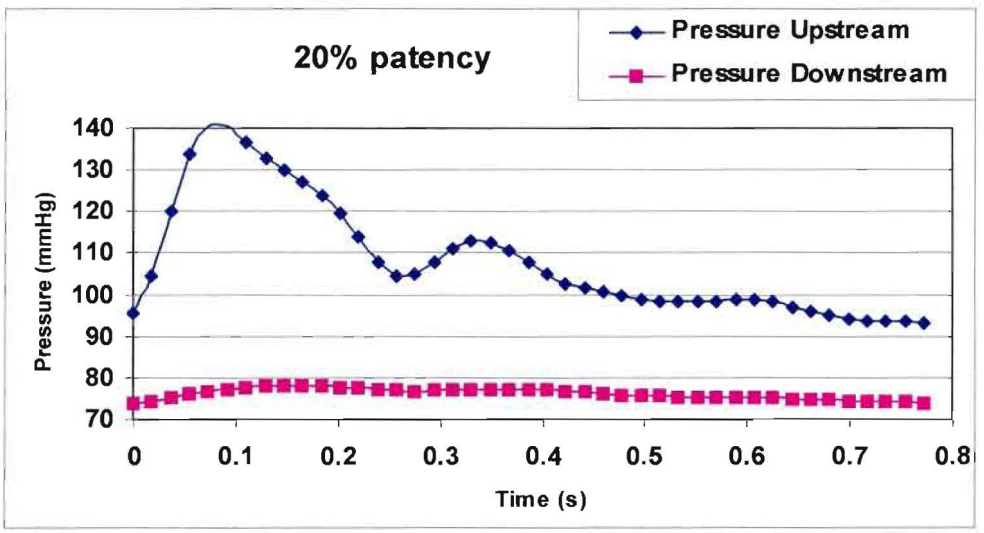

Figure V.VI : Computer simulated synchronous Pressure waveforms upstream and downstream from a 20% (radial) patent External Iliac artery.

APPENDIX VI
USING THE WOMERSLEY EQUATIONS TO MODEL RESISTANCE AND INDUCTANCE

1. Womersley's Equations :

In the electrical analogue of an arterial segment presented in Chapter 1, Resistance and Inductance (both per unit length) were assumed to be frequency independent. Nichols and O'Rourke [1990] cited the equations of Womersley (1955, 1957) which quantified the variation of both Resistance and Inductance (per unit length) with frequency. Note that this is not the same as Reactance.

Womersley's equations used Bessel functions to describe this frequency variation :

$$R = \frac{\omega.\rho}{\mu.R_0^{\,2}.M'_{10}}.\sin(\varepsilon'_{10}) \qquad \text{[Equation A6.1]}$$

$$L = \frac{\rho}{\mu.R_0^{\,2}.M'_{10}}.\cos(\varepsilon'_{10}) \qquad \text{[Equation A6.2]}$$

Where :

R = Resistance per unit length
L = Inductance per unit length
ω = angular frequency
ρ = blood density
μ = blood viscosity
R_0 = radius
M'_{10} = modulus of the Bessel Function of the first kind, and order = 0
ε'_{10} = phase angle of the Bessel function of the first kind, and order = 0

Note that for both Bessel Functions, the input parameter was α, where :

$$\alpha = \sqrt{\frac{R_0^2.\omega.\rho}{\mu}} \qquad \text{[Equation A6.3]}$$

More details on the use of Bessel Functions in the arterial analog context may be found in Nichols and O'Rourke [1990, Chapter 11, pp 286-287] and Milnor [1989, Appendix C, pp 398-400].

2. Frequency-Independent vs Frequency-Dependent Resistance & Inductance :

The frequency-independent equations for Resistance and Inductance [Equations 1.5-1.6] which were presented in Chapter 1 were used throughout the body of this thesis.

Whilst these frequency-independent equations allowed for faster computation times, the qualitative extent of the error introduced by the assumption frequency independent resistance and inductance, was investigated by comparing flow and pressure waveforms generated by the linear (frequency-independent) to the nonlinear (Womersley frequency-independent) equations.

This comparison was carried out at the External Iliac artery, which corresponds to Segment 92 of the arterial system model presented in Table 2.3 and Figure 2.3. The corresponding Flow and Pressure waveforms at 5 different degrees of radial patency are illustrated below :

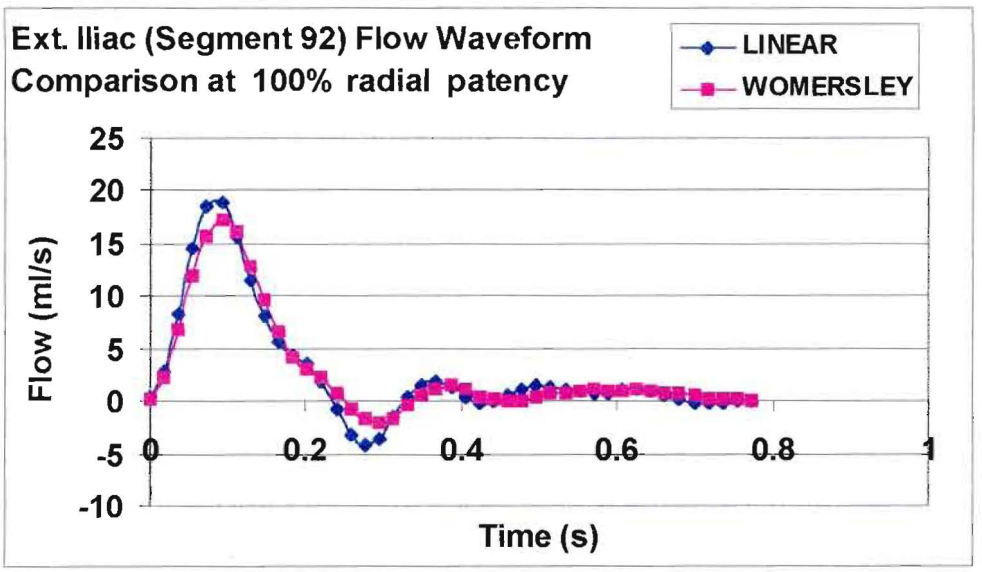

FIGURE A6.1 : Comparison between External Iliac flow waveforms produced by the Forward Model using linear Resistance and Inductance equations, to those produced by using the nonlinear Womersley equations, at 100% radial patency.

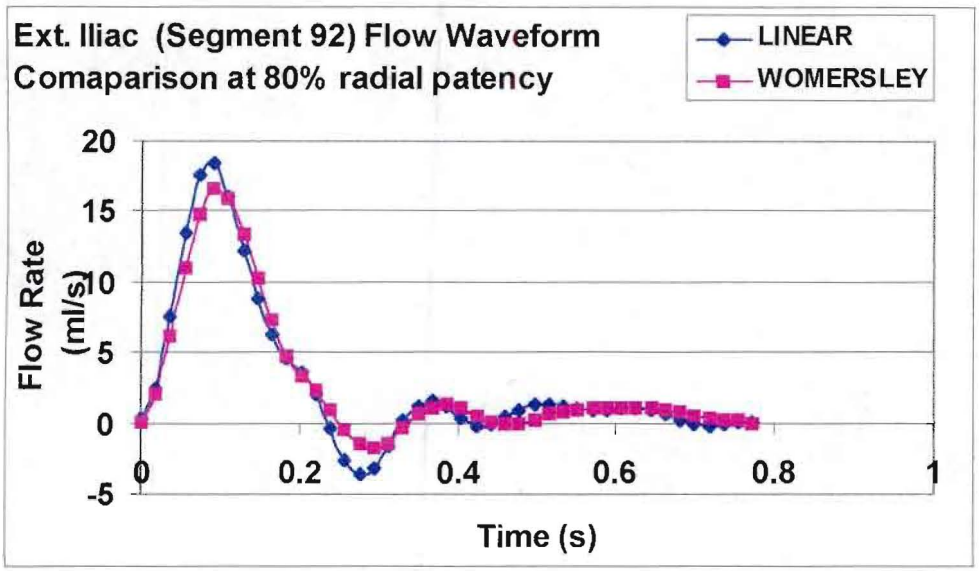

FIGURE A6.2 : Comparison between External Iliac flow waveforms produced by the Forward Model using linear Resistance and Inductance equations, to those produced by using the nonlinear Womersley equations, at 80% radial patency.

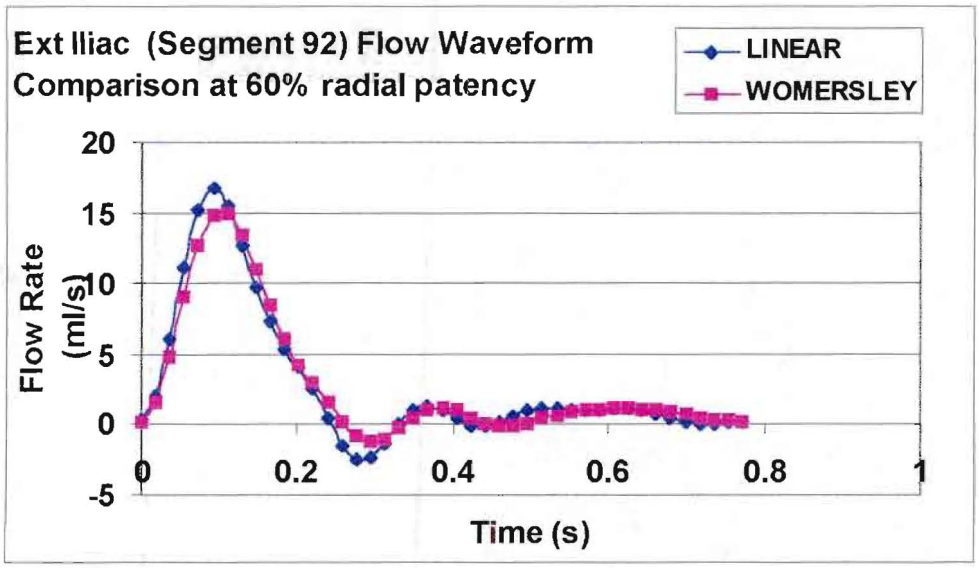

FIGURE A6.3 : Comparison between External Iliac flow waveforms produced by the Forward Model using linear Resistance and Inductance equations, to those produced by using the nonlinear Womersley equations, at 60% radial patency.

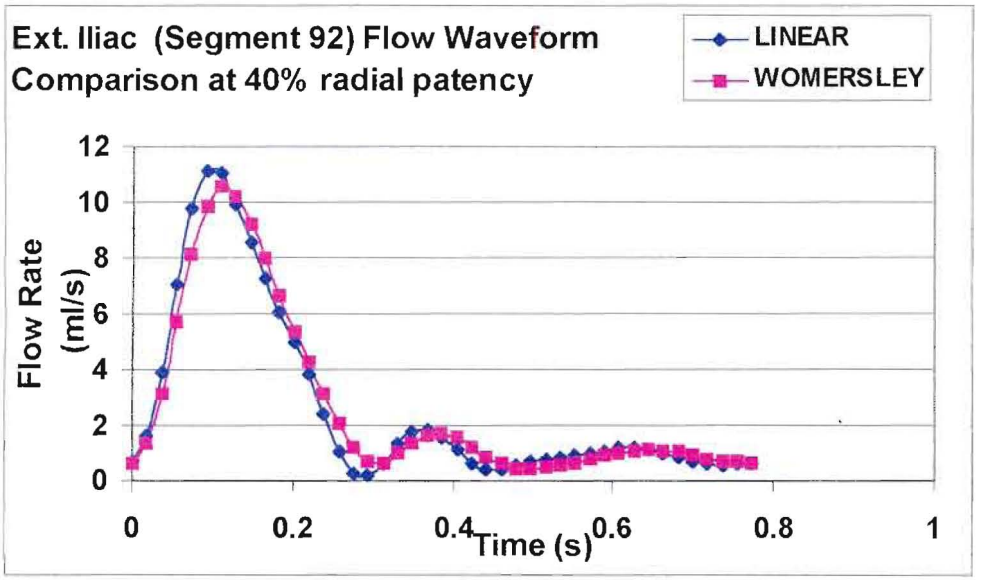

FIGURE A6.4 : Comparison between External Iliac flow waveforms produced by the Forward Model using linear Resistance and Inductance equations, to those produced by using the nonlinear Womersley equations, at 40% radial patency.

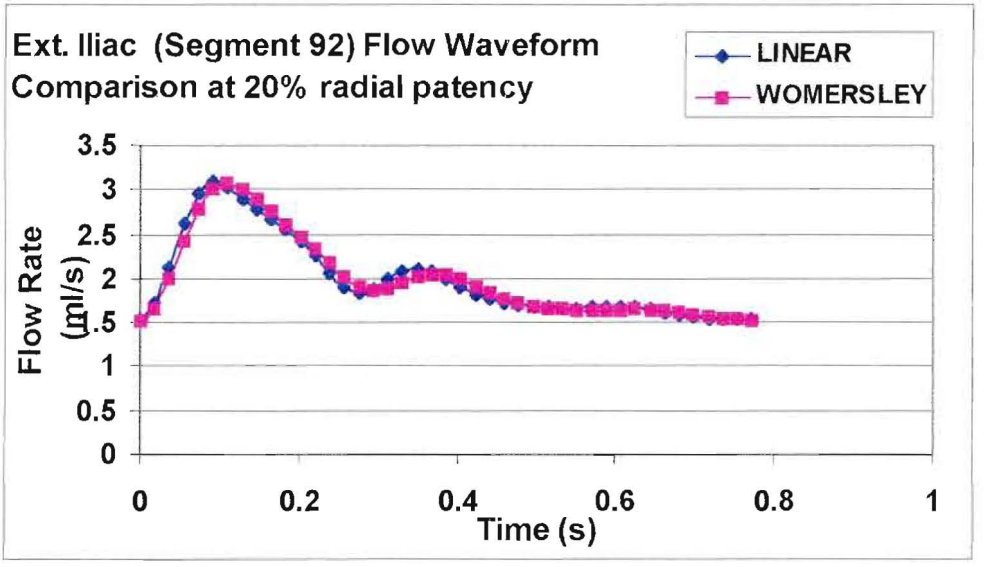

FIGURE A6.5 : Comparison between External Iliac flow waveforms produced by the Forward Model using linear Resistance and Inductance equations, to those produced by using the nonlinear Womersley equations, at 20% radial patency.

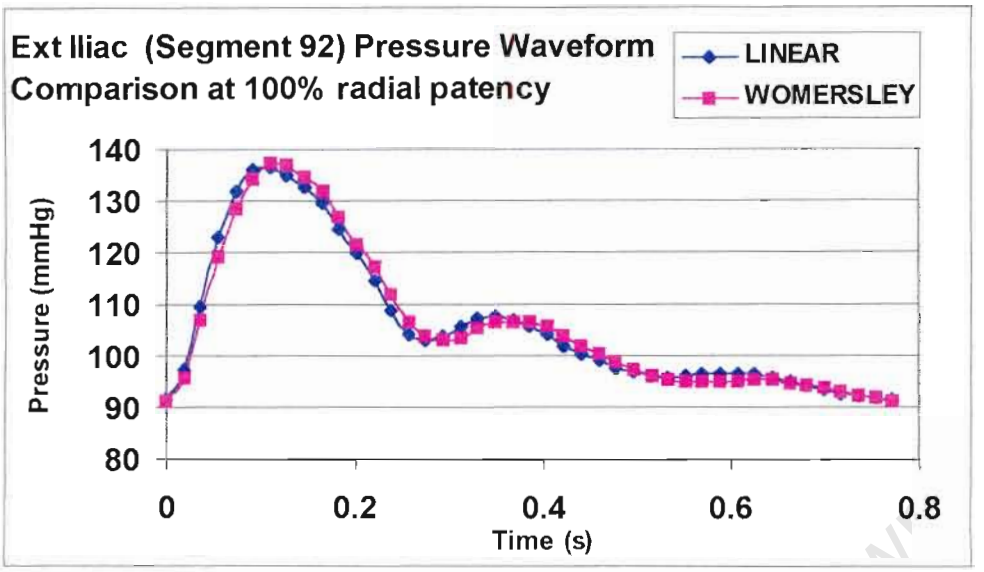

FIGURE A6.6 : Comparison between External Iliac pressure waveforms produced by the Forward Model using linear Resistance and Inductance equations, to those produced by using the nonlinear Womersley equations, at 100% radial patency.

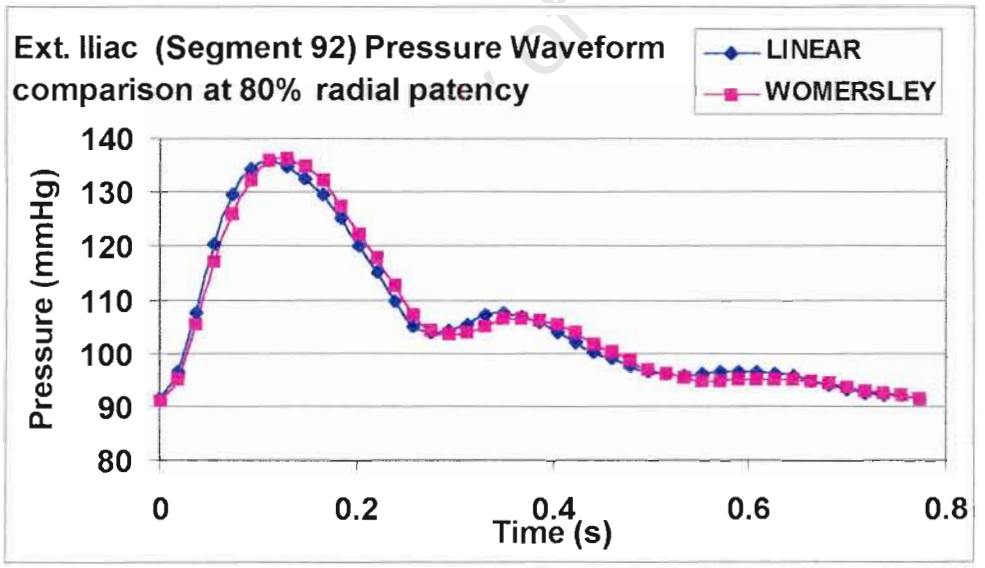

FIGURE A6.7 : Comparison between External Iliac pressure waveforms produced by the Forward Model using linear Resistance and Inductance equations, to those produced by using the nonlinear Womersley equations, at 80% radial patency.

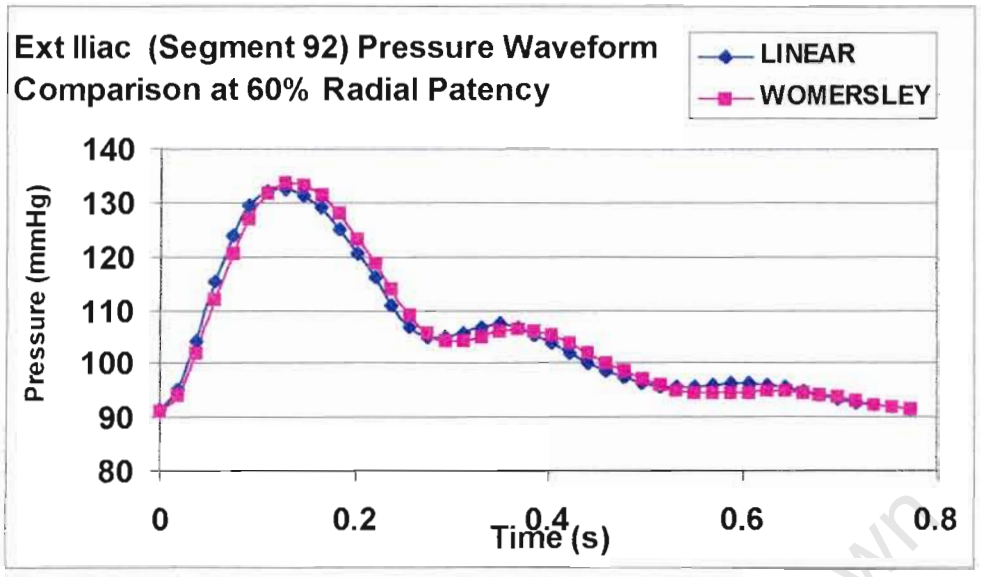

FIGURE A6.8 : Comparison between External Iliac pressure waveforms produced by the Forward Model using linear Resistance and Inductance equations, to those produced by using the nonlinear Womersley equations, at 60% radial patency.

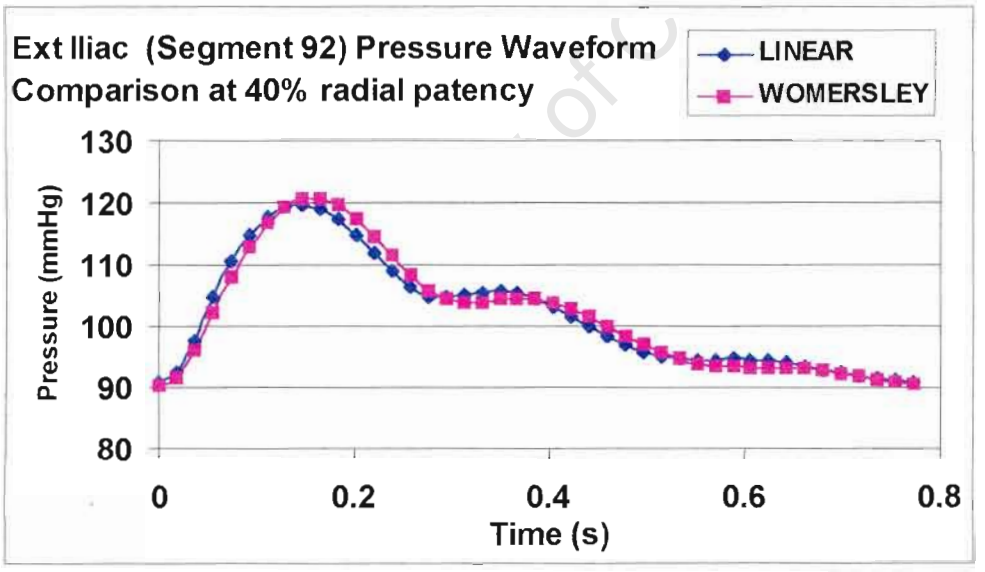

FIGURE A6.9 : Comparison between External Iliac pressure waveforms produced by the Forward Model using linear Resistance and Inductance equations, to those produced by using the nonlinear Womersley equations, at 40% radial patency.

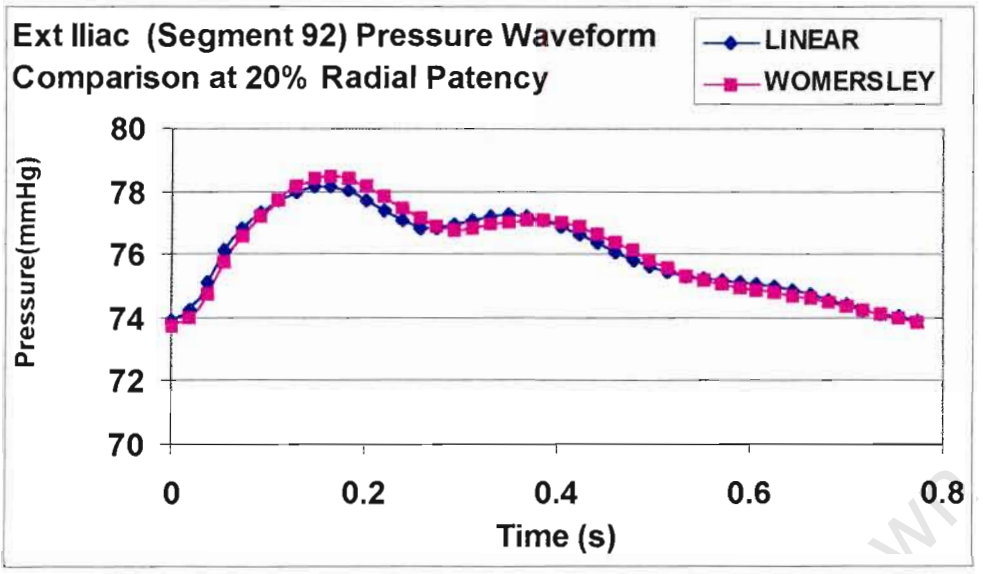

FIGURE A6.10 : Comparison between External Iliac waveforms produced by the Forward Model using linear Resistance and Inductance equations, to those produced by using the nonlinear Womersley equations, at 20% radial patency.

APPENDIX VII
FURTHER STUDIES OF THE FEMORAL DISTAL IMPEDANCE

A Computer-simulated study of the normalized absolute distal impedance spectrum was discussed in Chapter 15. That study attempted to investigate whether the extent and location of distal arterial disease could be quantified through inspection of the normalized absolute distal impedance spectrum.

The computer simulated study was then used as reference to investigate the clinically measured distal impedance spectrum. Clinical distal impedance was calculated as the frequency domain ratio of pressure and flow.

Chapter 11.4 discussed the use of amplitude scaling factors that were applied to both the clinically measured flow velocity and pressure waveforms. This scaling procedure introduced a possible amplitude error in both waveforms, and hence also in the calculated clinical distal impedance spectrum. For this reason, only the *normalized* impedance spectrum was analyzed in Chapter 15 (i.e. to reduce amplitude bias).

A pseudo-synchronous (Chapter 11.2) approach was also used for the clinical measurement of the Tonometric pressure and Doppler flow velocity waveforms. This approach introduced a possible phase error into the corresponding impedance spectrum. For this reason only the *absolute* distal impedance spectrum was analyzed in Chapter 15 (i.e. to reduce phase bias).

With the use of either invasive pressure and flow measurements, or with the future development of quantitatively accurate non-invasive pressure and flow measuring equipment, it would be possible to have an accurate representation of the distal impedance spectrum in both amplitude and phase.

For this reason, two computer simulated scenarios that were presented in Chapter 15 are illustrated in further detail here. These scenarios examined the effect of progressive stenosis in the External Iliac (Arterial Segment 99) and the Common Femoral (Arterial Segment 107) arteries , on the complex distal impedance spectrum measured at the level of the inguinal ligament.

Progressive stenosis was categorized in terms of percentage radial stenosis (0% - 80% radial stenosis in steps of 10%). Arterial impedance was in units of dynes.s.cm^{-3} and the Impedance angle was in radians.

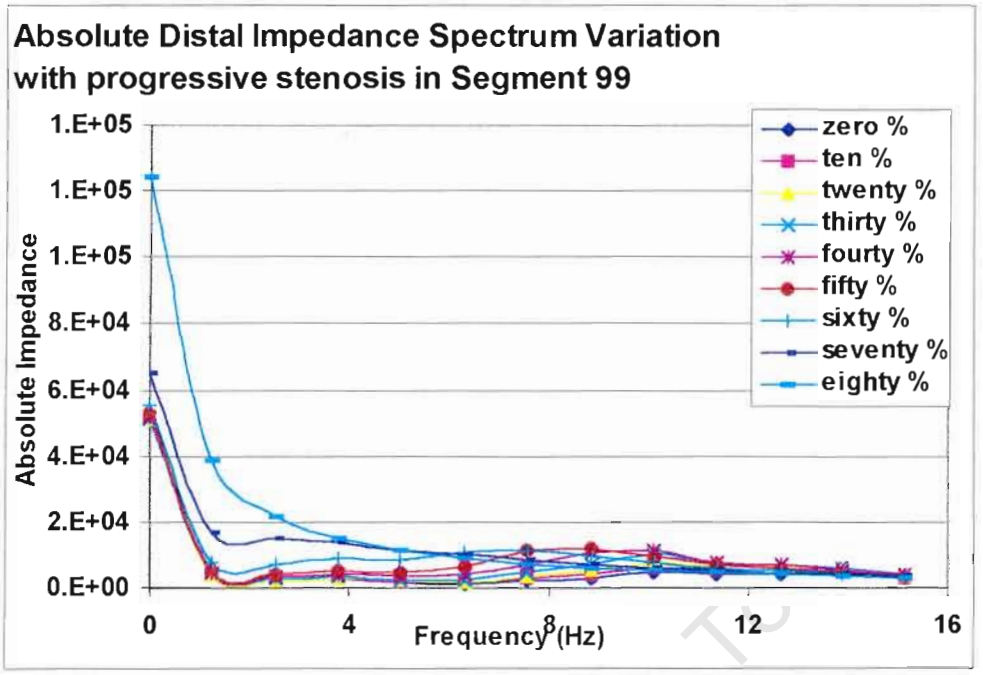

FIGURE A7.1 : Absolute Distal Impedance Spectrum (measured at the External Iliac, Segment 92) variation with stenosis in the Common Femoral (Segment 99). Segment numbering corresponds to Table 2.3 and Figure 2.3. Degrees of radial stenosis are indicated in the legend

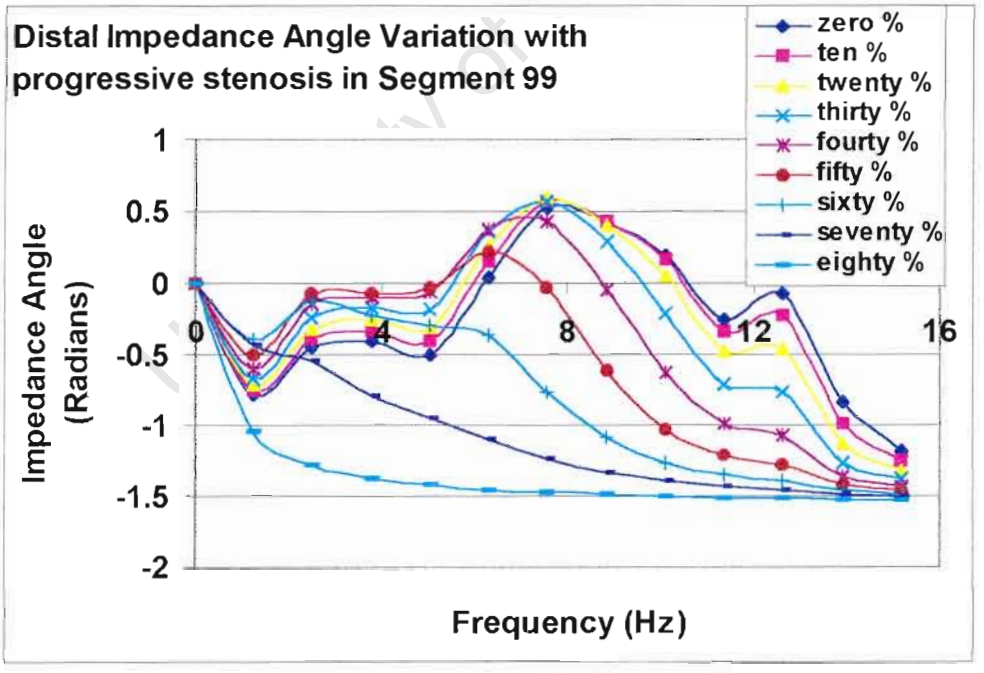

FIGURE A7.2 : Distal Impedance Spectrum Angle (measured at the External Iliac Artery, Segment 92) variation with stenosis in the Common Femoral (Segment 99). Segment numbering corresponds to Table 2.3 and Figure 2.3. Degrees of radial stenosis are indicated in the legend.

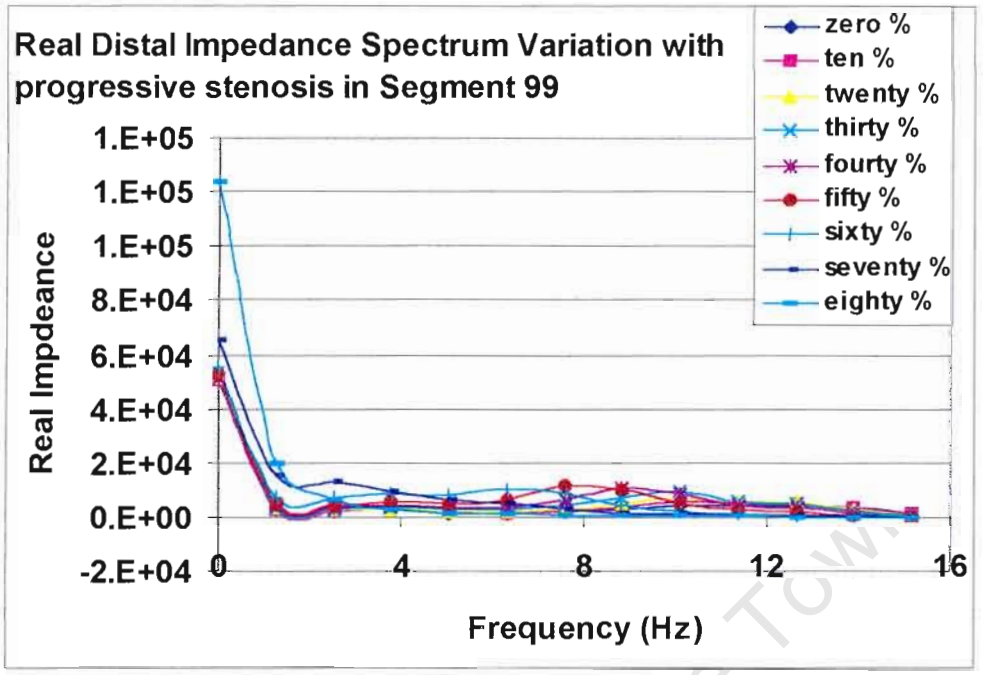

FIGURE A7.3 : Real Distal Impedance Spectrum (measured at the External Iliac Artery, Segment 92) variation with stenosis in the Common Femoral (Segment 99). Segment numbering corresponds to Table 2.3 and Figure 2.3. Degrees of radial stenosis are indicated in the legend.

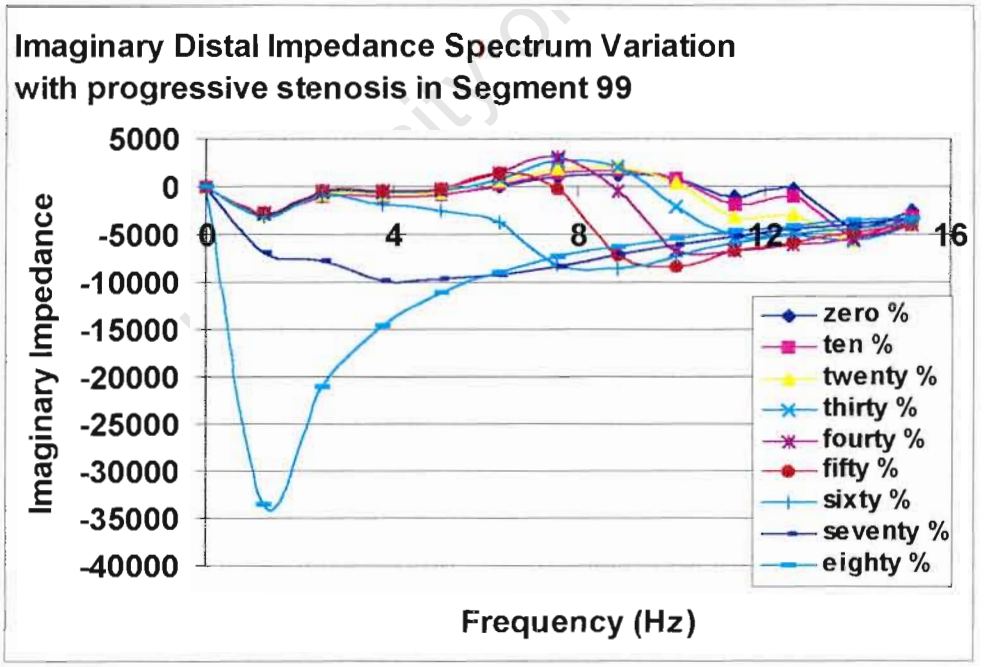

FIGURE A7.4 : Imaginary Distal Impedance Spectrum (measured at the External Iliac Artery, Segment 92) variation with stenosis in the Common Femoral (Segment 99). Segment numbering corresponds to Table 2.3 and Figure 2.3. Degrees of radial stenosis are indicated in the legend.

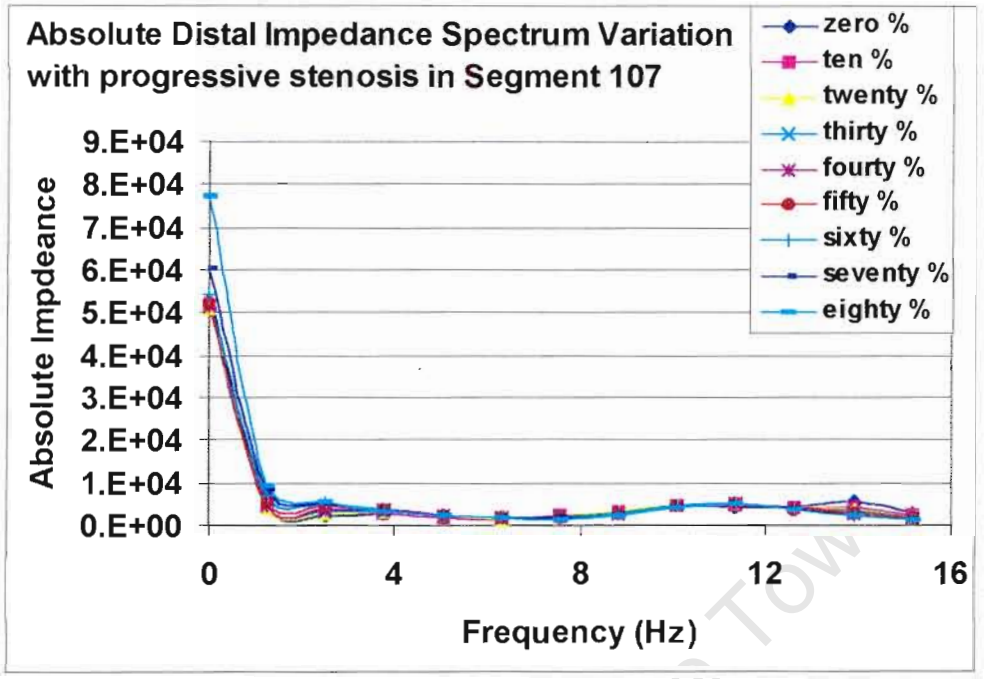

FIGURE A7.5 : Absolute Distal Impedance Spectrum (measured at the External Iliac, Segment 92) variation with stenosis in the Superficial Femoral (Segment 107). Segment numbering corresponds to Table 2.3 and Figure 2.3. Degrees of radial stenosis are indicated in the legend

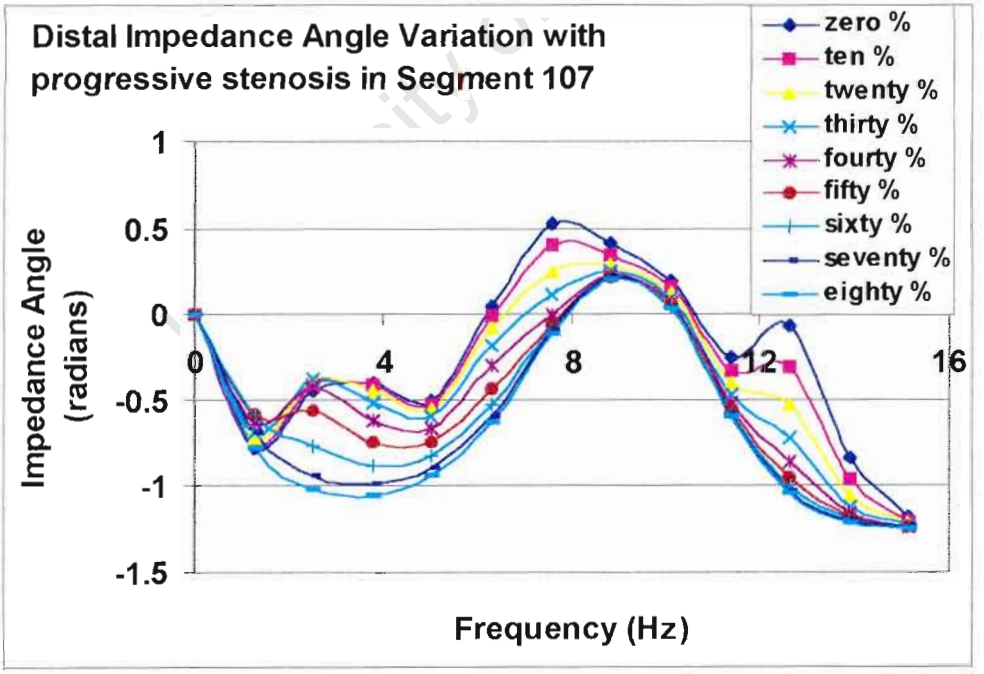

FIGURE A7.6 : Distal Impedance Spectrum Angle (measured at the External Iliac, Segment 92) variation with stenosis in the Superficial Femoral (Segment 107). Segment numbering corresponds to Table 2.3 and Figure 2.3. Degrees of radial stenosis are indicated in the legend

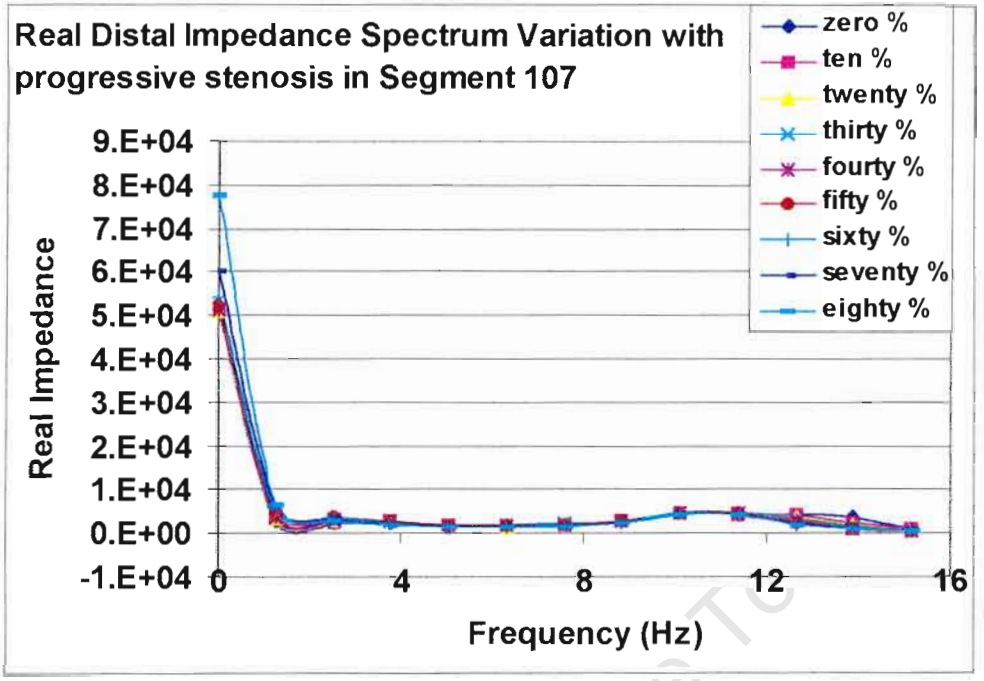

FIGURE A7.7 : Real Distal Impedance Spectrum (measured at the External Iliac, Segment 92) variation with stenosis in the Superficial Femoral (Segment 107). Segment numbering corresponds to Table 2.3 and Figure 2.3. Degrees of radial stenosis are indicated in the legend

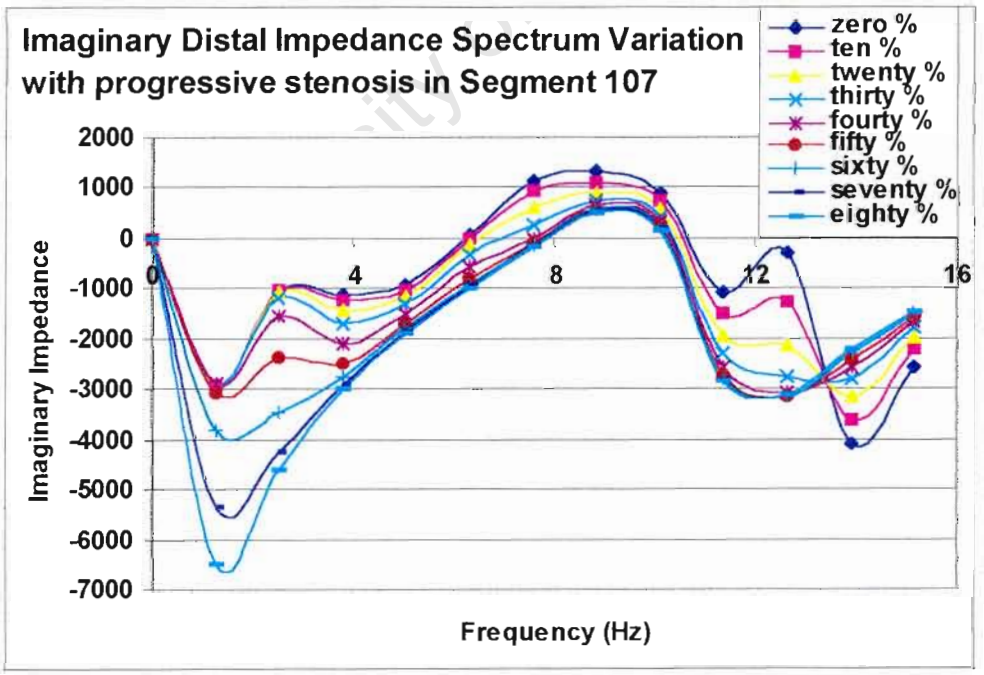

FIGURE A7.8 : Imaginary Distal Impedance Spectrum (measured at the External Iliac, Segment 92) variation with stenosis in the Superficial Femoral (Segment 107). Segment numbering corresponds to Table 2.3 and Figure 2.3. Degrees of radial stenosis are indicated in the legend

APPENDIX VIII
ADDITIONAL FACTORS AFFECTING PULSE ARRIVAL TIME ESTIMATION

1. Methods of measuring Arterial Pulse Arrival Time :

Pulse Arrival (or Delay Time) is the time taken for an arterial pulse to travel from one point to another. There are generally 3 physiological waveforms that may be used in the measurement of the arterial pulse delay time.

1.1 QRS complex of a single lead Electrocardiogram
1.2 Doppler Blood Velocity waveform
1.3 Blood Pressure Waveform

The pulse arrival time between two sites may be measured by comparing the time delay between specific features of flow velocity or pressure pulses, measured synchronously at both sites. The choice of a specific feature (eg. peak , or start of upstroke etc.) to be used for this measurement, may result in different calculated delays compared to those measured if a different waveform feature was used. Waveform harmonics may travel at different speeds (hence relative phases would alter) and be subject to different attenuation as they travel from site-a to site-b. A sharply defined feature often requires a high bandwidth (eg. upstroke of the Doppler Blood Velocity waveform) to be accurately measured.

If the time delay is measured by using either synchronous flow velocity or synchronous pressure waveforms, then the cardiac electro-mechanical would have no effect on the time measurement.

2. The Cardiac Electro-Mechanical Delay :

The cardiac electro-mechanical delay may be defined as the time from the beginning of the ECG QRS complex to the onset of the blood flow waveform in the aorta.

If the ECG QRS complex is used to determine the starting point for pulse delay time measurement, with the endpoint being determined by either the flow velocity or the blood pressure waveform measurement, then the cardiac electro-mechanical delay time must be subtracted from the measured delay time to determine the "true" delay time.

The cardiac electro-mechanical delay has also been referred to in the literature as the pre-ejection period or PEP [Bernstein A, 1976].

3. **Estimation of the Cardiac Electro-Mechanical Delay**

Pulse arrival (or delay) time was measured in 63 normal children from 7 months – 18 years old, by Bercu B. et al , 1979. Pre-ejection period was calculated using a formula that included subject age and heart rate :

$$PEP = 65 + 3.6A - 0.32\,P \qquad \text{[Equation A8.1]}$$

Where : PEP = pre-ejection period in ms
A = subject age in years
P = subject heart rate in beats per minute .

Another study of 27 normal subjects (mean age = 21.5 years, SD = 3.0) by Hasagawa M et al, 1991 showed a mean PEP = 86 ms (SD = 12).

If Pulse Arrival Time (P.A.T.) is to be measured clinically (using an ECG as a reference), then adjustment using PEP would improve the accuracy of the Pulse Arrival Time measurement, and hence also the accuracy of subsequent estimates of Pulse Wave Velocity.

$$PAT_{true} = PAT_{measured\ ECG\text{-}DOPPLER} - PEP \qquad \text{[Equation A8.2]}$$

3. **Effect of Age and Height on Arterial Length**

Arterial length is directly proportional to height, and in most arteries also directly proportional to age. These variables necessarily influence the estimation of arterial length, and have already been discussed in Chapter 6

4. **Electronic Equipment Time Delays**

Waveforms are measured using electronic equipment. For research studies this may consist of commercially available medical equipment (e.g. Doppler Ultrasound) interfaced to a Data Acquisition System with a finite time resolution. The finite time resolution obviously relates directly to the accuracy of any time measurement e.g. the prototype haemodynamic acquisition system described in Chapter 11 had a finite time resolution for QRS and Blood Pressure channels of 18ms. Higher accuracy measurements would require the use of higher performance data acquisition system. Furthermore the use of different front-end equipment interfaced via a common data acquisition card may result in small phase shifts between signals. Quantification of these phase delays may be used to improve the accuracy of relative time measurements.

APPENDIX IX
DOPPLER FLOW VELOCITY MEASUREMENT ERRORS

This appendix contains a short review of some error sources in Doppler Flow Velocity measurement. The minimization of Data Acquisition errors is an important consideration before a Pilot Clinical Study may be carried out. Such a study and also the development of custom haemodynamic data acquisition equipment is one of the recommendations of this thesis .

1. Doppler Angle :

The angle between the insonated vessel and the Ultrasound beam is referred to as the Doppler angle. The Doppler angle affects the amplitude of the measured flow velocity according to the Doppler equation :

$$F_D = 2.F_0.(v. \cos \Theta) / c \qquad \text{[Equation A11.1]}$$

Where :

F_D = Doppler shift frequency
F_0 = Doppler insonation frequency
V = velocity of moving particles
Θ = Doppler angle
c = speed of sound in the propagating medium (e.g. blood)

This angle must be constant for the duration of a measurement, and is usually between 45° - 60°. Movement of the patient, operator, or the blood vessel under consideration would introduce a Doppler angle error. Therefore it is important for both the operator and the patient not to move for the duration of a measurement.

In stenotic arteries, the presence of 3 dimensional haemodynamic jets (which may result only in the change of the flow angle and not in the flow magnitude), would be incorrectly depicted as a change in velocity magnitude. This is also true if measurements are taken from tortuous arteries [Beach KW and Phillips DJ in : Diagnostic Vascular Ultrasound, Labs K.H. et al (Editors), 1992].

Duplex Doppler systems allow visualization of the vessel and measurement of the Doppler Angle, and thus may be effective in minimizing the uncertainty in Doppler angle.

2. Vessel Insonation:

Partial insonation of a blood vessel would result in both shape and amplitude distortion of the Doppler signal. Therefore the diameter of the ultrasound transducer should be at least as large as the largest possible diameter of the vessel being investigated.

Proper transducer positioning to effect complete vessel insonation depends on operator skill in Continuous Wave Doppler systems. Duplex Doppler systems however, allow the vessel to be visualized and a sample volume to be specified, thus allowing for the minimization of vessel insonation error.

3. Doppler Frequency :

An ultrasound beam has a far-field and a near-field. In the near-field the beam has a cylindrical shape, and in the far-field the beam diverges. A higher frequency would provide a longer near-field. The length of the near field may be determined by :

$$D_{nf} = D^2/4.\lambda \qquad \text{[Equation A11.1]}$$

Where :

D_{nf} = near field distance
D = transducer diameter
λ = ultrasound wavelength

Ultrasonic power in a beam decays because of tissue absorption. This absorption is approximately proportional to frequency. Back scattering of power from moving red blood cells is proportional to frequency^4. Therefore a higher frequency would result in greater tissue absorption losses, but also better back scattering of power [Webster JG : Medical Instrumentation, Application and Design, 3rd Edition, 1998].

Clinically a compromise choice of Doppler frequency usually ranges between 5 MHz – 10 MHz for superficial blood vessels. For the preliminary Clinical feasibility study presented in Chapters 11- 15, a 5 MHz probe was used for subjects with deeper arteries (e.g. obese subjects), and a 10Mhz probe was used for subjects with more superficial arteries.

4. Vessel Compression :

Compression of the blood vessel during examination would distort the shape of the blood vessel and possibly also influence the flow profile. Use of a sufficient coupling gel, together with an understanding of the effect of vessel compression on the Doppler waveform is therefore important.

5. Aliasing :

Aliasing of the Doppler signal is an important consideration in pulsed Doppler systems. However, it is not a consideration of Continuous Wave Doppler systems, such as the system that was described in Chapter 11.

6. Averaged Doppler Flow Waveform :

Doppler waveforms from all Clinical subjects in the preliminary feasibility study were calculated as the mean of the Color Doppler spectrum (see Figure 11.2) . Further serial waveforms were then averaged to form a single average waveform. The number of serially averaged waveforms depended on subject heart rate, given that the window period for Doppler Waveform capture was 3 seconds (Figure 11.2).

It is important to note that that a series waveform was only captured under conditions of a stable repetitive Doppler spectrum. This indicated minimal movement on either the part of the operator or the subject and a stable heart rate. The averaged waveform in such a case would therefore not suffer bias from extreme values. Stability of subject heart rate and minimal operator and subject movement is important for an accurate average waveform to be constructed.

It may be necessary in future to create a longer visible window period (i.e. greater than 3 seconds) for the recording of sequential Doppler waveforms. However, a compromise must be reached on the length of that window. A long window period may appear to be able to provide a better average waveform, but it would also increase the possibility of operator or subject movement , as well as increase the chances of capturing subtle changes in the cardiovascular system (e.g. heart rate variation)

7. AR Spectral Analysis :

Further details on the Haemodynamic Data Acquisition system are available in the MSc Thesis of Smith L., 1993 and an unpublished document by Mehnert S., 1994 [both of the : Department of Biomedical Engineering, University of Cape Town, South Africa].

The Doppler Ultrasound aspect of the Data Acquisition system was based on two published works by Schlindwein FS and Evans DH [1989, 1990]. Spectral estimation was carried out using a 10^{th} order Auto-Regressive Model. The spectrogram implemented by the Data Acquisition System described in Chapter 11, captured a frequency spectrum every 18.5ms.

APPENDIX X
TECHNICAL DATA ON THE MILLAR ARTERIAL TONOMETER

The Haemodynamic Data Acquisition System (Chapter 11) used a Millar Arterial Tonometer (Model SPT-301, frequency response flat to 10kHz) interfaced via a Transducer Control Unit Module TC-510.

The Control Unit Module is a passive interface between the Tonometer and strain gauge pressure amplifiers. It also includes controls for balancing and calibration.

1. Transducer technical specifications (SPT-301) :

Type of Sensor :	diffused semiconductor
Pressure Range :	0 to +300 mmHg
Overpressure :	+4000 mmHg
Rated Excitation :	2.5-7.5 Vdc or Vac, rms
Sensitivity :	5 μV/V/mmHg nominal
Temperature error band at zero Pressure :	+- 3mmHg, BSL, 23-38^{0}C
Linearity and Hysteresis (combined) :	+- 1.5%, BSL of full scale
Natural Frequency :	35 kHz, nominal
Bridge Resistance :	1000 ohms, nominal
Reference Pressure :	Atmosphere
Electrical Leakage :	less than 10 A at 500 Vdc
Zero Offset :	less than +- 50mmHg
Probe Length :	13cm
Length of Cable :	1.5m

2. Artefact in Tonometric Recordings :

The correct positioning of the tonometer over the artery is the most important criterion for accurate recordings. Recording artefacts may result from transducer movement; excessive hold-down force; and angulation of the transducer with respect to the artery. These artefacts are discussed further by Kelly et al, 1989, who includes some empirical observations indicative of the presence of tonometer artefact.

Use of the tonometer requires some training, and Kelly et al, 1989 concluded that after 4-6 weeks of use of the probes intraobserver variability was 4.5% and interobserver variability was 11.6% (for human radial artery waveforms).

3. Correlation between intra-arterial pressure recordings and non-invasive Millar tonometer pressure recordings :

Kelly et al, 1989, carried out a comparative study of pressure waveforms recorded from a Millar non-invasive tonometer and invasive pressure measurements in the canine femoral artery and human radial artery.

The canine (3 male dogs) invasive readings were acquired using a microtip pressure transducer. The human (62 subjects; 21 females and 41 males; ages 17-79, mean age = 57 years) invasive readings were acquired using a fluid-filled catheter

connected to a Hewlett Packard pressure transducer. This fluid line had an average damped resonant frequency of 21 Hz and a damping coefficient of 0.38.

For the radial artery (i.e. human subjects) the tonometer tended to overestimate the first harmonic by less than 0.6 mmHg ($P<0.2$) and underestimate higher harmonics by less than 0.4 mm Hg. Phase differences between the tonometer and invasive catheter were small and showed no significant difference for harmonics 2-8. Studies in the adult dogs were also consistent with the human findings.

Zorn et al [1997] successfully evaluated a Colin arterial tonometer for compliance to guidelines established by the Association for the Advancement of Medical Instrumentation.

4. Use of the Arterial Tonometer in recent clinical modeling studies :

Besides an increasing number of purely clinical research studies, the arterial tonometer is also being used for the implementation of mathematical models in a clinical setting.

Diourte et al [1999] clinically implemented a nonlinear Forward Arterial Model that used Doppler Echocardiography to record the aortic stroke volume, and an arterial tonometer to record radial artery pulse pressure. That study compared the effects of using a nonlinear pressure-varying compliance model to a constant compliance model. Waveforms generated by both models were compared to tonometric blood pressure waveforms. At the level of the radial artery, the non-linear model, was shown to perform significantly better than the linear model. This study may be relevant to both the Forward and Inverse models (which used a linear compliance / capacitance analogue) introduced in this thesis.

McVeigh et al [1999] solved for the parameters of modified Windkessel-based arterial model that represented a section of artery between the brachial artery and the radial artery. Radial artery waveforms were acquired using a calibrated tonometer and Brachial artery waveforms were acquired intra-arterially. This model belongs to the class of transfer-function models that may be used to characterize an arterial segment provided both upstream and downstream pressure (or flow) waveforms are acquired. It is also important here to note one of the limitations of arterial tonometry i.e. it may only be used to acquire pressure waveform at points where an arterial pulse may be palpated (e.g. radial; femoral; and carotid arteries).

Radial tonometry in conjunction with mean peripheral (i.e. brachial in this case) blood pressure, has also been used to mathematically derive the central blood pressure waveform. Following this approach, a transfer function between central and peripheral blood pressure is first developed, through mathematical modeling and clinical studies. Once that transfer function has been verified, it is then used as a predictive function i.e. the clinically measured peripheral pressure serves as the output of the transfer function, and the input is then mathematically calculated. If this transfer function is an adequate representation of the arterial region between the ascending aorta and the radial artery, then the calculated input would correspond to the aortic pressure waveform. Such an approach may be used to indirectly determine the aortic (root) pressure. Siebenhofer et al [1999] investigated this technique with respect to inter-operator variability. That study concluded that inter-observer reproducibility of tonometric pressure waveforms had an 'excellent'

reproducibility for trained observers. The Transfer Function technique was also implemented by Wilkinson et al [1998] who concluded that the technique was highly reproducible. Sugimachi et al [1997] carried out a small study (8 patients) to derive the aortic-radial artery transfer function using radial tonometric pressure measurements and aortic root pressure.

Arterial tonometry has also been used to compare complex computer simulated geometric representations of the carotid artery to clinical studies. Zhao et al [2000] used MRI angiograms to reconstruct the geometry of the carotid bifurcation on computer. The subsequent computer simulated pressure and flow waveforms were then compared to clinically measured waveforms.

APPENDIX XI
TECHNICAL DATA RELATING TO SEGERS PHYSICAL MODEL

Technical data relating to flow and pressure measurement in the Segers physical arterial model (Chapter 7) is presented here.

1. Pressure measurement :

Pressure was measured using fluid-filled catheters. Segers [1997] compared the frequency response of those fluid catheters to that of a high-fidelity (Sentron) catheter-tip pressure transducer. Both catheters were used to simultaneously measure pressure, and the results of that comparison are presented here :

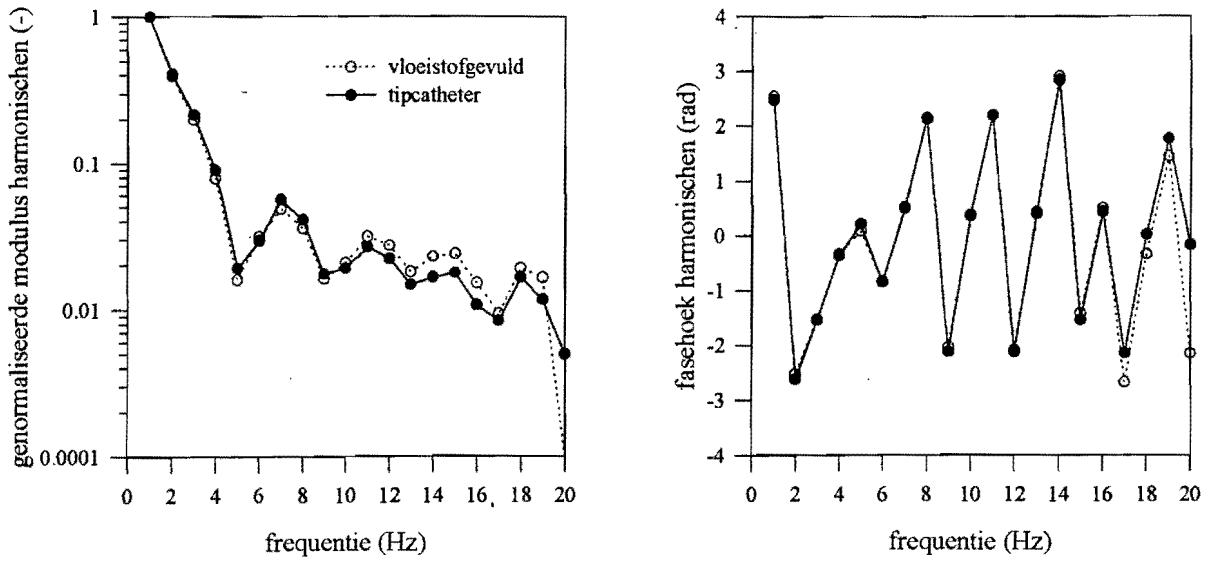

Figure A11.1 Comparison of the frequency content (left: modulus, right: phase) of pressure measured using a catheter-tip transducer (Sentron) to that measured using a fluid-filled catheter. The moduli were normalised with respect to the modulus of the first harmonic. Data provided courtesy of Patrick Segers.

2. Flow measurement :

Flow in the Segers Physical Model was measured using commercially available transonic flow probes. Detailed information on transonic flow probes is available at the internet site : http:\\www.transonic.com

The transonic flow probes consists of two transducers which are used to measure volume flow rate through transit time measurements. Their specified *absolute* accuracy is +- 10% for the R-Series (+-15 % for S-Series), however this may be improved to +- 2% for the R-Series (+- 3% for the S-Series) if the probes are *calibrated* before measurement. The method of measurement protected under US patent.

Transonics Website provides a list of approximately 100 publications that reference the use of transonic flow probes. A sample list of references to publications is provided below :

Comparative Measurements of Hemodialysis Access Blood Flow Using the Transonic Hemodynamic Monitor and The Critline Device. Sakiewicz, P, Paganini, E., Bednarz, D. American Journal of Kidney Diseases Abstract, Vol. 33, No. 4., P A-37, April 1999 Transonic Reference: HD104A

Evaluation of "Transonic HD01" Device to Monitor Access During HD Sessions. Barril, G, Fdez-Perpen, A., Cirujcda, A., Alvarez, V., Bemis, C., Schez Tomero, JA., Traver, JA., Selgas, R. Angioaccess for Hemodialysis 2nd International Multidisciplinary Symposium, May31-June 2, 1999 France, p. 175 Transonic Reference: HD109A

In Vitro Bench Validation of Glucose Infustion Test (GIT) Compared to Transonic Device. Magnasco, A., Alloatti, S., De Vincenzi, M., Paganni, F., Bisso, S., Solari, P.. JASN Abstracts, 11[A1008]:189A, 2000 Transonic Reference: HD157A

Setting Roller Pump Occlusion with the Transonic HT109 Flowmeter. Snyder, E.J., Harb, H.M., Cullen, J.A., McElwee, D.L. ASAIO Journal, Vol. 43, p. 60-64, 1997 Transonic Reference: 517AH

The Transonic Flowprobe in Clinical Cardiac Surgery. Transonic Reference: VP-6

US Dilution Method (Transonic Systems) For Evaluation of Native Access Flow. Bonforte, G, Grillo, P., Corso, R., Rovere G., Surian, M. 25th International Congress of Nephrology Abstract, May 1999, p. 321. Transonic Reference: HD91A